2013

Microstructure and Physics-Based Structural Models for Suspended Clay-Exopolymer Flocs

Xiaoling Tan
Louisiana State University and Agricultural and Mechanical College

MICROSTRUCTURE AND PHYSICS-BASED STRUCTURAL MODELS FOR SUSPENDED CLAY-EXOPOLYMER FLOCS

A Dissertation

Submitted to the Graduate Faculty of the
Louisiana State University and
Agricultural and Mechanical College
in partial fulfillment of the
requirements for the degree of
Doctor of Philosophy

in

The Department of Engineering Science

by
Xiaoling Tan
B.E., Huazhong University of Science and Technology, 2009
May 2014

ACKNOWLEDGMENTS

I would like to first express my deepest and sincerest appreciation to my committee chair and advisor, Dr. Guoping Zhang, who has offered me the precious opportunity for pursing this Ph.D. degree as well as the careful mentorship, enduring support, constant encouragement, and commitment. His wisdom, technical knowledge, and professional experience greatly assisted my technical writing and enriched my knowledge. Without his advice, corrections and guidance, this dissertation would never have been accomplished.

I also appreciate my co-advisor, Dr. Ying Wang, and all other committee members, Dr. Robert P. Gambrell, Dr. Murad Abu-Farsakh, and Dr. Richard F. Keim for their guidance, cooperation, constructive suggestions, and great patience, which enhance the quality of my work and dissertation. I also wish to acknowledge Dr. Yoko Furukawa and Dr. Allen H. Reed (Seafloor Sciences Branch, Naval Research Laboratory, Stennis Space Center) for their guidance, help, and supplied opportunities.

The Economic Development Assistantship (from the State of Louisiana), Supplement Award, and Dissertation Year Fellowship offered by Louisiana State University are fully acknowledged.

In addition, I would like to appreciate the help, support, and encouragement from my group mates (Dr. Hang Yin, Dr. Jie Gu, Dr. Zhenyu Lei, Rohit Pant, Zhen Liu, Hem Pant, and James Bouanchaud, etc.) and all friends (Zaihong Zhang, Yida Zhang, Yin Feng, Xi Tan, Dr. Jianglin Wang, and Qun Liu, etc.).

Last but not least, I am grateful to my parents, brother, and parents-in-law for their endless strong support. I would like to thank to my beloved husband, Dr. Hao Ying, for his encouragement, support, and patience.

TABLE OF CONTENTS

LIST OF TABLES

LIST OF FIGURES

ABSTRACT

Costal or shoreline waters are often characterized by high concentrations of suspended cohesive sediments (or clay) affected by varied organic matters (mostly extracellular polymeric substances or exopolymers), salt, and hydrodynamic disturbance. Resulting from the flocculation-disaggregation between the colloidal clay and exopolymer, the size and structure changes of the cohesive sediments are of key importance for understanding sediment transport processes (i.e., settling, breakage, and survivability) and the geotechnical and geophysical properties of the bottom bed. Because the coastal environment is extremely complicated, with many unpredictable and uncontrollable parameters, current knowledge is still insufficient to predict or fully explain the behavior of cohesive sediments.

To obtain a comprehensive and in-depth understanding of cohesive sediment properties, especially with focus on the flocculation mechanism and microstructure models of clay-exopolymers, a series of sediment samples were laboratory-prepared by using four model clays, including kaolinite, illite, Ca-montmorillonite (Ca^{2+}-Mt), and Na-montmorillonite (Na^{+}-Mt), and three representative exopolymers (xanthan, guar, and chitosan) with different polarities in both fresh and salt waters. In order to determine the influence of each main factor in coastal environments, the suspended cohesive sediments are separated as four systems and studied systematically, which are pure clay, clay-exopolymer, clay-salt, and clay-salt-exopolymer systems. Particle size distribution (PSD), settling velocity, and microstructure of these systems were characterized by state-of-the-art techniques and developed routines.

The primary PSDs of the four pure clays were first investigated via comparing different dispersion or disaggregation methods, which were used as the baseline for studying the PSD variations of other systems. Based on the synthesis of indirect PSD as well as settling velocity data and direct electron microscopy imaging, a conceptual microstructure model consisting of four hierarchical levels (i.e., primary particles, flocculi, microflocs, and macroflocs) was proposed for the clay-exopolymer flocs. The flocculation of clay-exopolymer was simplified and explained as a two-step process, including adsorption of exopolymer onto clay surfaces by intermolecular forces and packaging of clay-exopolymer groups into flocs via charge neutralization or polymer bridging. By synthesizing all the findings, a complete model was developed for clay-exopolymer floc ranging from submicron to micron scales.

CHAPTER 1 INTRODUCTION

This dissertation includes eight chapters. Except for the introduction (Chapter 1), literature review (Chapter 2), and conclusion (Chapter 8), all other chapters are constructed using the technical paper format (approved by the Graduate School of Louisiana State University) with papers that have been published, are under review, or are going to be submitted to peer-reviewed journals. This technical paper format is selected for encouraging and facilitating the Ph.D. candidate's technical publications. As a result, Chapters 3-7 are relatively independent and self-contained.

This chapter aims to present a brief but overall background for the related research in this dissertation, and offer an overview of each chapter. The detailed and specific information can be found in each paper.

1.1 Cohesive Sediments

All natural water systems (i.e., rivers, lakes, and ocean) contain sediments due to surface erosion from water sheds and bank erosion from riverbanks or coastlines (*Yang*, 2006). Particularly in nearshore and estuarine areas (*Lewis*, 2009), water is often characterized by high concentrations of suspended cohesiveless (or coarse) and cohesive (or fine) inorganic mineral sediments (*Duane and James*, 1980; *Elfrink and Baldock*, 2002; *Lewis*, 2009; *Nair et al.*, 1982; *Partheniades*, 2009; *Seo et al.*, 2009). Sediment transport has been widely studied by engineers and geologists because of its importance in economic and cultural development, such as predicting the roughness and frictional resistance of natural waterways and the magnitude of erosion and deposition (*Elfrink and Baldock*, 2002; *Huang et al.*, 2006; *Partheniades*, 2009; *Yang*, 2006). In addition, most pollutants and nutrients are attached to and transported with cohesive sediments (*Droppo et al.*, 1997; *Liu et al.*, 2008). The predication of sediment transport is the function of grain size of sediment and flow conditions. However, current understanding of cohesive sediment transport is quite limited compared to that of noncohesive sediments (*Yang*, 2006) due to the property of the fine grained mineral particles and their complex interaction with the composition of natural water (i.e., organic matter, salt).

Different from the coarse cohesiveless counterparts consisting of fine sand to coarse gravel, cohesive sediments are primarily composed of different types of fine grained clay particles (*Partheniades*, 2009; *Yang*, 2006), which are usually considered as colloids regarding their relatively small, submicrometer to micrometer sizes (e.g., <2 μm) and their charged, chemically active or reactive surfaces. These small-sized particles have large specific surface areas (SSA) so that the interparticle forces, instead of the gravitational force, dominate the behavior of cohesive sediment (*Huang et al.*, 2006) (e.g., they rarely settle in suspension as a result of Brownian motion). Basic properties, including particle size and structure, of different clays are usually different. As a result of particle-particle interaction and physical properties (i.e., irregular particle shape, flexible layers, pH dependent charge), even a pure clay can have a wide particle size distribution (PSD) ranging from submicron to tens of microns at a steady state (*Lagaly and Ziesmer*, 2003; *Murray*, 2000; *Wu*, 2001).

1.2 Nearshore or Coastal Environment

Water columns and bed sediments are usually loaded with abundant organic matter, particularly exopolymers or extracellular polymeric substances (EPS) of microbiological origin (*Azam and Malfatti*, 2007; *Bhaskar and Bhosle*, 2005; *Fabricius et al.*, 2003; *Harris and Mitchell*, 1973; *Molobela and Ilunga*, 2012). Depending on the functional groups, exopolymer molecules can exhibit different polarities, such as cationic, anionic, and neutral, and hence are chemically active in water. These organic substances are often considered as the primary mechanism for increasing sediment and soil stability through physico-chemical interactions between the clay minerals and exopolymers (*Chang and Cho*, 2012; *J. Tolhursf et al.*, 2002; *Nugent et al.*, 2009). For suspended inorganic minerals, the presence of dissolved exopolymer molecules and their interactions with clay particles can result in flocculation, particle size growth (can be as large as 500 μm), and structure and density change, which significantly alter the properties of cohesive sediments (e.g., settling, breakage, survivability) (*Furukawa and Watkins*, 2012).

Another feature of the costal environment is the change in salinity (*Alani et al.*, 1991). It can be lower in areas with mixing of fresh water from river mouths and surface runoff or higher in isolated pools as a result of evaporation. The salinity is 0 ppt (parts per thousand) for freshwater and an average of 35 ppt for seawater. The major ions in seawater are Na^{+}, Mg^{2+}, K^{+}, Ca^{2+}, Cl^{-}, SO_4^{2-}, and TCO_2 (total carbon dioxide) (*Atkinson and Bingman*, 1998). The presence of these ions and changes in their concentration in water columns quite often affect the clay-clay and clay-exopolymer interactions and hence the flocculation and properties of suspended particulate matter. For instance, divalent cations such as Mg^{2+} and Ca^{2+} may act as bridging agents to link anionic exopolymer molecules and negatively charged clays. On the other hand, the dielectric constant of water decreases as salinity increases (*Meissner and Wentz*, 2004; *Stogryn*, 1971), which can reduce the thicknesses of electrical double layers on charged colloid surfaces (*Israelachvili*, 2007).

In addition to all these constituent features, another critical feature of the nearshore zone is the large range of scales and types of fluid motion, including short and long waves, currents, turbulence, and vortices. The stability and strength of the clay-clay, clay-exopolymer, and clay-salt-exopolymer complexes are different under hydrodynamic turbulence; they may undergo disaggregation or break up into smaller sizes or grow into bigger ones due to two competing effects: (1) flocculation by the increased collision possibility and hence more adsorption; and (2) breakage into smaller flocs or particles due to the flow-induced shear stress (*Jarvis et al.*, 2005; *Mietta et al.*, 2009; *Yeung et al.*, 1997).

In summary, the nearshore zones are very complex environments where cohesive sediment is affected by biological, chemical, and hydrodynamic factors. Under these influences, the fine-grained, cohesive sediment particles can interact extensively with dissolved salts and exopolymer molecules to form aggregates or flocs of varied sizes with a typical value of 10-500 μm. Knowledge of their particle size and structure variation is of key importance for understanding a variety of sediment transport processes.

1.3 Overview of This Dissertation

The main objective of this dissertation is to get a fundamental and comprehensive understanding of clay-exopolymer flocculation mechanisms and develop a microstructure model for clay-exopolymer flocs within fresh and salt waters, which is separated and further discussed in the five paper-based chapters. Following are overviews for each chapter.

Chapter 2 first reviews the properties of different types of clay minerals and varies exopolymers, which were performed as the basis for selecting clay models (kaolinite, illite, Ca^{2+}-Mt, and Na^{+}-Mt) and exopolymer representatives (xanthan, guar, and chitosan). Then this chapter summarizes the interactions of clay and exopolymers as reported by other researchers, as well as the related characterization techniques.

Chapter 3 discusses the primary PSDs of the four selected clays. Both dry dispersion in pressurized air and wet dispersion in water and ethyl alcohol with and without an interlayer expanding agent, glycerol, were employed, along with ultrasound mechanical disaggregation and chemical dispersion. Results showed that all four clay minerals exhibit multimodal PSD consisting of superposed subordinate lognormal distributions with primary particles from submicron to 1-2 μm and flocculi at 10-20 μm (and trace impurities). The variability of these clay minerals' PSD is further discussed in terms of the complex interactions among clay particles, polar or less polar solvent, and dispersant, such as swelling, cation exchange, exfoliation, and electrical double layer repulsion. A significant practical implication is that most existing dispersion methods for PSD analysis tend to overestimate the silt-sized fraction but underestimate the clay-sized fraction, which may yield misleading classification for clay-rich soils.

Chapter 4 aims to investigate and further understand how a neutral exopolymer (guar) affects cohesive sediment transport and the final sediment yield by analyzing the PSDs and settling velocities of pure clay and clay-guar systems. The findings is that the neutral guar promotes flocculation for all four clays with the particle size significantly increasing from ~0.1-60 μm to as large as ~600 μm. Clays' layer charge has a profound influence on the clay-EPS flocculation. With the same floc size, the settling velocity of clay-EPS flocs is typically smaller than that of pure clay flocs, which is attributed to the reduced density of flocs caused by the EPS. However, for flocs of the same composition (e.g., pure clay or hybrid clay-EPS mixture), the settling velocity increases with size. The fractal dimension of these clay-EPS flocs estimated from settling velocity ranges from 1.39 to 1.47, which are smaller than that of pure clay flocs, indicating that these flocs are less compacted than the pure clay flocs.

Chapter 5 specifically shows focuses on properties of expansive clays, Ca^{2+}-Mt and Na^{+}-Mt, and investigated the influence of biological, chemical, and hydrodynamic factors on their flocculation and PSDs. All three exopolymers can facilitate flocculation through long-range polymer bridging and short-range ion-dipole, hydrogen bonding and Coulomb force. The influence of salinity is different for the two clays: the particle size of the Na^{+}-Mt increases with salinity, which is caused by flocculation resulting from the suppressed electrical double layer, while that of the Ca^{2+}-Mt is slightly reduced owing to the decreased basal spacing and cation exchange. For different hydrodynamic conditions, higher shear rate promotes the flocculation of Ca^{2+}-Mt, but breaks the Na^{+}-Mt flocs. The significance of understanding the flocculation and

PSD of expansive clays is also discussed in terms of sediment transport under different field environments.

Chapter 6 characterizes the microstructure of tenuous clay flocs modified by microbial exopolymers, in order to elucidate the effect of microbial activities (e.g., biofilms and associated exopolymers) on the flocculation and microstructure of suspended cohesive particulate matter that, after settling, forms the basic, loading-bearing skeleton of sedimentary clays. According to the particle size distribution (PSD) results, clay-guar mixture suspensions consist of four discrete particle groups, including primary particles (0.2-5 μm), flocculi (8-40 μm), microflocs (50-150 μm), and macroflocs (200-500 μm). While the first two are present in both pure clay and clay-guar suspensions, the latter two only exist in the mixture suspensions, suggesting that microflocs and macroflocs are induced by guar and composed of primary particles and flocculi. Direct electron microscopy characterization, which supports the PSD data, shows that densely packed flocculi are mainly formed via face-edge and face-face association of clay particles, and guar acts as fibrils and bundles coating, bridging, and surface gluing primary particles and flocculi, resulting in the formation of a loosely packed, porous microstructure for soft microflocs and macroflocs. Based on the synthesis of indirect PSD data and direct electron microscopy imaging, a conceptual microstructure model consisting of four hierarchical levels (i.e., primary particles, flocculi, microflocs, and macroflocs) is proposed for the clay-exopolymer flocs, and its engineering implications are also discussed.

Chapter 7 discusses the intermolecular forces and flocculation mechanisms for clay and exopolymer. Kaolinite, xanthan and guar were selected to prepare the clay-exopolymer models. Based on the flocculation study and theoretical analysis, it is found that the exopolymer-induced flocculation contains two main steps, adsorption of exopolymer onto kaolinite surface (1^{st}-step) and packaging of clay-exopolymer groups (2^{nd}-step). The 1^{st}-step results from submicroscale intermolecular forces including Coulomb force (i.e., charge-charge, ion-dipole), hydrogen bonding (H-bonding) and van der Waals force. According to the magnitude or energy of each force, as well as the chemical structure of kaolinite and exopolymers, adsorption of xanthan onto kaolinite is mainly controlled by Coulomb force, while that of guar mainly by H-bonding. Hence, the optimum concentration of exopolymers for maximum flocculation is determined by the amount of participating functional groups on exopolymers and kaolinite face surfaces. The 2^{nd}-step of flocculation is microscale interaction that usually occurs via charge neutralization or polymer bridging. Due to the lack of dissociable functional groups, nonionic guar and kaolinite packaging is only through the way of polymer bridging, while polyanionic xanthan occurs both ways. Addition of salt to a kaolinite-exopolymer system also shows different PSD change for xanthan and guar. Kaolinite-xanthan flocculation can be further promoted by divalent cation bridging and double layer compression induced more possibility in polymer bridging, which produces macroflocs in kaolinite-salt-xanthan system.

Finally, Chapter 8 gives a summary of this dissertation with some main conclusions. The findings are expected to be of interest to both geotechnical/geophysical engineers and researchers who study or use clays for different industrial applications or environmental processes. Based on current research, possible directions and work for further research are recommended.

1.4 References

[1] Alani, S., Dyer, K. R., and Huntley, D. A. 1991. Measurement of the influence of salinity on floc density and strength, *Geo-Marine Letters*, 11, 154-158.

[2] Atkinson, M. J., and Bingman, C. 1998. Elemental composition of commercial seasalts, *Journal of Aquariculture and Aquatic Sciences*, 8, 39-43.

[3] Azam, F., and Malfatti, F. 2007. Microbial structuring of marine ecosystems, *Nature Reviews Microbiology*, 5, 782-791.

[4] Bhaskar, P. V., and Bhosle, N. B. 2005. Microbial extracellular polymeric substances in marine biogeochemical processes, *Curr. Sci.*, 88, 45-53.

[5] Chang, I., and Cho, G.-C. 2012. Strengthening of Korean residual soil with beta-1,3/1,6-glucan biopolymer, *Construction and Building Materials*, 30, 30-35.

[6] Droppo, I. G., Leppard, G. G., Flannigan, D. T., and Liss, S. N. 1997. The freshwater floc: A functional relationship of water and organic and inorganic floc constituents affecting suspended sediment properties, *Water Air Soil Pollut.*, 99, 43-53.

[7] Duane, D. B., and James, W. R. 1980. Littoral transport in the surf zone elucidated by an Elerian sediment tracer experiment, *Journal of Sedimentary Petrology*, 50, 929-942.

[8] Elfrink, B., and Baldock, T. 2002. Hydrodynamics and sediment transport in the swash zone: A review and perspectives, *Coastal Engineering*, 45, 149-167.

[9] Fabricius, K. E., Wild, C., Wolanski, E., and Abele, D. 2003. Effects of transparent exopolymer particles and muddy terrigenous sediments on the survival of hard coral recruits, *Estuar. Coast. Shelf Sci.*, 57, 613-621.

[10] Furukawa, Y., and Watkins, J. L. 2012. Effect of organic matter on the flocculation of colloidal montmorillonite: A modeling approach, *Journal of Coastal Research*, 28, 726-737.

[11] Harris, R. H., and Mitchell, R. 1973. Role of Polymers in Microbial Aggregation, *Annual Review of Microbiology*, 27, 27-50.

[12] Huang, J., Hilldale, R. C., and Greimann, B. P. 2006, Chapter 4. Cohesive Sediment Transport, in Reclamation-Managing Water in the West-Erosion and Sedimentation Manual, edited, U.S. Department of the Interior, Bureau of Reclamation.

[13] Israelachvili, J. N. 2007, Intermolecular and surface forces, 2nd ed., Elsevier Academic Press.

[14] J. Tolhursf, T., Gust, G., and M. Paterson, D. 2002, The influence of an extracellular polymeric substance (EPS) on cohesive sediment stability, in Proceedings in Marine Science, edited by C. W. Johan and K. Cees, pp. 409-425, Elsevier.

[15] Jarvis, P., Jefferson, B., Gregory, J., and Parsons, S. A. 2005. A review of floc strength and breakage, *Water Research*, 39, 3121-3137.

[16] Lagaly, G., and Ziesmer, S. 2003. Colloid chemistry of clay minerals: the coagulation of montmorillonite dispersions, *Advances in Colloid and Interface Science*, 100, 105-128.

[17] Lewis, W. M. 2009, Ecological Zonation in Lakes, in Encyclopedia of Inland Waters, edited by E. L. Editor-in-Chief: Gene, pp. 416-422, Academic Press, Oxford.

[18] Liu, C., Sui, J., and Wang, Z.-Y. 2008. Sediment load reduction in Chinese rivers, *International Journal of Sediment Research*, 23, 44-55.

[19] Meissner, T., and Wentz, F. J. 2004. The complex dielectric constant of pure and sea water from microwave satellite observations, *Ieee Transactions on Geoscience and Remote Sensing*, 42, 1836-1849.

[20] Mietta, F., Chassagne, C., Manning, A. J., and Winterwerp, J. C. 2009. Influence of shear rate, organic matter content, pH and salinity on mud flocculation, *Ocean Dynamics*, 59, 751-763.

[21] Molobela, I. P., and Ilunga, F. M. 2012. Impact of bacterial biofilms: the importance of quantitative biofilm studies, *Annals of Microbiology*, 62, 461-467.

[22] Murray, H. H. 2000. Traditional and new applications for kaolin, smectite, and palygorskite: A general overview, *Applied Clay Science*, 17, 207-221.

[23] Nair, R. R., Hashimi, N. H., Purnachandra, and Rao, V. 1982. Distribution and dispersal of clay minerals on the western continental shelf of India, *Marine Geology*, 50, M1-M9.

[24] Nugent, R. A., Zhang, G., and Gambrell, R. P. 2009. Effect of exopolymers an the liquid limit of clays and Its engineering implications, *Transportation Research Record*34-43.

[25] Partheniades, E. 2009, Chapter 1. Introduction, in Cohesive Sediments in Open Channels - Properties, Transport, and Applications, edited, pp. 1-10, Elsevier.

[26] Seo, Y. J., Seol, J., Yeon, S. H., Koh, D. Y., Cha, M. J., Kang, S. P., Seo, Y. T., Bahk, J. J., Lee, J., and Lee, H. 2009. Structural, mineralogical, and rheological properties of methane hydrates in smectite clays, *Journal of Chemical and Engineering Data*, 54, 1284-1291.

[27] Stogryn, A. 1971. Equations for calculating the dielectric constant of saline water, *Microwave Theory and Techniques, IEEE Transactions on*, 19, 733-736.

[28] Wu, W. J. 2001. Baseline studies of the Clay Minerals Society Source Clays: Colloid and surface phenomena, *Clay Clay Min.*, 49, 446-452.

[29] Yang, C. T. 2006, Chapter 1. Introduction, in Reclamation-Managing Water in the West-Erosion and Sedimentation Manual, edited, U.S. Department of the Interior, Bureau of Reclamation.

[30] Yeung, A., Gibbs, A., and Pelton, R. 1997. Effect of shear on the strength of polymer-induced flocs, *J. Colloid Interface Sci.*, 196, 113-115.

CHAPTER 2 LITERATURE REVIEW

2.1 Clay and Clay Minerals

Clays are essentially composed of a small group of microcrystalline mineral particles (*Bergaya and Lagaly*, 2006). They are the major constituents of suspended sediments, cohesive soils, fine-grained rocks, and waters (*Bergaya and Lagaly*, 2006; *Çelik*, 2004; *Schroth and Sposito*, 1997). As a naturally occurring geomaterial, clays are also one of the most important mineral resources used in many industrial and ecological applications. The particle size or size distribution of clays is a key parameter for mineral identification and soil classification, as well as understanding the mechanical, physical, and chemical properties of soil, which are, in turn, of critical importance to many environmental processes (such as water quality monitoring, environmental abatement, sediment transport), agricultural applications (e.g., plant growth), and industrial engineering (e.g., oil well drilling, clay-polymer nanocomposites, and nanoclay catalysts) (*Anderson et al.*, 2010; *Harvey and Murray*, 1997; *Hill*, 1998; *Kiliaris and Papaspyrides*, 2010; *Murray*, 1999; *Pavlidou and Papaspyrides*, 2008; *Walling and Moorehead*, 1989; *Zbik and Smart*, 1998).

The two terms, "clay" and "clay mineral", are often confused and frequently misused because it is difficult to give them clear definitions. Usually, clay refers to a naturally occurring material composed of fine-grained materials, which contain one or more types of phyllosilicates, other materials that impart its plasticity (when present with appropriate water content) and harden when dried or fired, other materials that do not impart plasticity, and organic matters. While clay minerals can be either naturally occurring or synthesized, the term only refers to particularly phyllosilicate minerals with some cations and to the minerals which impart plasticity to clay and which harden upon drying or firing (*Bergaya and Lagaly*, 2006; *Guggenheim and Martin*, 1995). Thus, a clay mineral is only one of clay's constituents. In this study, these two terms may be used interchangeably but both mean the planar aluminum phyllosilicates with interlayer cations.

2.1.1 General Structure of Clay

Basic structural units and elements (Figure 2.1) are common to most ideal clay minerals. Si-O tetrahedron and Al-OH octahedron are their most basic units. Each tetrahedron is formed by a cation, Si^{4+}, coordinated to four oxygen atoms and linked to three neighboring tetrahedrons by sharing three basal oxygen atoms to form a Si-O tetrahedral sheet, an infinite two-dimensional hexagonal array along the *a*, *b* crystallo-graphic directions. For the octahedron unit, each cation (mostly Al^{3+}, but can be Fe^{3+} or Mg^{2+}) coordinates with six hydroxyl groups and the adjacent units connect by sharing edges. The edge-shared octahedrons form an Al-OH octahedral sheet as hexagonal or pseudo-hexagonal symmetry (*Brigatti et al.*, 2006).

Then, these two sheets again have two types of arrangements: 1) a tetrahedral and an octahedral sheets joint to form a TO (or 1:1) layer or plane with all the free apical oxygen atoms of tetrahedral sheet pointing to octahedral sheet; and 2) two tetrahedral and one octahedral sheets joint to generate a TOT (or 2:1) clay layer, with all the unshared corners of each tetrahedral sheet pointing toward each other and connecting to each face of octahedral sheet. At the junction

plane, OH anions lie near the center of each tetrahedral 6-fold ring, but are not shared with a tetrahedral sheet. Due to the different length scale of the units, the connection between the tetrahedral and octahedral sheets makes the tetrahedral twist or distort to a certain degree, while the octahedral sheet is flattened.

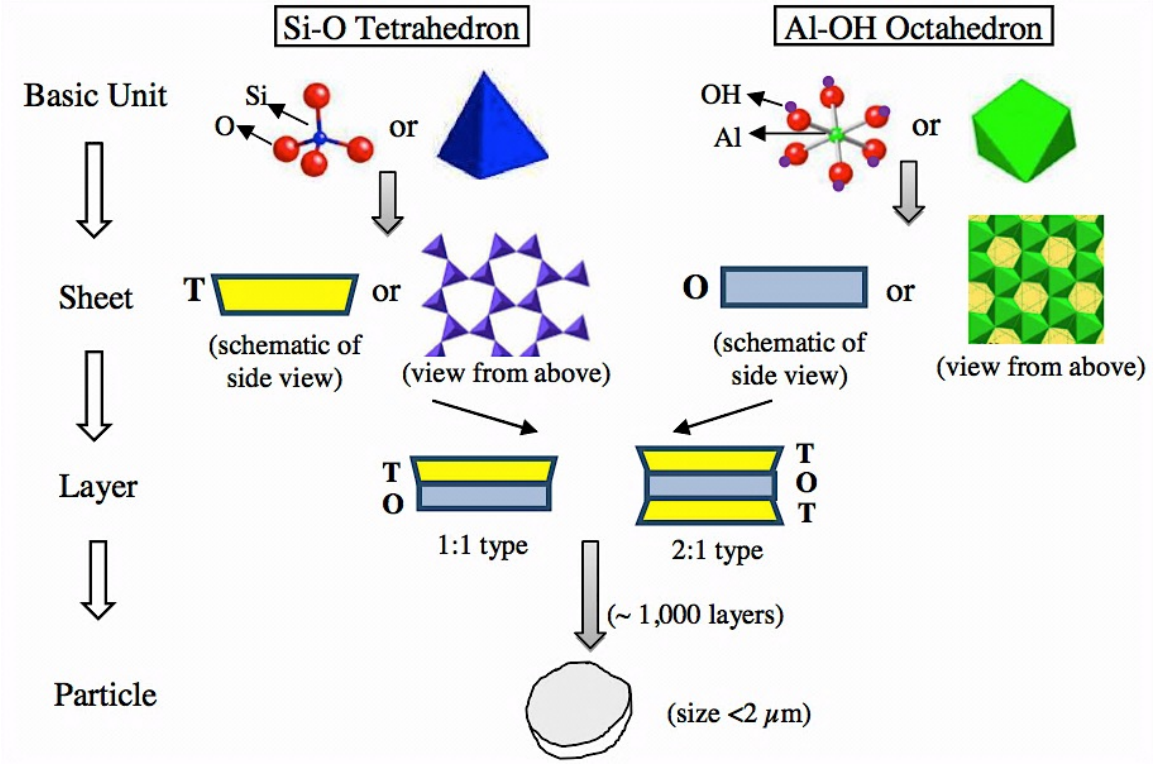

Figure 2.1 Unit and ideally crystalline structure of clay minerals.

At last, the repetition of TO layers via hydrogen bonding (H-bonding) forms 1:1 structured clay particles (e.g., kaolinite), and TOT layers are stacked and combined via Coulomb force, electrostatic attraction, and/or van der Waals, etc. forces to form 2:1 typed clay particles (e.g., illite, montmorillonite or smectite, vermiculite, mica). Besides, mixing of TO and TOT sheets generates other types of clay mineral, interstratified or mixed-layer clay minerals, which are complex in structure and less common with little literature available. Selected images for the common 1:1 type and 2:1 type clay are showed in Figure 2.2.

2.1.2 Property of Clay

Layer charge is the one of the most important features of clay, which dictates clay's physico-chemical properties (e.g., cation exchange capacity, swelling, activity of clay surface) including the aggregation/dispersion. Due to defects in crystalline structure, such as isomorphous substitution of Al^{3+}/Fe^{3+} for Si^{4+} (in tetrahedron) and Mg^{2+}/Fe^{2+} for Al^{3+} (in octahedron), and/or the presence of vacancies, naturally occurring clay minerals always have some negative charge (face charge). The negative charge is balanced by entering of the so-called interlayer or exchangeable cations (e.g., K^{+}, Na^{+}, Ca^{2+}) (*Çelik*, 2004). The presence of interlayer cations increases the basal spacing of clay particles to a typical range of 1-2 nm (Figure 2.3). The other

type of charge is the edge charge resulting from the broken bond or defects at the edge of clay particles, which is pH dependent (i.e., negative if pH >7 and positive if pH<7).

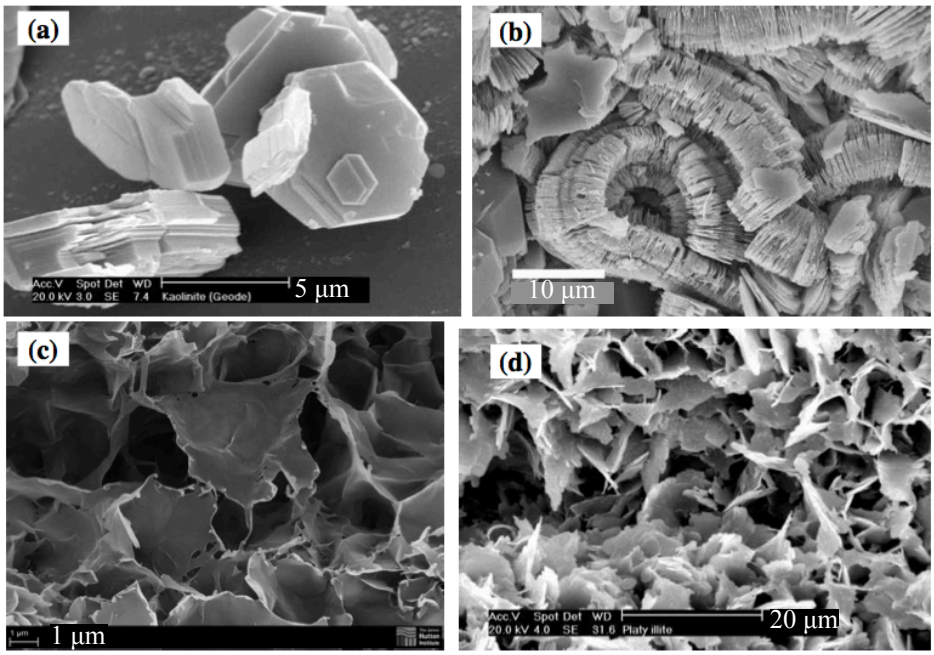

Figure 2.2 SEM images of clay particles: (a) well-crystallized kaolinite, (b) vermiform kaolinite, (c) smectite, and (d) platy illite (from the website of Mineralogical Society).

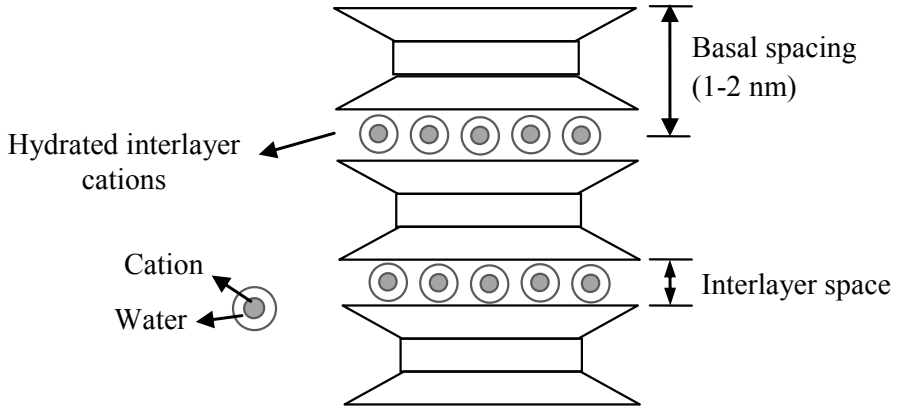

Figure 2.3 Schematic diagram of clay structure with basal spacing and interlayer spacing.

Property and type of the interlayer cations are another one of the most important feature for clays because they determine the clay-water interaction and clay swelling (*Foster*, 1995; *Theng*, 2012a). Usually, the same type of clay with different origins may be slightly different in crystalline structure (i.e., the isomorphous substitution at a different degree), but the types of their interlayer cations are the same. If the cation type or the amount of certain type varies, the property of the clay may be significantly changed. For example, in the Na-rich smectite and Ca-rich smectite, basal spacing of the former can be increased to >9 nm due to swelling (*Olejnik et al.*, 1974; *Posner and Quirk*, 1964), while the latter one can only swell to 1.9 nm (*Theng*, 1982). Swelling of clay is associated with, but not totally dependent on, the hydration of clay (*Foster*, 1995). Usually, the clays with Na^{+} and Ca^{2+} (with high valance/radius ratio or high hydration

capacity) as the major interlayer cations have high and limited expandability, respectively, while those ones with other poorly hydrated cations (e.g., K^+) rarely swell.

Cation exchange capacity (CEC) is another fundamental property of the fine-grained clay minerals (*Borden and Giese*, 2001), the studies of which predate those about the crystal structures of clay minerals. The exchange process determines many basic properties of clays, and it plays a critical role in many areas of clay research, such as the retention and release of nutrients, pesticides, and herbicides in soils; the physical and engineering properties of soils used in construction projects; the retention and isolation of wastes; water softening; and odor removal, etc. (*Churchman et al.*, 2006; *Czurda*, 2006; *Nir et al.*, 2006; *Pusch*, 2006; *Sposito et al.*, 1999). Clay minerals usually have high sorption capabilities, and the sorption of one cation must also be accompanied by desorption of another as showing in Equation 2.1. The value of CEC is usually obtained by measuring the quantity of a particular exchangeable cation and expressed in millequivalents per 100 grams (meq/100g).

$$Na^+ + K\text{-}X = Na\text{-}X + K^+ \qquad \text{Equation 2.1}$$

Additionally, specific surface area (SSA) of clay minerals, which controls the surface properties and phenomena, is also one of the most important features (*Douillard and Salles*, 2004; *Michot and Villiéras*, 2006). As the most convenient surface area parameter, it can be determined by some standard methods and is defined as area per unit gram (m^2/g). The value of SSA for non-swelling and non-microporous clays, ranging from as low as a fraction to as high as one hundred, is usually lower than that of swelling phyllosilicates.

2.1.3 Selected Clay Representatives

Among all the known minerals, kaolinite, illite, smectite (including montmorillonite), chlorite, and attapulgite are the most important and common types of clay minerals (*Çelik*, 2004). The structure and property of one type of clay mineral can be significantly different if the origins or locations are different. To offer a readily available and constant supply of materials and to correlate different groups' research to identical materials, the Clay Minerals Society (CMS) initiated the "Source Clay Mineral Project" half a century ago (*Moll*, 1973). These offered source clays are kaolinite, illite, smectite, chlorite, vermiculite and other minerals (*Chipera and Bish*, 2001). In this work, kaolinite (KGa-1b), illite (IMt-1), Ca-montmorillonite (Ca-M; STx-1b), and Na-montmorillonite (Na-M; SWy-2) were selected as clay representatives and purchased from the Clay Minerals Society Source Clay Repository. These four clays are the most abundant ones in both terrestrial soils and marine sediments and hence can represent four major species of clays with distinctly different behavior. Additionally, they have been well analyzed and widely used by many studies as reference clay minerals (*Chipera and Bish*, 2001; *Costanzo*, 2001; *Hower and Mowatt*, 1966; *Pruett and Webb*, 1993), and thus much literature is available. Geographic origins and basic properties of the four clays are summarized in Table 2.1.

Kaolinite, with the ideal formula of $Al_4Si_4O_{10}(OH)_8$, has very little isomorphous substitution in the structure lattice and thus a minimal layer charge and very low cation exchange capacity. It is produced by advanced weathering processes (*Miranda-Trevino and Coles*, 2003) and abundant in soil and sediments. As a typical 1:1 type clay mineral, the external surface

includes both the siloxane and hydroxide surfaces with negative and positive charge, respectively, for KGa-1b.

Table 2.1 Origin and basic properties of the four representative clay samples[a].

Name	Origin	CEC (meq/ 100g)	Layer charge[b] (unbalanced charge)		SSA (m^2/g)	pH[c]	Chemical formula
			T	O			
Kaolinite (KGa-1b)	Washington County, Georgia	2.00	-0.06 (0)		10.05	5.97	$(Mg_{.02}Ca_{.01}Na_{.01}K_{.01})$ $\{Al_{3.86}\ Fe^{3+}_{.02}Mn_{tr}Ti_{.11}\}$ $\{Si_{3.83}\ Al_{.17}\}O_{10}(OH)_8$
			-0.17	+0.11			
Illite (IMt-1)	Silver Hill, Montana	15.00[d]	-1.68 (0)		30.00[e] or 24.9[f]	8.61	$(Mg_{.09}\ Ca_{.06}\ K_{1.37})$ $\{Al_{2.69}Fe^{3+}_{.76}Fe^{2+}_{.06}$ $Mn_{tr}Mg_{.43}Ti_{.06}\}$ $\{Si_{6.77}Al_{1.23}\}O_{20}(OH)_4$
			-1.23	-0.44			
Ca-M (STx-1b)	Gonzales County, Texas	84.40	-0.68 (-0.08)		83.79	7.32	$(Ca_{.27}Na_{.04}K_{.01})$ $\{Al_{2.41}Fe^{3+}_{.09}Mn_{tr}$ $Mg_{.71}Ti_{.03}\}\{Si_{8.00}\}O_{20}(OH)_4$
			0	-0.68			
Na-M (SWy-2)	Crook County, Wyoming	76.40	-0.55 (+0.55)		31.82	6.44	$(Ca_{.12}Na_{.32}K_{.05})$ $\{Al_{3.01}Fe^{3+}_{.41}Mn_{.01}Mg_{.54}$ $Ti_{.02}\}\ \{Si_{7.98}Al_{.02}\}O_{20}(OH)_4$
			-0.53	-0.02			

[a] All data except those noted are from the Clay Minerals Society Source Clay Data Sheets.
[b] The charge is based on per $O_{10}(OH)_8$ for kaolinite and $O_{20}(OH)_4$ for the other three clays; T: charge from tetrahedral sheet; O: charge from octahedral sheet.
[c] pH of the suspension at a concentration of 0.4 g/L in deionized water at room temperature (23°C) obtained by a pH meter (Thermo Scientific Orion Star™ Series).
[d] Data from *Hower and Mowatt* (1966), and *Kinter and Diamond* (1958).
[e] Data from *Celis and Koskinen* (1999).
[f] Data from *Goldberg et al.* (1996).

Illite, which occurs in argillaceous sediments, is a member of the non-expanding, 2:1 type mica group (*Gaudette et al.*, 1966). The interlayer space is dominated by poorly hydrated potassium cations, thus, there is an absence of swelling. Among the four clays, illite has the highest layer charge with negative charges in both the octahedral and tetrahedral sheets for IMt-1. The CEC value of illite is usually higher than kaolinite but lower than montmorillonite.

Smectite and illite, together with vermiculate, are the most important groups of 2:1 layer clays. Specifically, the most common smemtites are calcium and sodium montmorillonite, which are dioctahedral structured with two thirds of the octahedral sites occupied by trivalent cations. The names given depend on the dominant exchangeable interlayer cation (*Çelik*, 2004). The ideal formula of montmorillonite is $M_y \bullet nH_2O(Al_{2y}Mg_y)Si_4O_{10}(OH)_2$, where M stands for cations (i.e., Ca^{2+}, Na^+). The layer charge, CEC, and SSA values are typically very high, which indicate their active surface properties. The most important feature of montmorillonite is its swelling behavior, which is summarized in Table 2.2. As shown in Table 2.1, the isomorphous substitution of Ca-M only occurs in the crystal lattice of the octahedral sheet and hence the face charge only generates from its external surface, while both octahedral and tetrahedral sheets of Na-M have isomorphous substitution. This kind of difference can be one reason for their different behaviors

in water. If the isomorphous substitution occurs in the tetrahedral sheet, the excess negative charge tends to be on single oxygen atoms, and hydrogen bonding between water molecules and the basal oxygen is possible, which is much stronger than that from the octahedral sheet (*Sposito and Prost*, 1982).

Table 2.2 Swelling of montmorillonite in water (from *Theng* (2012a)).

Region of swelling	State of Clay-Water System	Basal Spacing* (nm)	Water Content (g/g)	Interlayer Forces	
				Attractive	Repulsive
Region 1 (Crystalline swelling)	Solid, particulate	0.95-2.25	0-0.7	Electrostatic	Cation hydration
Region 2 (Osmotic swelling)	Paste-gel	2.25-4	0.7-20	Frictional, edge-to-face bonds	Diffuse double-layer interaction
Region 3	Gel-sol	> 4	> 20	Edge-to-face; Edge-to-edge bonds	Diffuse double-layer interaction; Thermal motion

* Basal spacing of Ca/Mg-montmorillonite does not exceed 1.9 nm.

2.2 Clay-Water Interface

Existence of the permanent negative surface charge results in the generation of the diffuse electrical double layer (EDL) on the basal surfaces of clay mineral particles in an aqueous suspension (Figure 2.4) (*Besra and Liu*, 2007; *Güven*, 1992; *Theng*, 2012a). The mutual repulsion of diffuse EDL is responsible for the stability of particles or unit silicate layers in water. In the clay-water system, a double layer consists of the negative charge on a clay surface and the balancing cation and negative co-ion. Characteristic length of the DL thickness, Debye length (t_D), on a clay surface can be estimated by using Equation 2.2 (*Block*, 1978):

$$t_D = \sqrt{\frac{\varepsilon_0 \cdot \varepsilon \cdot k \cdot T}{\sum_{j=1}^{N} n_j \cdot q_j^2}} \qquad \text{Equation 2.2}$$

where, ε_0 is the permittivity of vacuum, ε the dielectric constant; k the Boltzmann constant, T the absolute temperature, and n_j and q_j the mean concentration and valance of the *j-th* ion species, respectively.

Theoretically, the EDL in pure water is infinite according to Equation 2.2, but a value of 960 nm (at pH = 7) was reported by (*Israelachvili*, 2007). On the basis of the Derjaguin-Landau-Verwey-Overbeek (DLVO) theory, the interaction between negatively charged clay particles is essentially a summation of van der Waals attraction and the electrostatic repulsion due to diffuse EDL. If the thickness of double layer is decreased via lowering the dielectric constant (e.g., by adding salt, changing the temperature), aggregation or flocculation of clay mineral particles will be facilitated.

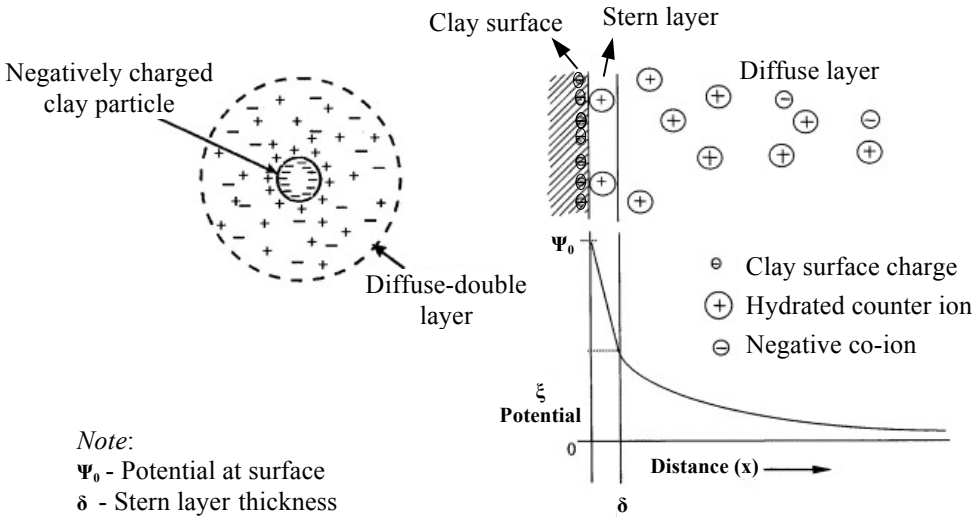

Figure 2.4 Structure of a diffuse electrical double layer at clay surface (*Besra and Liu*, 2007).

As an important characteristic for the aggregated or flocculated clay clusters, porosity is associated with clay's microstructure, property, and behavior (*Douillard and Salles*, 2004). Three types of pores can be generated in clay suspension due to flocculation (Figure 2.5): interlamellar pores within primary particles, intraaggregate pores between primary particles within aggregates, and interaggregate pores within the clay fabric (*Güven*, 1992). When the grain size decreases, either intraaggregate or interaggregate porosity usually increases (*Douillard and Salles*, 2004).

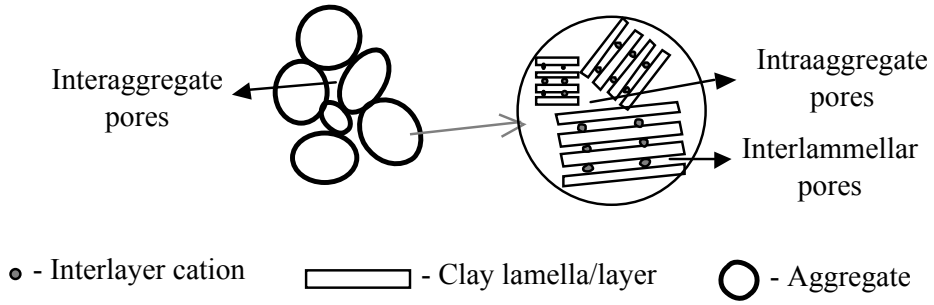

Figure 2.5 Three types of pores generated in clay flocs.

2.3 Influence of Additives on Clay Suspension

Both electrolyte addition and polymer adsorption can change the stability of clay mineral ssuspension (*Theng*, 2012b). This change and the corresponding concept (i.e., aggreation, coagulation, flcculation, charge stabilization, sensitization, and steric stabiliztion) are schematically shown in Figure 2.6. When clay particles (usually <2 μm) are completely dispersed in water, via particle-particle repulsion, they are able to reach a stabilization status, called "charge stabilztion". Otherwise, clay particles aggregate to form flocculi due to particle-particle attraction. If optimum amount of electrolyte or salt is added, coagulation of clays is generated, which results from double layer compression. If a very small amount of exopolymer added, these clay particles reach a sensitization status with the EPS molecules only adsorbed

onto clay surfaces. When the amount of exopolymer increases to a optimum amount or some electrolyte is added, floccualtion may be generated and the particle size can be significantly increased. If the exopolymer is overdosed, clay-exopolymer may reach the steric stabilization status, which impedes flocculation.

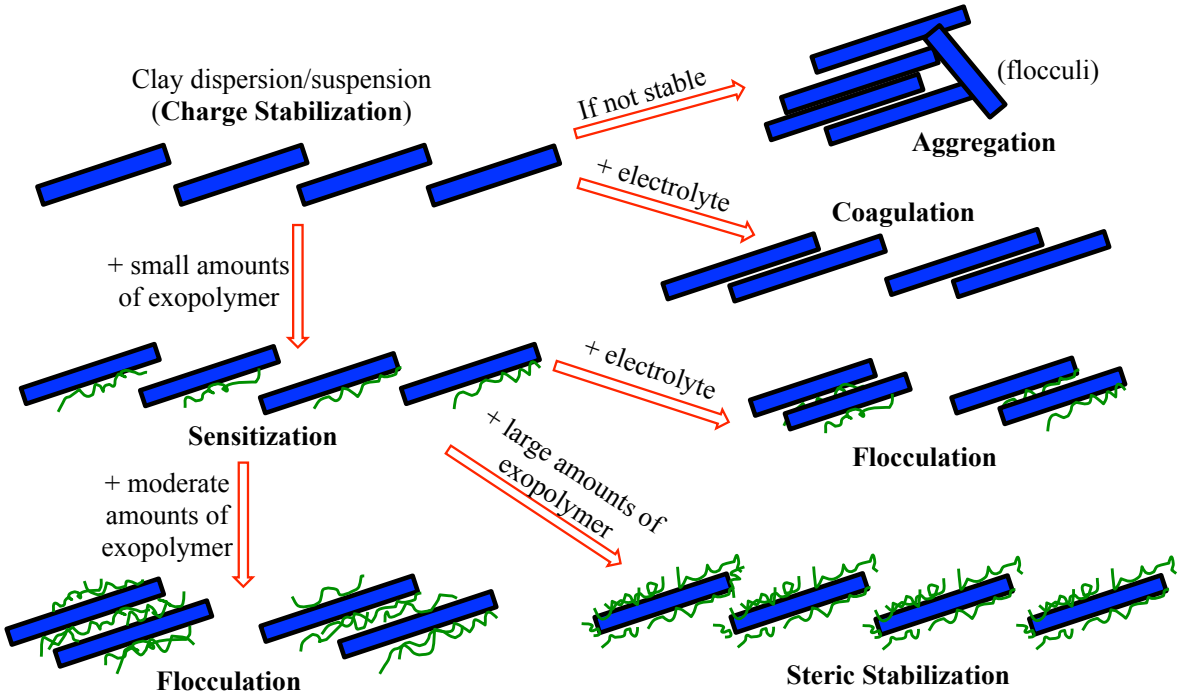

Figure 2.6 Influence of different additives on clay suspension (modified from *Theng* (2012b)).

2.4 EPS and Clay-EPS Interaction

2.4.1 EPS Representatives

The abundance of organic matters, particularly the EPS of microbiological origin (*Azam and Malfatti, 2007; Fabricius et al., 2003; Harris and Mitchell, 1973; Molobela and Ilunga, 2012*), is an important characteristic for the water column and bed sediment at nearshore environments. These expolymers or extracellular polymeric substances (EPS) are the primary compositions of biofilms and usually consist of mostly polysaccharides and a small quantity of proteins, DNAs, and humic substances (*Decho, 2000; Decho and Kawaguchi, 1999; Decho et al., 2003*). Structure of the EPS can range from simple polysaccharides assembled from identical monomeric units to complex muco-lipo-proteinaceous polymers and protein-nucleic acid polymers of nuclear origin (*Harris and Mitchell, 1973*). EPS usually play an important role in the stabilizing of clay aggregates in both soil and sediment (*Chang and Cho, 2012; J. Tolhursf et al., 2002; Nugent et al., 2009*). The interaction of clay mineral with EPS, usually involving water and ions, is very complicated, so the clay-EPS complexes are classified and discussed in terms of the charge or polarity characteristics of the polymers. Among all the types of EPS, polysaccharides are the most prevalent and the most abundant organic matter (*Theng, 2012c*) associated with the clay or soil stabilization. Thus, to account for the variety of EPS in the suspended cohesive sediment, three polysaccharides, anionic xanthan gum, neutral guar gum, and cationic chitosan, were chosen as the EPS representatives in this work. In fact, all three EPS

have been widely studied as coagulants (*Chen and Chung, 2011; Gupta and Ako, 2005; Kumar, 2000; Sashiwa and Aiba, 2004; Yokoi et al., 1996; Yokoi et al., 1998*). Chemical structures of these EPS are shown in Figure 2.7.

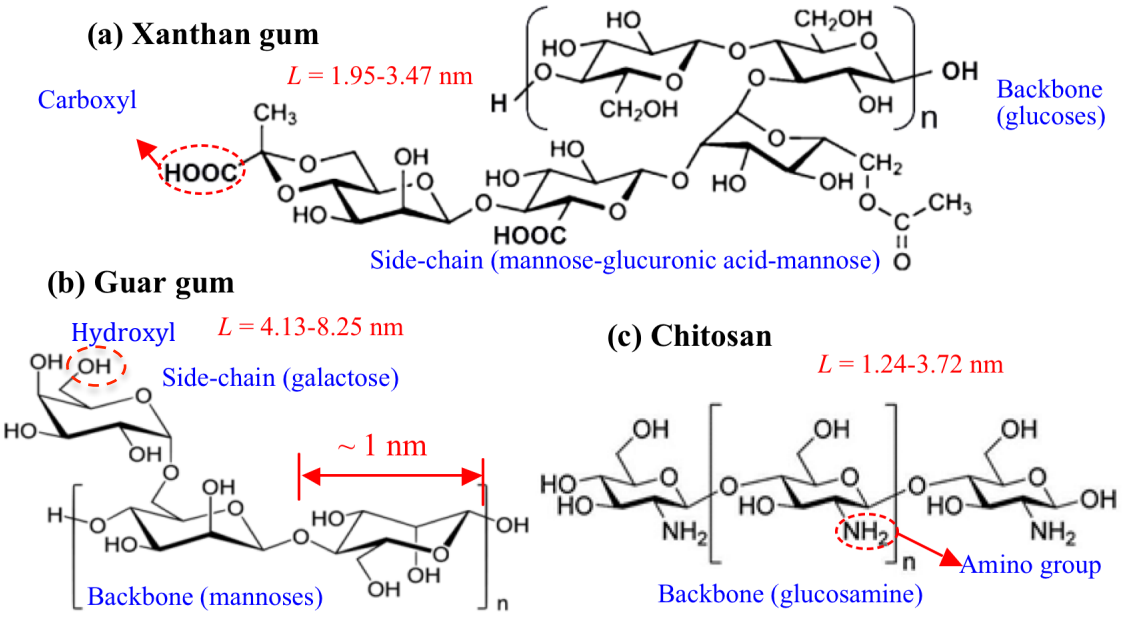

Figure 2.7 Chemical structure and molecule length (*L*) of (a) xanthan gum, (b) guar gum, and (c) (100% deacetylated) chitosan.

The polycationic xanthan gum (Spectrum®, Gardena, CA) is a water-soluble bacterial extracellular polysaccharide produced through fermentation by Xanthomonas campestris bacterium. Due to different bacterial strains and growth environments, the molecular weight of xanthan varies but typically ranges from 0.9-1.6 x 10^6 Da (Ian W, 1994). As shown in Figure 2.7 (a), xanthan consists of *β*-(1,4)-*D*-glucopyranose glucan backbone with extended side chains of (3→1)-*α*-linked *D*-mannopyranose-(2→1)-*β*-*D*-mannopyranose on alternating residues. Its negative charge is from carboxylic acid groups (-COOH) in glucuronic acid and pyruvic acid groups on side chains (*Ian W*, 1994). Its molecule length (of the backbone), as shown in Figure 2.7, can be estimated by using a published approach for polysaccharides (*Chang and Cho*, 2012).

The polyneutral guar gum (Fisher ChemAlert® Guide, Rochester, NY) is a water-soluble polysaccharide extracted from guar beans with a molecular weight of up to 2 x 10^6 Da (*Nugent et al.*, 2009; *Risica et al.*, 2005). It is not a true exopolymer, but is usually used as an EPS analog representative of neutral microbial exopolymers. Guar gum structurally consists of long, linear chains of *α*-*D*-manopyranosyl units linked together by *β*-*D*-(1,4)-glycosidic linkage mannose residues with a *α*-(1,6) linked *D*-galactose. There are 1.5-2 mannose residues for every galactose residue in average. After dissolving, guar gum can produce viscous, pseudoplastic aqueous solutions.

The polycationic chitosan (Acros Organics, New Jersey, USA) is obtained from the deacetylation process of chitin, which is the supporting material of shrimp and crab shells and other crustaceans or insects (*Kumar*, 2000). It is composed of *β*-(1,4) linked *D*-glucosamine

without any side chains. The molecular weight is 1~3 x 10^5 Da, and its positive charge is from the hydrolysis of amino groups in water.

The amount and distribution of EPS in waters is highly dependent on season, location, and some other environmental factors. Their concentration typically ranges from ~1 to ~1000 μg/g (*Collins et al.*, 1986; *Gerbersdorf et al.*, 2009; *Hirst et al.*, 2003). To account for this variation that may affect the flocculation of cohesive sediments, the EPS concentrations of 0, 1, 10, and 100 μg/g were chosen for the clay-EPS floc preparation.

2.4.2 Intermolecular Forces and Clay-EPS Interaction

To differentiate and classify/name the interaction mechanisms or interaction forces between clay particles and EPS molecules, the basic concepts and types of forces were reviewed and briefly summarized in Figure 2.8. The intermolecular force, a type of electromagnetic force in nature, can be roughly divided into three groups according to the polarity of molecules involved (*Briscoe*, 2010; *Israelachvili*, 2007): (1) Chemical bonding (i.e., covalent, ionic and metallic bonds with quantum mechanical nature) and steric repulsions (regarding to Pauli's exclusion principles), which are very short-ranged forces, e.g., covalent bond at 0.1-0.2 nm; (2) Coulomb force or electrostatic interaction between permanent charges and dipoles at a long range (~0.3 nm); (3) Polarisation force between dipoles induced by nearby charges and permanent dipoles, including van der Waals (VDW) force of three types (Keesom, Debye, and London dispersion forces). It is considered as long ranged on a molecular scale (several nanometer) but short ranged on a colloidal scale (1 nm – 10 μm), e.g., the range of VDW force is typically 0.25-0.46 nm; and (4) Hydrogen bonding (H-bonding), as special VDW force with some feature of covalent bond, of strong electromagnetic dipole-dipole attraction between hydrogen donor and acceptor (i.e., N, O, F), which is typically considered as a short-ranged force ranging 0.26-0.25 nm.

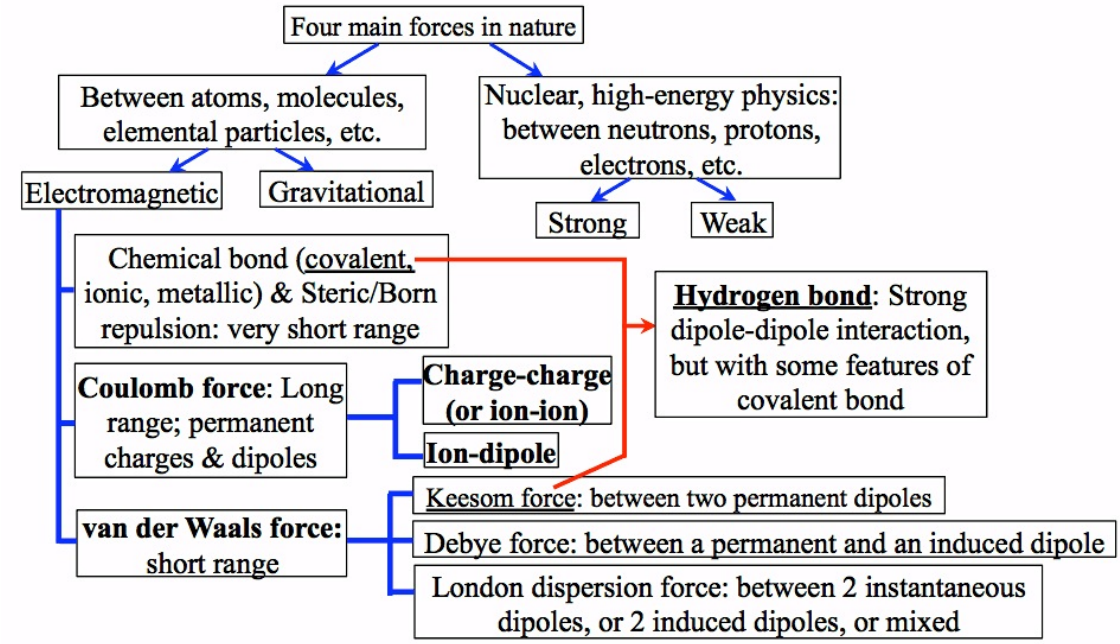

Figure 2.8 Basic concept and classification of molecular forces.

When dissolved EPS is added into clay suspension, the mixing, adsorption, and flocculation of clay and EPS take place by the following steps (*Gregory*, 1988) as shown in Figure 2.9: (a) mixing of EPS molecules among clay particles; (b) adsorption of EPS chains on particle surfaces; (c) re-arrangement or re-conformation of the adsorbed EPS from their initial state to an equilibrium configuration; (d) collisions between particles with adsorbed polymers to form aggregates (flocs), either by bridging or by charge effect; and (e) break-up of flocs. Instead of simply occurring in a sequence, these processes take place simultaneously at the rate determined by a number of factors, which make the whole process complicated and difficult to analyze in a straightforward manner. Among these five processes, (b) and (d) are the most important steps that mainly involve the clay-EPS intermolecular interactions. Hence, most of the literature review and analysis in this work are focused on these two processes.

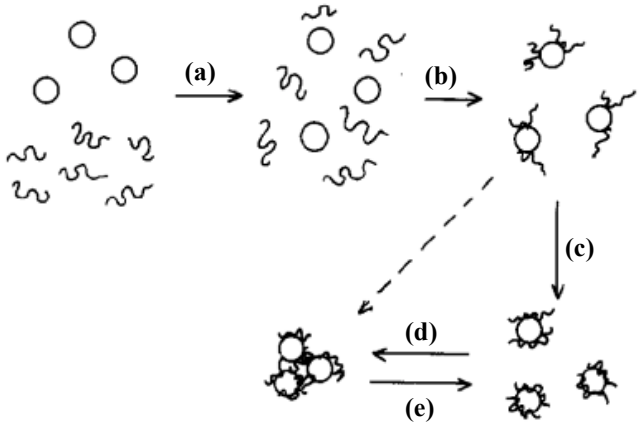

Figure 2.9 Schematic diagram showing the behavior of EPS molecules (polymeric flocculant) added to clay suspension *Gregory* (1988).

Different interaction mechanisms of clay and EPS molecules can coexist in the clay-EPS-water system controlled by surface or molecule functional groups, chemical structure, and conformation, which are further influenced by the presence of different ions. As illustrated by *Gregory* (1988) and *Theng* (2012b), this kind of interaction can be divided into two main steps: (1) adsorption of EPS molecules onto clay particles; and (2) flocculation of clay particles with absorbed EPS. EPS molecule adsorption, competing with water molecules attached on clay surface, is driven by the translational entropy from replacing water with a single macromolecular chain on a clay surface (*Theng*, 1982; 2012a). After the adsorption of EPS molecules onto clay surfaces, they rearrange their status into an equilibrium train-loop-tail conformation (*Adachi et al.*, 2012; *Theng*, 1982; 2012b). As a special case for swelling clay, the neutral EPS molecules can be inserted into the interlayers (intercalation) (*Theng*, 1982). Some details of clay-EPS flocculation have been reported. Electrostatic attraction and hydrogen bonding are the main attraction between clay edges and EPS molecules (*Theng*, 1970). Ca-smectite tends to flocculate with negatively charged EPS through the bridge of divalent Ca^{2+} (*Dontsova and Bigham*, 2005) since the electrostatic repulsion is relatively weaker. *Nugent et al.* (2009) reported that kaolinite and guar can interact by ion-dipole and hydrogen bonding. While more detailed information regarding both of the two steps in flocculation, for example, the involved adsorption forces and flocculation for different clay-exopolymer systems, has not been reported yet. In addition, since interaction between the colloidal clay and exopolymer is complicated and change of the

composition may result from different flocculation condition, a systematic study and investigation of different types of clay-exopolymer systems is needed.

The process of clay-induced flocculation is induced by either polymer (or interparticle) bridging or charge neutralization (*Adachi et al.*, 2012; *Gregory*, 1988; *Harris and Mitchell*, 1973; *Lagaly*, 2006; *Theng*, 2012b). To meet the first type flocculation, EPS molecule chain should be absorbed by at least two clay particles at the same time, which indicates that the length of extended loops and/or tails should be greater than twice of the double layer thickness. The charge neutralization induced flocculation usually generates between negative clays and cationic EPS with the extending loops/tails shorter than twice of the clay's double layer thickness.

2.5 Salt and Clay-Salt System

Variation of salinity is also an important feature of the natural environment (*Alani et al.*, 1991) that affects the flocculation of suspended cohesive sediments. Salinity stands for the saltiness or dissolved salt content in water with the units of ppt (parts per thousand), ppm (parts per million), and *o/oo* interchangeably used (e.g., 1 g dissolved salt / kg seawater = 1 ppt = 1, 000 ppm = 0.1 % = 1 *o/oo*). The nearshore zone is where the land and sea meet between the high and low tides. Hence, the salinity level varies, as it can be high at low tide and low at high tide. The salinity is 0 ppt for freshwater and 35 ppt on average for seawater. It can be lower in areas where there is mixing of fresh water from river mouths and surface runoff or higher in isolated pools and lakes resulting from evaporation.

The major ions in seawater, in order from the greatest to the least presence, are Na^+, Mg^{2+}, K^+, Ca^{2+}, Cl^-, SO_4^{2-}, and TCO_2 (total carbon dioxide) with other trace ions. *Atkinson and Bingman* (1998) analyzed eight different, commercially available, synthetic seasalt mixes for thirty-five elements and ions and other chemical parameters, and found that Instant Ocean® seasalt has the most similar compositions to the water from a typical tropical ocean. Thus, this commercial seasalt was selected for preparing salt waters and simulating the salinity change from fresh to seawaters.

The dielectric constant of water decreases as the salinity increases; its values are 80.4, 79.2, 77.9, and 71.8 for water at 0, 5, 10, and 35 ppt, respectively (*Meissner and Wentz*, 2004; *Stogryn*, 1971). By using Equation 2.2, EDL thicknesses at a salinity of 5, 10, and 35 ppt can be obtained and estimated as 0.92, 0.64, and 0.32 nm, respectively. The thickness of the double layer in freshwater is ~960 nm (at pH = 7) reported by (*Israelachvili*, 2007). These parameters are summarized in Table 2.3. Besides the lowest and highest salinity value, the other two salinities were chosen for the reason that there is significant change of EDL thickness in the range of 0-10 ppt.

The change in salinity and presence of these ions in the water column quite often affect the clay-clay and clay-EPS interactions and hence the flocculation and settling behavior of suspended particulate matter. As the salinity increases, the EDL decreases (*Israelachvili*, 2007), which may facilitate the flocculation or aggregation of clay minerals by reducing the repulsive force. On the other hand, cations from the seasalt may exchange with the interlayer cation of clay particles and cause exfoliation. For instance, the presence of Na^+ may exchange with the interlayer divalent cation, such as Mg^{2+} and Ca^{2+} in montmorillonite, which may either increase

particle size by promoting swelling or decrease the size by exfoliation. In addition, the presence of salt in a clay-anionic EPS system can facilitate flocculation through divalent (e.g., Ca^{2+}) bridging on anionic EPS molecules and negatively charged clay surfaces.

Table 2.3 Dielectric constant and electric double layer thickness of clay in saltwater.

Salinity (ppt)	Dielectric constant	Thickness of electric double layer (nm)
0	80.4	~960
5	79.2	0.92
10	77.9	0.64
35	71.8	0.32

2.6 Particle Size Measurement

The cohesive sediments usually have a wide particle size range, even in pure water at a steady state, due to their properties of irregular particle shape, flexible layers, heterogeneous layer charge, pH dependent edge charge (e.g., positive if pH < 7, and negative if pH > 7), and different modes of flocculation (*Lagaly and Ziesmer*, 2003; *Murray*, 2000; *Wu*, 2001). Due to their micrometer to sub-micrometer sizes, determination and evaluation of clays' particle size distribution (PSD) are difficult and hence not routinely performed in most engineering or industrial practices. For example, according to the ASTM Standards (*D422-63*, 2007), PSD is a very important parameter for soil classification, yet no further effort is required to characterize PSD for the <2 μm fraction. As a result, all particles in this fraction are collectively treated as clays without further differentiating their sizes (e.g., submicrometer vs. micrometer). On the other hand, some well-crystallized clay minerals (e.g., kaolinite) may have relatively large, >2 μm particles. Although these particles are truly clay minerals with chemically active surfaces, they may be counted toward the silt-sized fraction, which may yield misleading soil classification and lead to inappropriate perception on soils' physico-chemical properties.

For clays with variable PSDs, another concern arises with the definition and determination of truly representative primary particles. According to the literature, primary particles usually refer to physically solid and homogeneous, individual particles without flocculation or aggregation (*Zhang et al.*, 2005). For swelling clays, primary particles are the physically coherent stacks of parallel, equally spaced clay platelets (*Güven*, 1992). Therefore, primary particles are intrinsic or inherent to the material, and their sizes should not be affected by different sample preparation techniques.

The majority of existing techniques for PSD measurements require preparing an ideally or appropriately dispersed clay suspension, mostly in water. A few issues arise from this sample preparation process. The first one is interactions between clay and water, including the formation of an electrical double layer on charged clay surfaces, adsorbed cation hydration, and intercalation of water into expandable clays. Of these interactions, water intercalation in swelling clays can cause an initial increase in particle thickness, which may then result in an increase or decrease in their size, depending on the types of interlayer cations or degree of swelling and other environmental conditions, as discussed below; the second one is stability of the suspension. An unstable clay suspension can lead to flocculation or aggregation, resulting in coarser PSDs; hence the third one is the use of chemical dispersants to obtain stable clay suspensions (i.e., no

flocculation or aggregation). Due to clays' cation or anion exchange capability, the cations or anions from dissolved dispersants may change clays' properties and hence alter their PSDs. For example, a Ca-smectite may be partially or completely converted via cation exchange to a Na-smectite if a Na-based dispersant is used. After the conversion, because Na^{+} has a stronger hydrability than Ca^{2+}, the Na-smectite can swell to a higher degree such that its interlayer spacing can theoretically increase to infinity, leading to the formation of exfoliated individual 2:1 layers as separate particles. In contrast, Ca-smectite or smectites with other divalent interlayer cations (e.g., Mg^{2+}) have limited swelling due to both the van der Waals attraction and electrostatic attraction between interlayer cations and negatively charged 2:1 layers (*Helmy*, 1998; *Segad et al.*, 2010). Therefore, clay swelling may result in either an increase in particle size via water intercalation or decrease by exfoliation.

It is worth noting further the importance of appropriate dispersion of suspended clay particles for PSD analysis, because clay suspension is a very complex system that contains both individual clay particles and most likely clay aggregates. Both mechanical and chemical methods can be used to facilitate disaggregating or dispersing of clay suspensions (*Zhang et al.*, 2005). The former usually involves the application of mechanical energy to break down and separate aggregated particles, such as ultrasound disruption or flow-induced shearing in a high-speed stirrer, while the latter refers to the use of dispersants to remove or eliminate the physical cementation or chemical bonds holding particles together (*Zhang et al.*, 2005; *Zhang et al.*, 2004b). Therefore, accurate measurement of intrinsic PSDs largely depends on the effectiveness of the employed dispersion methods to separate clay aggregates and to then keep them stable at their primary particles state (*Crowley and Welch*, 1954). This may also require a continuous dispersion process to maintain the clay suspension at a completely dispersed, equilibrated state even during measurement. With the development of some new instruments (e.g., laser diffraction based particle size analyzers), the size of clay particles and their size distribution can be accurately and quickly measured (*Deboer et al.*, 1987) when a clay suspension is continuously circulated. Additionally, different dispersion methods, either chemical or mechanical or both, in different solvents (e.g., air, water, or a nonpolar liquid) can be employed for PSD measurements.

2.7 Characterization of Flocs' Microstructure

In addition to the forces between particles, structure (e.g., porosity, density, and fractal dimension) is an essential factor in determining various mechanical and rheological properties of cohesive sediment flocs and bottom beds (*Kranenburg*, 1994). The micron sized floc is usually soft, tenuous, porous, cluster-like, and associated with water, which makes its structure characterization very difficult. Recent reviews (*Chu and Lee*, 2004; *Droppo et al.*, 1997; *Jarvis et al.*, 2005a; *Jarvis et al.*, 2005b; *Lintern and Sills*, 2006) have summarized and evaluated most of the available techniques for floc structure measurements. The common adopted direct observations of a floc's microstructure include conventional optical microscope, confocal lasers scanning microscopy (CLSM), scanning electron microscopy (SEM), environmental scanning electron microscopy (ESEM), transmission electron microscopy (TEM), and atomic force microscopy (AFM), etc.; the ordinary indirect examinations include free settling test and small-angle laser light scattering (SALS). Details of these routine techniques for floc structure characterization are given bellow.

2.7.1 Conventional Optical Microscopy

Although the resolution of conventional optical microscopy is limited for micron or submicron sized samples, it is convenient for observing the gross structure and estimating the shape factors (*Chu and Lee*, 2004). More importantly, this method almost does not need any pre-treatment for a sample, which can keep all the intact features of the delicate flocs (*Droppo et al.*, 1997).

2.7.2 CLSM

CLSM can be used to observe the internal floc structure and matrix (*Chu and Lee*, 2004; *Droppo et al.*, 1997). Accompanied by fluorescence in situ hybridization (FISH) to chemically fix a sample, the laser of CLSM can penetrate and scan a floc sample at a pre-specified depth and hence can obtain cross-sectional images of a floc from different depths. A series of images of each slice can be used to reconstruct the 3*D* image of the examined floc, and comparisons be made between the TEM (mentioned below) and CLSM-acquired structure. The detailed structural data (e.g., perimeter of each slice, surface area, and volume) can then be used to estimate the fractal dimension, using a reported successful approach for sludge flocs.

2.7.3 SEM/ESEM

SEM can be used to determine the surface features of flocs, such as presence of EPS, particle compactness, porosity, and particle/clay orientation (*Chu and Lee*, 2004; *Chu et al.*, 2005). Analysis of size, particle orientation, and/or fractal geometry for clay particles from SEM image has also been reported by (*Du et al.*, 2009; *Erzan and Gungor*, 1995). For SEM, the selected floc sample needs to be first chemically fixed, dehydrated using ethanol, dried with critical-point CO_2 or freeze-drying, and then coated with gold or platinum. The technique of critical point drying can prevent water evaporation and maintain the original morphology. Examination of wet (without drying or pre-processing) flocs is able to be performed in an ESEM, which is designed for studying hydrated or wet soils, biomaterials (*Zhang et al.*, 2004a), and other environmental samples. This extra investigation can at least assess possible disturbances to the floc's microstructure caused by chemical fixation, critical-point drying, and other pre-processing steps.

2.7.4 TEM

Due to its ultra-high resolution, TEM can be used for more detailed structural observation and ultrastructure determination (*Chu and Lee*, 2004; *Chu et al.*, 2005; *Droppo et al.*, 1997; *Kim et al.*, 2012). As for SEM, the sample for TEM also needs to be pre-processed for chemical fixing and dehydration first. After drying the floc sample will be post-fixed (embedded in a low viscosity resin), followed by slicing the resin-fixed flocs into very thin sections (e.g., thickness <70 nm) using an ultramicrotome. The prepared thin sections will then be probed in TEM. A complete series of thin section images can be used to reconstruct the 3*D* image of an individual floc. The pre-processing methods from different literature may vary. Their influence on the structure and constituent of sediment flocs should be considered. For example, the solvent-exchange (methanol-water) in the L.R. White embedding procedure may remove the organic

matter from the floc (*Kim et al.*, 2012). Instead, water-miscible Nanoplast resin can be used since it eliminates the dehydration step typically required by TEM.

2.7.5 AFM

AFM is a very high-resolution scanning probe microscopy. It is used for surface feature or configuration characterization. The most common tapping-mode AFM cannot perform *in situ* observation of sludge flocs in liquid phase; thus, selected floc samples need be pre-processed by chemical fixing, dehydration and CO_2 critical-point drying (*Chu and Lee*, 2004). The dried sample is then glued on a grid for scanning. According to the AFM image from (*Chu and Lee*, 2004), AFM may not be a good tool for the study of floc morphology. Tapping the soft surface of a floc, especially the EPS part, is difficult since it makes positioning. Also, the roughness of a floc surface is very high, which usually exceeds the allowable range of AFM.

2.7.6 Free Settling Velocity and Test

Settling velocity is important for sediments in all water systems. It is usually directly or indirectly used in the calculation of deposition and selective transport of sediments (*Basile et al.*, 2010; *Loch*, 2001). Particle and floc transport by gravitational sedimentation is also important in nearly every procedure for water and wastewater treatment (*Johnson et al.*, 1996).

The motion of individual flocs in water can be captured and used for analyzing their structural properties (i.e., density, fractal dimension, porosity). Usually, the floc sample is put in a transparent cylinder and the settling process is recorded by using an optical microscope. For example, (*Chu and Lee*, 2004) made a cylinder with two filters (to remove the floc that does not move along centerlines) and transparent glass (diameter 6 cm and height 50 cm). The settling processes were record by a CCD camera (MML2-120; Moritex, UK). Then, terminal velocity and the vertically projected area were determined for each floc by using the software *INSPECTOR* (Matrox), which is designed for flocs with sizes between 100 and 2000 μm. In the end, the log-log plot of terminal velocity (u_T) versus floc size (D) yields a curve with the slope related to fractal dimension (D_f) (Equation 2.3), similar routines of which have also been reported by (*Likos and Lu*, 2001; *Lintern and Sills*, 2006; *Miyahara et al.*, 2002).

$$u_T \propto D^{D_f - 1} \qquad \text{Equation 2.3}$$

Settling velocities of single particles are clearly understood, but settling velocities of flocs or aggregates are not (*Hill*, 1998). The suspended primary cohesive sediments or clay particles are typically small (e.g., <2 μm) and, if dispersed, do not readily settle in most natural waters. Settling velocity of floc is probably associated with suspended particle concentration and limited by turbulence-induced forces, which are considered as the dominant mechanisms for liberating mass from flocs. The resultant shear force caused by settling acceleration under gravity, as well as hydrodynamic turbulence, can cause floc breakage or de-flocculation and hence limit the terminal size during settling (*Kobayashi et al.*, 1999). Settling velocity is also affected by flocculation resulting from either salt or organic matter. It is expected that different degrees of flocculation result in flocs of varying sizes and densities. Flocculation can promote the settling of clay particles that otherwise do not settle by altering the size and density of these particles (*Droppo et al.*, 1997).

For particles or flocs of the same composition and density, larger ones are usually expected to settle faster than smaller ones. Due to the floc's porous structure and resulting creeping flow through the internal pores, a smaller drag force is expected when compared with solid, non-porous particles of the same size, and hence flocs should sink faster than the solid particles of the same density and size (*Huang*, 1993). However, the larger clay flocs may be more porous and less denser than the smaller ones (*Likos and Lu*, 2001), and this could be interpreted by the fact that, while the size increases, the ratio of surface-area-to-volume decreases, which makes smaller flocs more adsorptive per unit of mass. Therefore, the density of larger flocs is relatively smaller (*Hill*, 1998).

2.7.7 SALS

SALS test is based on a laser particle size analyzer and hence it can measure flocs with a broad size distribution. Information from the scattered light is collected. According to the theory of Rayleigh-Gans-Debye scattering of a fractal floc, the scattering light intensity (I) versus wave vector (Q) can be plotted in a log-log plot. The curve has a linear region with the slope related to the scattering fractal dimension (D_s). The relationship, as shown in Equation 2.4, is similar to that for the settling velocity test. Different types of flocs usually give various D_s, indicating the difference of their internal structure.

$$I \propto Q^{-D_S} \qquad \text{Equation 2.4}$$

2.8 References

[1] Adachi, Y., Kobayashi, A., and Kobayashi, M. 2012. Structure of colloidal flocs in relation to the dynamic properties of unstable suspension, *International Journal of Polymer Science*, 2012.

[2] Alani, S., Dyer, K. R., and Huntley, D. A. 1991. Measurement of the influence of salinity on floc density and strength, *Geo-Marine Letters*, 11, 154-158.

[3] Anderson, R. L., Ratcliffe, I., Greenwell, H. C., Williams, P. A., Cliffe, S., and Coveney, P. V. 2010. Clay swelling - A challenge in the oilfield, *Earth-Science Reviews*, 98, 201-216.

[4] Atkinson, M. J., and Bingman, C. 1998. Elemental composition of commercial seasalts, *Journal of Aquariculture and Aquatic Sciences*, 8, 39-43.

[5] Azam, F., and Malfatti, F. 2007. Microbial structuring of marine ecosystems, *Nature Reviews Microbiology*, 5, 782-791.

[6] Basile, P. A., Riccardi, G. A., Zimmermann, E. D., and Stenta, H. R. 2010. Simulation of erosion-deposition processes at basin scale by a physically-based mathematical model, *International Journal of Sediment Research*, 25, 91-109.

[7] Bergaya, F., and Lagaly, G. 2006, Chapter 1 General Introduction: Clays, Clay Minerals, and Clay Science, in Developments in Clay Science, edited by B. K. G. T. Faïza Bergaya and L. Gerhard, pp. 1-18, Elsevier.

[8] Besra, L., and Liu, M. 2007. A review on fundamentals and applications of electrophoretic deposition (EPD), *Progress in Materials Science*, 52, 1-61.

[9] Block, L. P. 1978. A double layer review, *Astrophysics and Space Science*, 55, 59-83.

[10] Borden, D., and Giese, R. F. 2001. Baseline studies of the Clay Minerals Society Source Clays: Cation exchange capacity measurements by the ammonia-electrode method, *Clay Clay Min.*, 49, 444-445.

[11] Brigatti, M. F., Galan, E., and Theng, B. K. G. 2006, Chapter 2 Structures and Mineralogy of Clay Minerals, in Developments in Clay Science, edited by B. K. G. T. Faïza Bergaya and L. Gerhard, pp. 19-86, Elsevier.

[12] Briscoe, W. 2010, Chapter 16 Surface Forces, in Colloid Science: Principles, Methods and Applications (2nd Edition), edited by T. Cosqrove, pp. 329-361, Wiley-Blackwell.

[13] Çelik, M. S. 2004, Electrokinetic behavior of clay surfaces, in Interface Science and Technology, edited by W. Fernando and S. Kestur Gundappa, pp. 57-89, Elsevier.

[14] Celis, R., and Koskinen, W. C. 1999. Sorption and desorption of triadimefon by soils and model soil colloids, *J. Agric. Food Chem.*, 47, 776-781.

[15] Chang, I., and Cho, G.-C. 2012. Strengthening of Korean residual soil with beta-1,3/1,6-glucan biopolymer, *Construction and Building Materials*, 30, 30-35.

[16] Chen, C. Y., and Chung, Y. C. 2011. Comparison of Acid-Soluble and Water-Soluble Chitosan as Coagulants in Removing Bentonite Suspensions, *Water Air Soil Pollut.*, 217, 603-610.

[17] Chipera, S. J., and Bish, D. L. 2001. Baseline studies of the Clay Minerals Society Source Clays: Powder X-ray diffraction analyses, *Clay Clay Min.*, 49, 398-409.

[18] Chu, C. P., and Lee, D. J. 2004. Structural analysis of sludge flocs, *Advanced Powder Technology*, 15, 515-532.

[19] Chu, C. P., Lee, D. J., and Tay, J. H. 2005. Floc model and intrafloc flow, *Chemical Engineering Science*, 60, 565-575.

[20] Churchman, G. J., Gates, W. P., Theng, B. K. G., and Yuan, G. 2006, Chapter 11.1 Clays and Clay Minerals for Pollution Control, in Developments in Clay Science, edited by B. K. G. T. Faïza Bergaya and L. Gerhard, pp. 625-675, Elsevier.

[21] Collins, M. R., Amy, G. L., and Steelink, C. 1986. Molecular-weight distribution, carboxylic acidity, and humic substances content of aquatic organic matter: implications for removal during water-treatment, *Environ. Sci. Technol.*, 20, 1028-1032.

[22] Costanzo, P. M. 2001. Baseline studies of The Clay Minerals Society Source Clays: Introduction, *Clay Clay Min.*, 49, 372-373.

[23] Crowley, M. S., and Welch, A. P. 1954. Clay-particle dispersion by ultrasons, *Journal of The American Ceramic Society*, 37 433-439.

[24] Czurda, K. 2006, Chapter 11.3 Clay Liners and Waste Disposal, in Developments in Clay Science, edited by B. K. G. T. Faïza Bergaya and L. Gerhard, pp. 693-701, Elsevier.

[25] D422-63, A. S. 2007, Standard test method for particle-size analysis of soils, edited, ASTM International, West Conshohocken, PA.

[26] Deboer, G. B. J., Deweerd, C., Thoenes, D., and Goossens, H. W. J. 1987. Laser diffraction spectrometry: Fraunhofer diffraction versus Mie scattering, *Particle Characterization*, 4, 14-19.

[27] Decho, A. W. 2000. Microbial biofilms in intertidal systems: an overview, *Continental Shelf Research*, 20, 1257-1273.

[28] Decho, A. W., and Kawaguchi, T. 1999. Confocal imaging of in situ natural microbial communities and their extracellular polymeric secretions using Nanoplast (R) resin, *Biotechniques*, 27, 1246-1252.

[29] Decho, A. W., Kawaguchi, T., Allison, M. A., Louchard, E. M., Reid, R. P., Stephens, F. C., Voss, K. J., Wheatcroft, R. A., and Taylor, B. B. 2003. Sediment properties influencing upwelling spectral reflectance signatures: The "biofilm gel effect", *Limnology and Oceanography*, 48, 431-443.

[30] Dontsova, K. M., and Bigham, J. M. 2005. Anionic polysaccharide sorption by clay mineras, *Soil Science Society of America Journal* 69, 1026-1035.

[31] Douillard, J. M., and Salles, F. 2004, Phenomenology of water adsorption at clay surfaces, in Interface Science and Technology, edited by W. Fernando and S. Kestur Gundappa, pp. 118-152, Elsevier.

[32] Droppo, I. G., Leppard, G. G., Flannigan, D. T., and Liss, S. N. 1997. The freshwater floc: A functional relationship of water and organic and inorganic floc constituents affecting suspended sediment properties, *Water Air Soil Pollut.*, 99, 43-53.

[33] Du, J., Pushkarova, R. A., and Smart, R. S. C. 2009. A cryo-SEM study of aggregate and floc structure changes during clay settling and raking processes, *International Journal of Mineral Processing*, 93, 66-72.

[34] Erzan, A., and Gungor, N. 1995. Fractal geometry and size distribution of clay particles, *J. Colloid Interface Sci.*, 176, 301-307.

[35] Fabricius, K. E., Wild, C., Wolanski, E., and Abele, D. 2003. Effects of transparent exopolymer particles and muddy terrigenous sediments on the survival of hard coral recruits, *Estuar. Coast. Shelf Sci.*, 57, 613-621.

[36] Foster, M. 1995. The relation between composition and swelling in clay, *Clay Clay Min.*, 3, 205-220.

[37] Gaudette, H. E., GEades, J. L., and Grim, R. E. 1966. The nature of illite, *Clays and Clay Minerals 13th Conference*33-48.

[38] Gerbersdorf, S., Westrich, B., and Paterson, D. 2009. Microbial extracellular polymeric substances (EPS) in fresh water sediments, *Microbial Ecology*, 58, 334-349.

[39] Goldberg, S., Forster, H. S., and Godfrey, C. L. 1996. Molybdenum adsorption on oxides, clay minerals, and soils, *Soil Science Society of America Journal*, 60, 425-432.

[40] Gregory, J. 1988. Polymer adsorption and flocculation in sheared suspensions, *Colloids and Surfaces*, 31, 231-253.

[41] Guggenheim, S., and Martin, R. T. 1995. Definition of clay and clay mineral - Joint report of the AIPEA nomenclature and CMS nomenclature committees, *Clay Clay Min.*, 43, 255-256.

[42] Gupta, B. S., and Ako, J. E. 2005. Application of guar gum as a flocculant aid in food processing and potable water treatment, *European Food Research and Technology*, 221, 746-751.

[43] Güven, N. (Ed.) 1992, Molecular aspects of clay-water itneractions, Clay Minerals Society.

[44] Harris, R. H., and Mitchell, R. 1973. Role of Polymers in Microbial Aggregation, *Annual Review of Microbiology*, 27, 27-50.

[45] Harvey, C. C., and Murray, H. H. 1997. Industrial clays in the 21st century: A perspective of exploration, technology and utilization, *Applied Clay Science*, 11, 285-310.

[46] Helmy, A. K. 1998. The limited swelling of montmorillonite, *J Colloid Interface Sci*, 207, 128-129.

[47] Hill, P. S. 1998. Controls on floc size in the sea, *Oceanography* 11, 13-18.

[48] Hirst, C. N., Cyr, H., and Jordan, I. A. 2003. Distribution of exopolymeric substances in the littoral sediments of an oligotrophic lake, *Microbial Ecology*, 46, 22-32.

[49] Hower, J., and Mowatt, T. C. 1966. The mineralogy of illites and mixed-layer illite/montmorilonites, *American Mineralogist*, 51, 825-854.

[50] Huang, H. N. 1993. Porosity-size relationship of drilling mud flocs - Fractal structure, *Clay Clay Min.*, 41, 373-379.

[51] Ian W, S. 1994. Structure-function relationships in microbial exopolysaccharides, *Biotechnology Advances*, 12, 393-448.

[52] Israelachvili, J. N. 2007, Intermolecular and surface forces, 2nd ed., Elsevier Academic Press.

[53] J. Tolhursf, T., Gust, G., and M. Paterson, D. 2002, The influence of an extracellular polymeric substance (EPS) on cohesive sediment stability, in Proceedings in Marine Science, edited by C. W. Johan and K. Cees, pp. 409-425, Elsevier.

[54] Jarvis, P., Jefferson, B., and Parsons, S. A. 2005a. Breakage, regrowth, and fractal mature of natural organic matter flocs, *Environ. Sci. Technol.*, 39, 2307-2314.

[55] Jarvis, P., Jefferson, B., Gregory, J., and Parsons, S. A. 2005b. A review of floc strength and breakage, *Water Research*, 39, 3121-3137.

[56] Johnson, C. P., Li, X. Y., and Logan, B. E. 1996. Settling velocities of fractal aggregates, *Environ. Sci. Technol.*, 30, 1911-1918.

[57] Kiliaris, P., and Papaspyrides, C. D. 2010. Polymer/layered silicate (clay) nanocomposites: An overview of flame retardancy, *Prog. Polym. Sci.*, 35, 902-958.

[58] Kim, J., Furukawa, Y., Curry, K. J., and Bennett, R. H. 2012. Role of chitin in montmorillonite fabric: transmission electron microscope observations, *Clay Clay Min.*, 60, 89-98.

[59] Kinter, E. B., and Diamond, S. 1958. Gravimetric determination of monolayer glycerol complexes of clay minerals, *Clay Clay Min.*, 5, 318-333.

[60] Kobayashi, M., Adachi, Y., and Ooi, S. 1999. Breakup of fractal flocs in a turbulent flow, *Langmuir*, 15, 4351-4356.

[61] Kranenburg, C. 1994. The fractal structure of cohesive sediment aggregates, *Estuar. Coast. Shelf Sci.*, 39, 451-460.

[62] Kumar, M. 2000. A review of chitin and chitosan applications, *Reactive & Functional Polymers*, 46, 1-27.

[63] Lagaly, G. 2006, Chapter 5 Colloid Clay Science, in Developments in Clay Science, edited by B. K. G. T. Faïza Bergaya and L. Gerhard, pp. 141-245, Elsevier.

[64] Lagaly, G., and Ziesmer, S. 2003. Colloid chemistry of clay minerals: the coagulation of montmorillonite dispersions, *Advances in Colloid and Interface Science*, 100, 105-128.

[65] Likos, W. J., and Lu, N. 2001. A laser technique to quantify the size, porosity, and density of clay clusters during sedimentation, *Geotech. Test. J.*, 24, 83-91.

[66] Lintern, G., and Sills, G. 2006. Techniques for automated measurement of floc properties, *Journal of Sedimentary Research*, 76, 1183-1195.

[67] Loch, R. J. 2001. Settling velocity – a new approach to assessing soil and sediment properties, *Computers and Electronics in Agriculture*, 31, 305-316.

[68] Meissner, T., and Wentz, F. J. 2004. The complex dielectric constant of pure and sea water from microwave satellite observations, *Ieee Transactions on Geoscience and Remote Sensing*, 42, 1836-1849.

[69] Michot, L. J., and Villiéras, F. 2006, Chapter 12.9 Surface Area and Porosity, in Developments in Clay Science, edited by B. K. G. T. Faïza Bergaya and L. Gerhard, pp. 965-978, Elsevier.

[70] Miranda-Trevino, J. C., and Coles, C. A. 2003. Kaolinite properties, structure and influence of metal retention on pH, *Applied Clay Science*, 23, 133-139.

[71] Miyahara, K., Adachi, Y., Nakaishi, K., and Ohtsubo, M. 2002. Settling velocity of a sodium montmorillonite floc under high ionic strength, *Colloids and Surfaces a-Physicochemical and Engineering Aspects*, 196, 87-91.

[72] Moll, W. F. 1973. Source Clay Minerals Project, *Clay Clay Min.*, 21, 71-73.

[73] Molobela, I. P., and Ilunga, F. M. 2012. Impact of bacterial biofilms: the importance of quantitative biofilm studies, *Annals of Microbiology*, 62, 461-467.

[74] Murray, H. H. 1999. Applied clay mineralogy today and tomorrow, *Clay Minerals*, 34, 39-49.

[75] Murray, H. H. 2000. Traditional and new applications for kaolin, smectite, and palygorskite: A general overview, *Applied Clay Science*, 17, 207-221.

[76] Nir, S., El Nahhal, Y., Undabeytia, T., Rytwo, G., Polubesova, T., Mishael, Y., Rabinovitz, U., and Rubin, B. 2006, Chapter 11.2 Clays and Pesticides, in Developments in Clay Science, edited by B. K. G. T. Faïza Bergaya and L. Gerhard, pp. 677-691, Elsevier.

[77] Nugent, R. A., Zhang, G., and Gambrell, R. P. 2009. Effect of exopolymers an the liquid limit of clays and Its engineering implications, *Transportation Research Record*34-43.

[78] Olejnik, S., Posner, A. M., and Quirk, J. P. 1974. Swelling of montmorillonite in polar organic liquids, *Clay Clay Min.*, 22, 361-365.

[79] Pavlidou, S., and Papaspyrides, C. D. 2008. A review on polymer-layered silicate nanocomposites, *Prog. Polym. Sci.*, 33, 1119-1198.

[80] Posner, A. M., and Quirk, J. P. 1964. Changes in basal spacing of montmorillonite in electrolyte solutions, *Journal of Colloid Science*, 19, 798-&.

[81] Pruett, R. J., and Webb, H. L. 1993. Sampling and analysis of KGa-1b well-crystallized kaolin source clay, *Clay Clay Min.*, 41, 514-519.

[82] Pusch, R. 2006, Chapter 11.4 Clays and Nuclear Waste Management, in Developments in Clay Science, edited by B. K. G. T. Faïza Bergaya and L. Gerhard, pp. 703-716, Elsevier.

[83] Risica, D., Dentini, M., and Crescenzi, V. 2005. Guar gum methyl ethers - Part I. Synthesis and macromolecular characterization, *Polymer*, 46, 12247-12255.

[84] Sashiwa, H., and Aiba, S. I. 2004. Chemically modified chitin and chitosan as biomaterials, *Prog. Polym. Sci.*, 29, 887-908.

[85] Schroth, B. K., and Sposito, G. 1997. Surface charge properties of kaolinite, *Clay Clay Min.*, 45, 85-91.

[86] Segad, M., Jonsson, B., Akesson, T., and Cabane, B. 2010. Ca/Na montmorillonite: structure, forces and swelling properties, *Langmuir*, 26, 5782-5790.

[87] Sposito, G., and Prost, R. 1982. Structure of water adsorbed on smectites, *Chemical Reviews*, 82, 553-573.

[88] Sposito, G., Skipper, N. T., Sutton, R., Park, S. H., Soper, A. K., and Greathouse, J. A. 1999. Surface geochemistry of the clay minerals, *Proceedings of the National Academy of Sciences of the United States of America*, 96, 3358-3364.

[89] Stogryn, A. 1971. Equations for calculating the dielectric constant of saline water, *Microwave Theory and Techniques, IEEE Transactions on*, 19, 733-736.

[90] Theng, B. K. G. 1970. Interactions of Clay Minerals With Organic Polymers - Some Practical Applications, *Clay Clay Min.*, 18, 357-&.

[91] Theng, B. K. G. 1982. Clay-polymer Interactions - Summary and perspectives, *Clay Clay Min.*, 30, 1-10.

[92] Theng, B. K. G. 2012a, Chapter 1 - The Clay Minerals, in Developments in Clay Science, edited by B. K. G. Theng, pp. 3-45, Elsevier.

[93] Theng, B. K. G. 2012b, Chapter 2 - Polymer Behaviour at Clay and Solid Surfaces, in Developments in Clay Science, edited by B. K. G. Theng, pp. 47-75, Elsevier.

[94] Theng, B. K. G. 2012c, Chapter 11 - Polysaccharides, in Developments in Clay Science, edited by B. K. G. Theng, pp. 351-390, Elsevier.

[95] Walling, D. E., and Moorehead, P. W. 1989. The particle size characteristics of fluvial suspended sediment: an overview., *Hydrobiologia*, 176/177, 125-149.

[96] Wu, W. J. 2001. Baseline studies of the Clay Minerals Society Source Clays: Colloid and surface phenomena, *Clay Clay Min.*, 49, 446-452.

[97] Yokoi, H., Shiraki, M., Hirose, J., Hayashi, S., and Takasaki, Y. 1996. Flocculation properties of xanthan produced by Xanthomonas campestris, *Biotechnol. Tech.*, 10, 789-792.

[98] Yokoi, H., Yoshida, T., Hirose, J., Hayashi, S., and Takasaki, Y. 1998. Biopolymer flocculant produced by an Pseudomonas sp., *Biotechnol. Tech.*, 12, 511-514.

[99] Zbik, M., and Smart, R. S. C. 1998. Nanomorphology of kaolinies: comparative SEM and AFM studies, *Clay Clay Min.*, 46, 153-160.

[100] Zhang, G., Germaine, J. T., and Whittle, A. J. 2005. An evaluation of the mechanical and chemical dispersion methods for a tropical old alluvium, *Geotech. Test. J.*, 28, 123-132.

[101] Zhang, G., Germaine, J. T., Whittle, A. J., and Ladd, C. C. 2004a. Soil structure of a highly weathered old alluvium, *Géotechnique*, 54, 453-466.

[102] Zhang, G., Germaine, J. T., Whittle, A. J., and Ladd, C. C. 2004b. Index properties of a highly weathered old alluvium, *Géotechnique*, 54, 441-451.

CHAPTER 3 EVALUATION OF THE PARTICLE SIZES OF FOUR CLAY MINERALS

3.1 Introduction

Clay minerals are the major constituents of dispersed sediments, cohesive soils, and fine-grained rocks. As a naturally occurring geomaterial, clay minerals are also one of the most important mineral resources used in many industrial and domestic applications. The particle size or size distribution of clay minerals is a key parameter for mineral identification and soil's engineering classification, as well as understanding a soil's mechanical, physical, and chemical properties that are in turn of critical importance for many environmental processes and industrial applications, such as water quality monitoring, environmental abatement, sediment transport, oil well drilling, clay-polymer nanocomposites, and nanoclay catalysts (*Anderson et al.*, 2010; *Harvey and Murray*, 1997; *Hill*, 1998; *Kiliaris and Papaspyrides*, 2010; *Murray*, 1999; *Pavlidou and Papaspyrides*, 2008; *Walling and Moorehead*, 1989; *Marek. Zbik and Smart*, 1998). In addition, particle size affects a soil's hydraulic conductivity and moisture retention capability (*Daoud and Robert*, 1992) and dye and clay interactions (*Neumann et al.*, 2002).

However, owing to their micrometer to sub-micrometer sizes, determination and evaluation of clay minerals' particle size distributions (PSD) are difficult and hence not routinely performed in most engineering or industrial practices. For example, according to the ASTM Standards (*ASTM*, 2007), PSD is a very important parameter for soil classification, yet no further effort is required to characterize PSD for the <2 μm fraction. As a result, all particles in this fraction are collectively treated as clays without further differentiating their sizes (e.g., submicrometer vs. micrometer). On the other hand, some well-crystallized clay minerals (e.g., kaolinite) may have relatively large, >2 μm particles. Although these particles are truly clay minerals having chemically active surfaces, they may be counted toward the silt-sized fraction, which may yield misleading soil classification and lead to inappropriate perception on soils' physico-chemical properties.

The majority of existing techniques for PSD measurements require preparing an ideally or appropriately dispersed clay mineral dispersion, mostly in water. A few issues arise from this sample preparation process. The first one is interactions between clay mineral and water, including the formation of electrical double layer on charged clay surfaces, adsorbed cation hydration, and intercalation of water into expandable clay minerals. Of these interactions, water intercalation in swelling clay minerals can cause an initial increase in particle thickness, which then may result in an increase or decrease in size, depending on the types of interlayer cations or degree of swelling and other environmental conditions, as discussed below; The second one is stability of the suspension. An unstable clay mineral dispersion can lead to particle aggregation, resulting in coarser PSD; The third one is the use of chemical dispersants to obtain stable clay mineral dispersions (i.e., no flocculation or aggregation). Owing to clay minerals' cation or anion exchange capability, the cations or anions from dissolved dispersants may change clay minerals' properties and hence alter their PSD. For example, a Ca-smectite may be partially or completely converted via cation exchange to a Na^+-smectite if a Na^+-based dispersant is used. After the conversion, because Na^+ has a stronger hydration tendency than Ca^{2+}, the Na^+-smectite can swell to a higher degree such that its interlayer spacing can theoretically increase to infinity, leading to

the formation of exfoliated individual 2:1 layers as separate particles. In contrast, Ca-smectite or smectites with other divalent interlayer cations (e.g., Mg^{2+}) have limited swelling due to both the van der Waals and electrostatic attractions between interlayer cations and negatively charged 2:1 layers (*Helmy*, 1998; *Segad et al.*, 2010). Therefore, swelling may result in either an increase in particle size via water intercalation or decrease by exfoliation.

For clay minerals with variable PSD, another concern arises with the definition and determination of truly representative primary particles. According to the literature, primary particles usually refer to physically solid, homogeneous, individual particles without aggregation (*G Zhang et al.*, 2005). For swelling clay minerals, primary particles are the physically coherent stacks of parallel, equally spaced clay platelets (*Güven*, 1992). Therefore, primary particles are intrinsic or inherent to the material, and their sizes should not be affected by different sample preparation techniques.

It is worth noting further the importance of appropriate dispersion of dispersed clay mineral particles for PSD analysis. Due to crystal imperfections and isomorphous substitutions, most clay mineral particles possess net negative charges on face surfaces, which are balanced by adsorbed and/or interlayer cations (e.g., Na^{+}, K^{+}, Ca^{2+}). The broken bonds on edge surfaces result in pH dependent charges (e.g., positive if pH is <7). As such, electrostatic forces together with other interactions, such as van der Waals attraction and double layer repulsion, between dispersed clay mineral particles usually lead to aggregation. Therefore, a clay mineral dispersion is a very complex system that contains both individual clay mineral particles and most likely clay mineral aggregates. Together with other unique features of clay mineral particles, such as irregular shapes, flexible layers, and heterogeneous layer charges, clay minerals usually exhibit a wide range of particle sizes even in pure water under a stable equilibrium condition (*Lagaly and Ziesmer*, 2003; *Murray*, 2000; *Wu*, 2001).

Both mechanical and chemical methods can be used to facilitate dispersion or disaggregation of clay mineral suspensions (*G Zhang et al.*, 2005). The former usually involves the application of mechanical energy to breakdown and separate aggregated particles, such as ultrasound disruption, flow-induced shearing in a high-speed stirrer, while the latter refers to the use of dispersants to remove or eliminate the physical cementation or chemical bonds holding particles together (Zhang *et al*., 2004, 2005). Therefore, accurate measurement of intrinsic PSD largely depends on the effectiveness of the employed dispersion methods to separate clay mineral aggregates or flocs and then keep them stable at their primary particles (*Crowley and Welch*, 1954). This may also require a continuous dispersion process to maintain the clay mineral dispersion at a completely dispersed, equilibrated state even during measurement. With the development of some new instruments (e.g., laser diffraction based particle size analyzers), the size of clay mineral particles and their size distribution can be accurately and quickly measured (*de Boer et al.*, 1987) when a clay mineral dispersion is continuously circulated. Additionally, different dispersion methods, either chemical or mechanical or both, in different solvents (e.g., air, water, or a less polar liquid) can be employed for PSD measurements.

This chapter presents an experimental study to evaluate the PSD of four source clay minerals, kaolinite, illite, Na^{+}-montmorillonite (Na^{+}-Mt), and Ca^{2+}-montmorillonite (Ca^{2+}-Mt),, which are abundant in natural soils and are representative of four major species of clay minerals with distinctly different behavior. Kaolinite and illite are non-swelling 1:1 and 2:1 minerals,

respectively, while the two montmorillonites are swelling 2:1 minerals but with different interlayer cations. The objectives of this chapter are three-fold: (1) to investigate the effect of different dispersion methods on the PSD of different clay minerals, (2) to evaluate the PSD variability of different clay minerals, and (3) to obtain systematical reference data on the intrinsic PSD of these representative clay minerals. The findings are expectedly of interest to primarily geotechnical engineers and secondarily researchers who study or use clay minerals for different industrial applications or environmental processes.

3.2 Experimental

3.2.1 Materials

Four high-purity clay minerals, kaolinite (KGa-1b), illite (IMt-1), Ca^{2+}-montmorillonite (STx-1b), and Na^{+}-montmorillonite (SWy-2), which have been well analyzed and widely used by many studies as reference clay minerals, were purchased from the US Clay Minerals Society Source Clay Repository (*Chipera and Bish*, 2001; *Costanzo*, 2001; *Hower and Mowatt*, 1966; *Pruett and Webb*, 1993). Their geographic origins and basic properties are summarized in Table 3.1. Kaolinite and two montmorillonites were supplied as dry powder, which had been pre-processed by wet-sieving through a #325 mesh to remove the >44 μm fractions before shipping to users (*Pruett and Webb*, 1993). These three "*as-received*" dry powdery clay minerals were directly used without further treatment. The "*as-shipped*" illite sample consisted of small rock chips. To obtain powdery illite, the sample was first hand ground by a mortar and pestle and then wet ground with ethyl alcohol using a McCrone micronizing mill (McCrone Accessories & Components, Westmont, IL, USA) for 3 mins, which typically results in a fine powder with ≤38 μm particles for most silicate minerals. To identify clay minerals and impurities, the processed powdery illite was side-packed into a sample holder and analyzed by X-ray diffraction (XRD) using a Bruker/Siemens D5000 automated powder diffractometer using a Cu *K*α radiation at 40 kV and 30 mA with a scan range of 2-40° 2θ, a scan speed of 0.02° 2θ per 2 sec, and a step size of 0.02° 2θ. The XRD pattern validates illite as the major clay mineral phase and trace quartz as an impurity (Figure 3.1).

3.2.2 Preparation of Clay Mineral Dispersions

PSD measurements require the preparation of clay mineral dispersions either in air or liquid. Table 3.2 summarizes the different methods employed to prepare clay mineral dispersions. Details for each method are also provided as follows:

- I-A: To obtain the <2 μm fractions and hence their PSD, 0.2 g dry powder was first dispersed in 80 mL deionized (DI) water by using a Sonic Dismembrator Model 300 probe-type ultrasonic disruptor (Fisher Scientific, Pittsburgh, PA, USA) for 15 mins, followed by diluting with DI water to 1000 mL in a beaker. The resulting dispersion was allowed to settle for 3.5 hrs. The upper 5 cm supernatant was extracted as the dispersion for subsequent PSD measurement.

- I-B: To investigate the necessity of "*overnight soaking*" or "*pre-equilibrating with water*" that is usually required for sample preparation and hence its influence on PSD, 0.2 g dry clay mineral was used directly to prepare a dispersion and pre-soaked overnight (i.e., >16 hrs) before preparing a clay mineral dispersion.

Table 3.1 Origins and basic properties of the four clay minerals[a].

Name	Origin	CEC (meq/100g)	Layer charge[b] (unbalanced charge)		SSA (m^2/g)	pH[c]	Chemical formula
			T	O			
Kaolinite (KGa-1b)	Washington County, Georgia	2.00	-0.06 (0)		10.05	5.97	$(Mg_{.02}Ca_{.01}Na_{.01}K_{.01})$ $\{Al_{3.86}\ Fe^{3+}_{.02}Mn_{tr}Ti_{.11}\}$ $\{Si_{3.83}\ Al_{.17}\}O_{10}(OH)_8$
			-0.17	+0.11			
Illite (IMt-1)	Silver Hill, Montana	15.00[d]	-1.68 (0)		30.00[e] or 24.9[f]	8.61	$(Mg_{.09}\ Ca_{.06}\ K_{1.37})$ $\{Al_{2.69}Fe^{3+}_{.76}Fe^{2+}_{.06}Mn_{tr}Mg_{.43}Ti_{.06}\}$ $\{Si_{6.77}Al_{1.23}\}O_{20}(OH)_4$
			-1.23	-0.44			
Ca-M (STx-1b)	Gonzales County, Texas	84.40	-0.68 (-0.08)		83.79	7.32	$(Ca_{.27}Na_{.04}K_{.01})$ $\{Al_{2.41}Fe^{3+}_{.09}Mn_{tr}$ $Mg_{.71}Ti_{.03}\}\{Si_{8.00}\}O_{20}(OH)_4$
			0	-0.68			
Na-M (SWy-2)	Crook County, Wyoming	76.40	-0.55 (+0.55)		31.82	6.44	$(Ca_{.12}Na_{.32}K_{.05})$ $\{Al_{3.01}Fe^{3+}_{.41}Mn_{.01}Mg_{.54}$ $Ti_{.02}\}\ \{Si_{7.98}Al_{.02}\}O_{20}(OH)_4$
			-0.53	-0.02			

[a] All data except those noted are taken from the Clay Minerals Society Source Clay Data Sheets.
[b] CEC = cation exchange capacity.
[c] The layer charge is based on per $O_{10}(OH)_8$ for kaolinite and $O_{20}(OH)_4$ for the other three clay minerals; O: charge from octahedral sheet; T: charge from tetrahedral sheets.
[d] SSA = specific surface area.
[e] pH of the suspension at a concentration of 0.4 g/L in deionized water at room temperature (23°C) obtained by a pH meter (Thermo Scientific Orion Star™ Series).
[f] Data from *Hower and Mowatt* (1966), and *Kinter and Diamond* (1958).
[g] Data from *Celis and Koskinen* (1999).
[h] Data from *Goldberg et al.* (1996).

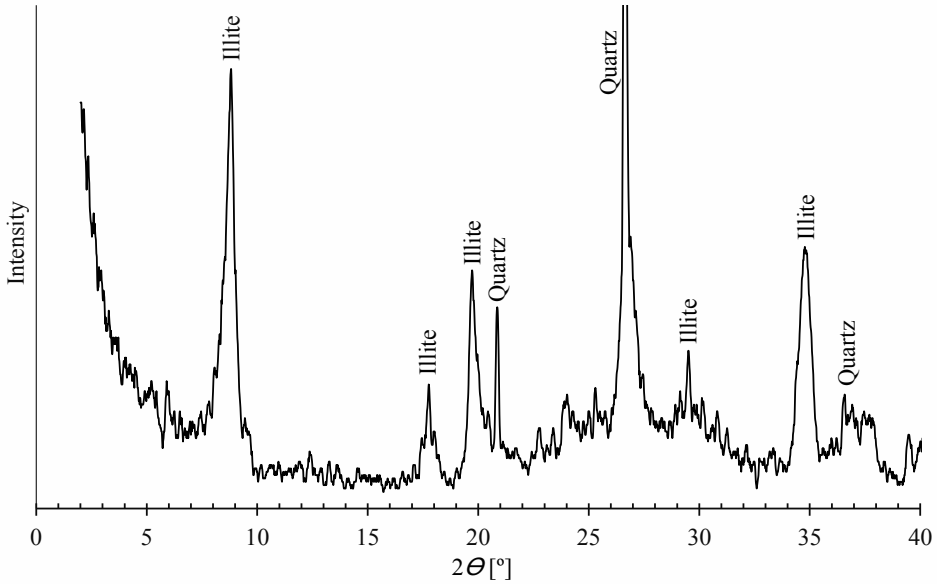

Figure 3.1 X-ray diffraction pattern of the processed illite powdery sample.

- I-C: To evaluate the effectiveness of mechanical disaggregation, 0.2 g overnight pre-soaked clay mineral was dispersed in 80 mL DI water by the aforementioned probe-type ultrasonic disruptor for 15 mins.

- I-D: To evaluate the influence of chemical dispersant, Na-hexametaphosphate (NaHMP; Mallinckrodt Baker Inc., Philipsburg, NJ, USA) solution at a concentration of 40 g/L was used to replace DI water for clay mineral dispersion preparation (*ASTM*, 2007).

- I-E: To investigate the influence of swelling on the PSD of two montmorillonites, ethyl alcohol (EA; 190 Proof, Pharmco-AAPER, Brookfield, CT, USA), a glycerol (EMD Chemicals Inc., Darmstadt, Germany) solution in EA with a 2 vol.% concentration (*Burt*, 2004; *Kinter and Diamond*, 1958), and a glycerol solution in DI water with a 2 vol.% concentration were used as solvents to prepare clay mineral dispersions.

- II: To evaluate the effectiveness of dry dispersion that may avoid the clay mineral-water interactions, four dry clay minerals were also dispersed in and transported by pressurized dry air.

In summary, air, water, EA, NaHMP, and glycerol were used as a dry dispersion medium, polar solvent, less polar solvent, chemical dispersant, and layer expanding agent, respectively, to prepare clay mineral dispersions so that the effectiveness of different dispersion methods can be evaluated.

Table 3.2 Summary of all clay mineral dispersions prepared by different methods.

Method		Sample preparation	Samples	Purpose
I (Liquid mode)	A	Probe-type ultrasound for 15 mins, followed by 3.5 hrs settling	All 4 clay minerals	Obtain the <2 μm fractions
	B	Unsoaking vs. overnight soaking in water	All 4 clay minerals	Investigate the influence of overnight soaking
	C	Probe-type ultrasound for 15 mins	All 4 clay minerals	Evaluate mechanical disaggregation
	D	Disperse in a 40g/L sodium hexametaphosphate solution	All 4 clay minerals	Evaluate a chemical dispersant
	E	3 solvents: EA, 2 vol.% glycerol in EA, and 2 vol.% glycerol in DI water	Only Ca^{2+}-Mt and Na^{2+}-Mt	Investigate the influence of swelling
II (Dry mode)		Dispersed in and transported by pressurized dry air	All 4 clay minerals	Evaluate dry dispersion

3.2.3 Methods

All PSD measurements were conducted in a Cilas® 1190 laser particle size analyzer (PSA) (Cilas Particle Size, Madison, WI, USA) under either wet or dry mode (Figure 3.2). In the wet mode, clay mineral dispersions at a concentration of 0.2 g dry clay mineral in 80 mL solvent prepared by the above methods were transferred to the PSA's liquid bath and then diluted to 500 mL, which is the total volume of the PSA's closed-loop liquid circulation system (including the liquid bath and circulation tubes), followed by running a built-in ultrasound disperser beneath the liquid bath for 1.0 min to achieve better dispersion. To prevent unnecessary flocculation and settling, all clay mineral dispersions were continuously agitated by a pedal-like stirrer located in the middle of the liquid bath at a constant speed of 180 rpm and continuously circulated in the PSA's circulation system by a peristaltic pump at a constant speed of 30 rpm, while the PSD was continuously monitored by three laser beams. The pump resulted in an average flow velocity of 0.15 m/s and a Reynolds number of ~1091, which indicates one-dimensional laminar flow inside the circulation tubes. Sufficient time (usually 15-20 mins) was allowed for the circulating dispersions to reach a steady state (i.e., no further significant change in the measured PSD even for prolonged circulation). After validating an equilibrated state, PSD measurement was then conducted. Selective images of particles were also taken using a 3032 series preconfigured, inverted microscope (Accu-Scope® Inc., Commack, NY, USA) that is externally connected to the PSA's liquid circulation system.

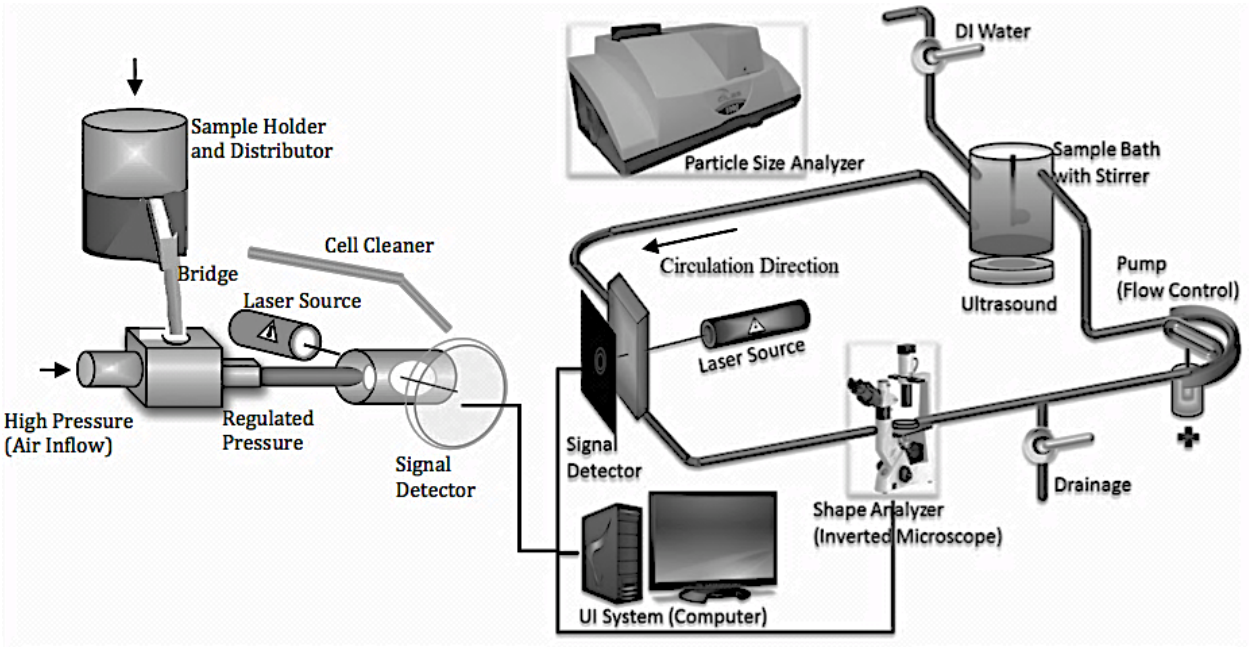

Figure 3.2 Schematic diagram showing the dry mode system (left) and liquid dispersion and circulation system with an inverted microscope for particle imaging (right) of the Cilas PSA.

In the dry mode, dry powdery samples were placed in a vibrating mass distributor and then transported and dispersed by pressurized dry air. Table 3.3 summarizes the optimal dispersing parameters (determined by trial and error) used for the four clay minerals, including vibration frequency, vibration ratio, and air pressure.

Table 3.3 Parameters of dry mode dispersion for the four clay minerals.

Sample	Mass of sample per measurement (g)	Obscuration rate	Vibration frequency (Hz)	Cyclic ratio of vibration	Air pressure (mbar)
Kaolinite	1.8	18%	50	40%	400
Illite	1.0	14%	50	35%	350
Ca^{2+}-Mt	2.0	16%	50	40%	500
Na^{2+}-Mt	3.0	14%	50	40%	400

For both modes, the laser diffraction data was analyzed using the Lorenz-Mie theory, which is an exact description of the diffraction field. This theory is more accurate than the Fraunhofer theory (an approximation of Lorenz-Mie theory) for PSD characterization of clay minerals, especially when the sizes are close to the laser wave length of 635-830 nm (*de Boer et al.*, 1987). Particle size obtained by the PSA was defined as the diameter of equivalent spheres calculated based on the volume moment mean value of multiple particles at a given size range. That is:

$$D = \frac{\sum n l^4}{\sum n l^3} \qquad \text{Equation 3.1}$$

where D is the mean diameter of all particles or flocs within a given size range, n the number of particles of a fixed size in the considered size range, and l the diameter of a particle or floc.

3.3 Results and Discussion

3.3.1 PSD of the <2 μm Fractions

The PSD curves of the <2 μm fractions (Figure 3.3) show that their particle size ranges from 0.04 (the smallest particle size that the PSA can detect) to ~4 μm and more than 90-95% (by number) particles are <2 μm. This is consistent with the purpose of ultrasound disaggregation and subsequent settling (or fractionation) used to disperse clay mineral flocs and remove impurities (e.g., quartz), which typically leaves only the <2 μm individual clay mineral particles in the supernatant (*Chipera and Bish*, 2001; *Chipera et al.*, 1993; *Furukawa et al.*, 2009; *Moore and Reynolds*, 1997). In fact, this also serves as an indirect and partial calibration of the accuracy of the PSA.

Of the four clay minerals, kaolinite and illite exhibit a trimodal lognormal distribution with the local maxima at 0.075, 0.3, and 1.2 μm (Figure 3.3b). The first one at ~0.075 μm is extremely small with only 10-15% particles finer than this value. It may be caused by the very small number of measurements on edge surface, and thus this value may represent particle thickness. The other two maxima represent the true basal plane dimensions of kaolinite and illite, resulting in two aspect ratios of 16 and 4 for both clay minerals. Other studies reported that this kaolinite has an aspect ratio of ~10 (*M. Zbik and Smart*, 2002) with an average of 5.3 (*M S Zbik*

and Frost, 2009). In addition, other studies (e.g., (*Mackinnon et al.*, 1993)) found that a similar kaolinite has two different sizes, ~0.3 and ~1.2 μm, in its <2 μm fraction. The aspect ratio of this illite has not been reported in the literature, but it can be reasonably assumed to have similar values.

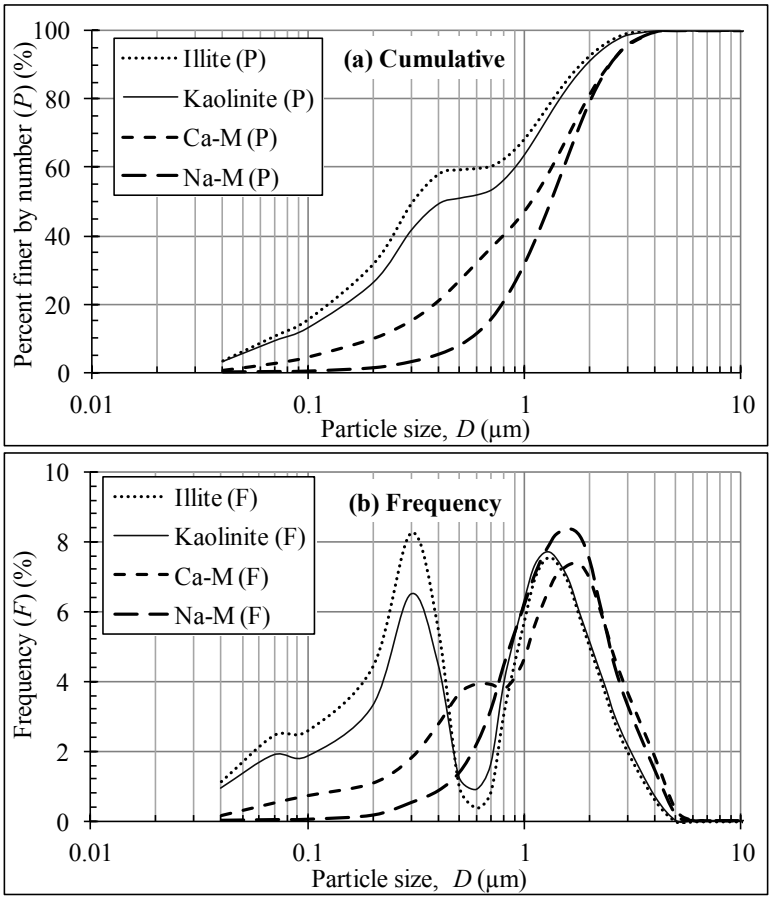

Figure 3.3 PSD curves of the < 2 μm fraction of the four clay minerals.

For the two montmorillonites, Ca^{2+}-Mt exhibits a superposed bimodal lognormal distribution with two maxima at 0.6 and ~1.5 μm, while Na^{+}-M has a monomodal distribution with a maximum at ~1.5 μm. Such different PSD stem from their different chemical compositions and distinct swelling behavior. According to their chemical formulas (Table 3.1), both clay minerals can be regarded as a mixed Ca^{2+}/Na^{+}-montmorillonite, but with different mole ratios of Ca^{2+}/Na^{+} (i.e., 27/4 and 3/8 for the Ca^{2+}-Mt and Na^{+}-Mt, respectively). As reported by (*Laird*, 2006), during swelling in water, cation demixing in montmorillonite occurs so that Na^{+} and Ca^{2+} are separated and relocated into different interlayers. The basal spacing, *d*(001), of Na^{+}-dominated interlayers can swell to >9 nm (*Olejnik et al.*, 1974; *Posner and Quirk*, 1964), while that of Ca^{2+}-dominated interlayers is <1.9 nm (*Theng*, 1982). When mechanically dispersed by a probe-type ultrasound disruptor, the swollen montmorillonite particles readily break apart or exfoliate at the interlayers dominated by Na^{+}, leading to the formation of two types of particles (Figure 3.4): (1) ~1.0 nm thick, Na^{+}-based individual 2:1 layers as single particles and (2) particles with Ca^{2+} as the dominant interlayer cations. The latter are stacks of parallel 2:1 layers (also called tactoids or domains) (*Kleijn and Oster*, 1982; *Quirk and Aylmore*, 1971), which are

relatively stable under shaking, stirring, sonication, and even certain pressure (*Kjellander et al.*, 1988; *Laird*, 2006; *Yariv and Lapides*, 2003). For both Ca^{2+}-Mt and Na^{+}-Mt, the process of 3.5 hr sedimentation can eliminate those relatively large Ca^{2+}-based tactoids (i.e., they readily settle down), resulting in a supernatant containing the relatively smaller tactoids and exfoliated 2:1 layers. As the major particles in the Na^{+}-Mt supernatant, the very thin, flexible, and soft (*Bihannic et al.*, 2001) Na^{+}-based individual 2:1 layers can easily curl in the PSA's circulation system, which yields a monomodal distribution for the Na^{+}-Mt. However, for the Ca^{2+}-Mt, the extracted supernatant may contain both relatively smaller Ca^{2+}-based tactoids and Na^{+}-based individual 2:1 layers (*Lagaly*, 2006), resulting in a bimodal distribution.

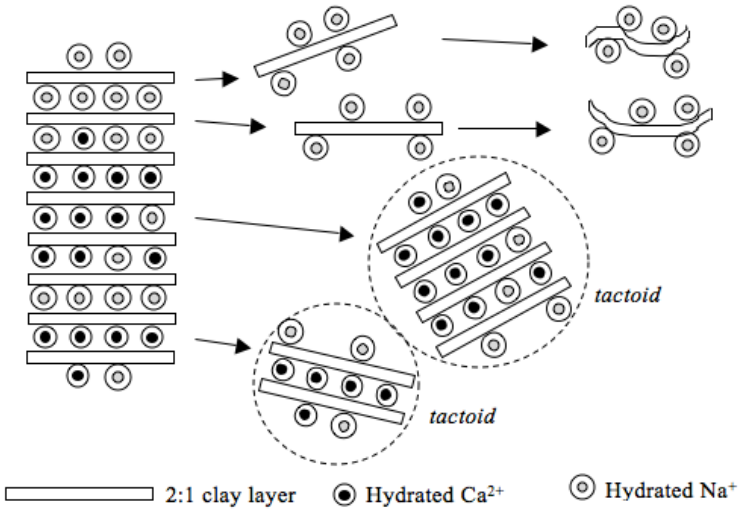

Figure 3.4 Schematic diagram showing the swelling of mixed Ca^{2+}/Na^{+}-montmorillonite in water.

3.3.2 Effect of Overnight Soaking in Water

Figure 3.5 compares the PSD of the DI water-soaked vs. unsoaked samples for the four clay minerals. All curves show a maximum size of 30-60 μm. The two non-swelling clay minerals, kaolinite and illite, exhibit a trimodal distribution with three maxima at 0.3, 1.5-2.5, and 13-20 μm, while the two swelling clay minerals, Ca^{2+}-Mt and Na^{+}-Mt, have a bimodal distribution with local maxima at 2.1-2.5 and 13-16 μm. The PSD value of the soaked kaolinite is in agreement with that of another similar kaolinite (KGa-1) reported by (*Franco et al.*, 2004). For all samples, the two maxima at smaller sizes (e.g., <10 μm) of water-soaked sample (Figure 3.5) are almost at the same locations as those from the <2 μm fractions (Figure 3.3), indicating that they are caused by dispersed, primary clay mineral particles. The third maximum located between 10-20 μm is not observed in the <2 μm fractions. As reported in the literature (*Lee et al.*, 2012), flocculi, the smallest clay mineral-based aggregates of 10-20 μm in size, are relatively strong and hence hardly break down to the lower level primary clay mineral particles (*Vandeven and Hunter*, 1977). In addition, impurities (e.g., quartz) and bulk sample residues may also contribute to this peak (*Pruett and Webb*, 1993). Figures 3.6 a-d show some representative optical microscope images of soaked clay mineral samples. The particle sizes observed from these images are consistent with the above analysis. For instance, Ca^{2+}-Mt has larger flocculi than other samples, while illite has the smallest flocculi.

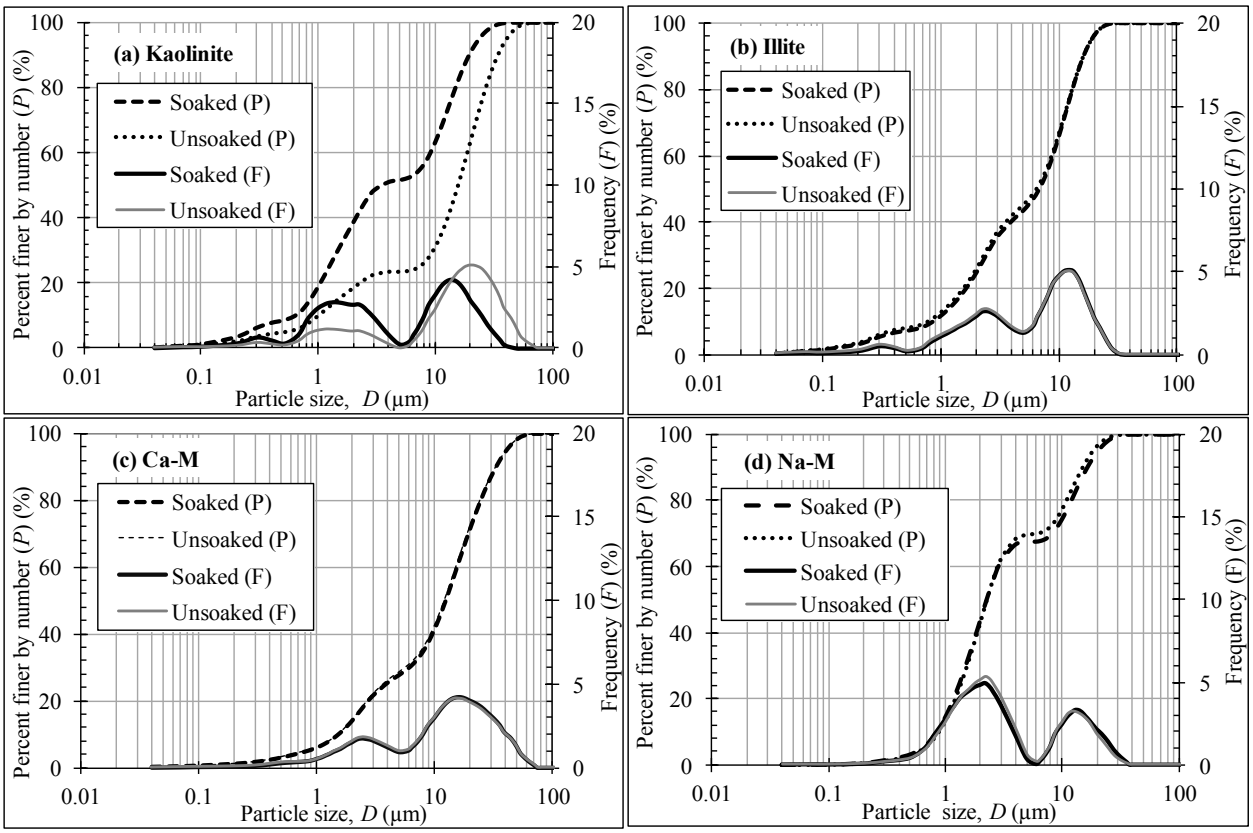

Figure 3.5 Effect of overnight soaking in water on the PSD of the four clay minerals.

Except kaolinite, the PSD of the soaked and un-soaked samples of the other three clay minerals are identical, indicating that the PSD of these three highly charged clay minerals are not sensitive to overnight soaking. For kaolinite, overnight soaking shifts the cumulative PSD curve toward left, or makes the PSD finer, as indicated by the change in the D_{50} from 16 to 4 μm for the unsoaked and soaked samples, respectively. This well-crystallized kaolinite has low defects (*Pruett and Webb*, 1993), with very low but opposite electrical charges of -0.17 and +0.11 in the tetrahedral and octahedral sheets per $O_{10}(OH)_8$, respectively (Table 3.1). The kaolinite dispersion has a measured pH 5.97 (Table 3.1). Under such a slightly acidic condition, the outmost octahedral sheet (as one face surface) exhibits its positive charge, while the outmost tetrahedral sheet (as the other face surface) exhibits its negative charge (*Gupta et al.*, 2011). As such, the electrical field generated by charges on face surfaces is very weak and there is also a weak electrostatic attraction between the octahedral face surface of one particle and the tetrahedral face of the other particle. Therefore, it may take a relatively long time for kaolinite particles to reach a fully hydrated and dispersed state. In contrast, illite, Ca^{2+}-Mt, and Na^{+}-Mt have relatively higher electrical charges of same polarity on face surfaces (Table 3.1), resulting in a stronger electrical field generated by the face surface as well as a stronger electrostatic repulsion between the face surfaces of individual particles. As such, they can hydrate quickly and then reach a fully dispersed or swollen state. In addition, compared with the kaolinite dispersion of the same concentration (e.g., 0.4 g/L), the much higher specific surface area (SSA) of the other three clay minerals renders them a larger surface density (i.e., total surface area per unit volume of dispersion) for particle-particle interactions, which may facilitate a quicker hydration and

dispersion (*Kleijn and Oster*, 1982; *Laird*, 2006; *Quirk and Aylmore*, 1971; *Rengasamy et al.*, 1976).

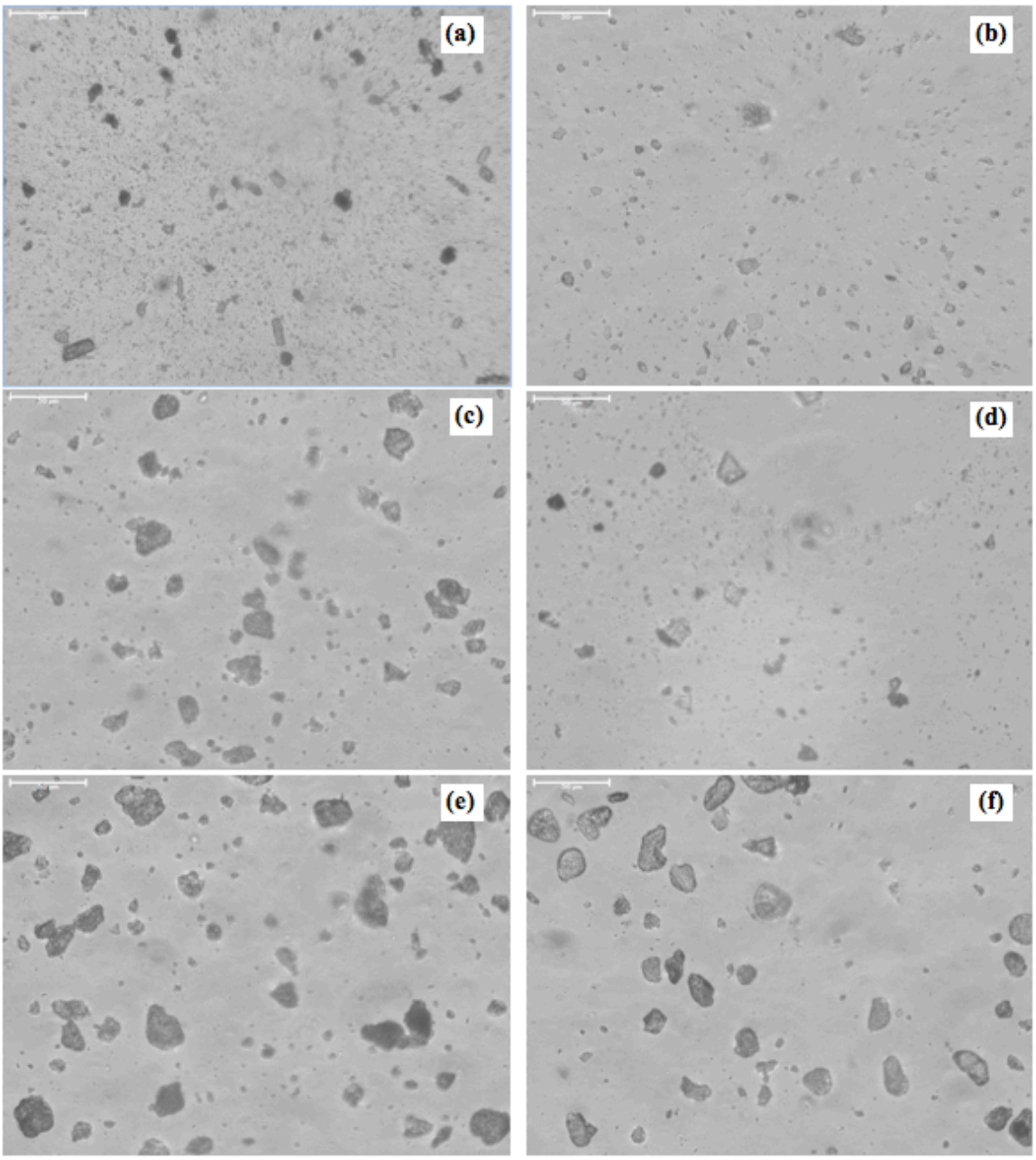

Figure 3.6 Optical microscope images of clay minerals: (a) kaolinite in DI water, (b) illite in DI water, (c) Ca^{2+}-Mt in DI water, (d) Na^{+}-Mt in DI water, (e) Ca^{2+}-Mt in EA, and (f) Na^{+}-Mt in EA (Scale bar: 50 μm).

In summary, although overnight soaking is recommended as a routine step to prepare clay mineral dispersions for particle size analysis, its necessity or influence has rarely been reported. Based on the above analysis, prolonged soaking is necessary for clay minerals with relatively small layer charges, such as kaolinite. Although this step may not be very important for highly charged clay minerals, it is still recommended to perform this step for most PSD measurements.

3.3.3 Effect of dispersion methods

Figure 3.7 shows the PSD of the four clay minerals treated by different dispersion methods, including overnight soaking, NaHMP dispersion, ultrasound (US) dispersion, and dry dispersion in air (Dry). The most striking feature is that, compared with dispersion methods in the liquid mode, the PSD curves obtained in the dry mode lie on the rightmost for all four clay minerals, indicating that much coarser particles or aggregates exist in the air-dispersed samples or, in other words, the samples are not well dispersed. The frequency distribution curves show four major peaks, with the largest one at 40-320 μm. In this mode, pressurized dry air is used as both a solvent for transporting and floating clay mineral particles and a mechanical disaggregation tool, which is hoped to eliminate the influence of complex clay mineral-water interactions on PSD measurements. However, it is known that air-dried clay minerals still contain some water adsorbed from the moisture in air, and hence clay mineral particles can still interact with each other to form aggregates via clay mineral-water interactions (e.g., van der Waals attraction, hydration, capillary, and Coulomb force). In addition, the air-dispersed clay mineral in dry mode is not circulated in a closed-loop system in the PSA, but is quickly transported through the laser measurement window. Therefore, an equilibrium state may not be reached during the measurement. In conclusion, dry dispersion cannot be employed to characterize the PSD of source clay minerals.

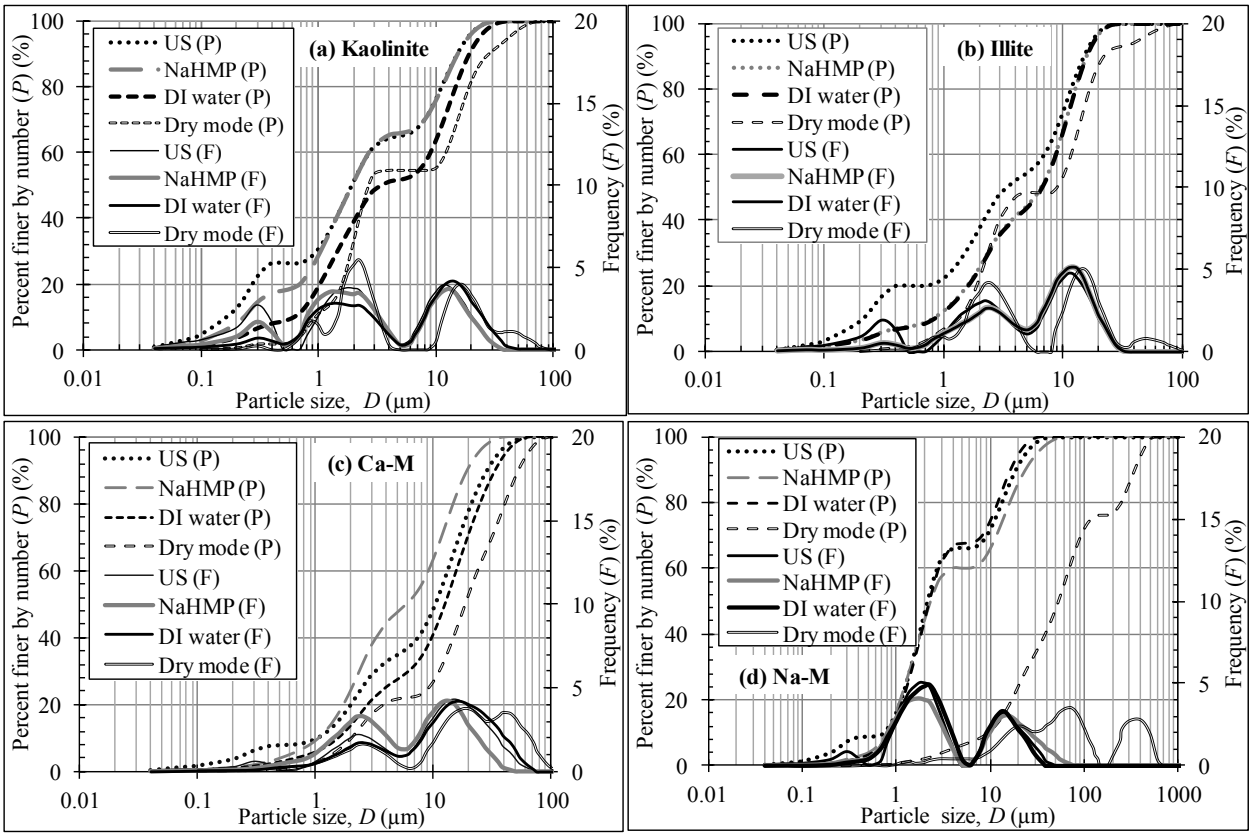

Figure 3.7 PSD curves of the four clay minerals obtained by different dispersion methods.

For other dispersion methods in liquid mode, all four clay minerals show a trimodal, lognormal distribution with a size range of 0.04-50 μm. The three maxima are at 0.3-0.6, ~2, and

~13 μm. Again, the former two represent primary clay mineral particles, while the last is caused by clay mineral flocculi. The effect of chemical dispersion and ultrasound disaggregation on each clay mineral's PSD is further discussed separately below.

3.3.3.1 Kaolinite

Compared with the water-soaked sample, both chemical and mechanical dispersions generate finer PSD, although the latter even results in a higher population of <1 μm particles. This result is consistent with other literature (*Crowley and Welch*, 1954; *Genrich and Bremner*, 1972a; b). As mentioned above, the two face surfaces (i.e., one is the outmost tetrahedral sheet, and the other is the outmost octahedral sheet) with opposite, low charges can generate electrostatic attraction between the basal planes of two different particles, leading to the formation of flocs. Another reason for floc formation is that kaolinite's edge charge is positive at pH <7 (i.e., a pH 5.97 was measured) and the interaction of positively charged edge to negatively charged tetrahedral face can also contribute to flocculation (*Du et al.*, 2010). However, kaolinite has very low layer charges, which means that the electrostatic attraction is not very strong, and hence kaolinite flocs can be dispersed by ultrasonic dispersion. Chemical dispersion by NaHMP is achieved by the edge charge reversal through adsorption of PO_3^-.

3.3.3.2 Illite

The cumulative PSD curve obtained by the ultrasound disaggregation lies in the leftmost, while that by chemical dispersant just overlays with the one of soaked sample (Figure 3.7 b). This suggests that NaHMP dispersion is not effective for illite. Two reasons may possibly contribute to this: (1) illite possesses a very high layer charge (e.g., -1.68 for this sample, Table 3.1) and (2) the amount of used dispersant may not be enough to reverse the edge charges. Therefore, for the highly charged, non-swelling illite, chemical dispersion by NaHMP is not as effective as ultrasound dispersion.

3.3.3.3 Ca^{2+}-Mt

According to the relative locations of the cumulative PSD curves (Figure 3.7 c), chemical dispersion is more effective than ultrasound dispersion, although both methods yield finer particles than soaking. Moreover, ultrasound dispersion generates more <1 μm particles, while chemical dispersion yields more >1 μm particles. The chemical dispersant, NaHMP, may alter the particle sizes in two ways: (1) it can partly reverse the clay mineral's positive edge charges by $(PO_3^-)_6$ and hence reduce the tendency of aggregation via edge-face interactions (*Levy et al.*, 1991) and (2) the added Na^+ can exchange with the interlayer Ca^{2+}, resulting in a change of Ca^{2+}-Mt to Na^+-Mt that can swell further and then exfoliate into smaller particles (as discussed previously). Therefore, adding the dispersant, NaHMP, to Ca^{2+}-Mt may generate misleading PSD results because of the partial conversion of Ca^{2+}-Mt to Na^+-Mt.

3.3.3.4 Na^+-Mt

It appears that either ultrasound dispersion or overnight soaking can yield the finest PSD for Na^+-Mt, although the former can generate more <1 μm particles. Chemical dispersion causes the presence of more >1 μm particles. Therefore, NaHMP is not effective for dispersing this Na^+-

Mt. Similar observations have been reported in the literature. For instance, (*Frenkel et al.*, 1992) stated that NaHMP is less effective in dispersing Na^+-Mt than kaolinite.

Finally, it is noteworthy to further discuss the effectiveness of ultrasonic dispersion. For all four clay minerals, the population of the smallest primary particles (i.e., <1-2 μm) obtained by ultrasound dispersion is the highest of all dispersion methods, indicating that this mechanical disaggregation method helps breakdown clay mineral flocs. Ultrasound dispersion, by creating and fracturing microbubbles in an aqueous medium, results in a sudden energy release, which generates local high temperature, high pressure, and strong shock waves to help disperse, expand, or split clay mineral particles (*Lapides and Yariv*, 2004; *Z P Zhang et al.*, 2010). Thus, the microprobe-type ultrasonication indeed facilitates the swelling and exfoliation of the two montmorillonites. As reported by (*Franco et al.*, 2004), ultrasound can cause both exfoliation and size reduction in other particle dimensions. As such, for the non-swelling kaolinite and illite, and limited swelling Ca^{2+}-Mt, the ultrasound processed samples show a size reduction in all size ranges when compared with their corresponding soaked samples. This reduction can be attributed to either the tactoid delamination (as for Ca^{2+}-Mt) or breakdown of clay mineral particles into smaller sizes (as measured on the basal plane dimension) or both. While the former can occur only in the two montmorillonites, the latter may happen in all four clay minerals.

3.3.4 Effect of Different Solvents for Swelling Clay Minerals

Figure 3.8 shows the PSD of the two montmorillonites dispersed in DI water, EA, a glycerol in DI water solution (Gly-DI), and a glycerol in EA solution (Gly-EA). The PSD obtained from the water-soaked samples are used as a reference for comparison. For all four solvents, both Ca^{2+}-Mt and Na^+-Mt exhibit a bimodal lognormal distribution with a size range of 0.1 to 70 μm and two maxima at ~2.2-2.5 and ~13-15 μm for primary particles and flocculi, respectively. Moreover, the PSD change in Ca^{2+}-Mt caused by different solvents is not as significant as that in Na^+-Mt.

For Ca^{2+}-Mt, although the PSD dependence on the type of solvent is not so significant, some changes in PSD are still discernable. Of the four solvents, the Gly-EA yields the coarsest PSD, while water generates the finest PSD. Also, the Gly-DI yields a coarser PSD than the DI water, and the PSD obtained from the EA is finer than that from Gly-EA, but coarser than that from DI water. The dielectric constant of water, EA, and glycerol at 20-25 °C is 80.3, 24.3, and 42.5, respectively (Table 3.4). If the interlayer of Ca^{2+}-Mt is filled with EA (to replace water), the Coulomb attraction between the interlayer exchangeable cations (i.e., Ca^{2+}) and negatively charged 2:1 layers will be much stronger, thus preventing the Ca^{2+}-Mt from swelling. In fact, neither Ca^{2+}-Mt nor Na^+-Mt swells in pure alcohol (*Brindley et al.*, 1969). For Ca^{2+}-Mt, the difference between the PSD in water and in EA is not significant, even though the clay mineral swells in water but not in pure EA. This can be reasoned by the fact that the increase in particle size caused by swelling in water is counterbalanced by the decrease in particle size caused by exfoliation, which in turn is promoted by the existence of Na^+ in some interlayers (as discussed previously) and flow-induced shearing (causing exfoliation).

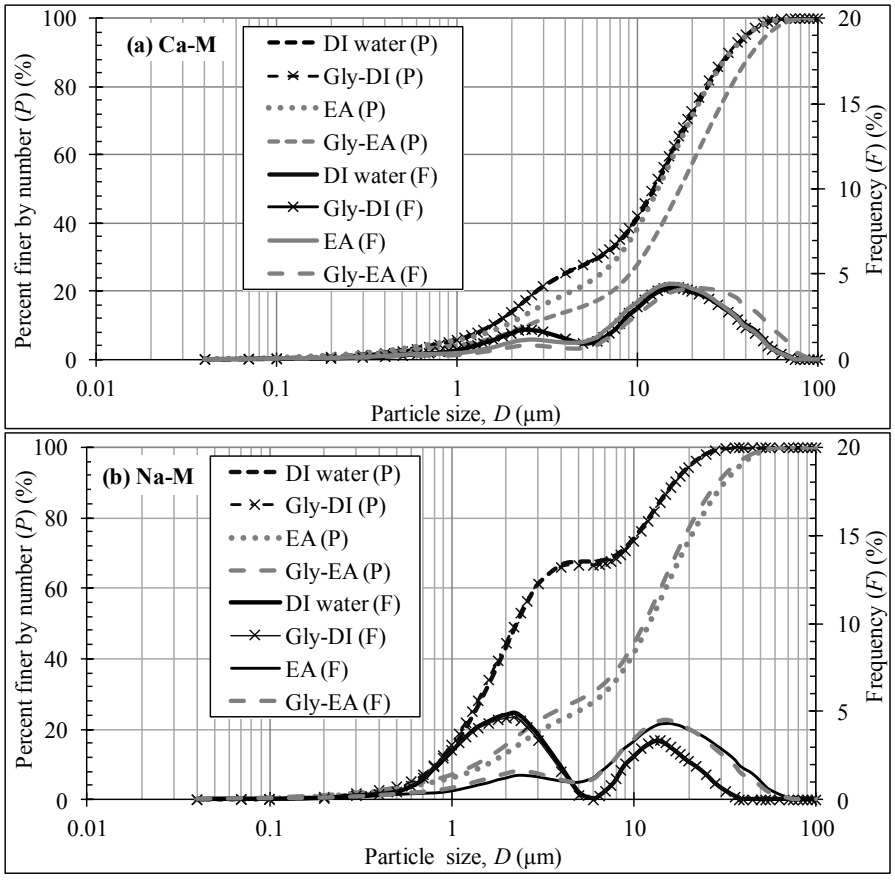

Figure 3.8 PSD curves of two montmorillonites in different dispersion solvents.

Table 3.4 Dielectric constant of different solvents at 25°C.

Solution or solvent	Dielectric constant
Deionized water	80.3
Ethyl alcohol	24.3
Glycerol	42.5
2 vol.% glycerol in deionized water*	79.5
2 vol.% glycerol in ethyl alcohol*	24.7

* Dielectric constant estimated based on a relationship proposed by (*Jouyban et al.*, 2004).

It is also interesting to discuss the influence of glycerol as an expanding agent on PSD (Figure 3.8). Glycerol is completely soluble in water and alcohol. According to (*Kinter and Diamond*, 1958), glycerol molecules can enter the interlayer space of montmorillonite and easily form a stable glycerol complex without heating. The basal spacing *d*(001) for montmorillonite with two layers of glycerol, monolayer of glycerol, and absence of glycerol as its interlayer is 1.84, 1.42, and 0.99 nm, respectively. The partial replacement of water molecules by larger glycerol molecules in the interlayer may further increase repulsive interlayer force (*Brindley et al.*, 1969), which results in an increase in tactoid's basal spacing and hence the particle size. As

shown in Figure 3.8, the Gly-DI slightly increases the size of particles within the size range of ~1-10 μm, but without the change in the mean particle size (D_{50}), when compared with the PSD from DI water. The Gly-EA can further increase the particle sizes, with a change in D_{50} from 12 to 17 μm. In the Gly-EA solvent, montmorillonite's basal spacing increases by intercalating glycerol molecules into its interlayer space, which causes the size increases (i.e., when compared with the DI water as a solvent). Again, due to the smaller dielectric constants of both glycerol and EA, the interlayer attraction force is stronger in the Gly-EA solvent than in water, and hence the swollen montmorillonite particles cannot be easily exfoliated by hydraulic shearing force. Therefore, there are two reasons why the PSD in the Gly-EA is much coarser than in the DI water: (1) particle swelling due to the intercalation of glycerol and (2) less hydraulic shear-induced particle exfoliation.

For Na^+-Mt, the PSD dependence on different solvents is more significant (Figure 3.8 b). The four PSD curves can be separated into two groups: DI water and Gly-DI as the first group, and EA and Gly-EA as the second group. The difference in PSD within each of the two groups is very small. As mentioned above, Na^+-Mt can swell to infinity in water, and hence an individual 2:1 layer is a particle. Moreover, glycerol can be intercalated into Na^+-Mt's interlayers. For Na^+-dominated interlayers, glycerol intercalation causes exfoliation, resulting in a decrease in size, while for Ca^{2+} or K^+-dominated interlayers, glycerol intercalation further expands basal spacing but will not cause exfoliation, resulting in an increase in size. Therefore, the Gly-DI yields a slightly coarser PSD than DI water.

For the second group where EA and Gly-EA are used as solvents, Na^+-Mt does not readily swell in EA. As such, Na^+-Mt in EA exhibits a much coarser PSD than in DI water. In fact, its D_{50} increases from ~2.2 μm in water to ~13 μm in EA. Because Na^+-Mt swells in the Gly-EA by intercalating glycerol (but probably not EA), some of which can be exfoliated into smaller particles or tactoids by hydraulic shearing, resulting in a finer PSD in the Gly-EA than in EA. However, due to the smaller dielectric constants of glycerol and EA (Table 3.4), which can results in stronger interlayer Coulomb attraction force (between interlayer cations and 2:1 layers), the exfoliation can be very limited, and hence the change in the PSD is very small.

The PSD dependence on different levels of clay mineral swelling in different solvents is also demonstrated by the images shown in Figure 3.6. Both the Ca^{2+}-Mt and Na^+-Mt in EA (Figure 3.6 e and f) exhibit larger particles than in DI water, because they can swell in water and subsequently exfoliate into smaller particles (Figure 3.6 c and d).

3.3.5 Intrinsic PSD of the Four Clay Minerals

As pointed early, intrinsic PSD should truly represent the sizes of original, physically individual particles that are not affected by sample preparation, such as chemical dispersants, excessive physical disruption or disaggregation, or solvent-clay mineral interactions, nor affected by aggregation or flocculation in the prepared clay mineral dispersions. Strictly speaking, because of the presence of flocculi, a kind of clay mineral aggregates, it is difficult to obtain the intrinsic PSD of the four source clay minerals. However, if the 10-20 μm flocculi are treated as inherent to the clay minerals, the above analyses can be used to find their intrinsic PSD, as discussed below.

For the non-swelling kaolinite and illite, although ultrasound dispersion yields the finest PSD (Figure 3.7), it may also cause particle disruption or breakage along the basal plane dimension or delamination along the *c*-axis. Thus the obtained PSD are not intrinsic. The difference in the PSD from NaHMP dispersion and overnight soaking is not so significant for illite, but there is difference for kaolinite. Therefore, it is reasonably to conclude that the kaolinite PSD obtained by NaHMP dispersion represents the intrinsic one and the illite PSD obtained by overnight soaking or NaHMP is intrinsic.

For the swelling clay minerals, primary particles should be the individual particles at their non-swelling state. The PSD obtained in water-based dispersions (e.g., DI water, NaHMP solution, glycerol in water solution) also reflect the swollen particles. Additionally, powdery clay minerals cannot be fully dispersed in dry mode. The use of an interlayer expanding agent, glycerol, certainly alters the original particle thickness. Therefore, the PSD of the two montmorillonites dispersed in ethyl alcohol, a much less polar liquid where they do not readily swell, are regarded as intrinsic. This is due to the fact that dispersion in a less polar liquid avoids swelling (due to intercalation of water molecules into interlayers), cation exchange between the clay mineral and solution, and exfoliation. Table 3.5 summarizes the intrinsic PSD parameters for all four clay minerals.

Table 3.5 Intrinsic PSD parameters of the four clay minerals.

Sample	Dispersion method	D_{10} (μm)	D_{50} (μm)	D_{90} (μm)	$C_u = D_{60}/D_{10}$	$C_c = (D_{30})^2/(D_{10}*D_{60})$
Kaolinite	Dispersed in NaHMP solution	0.63	3.56	19.41	14.44	0.39
Illite	Overnight soaking / Dispersed in NaHMP solution	0.76	6.37	15.94	11.32	0.81
Ca^{2+}-Mt	Dispersed in alcohol	1.87	12.98	32.75	8.56	2.14
Na^{2+}-Mt	Dispersed in alcohol	1.56	12.26	31.91	9.94	2.03

C_u is the coefficient of uniformity; C_c is the coefficient of curvature.

3.3.6 Practical Implications

PSD is one of the most fundamental physical properties of soils. It is required by current soil classification standards (e.g., the unified soil classification system). Based on the above analyses, relatively strong clay mineral-based flocculi of 10-20 μm in size are quite resistant to mechanical disaggregation and chemical dispersion and can exist in different types of clay minerals. As such, this type of clay mineral aggregates is usually counted toward the silt-sized fraction, which may lead to misleading soil classifications or incorrect soil properties (e.g., activity). On the other hand, better dispersion techniques that can disaggregate clay mineral flocculi should be developed in future studies.

In addition, several other factors warrant more thorough considerations when selecting appropriate sample preparation methods for PSD analysis. First, soaking in water for sufficient time (e.g., overnight) should be always performed for most soils, especially those containing a significant fraction of kaolinite or other low charge clay minerals; Second, caution should be taken when Na^+-based dispersants are used, particularly for soils with non-sodium based

smectites, although NaHMP is specified in the ASTM or other standard methods for PSD analysis. As a general guideline, when selecting proper dispersants for soils containing Ca or other divalent cation dominant smectites, cation exchange between smectites and dissolved dispersants that can lead to alteration to the particle size should be avoided; Finally, the solvent used to prepare soil dispersions should not be limited to water only, and other polar or less polar liquids may also be selected to prevent the unnecessary clay mineral-water or clay mineral-solvent interactions.

3.4 Conclusions

An experimental study was conducted to evaluate the PSD and their variability of four source clay minerals, kaolinite, illite, Ca^{2+}-Mt, and Na^{+}-Mt, under different dispersion methods, including dry dispersion in pressurized air and wet dispersion in water and EA with and without an interlayer expanding agent, glycerol, along with ultrasound disaggregation and NaHMP dispersion. Based on the results and above discussion, the following conclusions can be drawn:

- Ultrasound disaggregation followed by settling can be used to obtain the <2 μm fraction of all four clay minerals, and this fraction is usually free of aggregates and non-clay mineral impurities.

- Overnight soaking in water should always be included in the preparation of clay mineral dispersions for PSD analysis, especially for kaolinite or other low charge clay minerals.

- Prolonged ultrasound disaggregation should be avoided in sample preparation for PSD measurement in order to prevent unnecessary particle exfoliation or breakage.

- Dry dispersion in pressurized air is not effective to disperse clay mineral aggregates for PSD analysis.

- A much less polar solvent such as EA should be used to prepare the dispersions of swelling clay minerals for PSD analysis.

- Most clay minerals contain relatively strong clay mineral-based flocculi of 10-20 μm in size that is resistant to disaggregation, and hence the resulting PSD overestimate the silt-sized fraction, but underestimate the clay mineral-sized fraction.

- The intrinsic PSD of kaolinite and illite should be obtained by NaHMP dispersion, while those of the two smectites can be obtained by dispersing in EA or other less- or non-polar solvents.

- In general, caution should be taken in selecting an appropriate chemical dispersant for PSD analysis, especially when selecting a Na^{+}-based dispersant for soils containing non-sodium based smectites.

- The PSD of most clay minerals show a multimodal lognormal distributions with local maxima representing <2 μm primary clay mineral particles, 10-20 μm flocculi, and sometimes 50-500 μm microflocs.

3.5 Notations

θ – Diffraction angle

D – Volume moment based mean diameter of particles within a given size range

n – Number of particles

l – Diameter of a particle in that given size range

d – Basal spacing of clay minerals

P – Percent finer of particles by number

F – Frequency as a percentage of a particle in the whole sample

3.6 Acknowledgments

This work was partially supported by the Office of Naval Research through Naval Research Laboratory base funding under Award No. N00173-10-1-G013 as part of the NRL ARI "Biogeochemical Influences on Cohesive Sediment Strength in Marine and Estuarine Environments (PE No. 061153N)". The facilities used in this study were purchased using the fund from the Louisiana Board of Regents Enhancement Program.

3.7 References

[1] Anderson, R. L., Ratcliffe, I., Greenwell, H. C., Williams, P. A., Cliffe, S., and Coveney, P. V. 2010. Clay swelling - A challenge in the oilfield, *Earth-Science Reviews*, 98, 201-216.

[2] ASTM 2007, Standard Test Method for Particle-Size Analysis of Soils, edited, pp. D422-463, ASTM International, West Conshohocken, PA.

[3] Bihannic, I., Tchoubar, D., Lyonnard, S., Besson, G., and Thomas, F. 2001. X-Ray scattering investigation of swelling clay fabric: 1. The Dry State, *J. Colloid Interface Sci.*, 240, 211-218.

[4] Brindley, G. W., Wiewiora, K., and Wiewiora, A. 1969. Intracrystalline swelling of montmorillonite in some water-organic mixtures (clay-organic studies. XVII), *American Mineralogist*, 54, 1635-1644.

[5] Burt, R. 2004, Soil Survey Laboratory Methods Manual, edited, p. 735, Soil Survey Investigations Report No. 42 Version 4.0, Lincoln, NE: Natural Resources Conservation Service, U.S. Department of Agriculture.

[6] Chipera, S. J., and Bish, D. L. 2001. Baseline studies of the Clay Minerals Society Source Clays: Powder X-ray diffraction analyses, *Clay Clay Min.*, 49, 398-409.

[7] Chipera, S. J., Guthrie, G. D., and Bish, D. L. 1993. Preparation and purification of mineral dusts, *Reviews in Mineralogy*, 28, 235-249.

[8] Costanzo, P. M. 2001. Baseline studies of The Clay Minerals Society Source Clays: Introduction, *Clay Clay Min.*, 49, 372-373.

[9] Crowley, M. S., and Welch, A. P. 1954. Clay-particle dispersion by ultrasons, *Journal of The American Ceramic Society*, 37 433-439.

[10] Daoud, Y., and Robert, M. 1992. Influence of particle size and clay organization on hydraulic conductivity and moisture retention of clays from saline soils, *Applied Clay Science*, 6, 293-299.

[11] de Boer, G. B., de Weerd, C., Thoenes, D., and Goossens, H. W. 1987. Laser diffraction spectrometry: Fraunhofer diffraction versus Mie scattering, *Particle Characterization*, 4, 14-19.

[12] Du, J., Morris, G., Pushkarova, R. A., and Smart, R. S. 2010. Effect of surface structure of kaolinite on aggregation, settling rate, and bed density, *Langmuir*, 26, 13227-13235.

[13] Franco, F., Perez-Maqueda, L. A., and Perez-Rodriguez, J. L. 2004. The effect of ultrasound on the particle size and structural disorder of a well-ordered kaolinite, *J. Colloid Interface Sci.*, 274, 107-117.

[14] Frenkel, H., Levy, G. J., and Fey, M. V. 1992. Clay dispersion and hydraulic conductivity of clay-sand mistures as affected by the addition of vairous anions, *Clay Clay Min.*, 40, 515-521.

[15] Furukawa, Y., Watkins, J. L., Kim, J., Curry, K. J., and Bennett, R. H. 2009. Aggregation of montmorillonite and organic matter in aqueous media containing artificial seawater, *Geochemical Transactions*, 10.

[16] Genrich, D. A., and Bremner, J. M. 1972a. A reevaluation of the ultrasonic-vibration method of dispersing soils, *Soil Sci. Soc. Am. Proc.*, 36, 944-947.

[17] Genrich, D. A., and Bremner, J. M. 1972b. Effect of probe condition on ultrasonic dispersion of soils by probe-type ultrasonic vibrators, *Soil Sci. Soc. Am. Proc.*, 36, 975-976.

[18] Goldberg, S., Forster, H. S., and Godfrey, C. L. 1996. Molybdenum adsorption on oxides, clay minerals, and soils, *Soil Science Society of America Journal*, 60, 425-432.

[19] Gupta, V., Hampton, M. A., Stokes, J. R., Nguyen, A. V., and Miller, J. D. 2011. Particle interactions in kaolinite suspensions and corresponding aggregate structures, *J Colloid Interface Sci*, 359, 95-103.

[20] Güven, N. (Ed.) 1992, Molecular aspects of clay-water itneractions, Clay Minerals Society.

[21] Harvey, C. C., and Murray, H. H. 1997. Industrial clays in the 21st century: A perspective of exploration, technology and utilization, *Applied Clay Science*, 11, 285-310.

[22] Helmy, A. K. 1998. The limited swelling of montmorillonite, *J Colloid Interface Sci*, 207, 128-129.

[23] Hill, P. S. 1998. Controls on floc size in the sea, *Oceanography* 11, 13-18.

[24] Hower, J., and Mowatt, T. C. 1966. The mineralogy of illites and mixed-layer illite/montmorilonites, *American Mineralogist*, 51, 825-854.

[25] Jouyban, A., Soltanpour, S., and Chan, H.-K. 2004. A simple relationship between dielectric constant of mixed solvents with solvent composition and temperature, *International Journal of Pharmaceutics*, 269, 353-360.

[26] Kiliaris, P., and Papaspyrides, C. D. 2010. Polymer/layered silicate (clay) nanocomposites: An overview of flame retardancy, *Prog. Polym. Sci.*, 35, 902-958.

[27] Kinter, E. B., and Diamond, S. 1958. Gravimetric determination of monolayer glycerol complexes of clay minerals, *Clay Clay Min.*, 5, 318-333.

[28] Kjellander, R., Marcelja, S., Pashley, R. M., and Quirk, J. P. 1988. Double-layer ion correlation forces restrict calcium clay swelling, *J. Phys. Chem.*, 92, 6489-6492.

[29] Kleijn, W. B., and Oster, J. D. 1982. A model of clay swelling and tactoid formation, *Clay Clay Min.*, 30, 383-390.

[30] Lagaly, G. 2006, Chapter 5. Colloid Clay Science, in Developments in Clay Science, edited by F. Bergaya, B. K. G. Theng and G. Lagaly, pp. 141-245, Elsevier.

[31] Lagaly, G., and Ziesmer, S. 2003. Colloid chemistry of clay minerals: the coagulation of montmorillonite dispersions, *Advances in Colloid and Interface Science*, 100, 105-128.

[32] Laird, D. A. 2006. Influence of layer charge on swelling of smectites, *Applied Clay Science*, 34, 74-87.

[33] Lapides, I., and Yariv, S. 2004. The effect of ultrasound treatment on the particle-size of Wyoming bentonite in aqueous suspensions, *J. Mater. Sci.*, 39, 5209-5212.

[34] Lee, B. J., Fettweis, M., Toorman, E., and Molz, F. J. 2012. Multimodality of a particle size distribution of cohesive suspended particulate matters in a coastal zone, *Journal of Geophysical Research-Oceans*, 117, 17.

[35] Levy, G. J., Shainberg, I., Alperovitch, N., and Vandermerwe, A. J. 1991. Effect of Na-hexametaphosphate on the hydraulic conductivity of kaolinite-sand mistures, *Clay Clay Min.*, 39, 131-136.

[36] Mackinnon, I. D. R., Uwins, P. J. R., Yago, A., and Page, D. 1993. Kaolinite particle sizes in the < 2 micron range using laser scattering, *Clay Clay Min.*, 41, 613-623.

[37] Moore, D. M., and Reynolds, R. C. (Eds.) 1997, X-ray Diffraction and the Identification and Analysis of Clay Minerals, 2nd ed., 378 pp., Oxford University Press, New York.

[38] Murray, H. H. 1999. Applied clay mineralogy today and tomorrow, *Clay Minerals*, 34, 39-49.

[39] Murray, H. H. 2000. Traditional and new applications for kaolin, smectite, and palygorskite: A general overview, *Applied Clay Science*, 17, 207-221.

[40] Neumann, M. G., Gessner, F., Schmitt, C. C., and Sartori, R. 2002. Influence of the layer charge and clay particle size on the interactions between the cationic dye methylene blue and clays in an aqueous suspension, *Journal of Colloid and Interface Science*, 255, 254-259.

[41] Olejnik, S., Posner, A. M., and Quirk, J. P. 1974. Swelling of montmorillonite in polar organic liquids, *Clay Clay Min.*, 22, 361-365.

[42] Pavlidou, S., and Papaspyrides, C. D. 2008. A review on polymer-layered silicate nanocomposites, *Prog. Polym. Sci.*, 33, 1119-1198.

[43] Posner, A. M., and Quirk, J. P. 1964. Changes in basal spacing of montmorillonite in electrolyte solutions, *Journal of Colloid Science*, 19, 798-&.

[44] Pruett, R. J., and Webb, H. L. 1993. Sampling and analysis of KGa-1b well-crystallized kaolin source clay, *Clay Clay Min.*, 41, 514-519.

[45] Quirk, J. P., and Aylmore, L. A. G. 1971. Domains and quasi-crystalline regions in clay systems, *Soil Science Society of America Proceedings*, 35, 652-&.

[46] Rengasamy, P., van Assche, J. B., and Uytterhoeven, J. B. 1976. Particle size of wyoming bentonite and its relation to the cation exchange capacity and the homogeneity of the charge density, *Journal of the Chemical Society, Faraday Transactions 1: Physical Chemistry in Condensed Phases*, 72, 376-381.

[47] Segad, M., Jonsson, B., Akesson, T., and Cabane, B. 2010. Ca/Na montmorillonite: structure, forces and swelling properties, *Langmuir*, 26, 5782-5790.

[48] Theng, B. K. G. 1982. Clay-polymer Interactions - Summary and perspectives, *Clay Clay Min.*, 30, 1-10.

[49] Vandeven, T. G. M., and Hunter, R. J. 1977. Energy-dissipation in sheared coagulated sols, *Rheologica Acta*, 16, 534-543.

[50] Walling, D. E., and Moorehead, P. W. 1989. The particle size characteristics of fluvial suspended sediment: an overview., *Hydrobiologia*, 176/177, 125-149.

[51] Wu, W. J. 2001. Baseline studies of the Clay Minerals Society Source Clays: Colloid and surface phenomena, *Clay Clay Min.*, 49, 446-452.

[52] Yariv, S., and Lapides, I. 2003. Laser shadow analysis of particle-size distribution of montmorillonites in aqueous suspensions, *Clay Clay Min.*, 51, 23-32.

[53] Zbik, M., and Smart, R. S. C. 1998. Nanomorphology of kaolinies: comparative SEM and AFM studies, *Clay Clay Min.*, 46, 153-160.

[54] Zbik, M., and Smart, R. S. C. 2002. Dispersion of kaolinite and talc in aqueous solution: nano-morphology and nano-bubble entrapment, *Minerals Engineering*, 15, 277-286.

[55] Zbik, M. S., and Frost, R. L. 2009. Micro-structure differences in kaolinite suspensions, *J. Colloid Interface Sci.*, 339, 110-116.

[56] Zhang, G., Germaine, J. T., and Whittle, A. J. 2005. An evaluation of the mechanical and chemical dispersion methods for a tropical old alluvium, *Geotech. Test. J.*, 28, 123-132.

[57] Zhang, Z. P., Liao, L. B., and Xia, Z. G. 2010. Ultrasound-assisted preparation and characterization of anionic surfactant modified montmorillonites, *Applied Clay Science*, 50, 576-581.

CHAPTER 4 CHARACTERIZATION OF PARTICLE SIZE AND SETTLING VELOCITY OF COHESIVE SEDIMENTS AFFECTED BY A NEUTRAL EXOPOLYMER*

4.1 Introduction

Riverine, estuarine, and lake waters are usually loaded with various types of organic matter, one of which is exopolymers or extracellular polymeric substances (EPS) secreted by microorganisms (*Bhaskar and Bhosle, 2005*). In fact, EPS are the major constituent of biofilms that disperse into water upon maturation. Depending on the functional groups, EPS molecules can exhibit different polarities, such as cationic, anionic, and neutral, and hence are chemically active or reactive in solution or suspension. During transport, the dissolved EPS molecules interact extensively, via collision facilitated by a series of short-range surface and intermolecular forces (e.g., Coulomb force, van der Waals attraction, hydrogen bond), with other water-borne suspended particles or molecules, particularly those negatively charged clays—the primary constituent of cohesive sediments. As a result, micro-sized flocs of typically 10-500 μm in size form and develop. These flocs are usually soft and tenuous in nature, with a complex and fractal structure (*Kranenburg, 1994; Furukawa et al., 2009*).

Flocculation between inorganic, fine-grained clay particles and dissolved organic EPS molecules can have a profound influence on cohesive sediment dynamics, such as sediment transport, settling velocity, and sediment yield (i.e., the final volume of settled bottom sediment). The suspended primary cohesive sediments or clay particles are typically small (e.g., <2 μm) and, if dispersed, do not readily settle in most natural waters. It is expected that different degrees of flocculation result in flocs of varying sizes and densities. Flocculation can promote the settling of clay particles that otherwise do not settle by altering the size and density (*Droppo et al., 1997*). For particles or flocs of the same composition and density, larger ones are usually expected to settle faster than smaller ones. Due to the floc's porous structure and resulting creeping flow through the internal pores, a smaller drag force is expected when compared with solid, non-porous particles of the same size, and hence flocs should sink faster than the solid particles of same density and size (*Huang, 1993*). However, the larger clay flocs may be more porous and less dense than the smaller ones (*Likos and Lu, 2001*), and this could be interpreted by the fact that, while the size increases, the ratio of surface-area-to-volume decreases, which makes smaller ones more adsorptive per unit of mass. Therefore, the density of larger flocs is relatively smaller (*Hill, 1998*). Moreover, settling velocity is usually directly or indirectly used in the calculation of deposition and selective transport of sediments (*Loch, 2001; Basile et al., 2010*). On the other hand, the resultant shear force caused by settling acceleration under gravity as well as hydrodynamic turbulence can cause floc breakage or de-flocculation and hence limit the terminal size during settling (*Kobayashi et al., 1999*). As a result, floc formation and breakup are highly dynamic processes that are affected by many hydraulic or hydrodynamic factors.

---

* Reprinted by permission of *International Journal of Sediment Research*, Elsevier.

Knowledge of the particle size distribution (PSD) of primary clays and clay-EPS flocs is also of great significance to the characterization of sedimentary environments, selection of numerical sediment transport models and associated parameters (*Yang et al., 2009; Zhang et al., 2009*), and removal of nutrients and contaminants from water, as well as the influence of involved organic matter on sediment yield. With the development of some new instruments (e.g., laser diffraction-based particle size analyzers), the size of individual particles or flocs and their overall size distribution can be measured simultaneously while they are subjected to varying hydrodynamic flow conditions. However, with these systems, it is very challenging and difficult to determine flocs' microstructure and density, because of the micro/nano-meter size of clay particles that make up the flocs and the fact that flocculation is a complex, random process. Additionally**,** the porous, soft, and highly deformable nature of flocs adds extra difficulty in manipulating flocs for density measurement and microstructure characterization. According to the literature (*Huang, 1993; Johnson et al., 1996; Loch, 2001; Jarvis et al., 2005; Khelifa and Hill, 2006*), the density of flocs or particles can be indirectly measured by sedimentation experiments where the measured settling velocity is used to estimate the floc or particle density based on specific mathematical models (e.g., Stoke's Law).

Of all three types (i.e., cationic, anionic, and neutral) of EPS, the influence of the charged ones on clay flocculation has been extensively studied (*Dontsova and Bigham, 2005; Labille et al., 2005; Benchabane and Bekkour, 2006; Tripathy and Rajan De, 2006; Furukawa et al., 2009; Ghimici and Nichifor, 2009*). However, a systematic study of the influence of neutral EPS on the PSD and settling velocity has not been reported in the literature. This paper presents an experimental study of the flocculation of cohesive sediments caused by neutral EPS in fresh water at room temperature. Four types of clays that are abundant in natural waters and sediments, including kaolinite, illite, Na-montmorillonite (Na-mont.), and Ca-montmorillonite (Ca-mont.), were selected to account for the diversity of cohesive sediments. The guar gum was selected and used as an analog to neutral EPS. It is expected that adding EPS into clay suspensions can change their flocculation properties and promote the formation of clay-EPS flocs, whose settling velocity, microstructure, and density are unknown and difficult to characterize. The objectives of this study were two-fold: (1) to investigate the effects of exopolymers on the size of clay-EPS flocs, and (2) to determine the settling velocity of pure clay flocs and clay-EPS flocs. The relationships between settling velocity and floc size were also used to estimate the fractal dimension of flocs, and comparisons made between pure clay flocs and clay-EPS flocs.

4.2 Materials and Methods

4.2.1 Materials

Four clays, namely kaolinite, illite, Ca-mont., and Na-mont., were chosen as the model inorganic cohesive sediment particles. Samples of the four clays were purchased from the US Clay Minerals Society (CMS) Source Clay Repository (Purdue University, Indiana, USA). These high-purity source clays were well analyzed and used by many previous studies as reference clay minerals. Table 4.1 shows the geographic origin and some basic properties of these clay samples. Of the four samples, kaolinite (KGa-1b), Ca-mont. (STx-1b), and Na-mont. (SWy-2) were supplied as dry powder, while illite (IMt-1) as small rock chips. The +44 μm size fraction of the three powdery clays was initially removed by wet sieving through a #325 mesh (*Pruett and Webb, 1993*) during the clay mining and pre-processing before shipment to users. Thus, these

three clay samples were used without further pretreatment in this study. To obtain a powdery illite sample, the as-received rock chips were first hand-ground by a mortar and pestle and then wet-ground with ethyl alcohol by a McCrone micronizing mill (McCrone Accessories and Components, USA) for 3 mins, which typically results in a fine powder with particle sizes ≤38 μm for most silicate minerals.

Table 4.1 Origin and basic properties of the four clay samples[a].

Name	Origin	Layer type	Layer charge[b]	SSA[c] (m^2/g)	Chemical formula
Kaolinite (KGa-1b)	Washington County, Georgia	1:1	-0.03	10.05	$(Mg_{.02}Ca_{.01}Na_{.01}K_{.01})$ $[Al_{3.86}Fe^{3+}_{.02}Mn_{tr}Ti_{.11}]$ $[Si_{3.83}Al_{.17}]O_{10}(OH)_8$
Illite (IMt-1)	Silver Hill, Montana	2:1	-0.84	30.00[d]	$(Mg_{.09}Ca_{.06}K_{1.37})$ $[Al_{2.69}Fe^{3+}_{.76}Fe^{2+}_{.06}Mn_{tr}Mg_{.43}Ti_{.06}]$ $[Si_{6.77}Al_{1.23}]O_{20}(OH)_4$
Ca-mont. (STx-1b)	Gonzales County, Texas	2:1	-0.34	83.79	$(Ca_{.27}Na_{.04}K_{.01})$ $[Al_{2.41}Fe^{3+}_{.09}Mn_{tr}Mg_{.71}Ti_{.03}]$ $[Si_{8.00}]O_{20}(OH)_4$
Na-mont. (SWy-2)	Crook County, Wyoming	2:1	-0.28	31.82	$(Ca_{.12}\ Na_{.32}\ K_{.05})$ $[Al_{3.01}\ Fe^{3+}_{.41}\ Mn_{.01}\ Mg_{.54}Ti_{.02}]$ $[Si_{7.98}\ Al_{.02}]\ O_{20}(OH)_4$

[a] All data except those noted separately are from the Clay Minerals Society Source Clay Data Sheets.
[b] The layer charge is based on per $O_5(OH)_4$ or $O_{10}(OH)_2$.
[c] SSA = specific surface area.
[d] Data from *Celis and Koskinen (1999)*.

Guar gum (Fisher ChemAlert® Guide, Rochester, NY), a neutral plant polysaccharide found in the seed of *Cyamopsis tetragonoloba*, was selected as an EPS analog to be used as the organic constituent of flocs. Guar gum has a molecular weight of up to 2 x 10^6 Da (*Cheng et al., 2002*) and, once dissolved, results in a viscous and pseudoplastic aqueous solution. A low concentration guar gum solution can bring inorganic minerals to flocculation, while high concentration solutions may lead to steric re-dispersion (*Pawlik and Laskowski, 2006*). Figure 4.1 shows the chemical structure of guar gum. The lack of carboxylic acid groups (-COOH) and other ionizable functional groups that are commonly found on anionic or cationic EPS renders guar gum a neutral polarity in circum-neutral pH solutions. Its hydroxyl groups can dissociate only in very high pH solutions.

4.2.2 Particle Size Analyses

The PSD of clay particles and clay-EPS flocs was characterized by a Cilas® 1190 particle size analyzer (PSA) (Cilas Particle Size, Madison, WI, USA). This instrument has a liquid dispersion and circulation system. Sample dispersion in liquid is achieved by a speed-controllable stirrer and an ultrasound generator, while liquid circulation is driven by a peristaltic pump whose rotation rate is also controllable (Figure 4.2). Flocculation between suspended clay

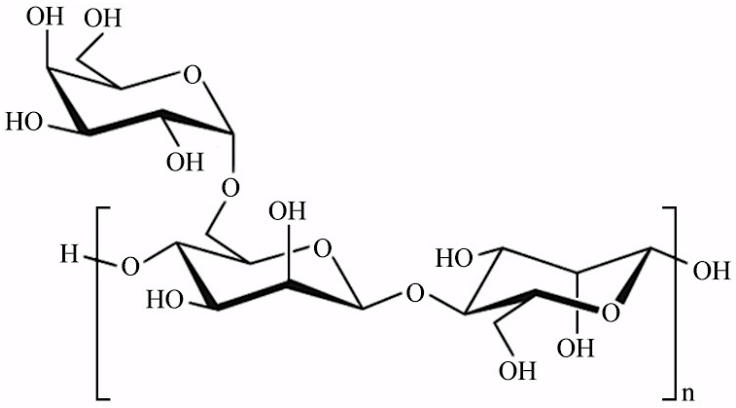

Figure 4.1 Chemical structure of guar gum.

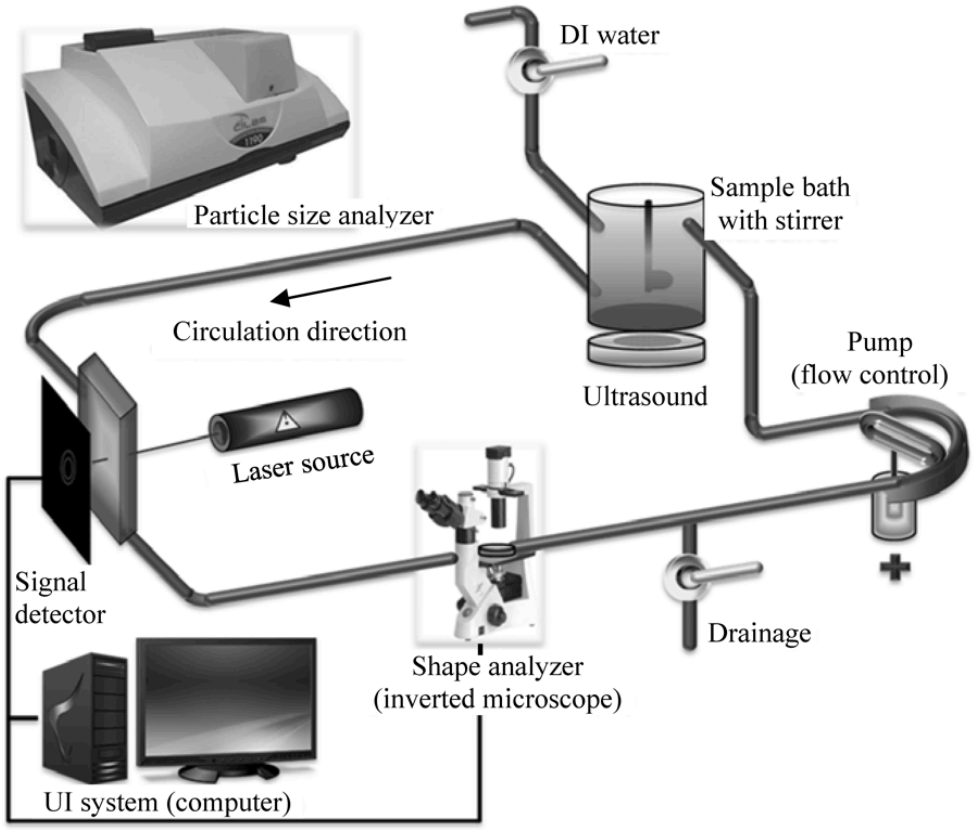

Figure 4.2 The liquid dispersion and circulation system of the PSA.

particles and EPS molecules in solution took place in the PSA's bath where, during stirring, collisions between particles, clay to clay and clay to EPS molecules, occurred frequently. At the same time, the suspension was circulated through the tube system where floc formation or breakage took place. The circulation was maintained until a steady state in particle size was achieved. A steady state in particle size was determined from the real-time PSD measurement via the analyzer's built-in laser diffraction instrument. During suspension circulation under a given constant flow velocity, flocs with a strength greater than the flow-induced shear force tended to form, while weaker ones would breakup and re-flocculate or remain disaggregated such that all

remaining flocs were strong enough to resist the flow-induced shear stress. For all particle size measurements, sufficient time (usually 5-10 mins) was allowed for the clay suspension in the circulation system to reach a steady state (i.e., no further significant change in the measured PSD even for prolonged circulation). The accuracy of the PSA was determined prior to evaluating floc sizes by measuring the size of standard spheres with a diameter of 40 μm. The result showed that more than 97% of the particles were in the size of ~40 μm, thus substantiating the instrument's accuracy.

Both pure clay and clay-EPS suspensions were prepared for particle size analysis. The experimental procedures are detailed in Figure 4.3. For each of the four clay samples, 0.2 g dry clay powder was soaked with deionized (DI) water for at least 16 hours, followed by dilution with DI water to obtain a 500 mL (which was the total volume of the PSA circulation system, including water bath and tubes) clay suspension with a concentration of 0.4 g L^{-1}. This solution was then transferred into the PSA bath. To identify the sole effect of EPS on clay flocculation, no other chemicals (e.g., sodium hexametaphosphate) were added to the suspension for further dispersion. However, to obtain accurate PSDs for the pure clay samples and to prevent the unnecessary formation of clay flocs, the built-in ultrasound dispenser beneath the PSA sample bath was turned on during the particle size measurement of the pure clay suspensions.

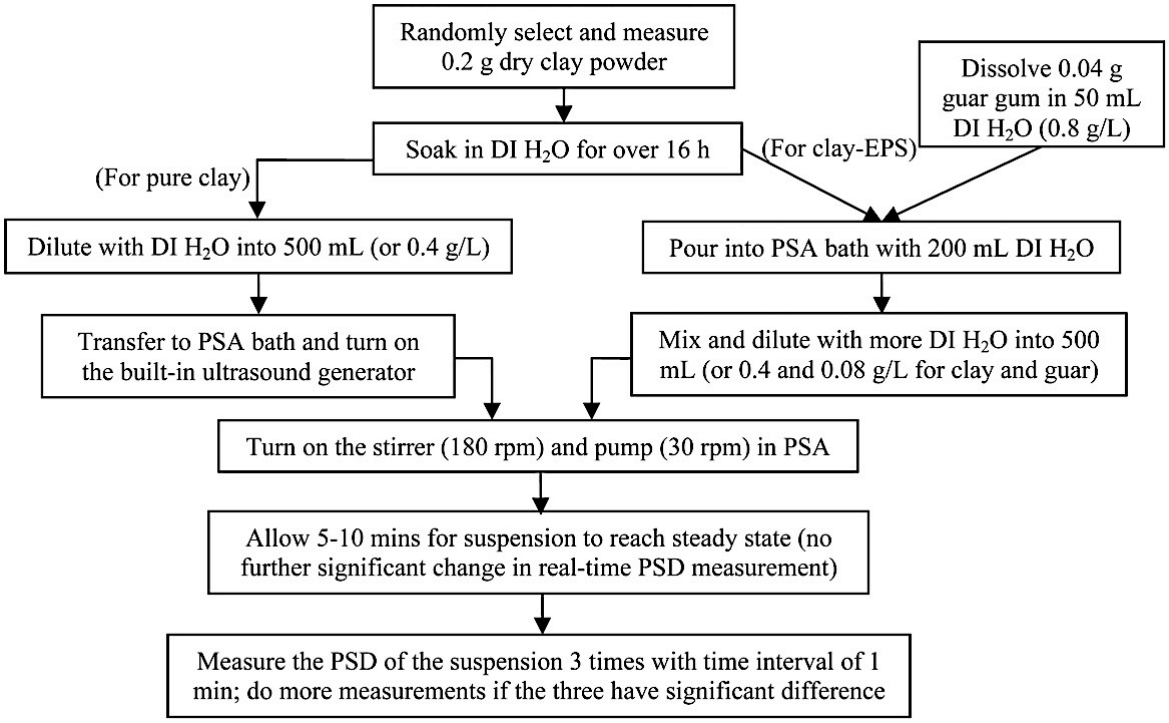

Figure 4.3 Flow chart showing the preparation of clay and clay-EPS suspensions and corresponding PSD measurements.

It was recognized in the preliminary testing that the most stable clay-guar gum flocs were generated when the mass ratio of clay to guar gum is 5:1. For the preparation of clay-guar flocs, 0.2 g dry clay powder was first soaked for at least 16 hours. A guar gum solution with a concentration of 0.8 g L^{-1} was prepared by dissolving facilitated by a magnetic stirrer 0.04 g guar gum slowly into 50 mL DI water. The mixing lasted for >30 minutes to completely dissolve the

guar gum. Then 200 mL DI water, the soaked clay suspension, and the 50 mL guar gum solution were added sequentially to the PSA bath. Finally, more water was added to the bath to bring the total volume of the mixture to 500 mL, resulting in a final concentration of 0.4 and 0.08 g L^{-1} for clay and guar gum, respectively.

The prepared suspensions were circulated in the PSA flow system under a fixed stirrer speed of 180 rpm and a pump speed of 30 rpm, which resulted in an average flow velocity of 150 mm s^{-1} in the recirculating flow-through system. The dynamic viscosity of the guar solution at a concentration of 0.08 g L^{-1} is 1.0156 mPa·s (*Wientjes et al., 2000*), resulting in a Reynolds number (*R*e) of 961 or laminar flow in the tube. This work focused on flocs that were formed in laminar flow.

The size of particles or flocs are defined as the diameter of equivalent spheres calculated based on the volume-moment-mean value of multiple particles at a given size range. That is (Equation 4.1):

$$D = \frac{\sum nl^4}{\sum nl^3} \qquad \text{Equation 4.1}$$

where D is the mean diameter of flocs or particles within a given range, n the number of particles at a fixed size, and l the diameter of a particle or floc at a size within the given range.

4.2.3 Settling Velocity Measurements

An acrylic cylinder with dimensions of 20 × 20 × 300 mm (*Miyahara et al., 2002*) filled with DI water was used as a sedimentation column for settling velocity measurements. According to previous studies (*Johnson et al., 1996*), the terminal velocity of flocs within a static water column can be reached at a vertical distance of <150 mm. The ratio of the diameter of the largest flocs (e.g., 600 μm in this study) to the width of the sedimentation cylinder is 0.03, which is small enough that the resulting edge effect is insignificant. In fact, an error of <10% was estimated for a 600 μm floc according to prior work (*McNown and Malaika, 1950; Loch, 2001*). In this study, the majority of flocs are much smaller than 600 μm, and hence this error is even smaller. Therefore, the size of the sedimentation cylinder is appropriate for the settling velocity measurement without causing significant edge effects. The pure clay and clay-EPS suspensions with the desired concentrations were prepared in the PSA by exactly following the procedures described above for particle size measurements. After the suspension in the PSA circulation system reached a steady state (as monitored by no further change in the measured PSD curves), a pipette with a relatively large orifice was used to slowly withdraw the floc suspension and then dispense a drop of the suspension onto the surface of water in the sedimentation cylinder. To record the terminal settling velocity, the process of settling was imaged at a settling distance of 150 mm by a Leica DVM 2000 optical microscope at a speed of one frame per second (Figure 4.4). The settling velocity was then estimated by analyzing the time-series images, where the traveling distance and time of a settling floc were measured. Magnifications of 150x and 100x were used for imaging pure clay and clay-EPS flocs, respectively, at a fixed resolution of 1624 × 1236 pixels. Furthermore, the maximum and minimum diameters of each particle or floc were directly measured in the image, and their average diameter is reported as the representative size.

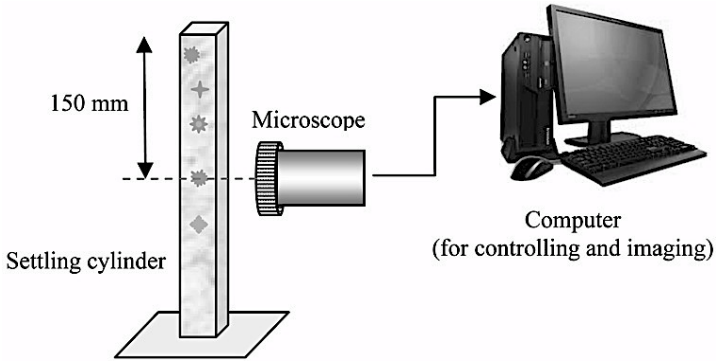

Figure 4.4 Schematic diagram showing the settling velocity measurement.

4.3 Results and Discussion

4.3.1 Particle Size Distribution

Figure 4.5 shows the results of particle size analyses performed on the four clays and clay-EPS mixtures. Clearly, the addition of guar gum to clay suspensions dramatically increases the particle size, as indicated by the shift of the cumulative PSD curves for each of the four clays. Table 4.2 summarizes the shape characteristics of these cumulative PSD curves. Of the four clays, Na-mont. has the smallest mean particle size (D_{50}) of 2.2 μm. However, after flocculation with guar gum, its D_{50} increases to 145 μm, which is the largest of all pure clays and clay-EPS mixtures. Kaolinite-EPS flocs have the second largest increase in the D_{50} (i.e., from 7.3 to 107 μm), while illite-EPS flocs have the smallest increase in the D_{50} (i.e., from 5.8 to 13.7 μm). The different degrees of PSD change are also indicated by the distance of the two cumulative PSD curves before and after EPS flocculation. Such a large increase in floc sizes implies that the final volume of settled sediments after flocculation by EPS is significantly increased. Table 4.2 also summarizes the coefficient of uniformity ($C_u = D_{60}/D_{10}$) and the coefficient of curvature ($C_c = (D_{30})^2/(D_{60}\cdot D_{10})$). The changes in both parameters appear to be irregular. For kaolinite and Na-mont., flocculation by EPS reduces the C_u or increases their uniformity, because the smallest particles seem to disappear after flocculation. As a result, the C_c values also decrease for these two clays. For illite and Ca-mont., their C_u values increase after flocculation by EPS, indicating a reduction in their uniformity, most likely caused by the presence of flocs as well as some smaller particles.

Regarding the particle size frequency distribution, all of the four pure clays show a tri-modal distribution with three peaks at 0.3, 2, and 10-20 μm. The first peak may represent the size of the individual primary clay particles (*Bennett et al., 1991*), while the second one may represent the size of the clay domains resulting from the claystone grinding procedure. The third one at 10-20 μm may represent the presence of clay flocs that were formed during the experiments. The maximum size of the four pure clays ranges from 30 to 70 μm, while that of the clay-EPS flocs from 150 to 600 μm, and some changes caused by flocculation exceed one order of magnitude. It is noticed that about 70-80% (by the number of particles) of the clay particles are greater than 2 μm, indicating that clay flocs are present in the pure clay suspensions. Without the presence of EPS or other chemicals, these flocs form as a result of force balance between the attraction caused by the van der Waals and edge-to-face attractive forces, and the face-to-face double layer repulsive force (*Thomas et al., 1999*).

For the clay-EPS mixture suspensions, floc formation depends on the interactions between clay particles and EPS molecules (such as collision, adhesion, and other forces). Generally, the hydraulic turbulence results in the collision of clay particles or EPS molecules, and the van der Waals and electro-chemical forces (e.g., hydrogen bond, Coulomb force, etc.) cause particles to adhere to each other (*Kranck and Milligan, 1980*). Clay-EPS flocculation is a simultaneous, competing multiple-step process involving the following five stages: (a) mixing of clay and EPS, (b) adsorption of EPS molecules onto clay particle surfaces (*Liu et al., 2000*), (c) re-conformation of the adsorbed EPS molecules, (d) flocculation of clay particles, and (e) floc breakup due to applied shearing (*Elimelech et al., 1995; Du et al., 2010*). Usually, owing to their relatively large size, guar gum molecules can also act as a bridging-chain that links multiple clay particles together, resulting in relatively loosely-packed flocs.

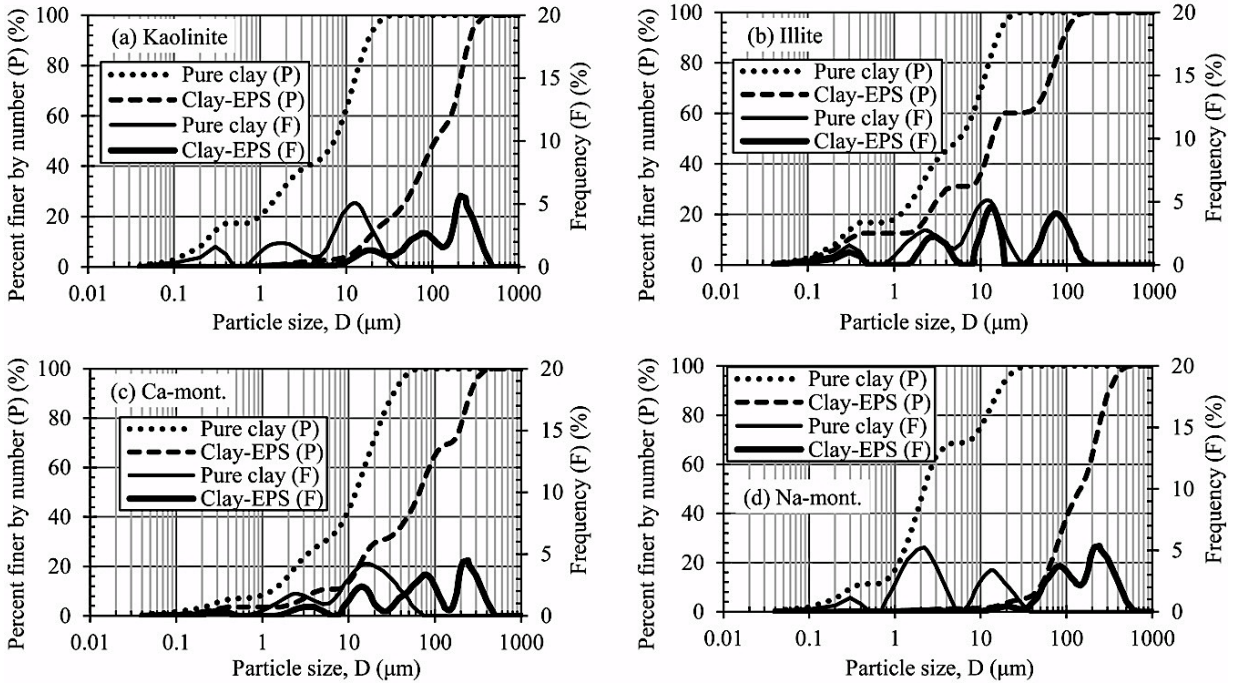

Figure 4.5 Particle size distribution of pure clay and clay-EPS flocs.

Table 4.2 Summary of the PSD characteristics of the pure clay and clay-EPS flocs.

Sample		Mean size D_{50} (μm)	Coefficient of uniformity, C_u	Coefficient of curvature, C_c
Kaolinite	Pure clay	7.3	40.87	1.50
	Clay-EPS	107	9.76	1.19
Illite	Pure clay	5.8	32.80	1.76
	Clay-EPS	13.7	59.33	3.00
Ca-Mont.	Pure clay	12.1	12.00	1.39
	Clay-EPS	68	19.11	1.25
Na-Mont.	Pure clay	2.2	8.75	2.35
	Clay-EPS	145	3.96	0.76

The adsorption of neutral EPS onto negatively charged clays is mainly “entropy-driven”. The size of illite-EPS flocs is smaller than that of Ca-mont. and Na-mont.-EPS flocs. Illite is a

non-swelling 2:1 clay, while the two montmorillonites are swelling clays. The layer charge of illite is much greater than that of the two montmorillonites (Table 4.1). As such, the electrostatic repulsion force between two illite particles inside the illite-EPS flocs is much stronger than that within the Ca-mont.-EPS or Na-mont.-EPS flocs. The strong electrostatic repulsion force can counteract the adhesion between EPS and illite, and hence the illite-EPS flocs are much weaker, as indicated by their significantly smaller size. Moreover, neutral EPS molecules can enter the interlayer space of expandable 2:1 clays such as smectites (*Theng, 1982*) where neutral EPS can be adsorbed onto clay surfaces by hydrogen bonds. This process is also called intercalation. For some intercalated EPS molecules, part of the molecular chain exists outside the clay interlayer space, and strong attachment of this part of the molecular chain to other clay particles tends to form. Therefore, the two montmorillonite clays generate significantly larger clay-EPS flocs than illite.

With respect to the two non-swelling clays, a 1:1 type kaolinite and a 2:1 type illite, the illite-EPS flocs are relatively smaller than the kaolinite-EPS flocs. This is reasoned as follows. Kaolinite is a well crystallized clay with low defect (*Pruett and Webb, 1993*)**,** while illite has complex nano-scale irregularities and high defect on the face surfaces and broken bonds on the edge surfaces. The defects in illite's crystal structure produce a higher quantity of charges that affect the site for hydrogen bond formation on the face surface. According to the bridging mechanisms proposed by *Du et al. (2010)*, effective adsorption of EPS onto clay surfaces requires relatively few attachment points so that the other parts of EPS molecule chain can stay in the surrounding suspension and be connected or adsorbed onto other particles. The relatively high layer charge of illite reflects its high degree of irregularity in its crystal structure, which results in the highest concentration of polarized oxygen atoms on illite surfaces and less attachment points on the already adsorbed EPS molecule chain for other clay particles. Thus, the highly charged illite forms the smallest clay-EPS flocs. In contrast, kaolinite has two types of basal surfaces: one consists of a plane of oxygen atoms, while the other contains only hydroxyls. Although kaolinite has very small layer charges, the hydroxyls on one of the two basal planes can readily form hydrogen bonds with the hydroxyls of guar gum (Figure 4.1). The small layer charge of kaolinite reduces the electrostatic repulsion between two kaolinite particles, and hence helps generate closer packing of clay particles in the kaolinite-EPS flocs.

Figure 4.6 shows a series of images taken by the optical microscope installed with the PSA for both pure clay and clay-EPS flocs. It should be noted that these flocs may not represent the average flocs and thus may not correctly reflect the measured PSD curves discussed above. Nevertheless, bimodal distributions of clay particles or flocs are discernable, and relatively larger clay-EPS flocs are introduced by the addition of EPS to the clay suspensions (e.g., Figure 4.6 b, f, and h). The absence of extensive flocculation or relatively large flocs is a typical phenomenon for both illite and illite-EPS suspensions.

In summary, the interactions responsible for the clay-EPS flocculation include: (1) relatively long-range EPS bridging of clay particles where the EPS molecules may be adsorbed to the surfaces of clay particles via hydrogen bonds; (2) the Coulombic repulsive force between two clay surfaces that prevents closer packing of clay particles; and (3) the clay surface structure that affects the density of available sites for hydrogen bond formation. According to these mechanisms, illite with the highest layer charge tends to form smaller and weaker clay-EPS (neutral) flocs, due to the strong repulsive force between two illite particles and the less polymer

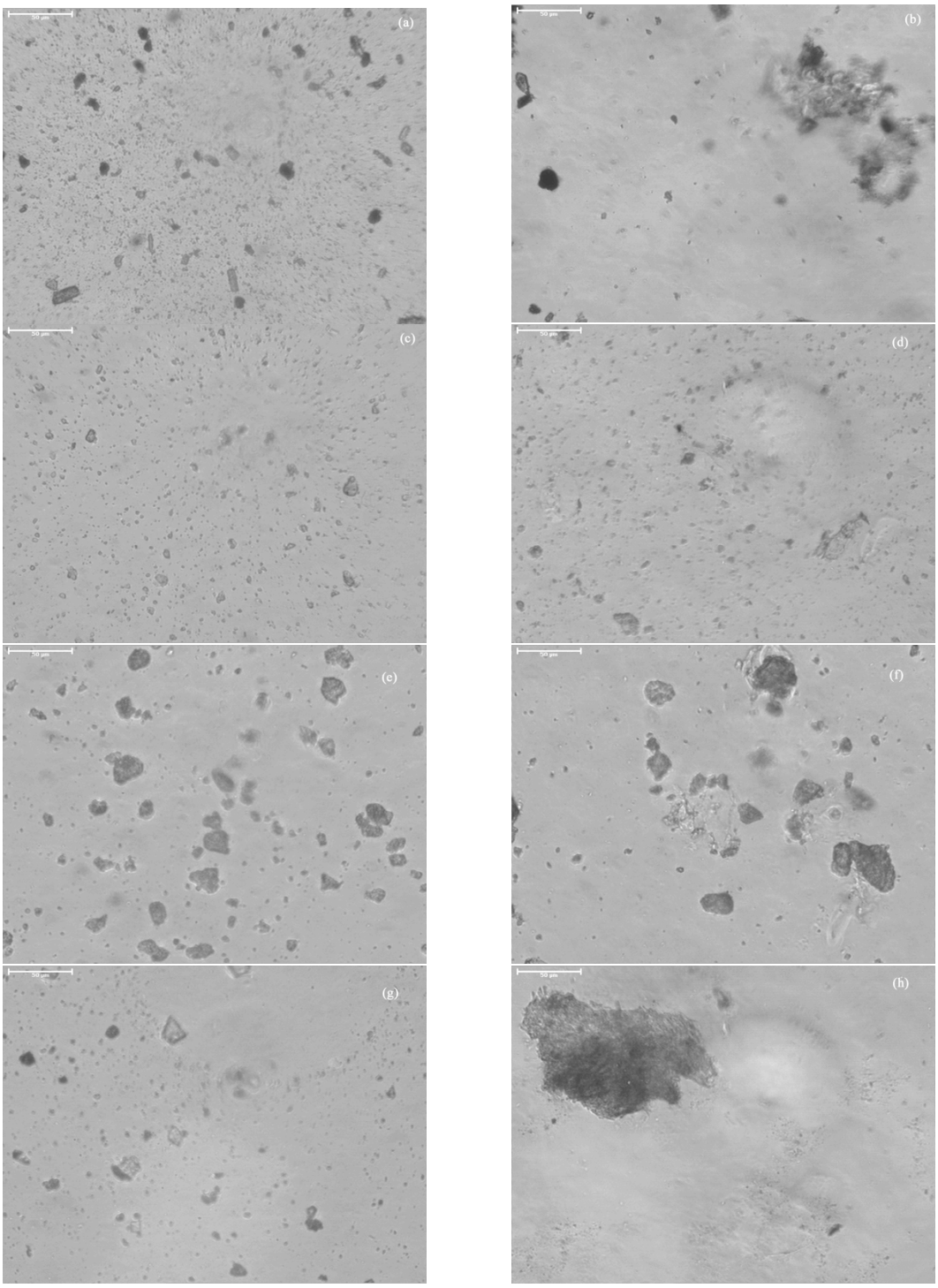

Figure 4.6 Optical microscope images showing the size and shape of flocs: (a) pure kaolinite; (b) kaolinite-EPS; (c) pure illite; (d) illite-EPS; (e) Ca-mont.; (f) Ca-mont.-EPS; (g) Na-mont.; and (h) Na-mont.-EPS (All scale bars: 50 μm).

bridging among different particles (because a larger portion of a polymer molecule may be adsorbed onto the surface of a single illite particle owing to its high charge); kaolinite with little layer charge and abundant surface hydroxyls on one of the two basal planes can interact

extensively with EPS molecules via hydrogen bond, and thus relatively larger flocs are formed; Na-mont. can swell to infinity and exfoliate into single 2:1 layers, and the layer charge is relatively small, and thus much larger flocs can be formed with EPS molecules.

4.3.2 Settling Velocity of Pure Clay and Clay-EPS Flocs

The clay-EPS flocculation and resulting alteration to the size of primary clay particles are expected to affect their settling velocity. Figure 4.7 shows the relationship between settling velocity and particle or floc size for both pure clays and clay-EPS mixtures. In general, the settling velocity increases with size for both pure clays and clay-EPS flocs of the same composition. The settling velocity of the pure clay flocs ranges from 0.07 to 0.9 mm s^{-1} at the corresponding size range of 10-60 μm, while that for the clay-EPS flocs 0.05 to 1 mm s^{-1} at the size range of 20-300 μm. Because the settling velocity is much smaller than the flow velocity of 150 mm s^{-1} in the PSA circulation system where the clay-EPS flocs were prepared, the flocs should not breakup during the settling process. The measured settling velocity of pure clays is consistent with some published data. For example, for particles/flocs taken from the suspensions of Yangtze and Jialing Rivers (China), their settling velocities are 0.016, 0.180, and 0.885 mm s^{-1} for floc sizes of 5, 16.9, and 36.8 μm, respectively (*Lu et al., 2010*); 0.001-3 mm s^{-1} for particles at a size of 1-300 μm in river or other freshwaters (*Droppo et al., 1997; Khelifa and Hill, 2006; Williams et al., 2008*). Due to the limitation imposed by the resolution of the optical microscope used in this study, the smallest particle size that can be analyzed is about 10 μm. Therefore, clay-sized (i.e., <2 μm) particles were not studied. An additional reason is that they took a long time (e.g., about 4 hours) to settle (*Moore and Reynolds, 1997*). Therefore, the particles from pure clay samples characterized in the settling process are mostly clay flocs.

The settling velocity data indicate that the pure clay flocs settle much faster than the porous and lighter clay-EPS flocs of the same size. The slope of the regression line in the log-log plot of settling velocity vs. floc size for clay-EPS flocs is smaller than that for primary clay particles, which indicates that clay particles or flocs are denser than the porous clay-EPS flocs. The reason is that both the internal structure and surface of flocs are heterogeneous and fractal in nature (*Jarvis et al., 2005*). Usually, higher-order compacted flocs have a lower density than lower-order compacted ones (*Loch, 2001*). The factor most affecting this is due to clay surface properties and resultant floc formation. Pure clay flocs form through flocculating individual clay particles by edge-edge, edge-face, or face-face interactions, and the floc size typically increases to 10-20 μm from <2 μm particles. However, the clay-EPS flocs were obtained by connecting the clay particles or flocs with EPS molecules through polymer bridging. In this case, the size increased from 10-20 μm to 200-300 μm with a higher-order packing. Therefore, the clay-EPS flocs have usually lower density than the pure clay flocs. In addition, even if the degree of packing is the same, the clay-EPS flocs are less dense than the pure clay flocs owing to the smaller density of pure EPS.

The effective density of the clay and clay-EPS flocs decreases as the floc size increases, while the settling velocity increases as the floc size increases (*Khelifa and Hill, 2006; Nguyen and Chua, 2011*). For flocs of the same composition, different sized ones have different densities and porosities, because the surface-area-to-volume ratio decreases as size increases, smaller flocs are more adsorptive per unit of mass (*Hill, 1998*). Another reason for the variation of settling velocity may be that, the porosity and permeability increase with floc size increasing, which

causes more creeping flow and relatively less drag force for larger flocs during settling (*Huang, 1993*). The density of EPS (guar gum) is smaller than that of clays. Incorporation of the EPS into flocs causes a decrease in flocs' density. Therefore, the clay-EPS flocs settle slower than the pure clay flocs. Examples of high-magnification images of clay flocs and clay-EPS flocs for settling analysis are shown in Figure 4.8. The clay-EPS floc (Figure 4.8 b) is much more porous and less dense than the clay flocs. In general, the density of flocs composited of expansive clays (i.e., Ca- and Na-mont.) is smaller than that of non-swelling clays (i.e., kaolinite and illite) (*Loch, 2001*).

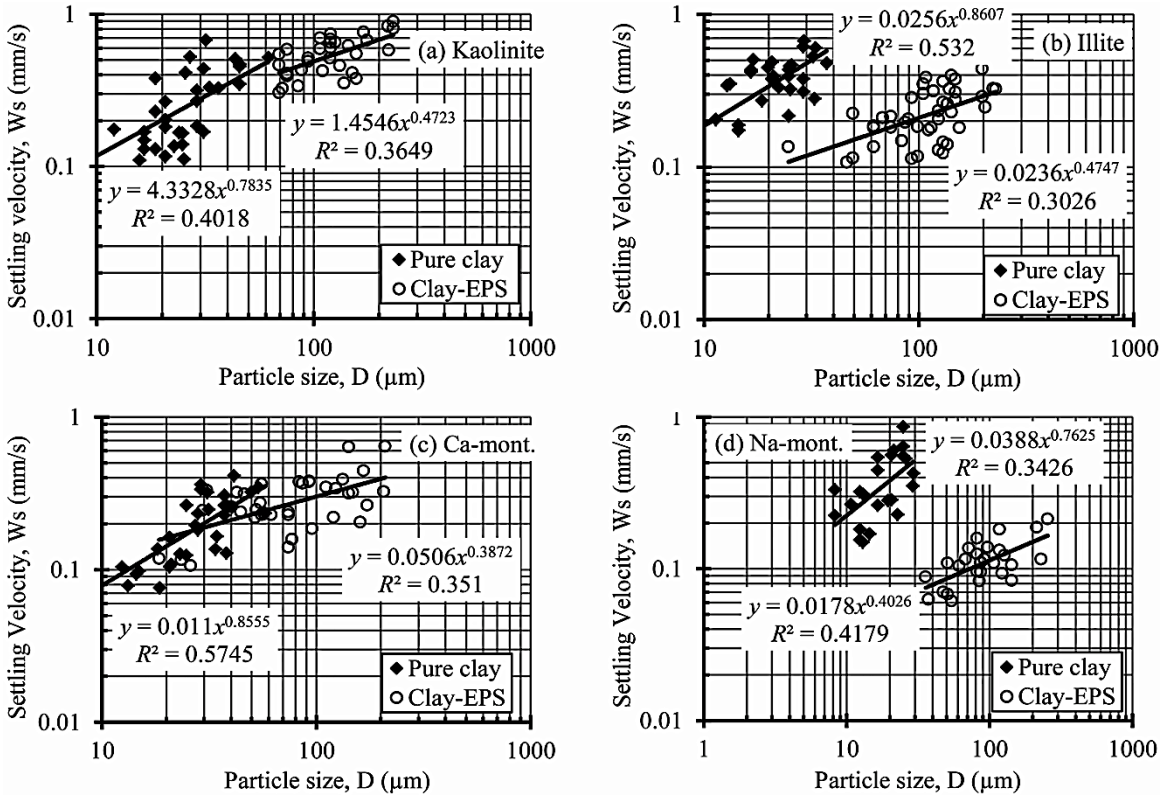

Figure 4.7 Settling velocity of pure clay and clay-EPS flocs.

In addition to the size, the settling velocity of a sediment floc has a complex relationship with its shape, porosity, and density. According to the literature (*Johnson et al., 1996; Winterwerp, 1998; Khelifa and Hill, 2006; Nguyen and Chua, 2011*), settling velocity (W_s) scales with D^{d-1} (Equation 4.2**):**

$$W_s \propto D^{d-1} \qquad \text{Equation 4.2}$$

where D is the floc size, and d the fractal dimension of the floc. Therefore, d can be found from the slope of the log-log plot of floc settling velocity against floc size, or (d-1) is equal to the slope of the linear relationship between log(W_s) and log(D). According to this relationship, the fractal dimension of pure clay flocs and clay-EPS flocs was estimated (Table 4.3) from the power-law regression equations shown in Figure 4.7. In general, pure clay flocs have a fractal dimension of 1.76 to 1.86, while the clay-EPS flocs 1.39 to 1.47. Owing to their swelling behavior, the fractal dimension of Ca- and Na-mont.-EPS flocs is expectedly smaller than that of the other two clays. Moreover, these values are consistent with published results. For example,

Engel and Schartau (1999) found that the fractal dimension of marine aggregates containing transparent EPS is 1.44, and *Miyahara et al. (2002)* reported the fractal dimension of Na-mont. flocs increases from 2.01 to 2.11 as the NaCl concentration increases from 0.5 to 3.0 M. Nevertheless, the higher *d* values of the pure clay flocs suggest that they are more compact than the clay-EPS ones. Moreover, these data also support the idea that the density of clay-EPS flocs is much smaller than that of pure clay flocs.

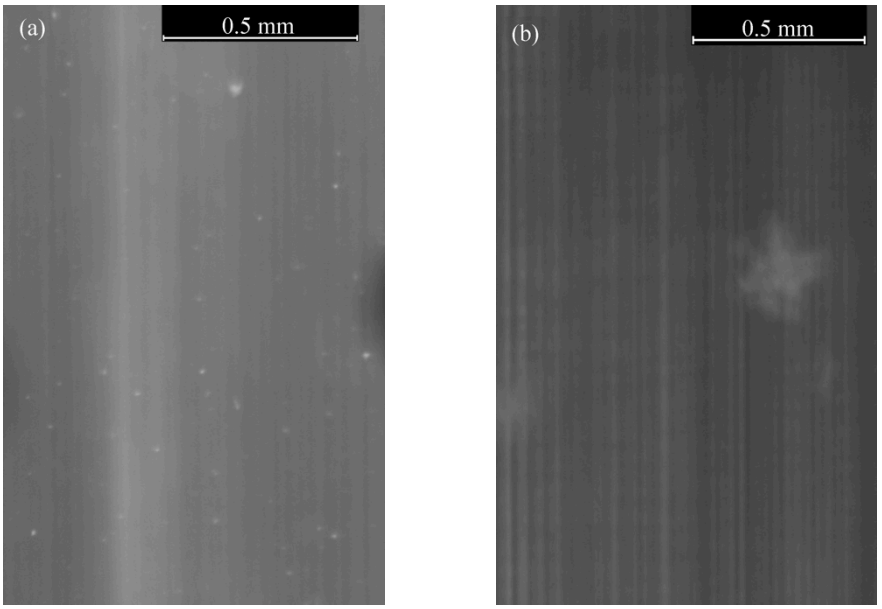

Figure 4.8 Representative images from settling velocity measurements: (a) several pure clay particles or flocs, and (b) one clay-EPS floc.

Table 4.3 Estimated fractal dimension of the pure clay and clay-EPS flocs.

Sample	kaolinite	illite	Ca-mont.	Na-mont.
pure clay flocs	1.78	1.86	1.86	1.76
clay-EPS flocs	1.47	1.47	1.39	1.40

4.4 Conclusions

A pilot experimental study was conducted to investigate the influence of a neutral exopolymer on the particle size and settling velocity of four types of cohesive sediments (i.e., kaolinite, illite, Ca-mont., and Na-mont.) in fresh water. In general, the presence of neutral EPS in natural waters dramatically changes the transport behavior of the four clays, including the flocculation, PSD, density, and settling velocity. The following conclusions can be drawn based on the experimental results:

(a) Neutral EPS significantly increase the size of suspended pure clay sediments, and the resulting clay-EPS flocs can be one order of magnitude larger than pure clay particles or flocs. Of the four studied clays, Na-mont. produces the largest clay-EPS flocs with sizes up to ~600 μm, while illite the smallest flocs with a maximum size of ~150 μm.

(b) For flocs or particles with the same composition (i.e., either pure clay or clay-EPS mixture), their settling velocity increases with size.

(c) The settling velocity of clay-EPS flocs is smaller than that of pure clay flocs of the same size. Additionally, fractal dimension of clay-EPS flocs is typically smaller than that of pure clay flocs. These indicate that the presence of neutral EPS significantly decreases the density of flocs, which results from the two possible reasons: (1) density of EPS is much lower than that of clay; (2) the bridging and bonding occurring between EPS and clay increase the porosity and make floc less dense.

(d) The fractal dimension of clay-EPS flocs estimated using the settling velocity data ranges from 1.39 to 1.47, which are much smaller than 3.0, suggesting that these clay-EPS flocs are not highly compacted but highly porous.

This work focused on the influence of a neutral exopolymer on the size of flocs generated under a laminar flow condition. Because other flow conditions (e.g., transitional and turbulent) also prevail in the field, it is recommended that further work is needed to take into account of these flow conditions, so that a complete understanding of floc sizes and settling velocity under different flow conditions can be achieved. Moreover, exopolymers with different polarity, such as anionic or cationic EPS, can also be included in future similar experimental studies.

4.5 Acknowledgments

This work was partially supported by the Office of Naval Research through Naval Research Laboratory base funding under Award No. N00173-10-1-G013 as part of the NRL ARI "Biogeochemical Influences on Cohesive Sediment Strength in Marine and Estuarine Environments (PE No. 061153N)". The facilities used in this study were purchased using the fund from the Louisiana Board of Regents Enhancement Program. X. Tan and H. Yin received partial support from the LSU Graduate School Supplement Award.

4.6 References

[1] Basile, P. A., Riccardi, G. A., Zimmermann, E. D., and Stenta, H. R. 2010. Simulation of erosion-deposition processes at basin scale by a physically-based mathematical model, *International Journal of Sediment Research*, 25, 91-109.

[2] Benchabane, A., and Bekkour, K. 2006. Effects of anionic additives on the rheological behavior of aqueous calcium montmorillonite suspensions, *Rheologica Acta*, 45, 425-434.

[3] Bennett, R. H., O'Brien, N. R., and Hulbert, M. H. 1991, Determinants of clay and shale microfabric signatures: processes and mechanisms, in Microstructure of Fine-Grained Sediments: From Mud to Shale, edited by R. H. Bennett, W. R. Bryant and M. H. Hulbert, pp. 5-32, Springer-Verlag, New York.

[4] Bhaskar, P. V., and Bhosle, N. B. 2005. Microbial extracellular polymeric substances in marine biogeochemical processes, *Current Science*, 88, 45-53.

[5] Celis, R., and Koskinen, W. C. 1999. Sorption and desorption of triadimefon by soils and model soil colloids, *Journal of Agricultural and Food Chemistry*, 47, 776-781.

[6] Cheng, Y., Brown, K. M., and Prud'homme, R. K. 2002. Characterization and intermolecular interactions of hydroxypropyl guar solutions, *Biomacromolecules*, 3, 456-461.

[7] Dontsova, K. M., and Bigham, J. M. 2005. Anionic polysaccharide sorption by clay mineras, *Soil Science Society of America Journal*, 69, 1026-1035.

[8] Droppo, I. G., Leppard, G. G., Flannigan, D. T., and Liss, S. N. 1997. The freshwater floc: A functional relationship of water and organic and inorganic floc constituents affecting suspended sediment properties, *Water Air and Soil Pollution*, 99, 43-53.

[9] Du, J. H., Morris, G., Pushkarova, R. A., and Smart, R. S. 2010. Effect of surface structure of kaolinite on aggregation, settling rate, and bed density, *Langmuir*, 26, 13227-13235.

[10] Elimelech, M., Gregory, J., Jia, X., and Williams, R. A. 1995. Particle deposition and aggregation - Measurement, modeling and simulation, Elsevier.

[11] Engel, A., and Schartau, M. 1999. Influence of transparent exopolymer particles (TEP) on sinking velocity of Nitzschia closterium aggregates, *Marine Ecology-Progress Series*, 182, 69-76.

[12] Furukawa, Y., Watkins, J. L., Kim, J., Curry, K. J., and Bennett, R. H. 2009. Aggregation of montmorillonite and organic matter in aqueous media containing artificial seawater, *Geochemical Transactions*, 10, 11.

[13] Ghimici, L., and Nichifor, M. 2009. Flocculation Properties of Some Cationic Polysaccharides, *Journal of Macromolecular Science Part B-Physics*, 48, 106-113.

[14] Hill, P. S. 1998. Controls on floc size in the sea, *Oceanography*, 11, 5.

[15] Huang, H. N. 1993. Porosity-size relationship of drilling mud flocs - Fractal structure, *Clays and Clay Minerals*, 41, 373-379.

[16] Jarvis, P., B., J., and P., S. A. 2005. Measuring floc structural characteristics, *Reviews in Environmental Science and Biotechnology*, 4, 1-18.

[17] Johnson, C. P., Li, X., and Logan, B. E. 1996. Settling velocities of fractal aggregates, *Environmental Science & Technology*, 30, 1911-1918.

[18] Khelifa, A., and Hill, P. S. 2006. Models for effective density and settling velocity of flocs, *Journal of Hydraulic Research*, 44, 390-401.

[19] Kobayashi, M., Adachi, Y., and Ooi, S. 1999. Breakup of fractal flocs in a turbulent flow, *Langmuir*, 15, 4351-4356.

[20] Kranck, K., and Milligan, T. 1980. Macroflocs - Production of marine snow in the laboratory, *Marine Ecology-Progress Series*, 3, 19-24.

[21] Kranenburg, C. 1994. The fractal structure of cohesive sediment aggregates, *Estuarine Coastal and Shelf Science*, 39, 451-460.

[22] Labille, J., Thomas, F., Milas, M., and Vanhaverbeke, C. 2005. Flocculation of colloidal clay by bacterial polysaccharides: effect of macromolecule charge and structure, *Journal of Colloid Interface Science*, 284, 149-156.

[23] Likos, W. J., and Lu, N. 2001. A laser technique to quantify the size, porosity, and density of clay clusters during sedimentation, *Geotechnical Testing Journal*, 24, 83-91.

[24] Liu, Q., Zhang, Y. H., and Laskowski, J. S. 2000. The adsorption of polysaccharides onto mineral surfaces: an acid/base interaction, *International Journal of Mineral Processing*, 60, 229-245.

[25] Loch, R. J. 2001. Settling velocity – a new approach to assessing soil and sediment properties, *Computers and Electronics in Agriculture*, 31, 305-316.

[26] McNown, J. S., and Malaika, J. 1950. Effects of particle shape on settling velocity at low Reynolds numbers, *Trans Am Geophys Union*, 31, 74-82.

[27] Miyahara, K., Adachi, Y., Nakaishi, K., and Ohtsubo, M. 2002. Settling velocity of a sodium montmorillonite floc under high ionic strength, *Colloids and Surfaces a-Physicochemical and Engineering Aspects*, 196, 87-91.

[28] Moore, D. M., and Reynolds, R. C. J. 1997. X-ray diffraction and the identification and analysis of clay minerals, pp212, 2nd ed., Oxford University Press,.

[29] Nguyen, H., and Chua, L. 2011. Simplified Physically Based Model for Estimating Effective Floc Density, *Journal of Hydraulic Engineering*, 137, 843-846.

[30] Pawlik, M., and Laskowski, J. S. 2006. Stabilization of mineral suspensions by guar gum in potash ore flotation systems, *Canadian Journal of Chemical Engineering*, 84, 532-538.

[31] Pruett, R. J., and Webb, H. L. 1993. Sampling and analysis of KGa-1b well-crystallized kaolin source clay, *Clays and Clay Minerals*, 41, 514-519.

[32] Theng, B. K. G. 1982. Clay-polymer interactions - Summary and perspectives, *Clays and Clay Minerals*, 30, 1-10.

[33] Thomas, D. N., Judd, S. J., and Fawcett, N. 1999. Flocculation modeling: A review, *Water Research*, 33, 1579-1592.

[34] Tripathy, T., and Rajan De, B. 2006. Flocculation: A new way to treat the waste water, *Journal of Physical Sciences*, 10, 93-127.

[35] Wientjes, R. H. W., Duits, M. H. G., Jongschaap, R. J. J., and Mellema, J. 2000. Linear rheology of guar gum solutions, *Macromolecules*, 33, 9594-9605.

[36] Williams, N. D., Walling, D. E., and Leeks, G. J. L. 2008. An analysis of the factors contributing to the settling potential of fine fluvial sediment, *Hydrological Processes*, 22, 4153-4162.

[37] Winterwerp, J. C. 1998. A simple model for turbulence induced flocculation of cohesive sediment, *Journal of Hydraulic Research*, 36, 309-326.

[38] Yang, C. T., Marsooli, R., and Aalami, M. T. 2009. Evaluation of total load sediment transport formulas using ANN, *International Journal of Sediment Research*, 24, 274-286.

[39] Zhang, Q.-H., Yan, B., and Wai, O. W. H. 2009. Fine sediment carrying capacity of combined wave and current flows, *International Journal of Sediment Research*, 24, 425-438.

CHAPTER 5 FLOCCULAITON AND PARTICLE SIZE ANALYSIS OF EXPANSIVE CLAY SEDIMENTS AFFECTED BY BIOLOGICAL, CHEMICAL, AND HYDRODYNAMIC FACTORS *

5.1 Introduction

Expansive clay sediments, such as smectite, vermiculite, and other mixed layer clays, are abundant in riverine and estuarine waters and bottom beds (*Nair et al.*, 1982; *Seo et al.*, 2009). For instance, the fine-grained marine sediment in deep Gulf of Mexico contains 26.2 wt.% smectite of all clay minerals (other non-expansive ones include 44.7 wt.% illite, 11.4 wt.% kaolinite, and 17.7 wt.% chlorite) (*Devine et al.*, 1972), and in the cohesive sediments from Mississippi River estuary, there are as much as 45 wt.% montmorillonite, but only 17 wt.% illite and 12 wt.% kaolinite (*Hiltabrand et al.*, 1973). As a member of the smectite group, montmorillonite is the best known and most common expansive clay. Basically, these clays, different from those non-swelling counterparts (e.g., kaolinite, illite, chlorite), expand or swell when they gain water and shrink when they lose water. According to the crystal structure, these clays belong to the 2:1 layer type with each layer consisting of two tetrahedral (T) silica sheets sandwiching a central octahedral (O) alumina sheet (Figure 5.1). Due to isomorphous substitutions such as the Si^{4+} by Al^{3+} in the T sheet and/or Al^{3+} by Mg^{2+} in the O sheet, these naturally occurring clays have permanent negative charges on face surfaces, which are balanced by positive counterions (also called "interlayer cations") adsorbed onto face surfaces. In these swelling clays, the interlayer cations are usually hydrated and also function as bonds to hold together adjacent 2:1 layers, resulting in relatively weak bonding. Smectite clays with Na^{+} or Ca^{2+} interlayer cations usually exhibit a higher expansive capability. Therefore, for these clays, the potential of water penetration into the interlayer spacing is much higher compared with those non-swelling kaolinite, illite, and chlorite (*Luckham and Rossi*, 1999). Additionally, at the edge surface of each clay, the broken Si-O and Al-O covalent bonds expose and bestow them a pH dependent charge: positive and negative in acidic and alkaline conditions, respectively (*van Olphen*, 1964).

Cohesive sediments usually exhibit a wide range of particle sizes even in pure water at a steady state condition, owing to their special properties such as irregular particle shape, flexible layer, heterogeneous layer charge, pH dependent edge charge, and various modes of flocculation (*Lagaly and Ziesmer*, 2003; *Murray*, 2000; *Wu*, 2001). For expansive clays, their swelling nature also renders them to change their sizes with swelling, and different interlayer cations can further alter the degree of swelling (*Kleijn and Oster*, 1982) and hence particle sizes. The natural sediment-water system is usually loaded with various types of organic matter, background ions, and flow conditions, which can further alter the aggregation or flocculation of expansive clays by different mechanisms (*Hill*, 1998; *Mietta et al.*, 2009). Complex change in the particle size of expansive clays can result from the increase in interlayer space, layer exfoliation, and flocculation under different biological, chemical, and hydrodynamic conditions. Besides, flocculation and associated size change usually generate flocs with relatively smaller density in

* Reprinted by permission of *Ocean Dynamics*, Springer.

the order of 50-300 kg/m^3 (*Winterwerp*, 1998), which alters the settling velocity and hence the transport and fate of cohesive sediment. Knowledge of their intrinsic particle size distributions (PSD) and variations in different biological, chemical, and hydrodynamic conditions is of key importance to the understanding of sediment hydrodynamics and transport in natural waters, nutrient or contaminant removal from water column, and the influence of involved organic matter on sediment yield (*T S Chang et al.*, 2006; *Hill*, 1998; *van Leussen*, 2011).

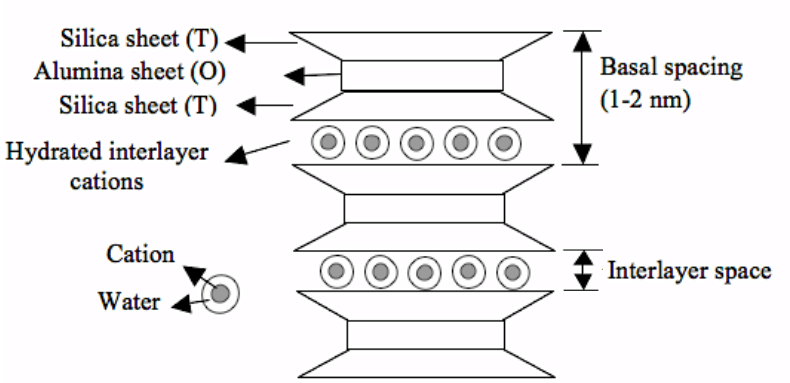

Figure 5.1 A schematic diagram showing the montmorillonite structure.

One type of the abundant, naturally occurring organic matter is the extracellular polymeric substances (EPS), which may vary significantly in different seasons and locations. Their concentration in natural waters typically ranges from 0 to ~1000 μg/g (*Gerbersdorf et al.*, 2009; *Hirst et al.*, 2003). Owing to the chemically active surfaces of clays, EPS can interact extensively with clay particles via a series of mechanisms, including polymer bridging, polymer intercalation into the interlayer space of expandable clays, ion-dipole interaction on clay surfaces, hydrogen bonding, and electrostatic forces (*Lagaly et al.*, 2006; *Theng*, 1982). Depending upon their type, concentrations and polarity, EPS can facilitate the flocculation of clay sediments and hence result in the change in the PSD. Moreover, the existence of permanent negative charges on clay face surfaces results in the formation of an electrical double layer (DL), which can be altered by the concentration of cations or salinity in the suspension liquid. The pronounced cation exchange capacity (CEC) of expansive clays also enables the exchange of the interlayer cations with different background cations, resulting in swelling or shrinkage. Therefore, the presence of salt (including different ions) in riverine or estuarine waters can lead to the compression of the DL as well as the exchange of interlayer cations, and hence the flocculation of primary clay particles or strengthening of the clay flocs may take place. The stability and strength of clays flocs can in turn change the PSD under different hydrodynamic conditions that can exert flow-induced shear stress to breakup larger flocs into smaller ones or help grow smaller flocs into larger ones (*Jarvis et al.*, 2005; *Yeung et al.*, 1997).

Due to the distinct crystal structure and properties of expansive clays, their particle sizes are more sensitive to different solvents and environmental conditions. Additionally, the natural water systems are usually very complex, and the in-situ monitoring of cohesive sediment flocculation behavior is difficult. Therefore, this paper presents a laboratory study of the flocculation behavior and particle size change of expansive clay sediments under controlled conditions in order to isolate different factors influencing the flocculation of expansive clays. The major objective of this study was to characterize the intrinsic PSD and PSD variations of

two common swelling clays, a Ca- and a Na-montmorillonite, affected by different dispersion methods, different solvents, as well as the presence of EPS, salt, and different hydrodynamic conditions.

5.2 Materials and Methods

The flocculation behavior and PSD of two selected expansive clays were characterized by a laser based particle size analyzer installed with a liquid circulation system. To evaluate their intrinsic PSD, different dispersion methods, including dispersing in solvents of varied polarity (i.e., water and alcohol), with and without chemical dispersant or ultrasound disintegration, and dry dispersing in air. Three different EPS at various concentrations were selected to evaluate the influence of biological factors on their PSD. Salt water with different, gradient salinities was then used to study the influence of chemical factors. Finally, the hydrodynamic conditions were varied by controlling the flow speed in the liquid circulation system of the particle size analyzer. In summary, a total of 10 particle size tests (2 samples and 5 dispersion methods for each sample) was performed to measure the intrinsic PSD, and of 90 tests to characterize the influences of 3 different EPS at 3 concentrations, 4 salinities, and 3 hydrodynamic conditions on the PSD of two clays.

5.2.1 Materials

5.2.1.1 Expansive Clays

Two members of montmorillonite, a Ca-montmorillonite (Ca-M) and a Na-montmorillonite (Na-M), from the US Clay Minerals Society Source Clay Repository, were chosen as the representatives of the limited and unlimited swelling clays, respectively. Their geographic origin and basic properties are summarized in Table 5.1. The main interlayer cations are Ca^{2+} for Ca-M and Na^{+} for Na-M, which are both hydrated in these two clays. Na-M swells much more than Ca-M in suspensions, which could lead the formation of exfoliated 2:1 layers as individual particles. However, in a nonpolar or less polar liquid such as ethyl alcohol, these two clays do not readily swell.

Table 5.1 Origin and basic properties of the two expansive clays[a].

Name	Origin	CEC (meq/100g)	Layer charge[b] (*unbalanced*)	SSA[c] (m^2/g)	pH[d]	Chemical formula
Ca-montmorillonite (STx-1b)	Gonzales County, Texas	84.4	-0.34 (*-0.04*)	83.79	6.44	$(Ca_{.27}Na_{.04}K_{.01})$ $[Al_{2.41}Fe^{3+}_{.09}Mn_{tr}Mg_{.71}Ti_{.03}]$ $[Si_{8.00}]O_{20}(OH)_4$
Na-montmorillonite (SWy-2)	Crook County, Wyoming	76.4	-0.28 (*+0.025*)	31.82	7.32	$(Ca_{.12}\ Na_{.32}\ K_{.05})$ $[Al_{3.01}\ Fe^{3+}_{.41}\ Mn_{.01}Mg_{.54}Ti_{.02}]$ $[Si_{7.98}\ Al_{.02}]\ O_{20}(OH)_4$

[a] All data are from the Clay Minerals Society Source Clay Data Sheets.
[b] The layer charge is based on per $O_{10}(OH)_2$ unit.
[c] SSA = specific surface area.
[d] pH of suspension at concentration of 0.4 g/L in deionized water.

5.2.1.2 Chemical Reagents

To evaluate the influence of different chemical factors on the PSD and hence obtain the intrinsic PSD of the two clays, deionized (DI) water, ethyl alcohol (EA), and Na-hexametaphosphate (NaHMP) were selected as a polar solvent, less polar solvent, and chemical dispersant, respectively, to prepare clay suspensions for subsequent particle size analysis. The alcohol, 190 Proof (95% purity), was purchased from Pharmco-AAPER. The NaHMP was obtained from Mallinckrodt Baker Inc., Philipsburg, NJ. According to the American Society for Testing and Materials (ASTM) Method D422-63 (*D422-63*, 2007), a NaHMP solution with a concentration of 40 g/L was used as the liquid for clay suspension preparation. In addition, an Instant Ocean® sea salt was chosen to prepare clay suspensions with varied salinities.

5.2.1.3 EPS

Interaction of clay and EPS typically depends on the charge or polarity of EPS, thus EPS can be roughly classified into three types: anionic, neutral, and cationic (*Theng*, 2012). To account for a variety of microbial EPS in natural waters, polyanionic xanthan gum (Spectrum®, Gardena, CA), neutral guar gum (Fisher ChemAlert® Guide, Rochester, NY), and polycationic chitosan (Acros Organics, New Jersey, USA) were chosen as the EPS representatives that may induce flocculation of clay sediments. In fact, all of the three EPS have been widely used and studied as coagulants (*Chen and Chung*, 2011; *Gupta and Ako*, 2005; *N.V and Kumar*, 2000; *Sashiwa and Aiba*, 2004; *Yokoi et al.*, 1996; *Yokoi et al.*, 1998). Their chemical structure is shown in Figure 5.2. Xanthan gum is a water-soluble bacterial extracellular polysaccharide produced through fermentation by *Xanthomonas campestris* bacterium. Due to different bacterial strains and the growth environments, the molecular weight of xanthan varies but typically ranges 0.9 - 1.6 x 10^6 Da (*Ian W*, 1994). As shown in Figure 5.2 a, xanthan consists of *β*-(1,4)-*D*-glucopyranose glucan backbone with extended side chains of (3→1)-*α*-linked *D*-mannopyranose-(2→1)-*β*-*D*-mannopyranose on alternating residues. Its negative charge is from the carboxylic acid groups (-COOH) in glucuronic acid and pyruvic acid groups on side chains (*Ian W*, 1994). Guar gum is a water-soluble polysaccharide extracted from guar beans with a molecular weight of up to 2 x 10^6 Da (*Nugent et al.*, 2009; *Risica et al.*, 2005). It is not a true

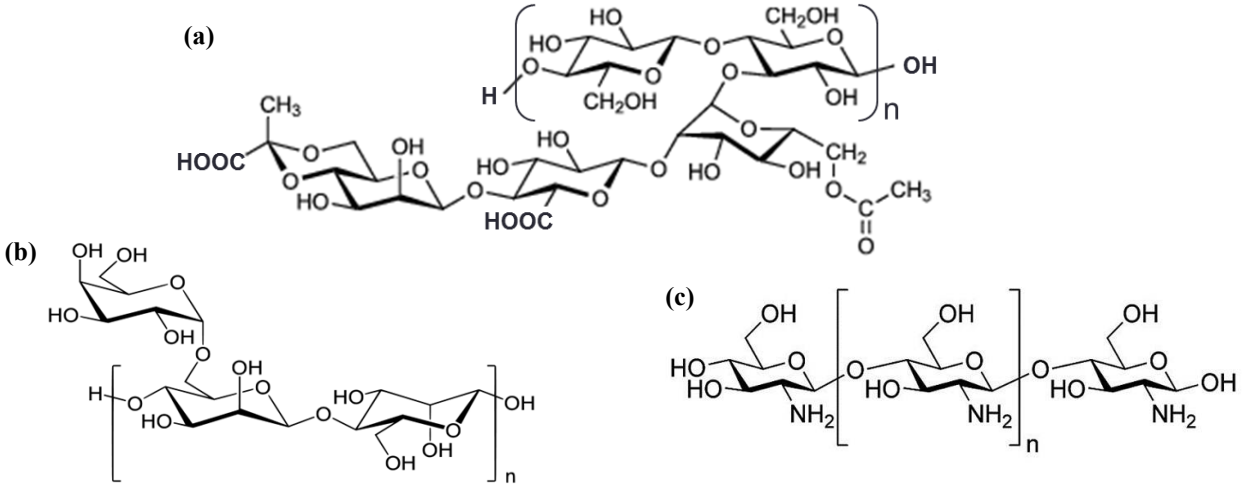

Figure 5.2 Chemical structure of (a) xanthan gum, (b) guar gum, and (c) 100% deacetylated chitosan.

exopolymer, but usually used as an EPS analog representative of neutral microbial exopolymers. Guar gum structurally consists of long, liner chains of *α-D*-manopyranosyl units linked together by *β-D*-(1,4)-glycosidic linkage mannose residues with a *α*-(1,6) linked *D*-galactose. There are 1.5-2 mannose residues for every galactose residue in average. Upon dissolving, guar gum can produce viscous, pseudoplastic aqueous solutions. Chitosan is obtained from the deacetylation process of chitin, which is the supporting material of shrimp and crab shells and other crustaceans or insects (*N.V and Kumar*, 2000). It is composed of *β*-(1,4) linked *D*-glucosamine without side chains. The molecular weight is 1 - 3 x 10^5 Da, and its positive charge is from the hydrolysis of amino groups in water.

5.2.2 Preparations and Size Analysis of Clay Suspensions

The PSD of the two expansive clay samples and clay-EPS mixtures was characterized by a Cilas® 1190 particle size analyzer (PSA) (Cilas Particle Size, Madison, WI, USA) (Figure 5.3). This instrument can perform measurement in both liquid mode and dry mode. In the liquid mode, a sample is dispersed in a liquid (usually water) bath assisted by a stirrer and/or a built-in ultrasound disperser, and then the suspension is continuously circulated by a peristaltic pump whose speed can be varied. The dry mode is designed to measure the PSD of dry powdery samples without the need of preparing a suspension. Instead, a dry powdery sample is directly placed in the vibrating bowl of a mass distributor. The optimal dispersing parameters, including the vibrator's frequency and cyclic ratio of vibration, and air pressure are usually obtained by trial and error. In this work, the dry mode was only chosen to evaluate the intrinsic PSD of the two expansive clays.

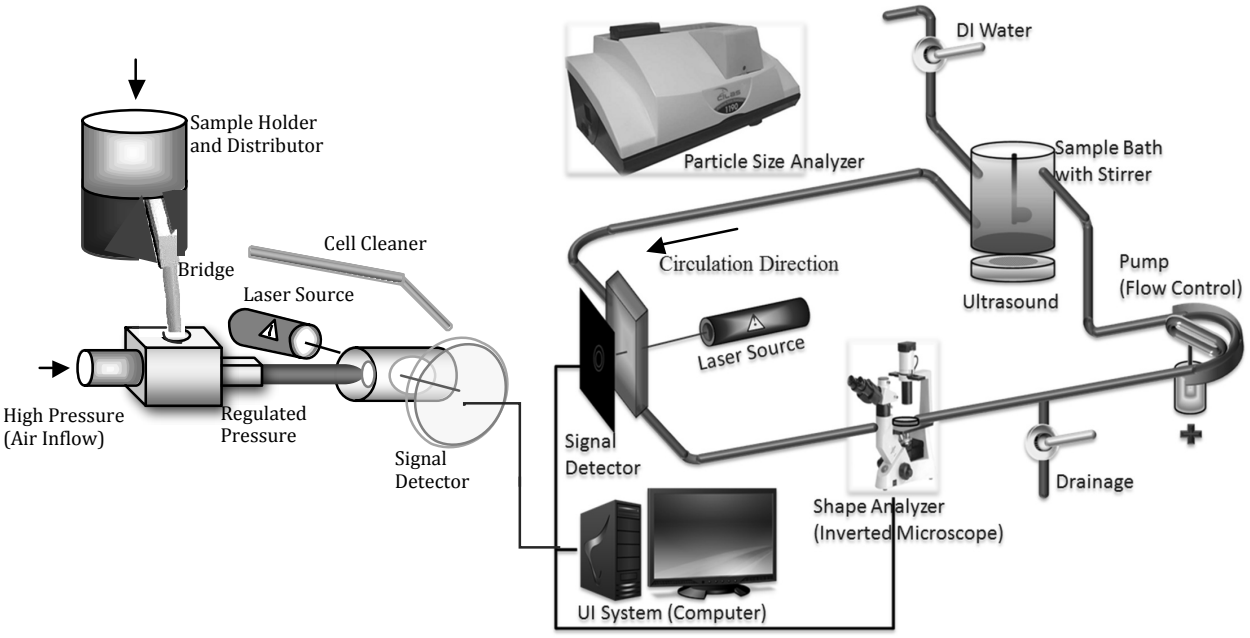

Figure 5.3 Schematic diagrams of dry mode system (left) and liquid dispersion and circulation system (right) in the PSA.

Both pure clay and clay-EPS suspensions were prepared for size analysis under the liquid mode. For each of the two clays, 0.2 g dry powder was soaked overnight with DI water, followed by dilution with DI water into a 500 mL (which was the total volume of the PSA's liquid

circulation system, including the liquid bath and connecting pipes) clay suspension with a final concentration of 0.4 g/L in the PSA liquid system while both the stirrer and pump were running at their lowest speed. The flow pattern inside this PSA liquid circulation system is very complex because it consists of several different sections with different flow areas (i.e., the stirring bath, flow pipe, connection parts, the laser diffraction and optical microscope observation windows, and squeezed section of the pipe in the peristaltic pump). Therefore, different flow conditions are expected to take place in different sections of the pipe. However, because other sections were very short and hence their effects could be ignored, only the hydrodynamic conditions of flow in the stirring bath and pipe were specifically considered in this study. Reynolds number (R_e) and average shear rate (G) of these two parts are calculated as below:

(1) In stirring bath

According to (*Camp and Stein*, 1943) and (*Spicer and Pratsinis*, 1996), the Reynolds number is

$$R_e = \frac{\rho * \Omega * D_A^2}{\mu} \qquad \text{Equation 5.1}$$

and the average shear rate is

$$G = \sqrt{\frac{\bar{\varepsilon}}{v}} \qquad \text{Equation 5.2}$$

and $\bar{\varepsilon}$, the average turbulent energy dissipation per unit time and mass, is

$$\bar{\varepsilon} = \frac{N_p * \Omega^3 * D_A^5}{V} \qquad \text{Equation 5.3}$$

where ρ is the fluid density, Ω the angular velocity of impeller, D_A the impeller diameter, μ the fluid dynamic viscosity, v is the kinematic viscosity of the liquid, N_p the power number of stirrer (*Holland and Chapman*, 1966), and V the volume of the stirring bath.

(2) In pipe

The Reynolds number for pipe flow is

$$R_e = \frac{\rho * v_0 * D_0}{\mu} \qquad \text{Equation 5.4}$$

According to (*Eirich*, 1967) and (*Matsuo and Unno*, 1981), the average shear rate for laminar pipe flow is

$$G = \frac{2Q}{\pi * R_0^3} = \frac{2v_0}{R_0} \qquad \text{Equation 5.5}$$

According to (*Camp and Stein*, 1943), the average shear rate for transient and turbulent pipe flow is

$$G = \sqrt{\frac{f * v_0^3}{v * 8R_0}} \qquad \text{Equation 5.6}$$

where ρ is the fluid density, v_0 the mean flow velocity in pipe, D_0 the internal diameter of pipe, μ the fluid dynamic viscosity, Q is the flow rate in pipe, R_0 the internal radius of pipe, v the kinematic viscosity of liquid, and f the friction factor (*Moody*, 1944) as

$$f = 0.316 * R_e^{-0.25} \qquad \text{Equation 5.7}$$

Flocculation of clay particles and EPS molecules in suspension took place in the PSA's liquid bath where continuous stirring caused collisions of clay to clay and clay to EPS molecules. At the same time, the suspension in the liquid bath was circulated in the pipe circulation system. For all particle size analyses, sufficient time (usually 15-20 mins) was allowed for the clay suspension in the circulation system to reach a steady state (i.e., no further significant change in the measured PSD curves even for a prolonged period of liquid circulation). As illustrated in Figure 5.4, no significant change can be observed among the PSD curves captured at a circulating time of 6, 12, and 18 mins for a typical clay-EPS sample. After validating that a steady state was reached, particle size analysis was then conducted in the Cilas PSA. The following sets of experiments were performed, each with its specific purposes:

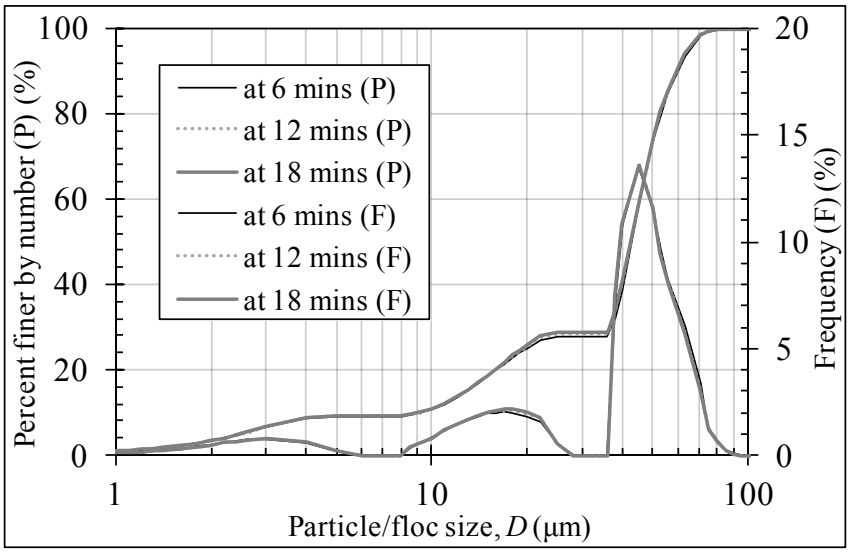

Figure 5.4 Example PSD of a clay sample (Ca-M with 100 μg/g guar gum at high pump speed) after dispersed for 6, 12, and 18 mins in the PSA.

(1) To obtain the intrinsic PSD, the two clays were dispersed in DI water, EA, NaHMP solution (in DI water), and in dry mode. To achieve better dispersion, the built-in ultrasound disperser was turned on for this process, and the stirrer and pump were running at a speed of 180 rpm and 30 rpm, respectively.

(2) To investigate the effect of some microbial EPS on the flocculation of the two expansive clays, each of the three EPS was first dissolved in 50 mL DI water assisted by a magnetic stirrer for 30 mins mixing (to ensure that the EPS were evenly wetted), followed by mixing the EPS solution into the clay suspensions. For each EPS, three different final EPS

concentrations of 1, 10, and 100 μg/g were prepared, leading to totally 9 different EPS solutions and 18 different clay-EPS suspensions. No chemicals were added to these suspensions for further dispersion in this process.

(3) To examine the chemical influence (i.e., salinity) on the PSD, the aforementioned sea salt was used to prepare salt water at 0, 5, 10, and 35 ppt salinities to simulate the salinity gradient change from river to ocean in estuaries.

(4) To investigate the effect of hydrodynamic conditions on the PSD, the peristaltic circulation pump driving liquid flow in circulation system was run at 3 different speeds (i.e., low (30 rpm), medium (120 rpm), and high (240 rpm)), while the stirrer's speed remained the same at 180 rpm. Based on a careful calibration, these three pump speeds resulted in the approach flow velocities of 0.15, 0.4, and 0.8 m/s for the liquid inside the circulation system, respectively. To minimize the influence of hydrodynamic shear force on the particle size analysis, the lowest pump speed (i.e., 30 rpm or 0.15 m/s for flow velocity) was selected for evaluating the intrinsic PSD and the influence of biological and chemical factors on the PSD of the two clays.

Finally, in this paper, the particle size obtained by the Cilas PSA is defined as the diameter of equivalent spheres calculated based on the volume moment mean value of multiple particles at a given size range. That is:

$$D = \frac{\sum n*l^4}{\sum n*l^3} \qquad \text{Equation 5.8}$$

where D is the mean diameter of all flocs and particles within a given size range, n the number of particles at a fixed size, and l the diameter of a particle or floc.

5.3 Results and Discussion

5.3.1 Intrinsic PSD

All PSD curves of the two expansive clays obtained by different dispersion methods are shown in Figure 5.5. Both clays exhibit multimodal, lognormal PSD curves consisting of primary particles (submicron to 1-2 μm) and flocculi (10-20 μm) (*Lee et al.*, 2012), except those obtained by the dry dispersion method. In fact, the dry method yields the largest particle sizes of 100 and ~600 μm for the Ca-M and Na-M, respectively. The PSD curve obtained by the dry dispersion method is situated at the rightmost location (Figure 5.5), indicating that these two as-received powdery clay samples are not readily dispersed by dry dispersion in air. In other words, their intrinsic PSD cannot be obtained by dry dispersion.

The two as-received clay samples possess some impurities, which are usually greater than clays (*Mermut and Cano*, 2001; *Mosser-Ruck and Cathelineau*, 2004). In fact, according to their Materials Safety and Data Sheets, the Ca-M and Na-M contain 1-5 wt.% and 5-10 wt.% quartz as impurity, respectively. In addition, some clay particles may be greater than 2 μm. Therefore, the <2 μm fractions of the two samples were also extracted via sedimentation (i.e., gravitational settling for 3.5 hours (Moore and Reynolds, 1997)). The leftmost curves in Figure 5.5 are obtained from the <2 μm fractions of the two samples, and both curves show the existence of particles of <2-3 μm. This can also serve as an indirect and partial calibration of the Cilas PSA.

For Ca-M, the PSD of the <2 μm fraction shows a bimodal distribution with two maxima at 0.6 and 1.8 μm, respectively. The PSD of Na-M's <2 μm fraction exhibits a monomodal distribution with one maximum at 1.6 μm, which agrees well with previous results (e.g., a peak maximum at ~1.3 μm (*Poli et al.*, 2008; *Theng*, 1982)).

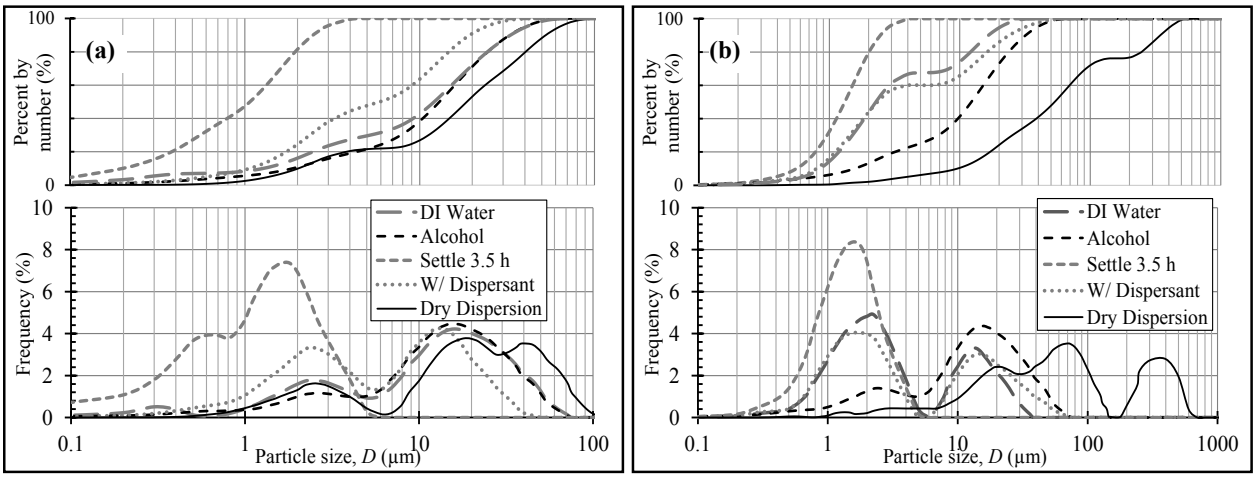

Figure 5.5 Effects of different dispersion methods on the PSD of (a) Ca-M and (b) Na-M.

The Ca-M has limited swelling in water and remains its layer structure, since Ca-M doesn't swell beyond a basal spacing of 1.9 nm (*Theng*, 1982) and this spacing is relatively stable under stirring, sonication, or certain pressure (*Kjellander et al.*, 1988; *Laird*, 2006). Thus, each particle is a stack of parallel 2:1 layers (also called "*tactoid*"). However, the basal spacing of Na-M in water can reach as high as 9 nm (*Olejnik et al.*, 1974). Thus, the highly swelling Na-M particles can exfoliate into individual 2:1 layers of ~1.0 nm in thickness. Such thin 2:1 layers (as individual particles) can easily curl up in the circulation system. As a result, the <2 μm fraction of Na-M shows a monomodal distribution.

It is also interesting to compare the PSD of the two clays dispersed in three different solvents: water, alcohol, and NaHMP solution. From Figure 5.5 a and b, the D_{50} in DI water and alcohol is 12 and 13 μm for Ca-M, and 2.3 and 13 μm for Na-M, respectively. The particle size of both clays in DI water is smaller than that in alcohol, and the difference for Na-M is greater than that of Ca-M. The dielectric constant (at 20-25°C) of DI water and ethyl alcohol is 80.4 and 24.3, respectively. If the interlayer space of swelling clays were filled with alcohol, the interlayer attraction force (i.e., Coulomb force) would be much stronger, thus preventing the swelling of montmorillonite. In fact, either Na-M or Ca-M does not swell in pure alcohol (*Brindley et al.*, 1969). As mentioned above, Na-M can swell to infinity in water, and hence one single 2:1 layer is a particle. Therefore, Na-M in water exhibits a much finer PSD than in alcohol. For Ca-M, the difference of the PSD in water and alcohol is not significant, even though it swells in water but not in alcohol. This can be reasoned by the fact that the increase in particle size caused by swelling in water is counterbalanced by the decrease in particle size caused by the exfoliation (which in turn is promoted by the flow-induced shearing). In addition, when compared with the <2 μm fraction (i.e., after settling for 3.5 hrs), each clay in water has almost the same PSD peaks, but with one more larger-sized peak, which is likely due to the existence of impurity, flocs, or bulk sample residue (*Pruett and Webb*, 1993).

Finally, for Ca-M, dispersion in the NaHMP solution results in a much finer PSD than in water, due to partly the cation exchange of Ca^{2+} by Na^{+} and partly the reversal of positive edge charge by $(PO_3^-)_6$. The former can definitely results in smaller particles, while the latter can reduce the tendency of clay flocculation. For Na-M, the PSD in the NaHMP solution and water are nearly the same. Therefore, adding Na-based dispersant such as NaHMP may generate misleading results for both clay samples, and this is particularly the case for Ca-M.

In summary, due to their swelling nature, both Ca-M and Na-M exhibit different PSD in different dispersion liquids. Dry dispersion in air cannot yield accurate results for clays. The intrinsic particle size of both Ca-M and Na-M should be measured in alcohol or other liquids that should not cause significant swelling. The desired particle size should be determined by dispersion under conditions representative of the environment where the swelling clays are present.

5.3.2 Effects of EPS

The influence of different EPS at various concentrations (all in zero salinity) on the flocculation of expansive clays is summarized in Figure 5.6 and Figure 5.7. All of the three EPS, anionic xanthan, neutral guar, and cationic chitosan, can change the particle size or cause flocculation of both clays. For all three EPS, the Ca-M always exhibits a tri-modal distribution, while the mode of distribution of the Na-M changes with the concentration of xanthan and guar gum. The molecule length of xanthan, guar, and chitosan can be estimated as 1.95-3.47, 4.13-8.25, and 1.24-3.72 μm, respectively, using a published approach (*I Chang and Cho*, 2012). Such molecular lengths are in the same size range of clay particles (i.e., mostly <2 μm), and hence flocculation of the two expansive clays through polymer bridging is possible for all of the three EPS.

As shown in Figure 5.6a, xanthan gum causes little additional flocculation of Ca-M. As xanthan concentration increases from 0 to 1, 10, and 100 μg/g, the D_{50} of Ca-M increases from 32.4 to 32.8, 32.8, and 33.5 μm (Figure 5.7 a). Such small changes can be ignored when compared with the influence of the other two EPS. In the primary xanthan structure (Figure 5.2a), the anionic side chains are very close to each other, resulting in a high charge density and strong electrostatic repulsion, and hence xanthan keeps a rigid double helix conformation, which does not facilitate bridging (*Labille et al.*, 2005). Although the optimum concentration of 10 μg/g xanthan used as a flocculating agent for kaolin was reported (*Yokoi et al.*, 1996), the negative layer charge of Ca-M (-0.34, Table 5.1) is usually much higher than that of kaolin (typically -0.03), and thus the repulsion between Ca-M particle and xanthan molecule is much stronger. Additionally, anionic xanthan molecules cannot enter into the interlayer of swelling clays (*Benchabane and Bekkour*, 2006; *Theng*, 1982). Xanthan gum interacts only with the clay surface principally through an adsorption mechanism, which may be the electrostatic attraction between the negatively charged xanthan and positively charged clay edges at pH <7 (Table 5.1), and/or the hydrogen bonding between the carboxyl groups on xanthan side chains and the oxygen of the clay lattice (Figure 5.8 a) (*Theng*, 1970).

For the highly swelling Na-M, the addition of a very small amount of xanthan (1 μg/g) causes no change in the PSD. As xanthan concentration increases to 10 μg/g, the D_{50} increases from 2.3 to 2.9 μm and one extra peak appears at ~30-40 μm, while the other two peaks at the

smaller size ranges become smaller. This indicates that flocculation takes place, resulting in the formation of coarser flocs that are not previously present. As the xanthan concentration continues to increase to 100 μg/g, the PSD becomes even finer than that of the pure clay with no xanthan, which is further explained below.

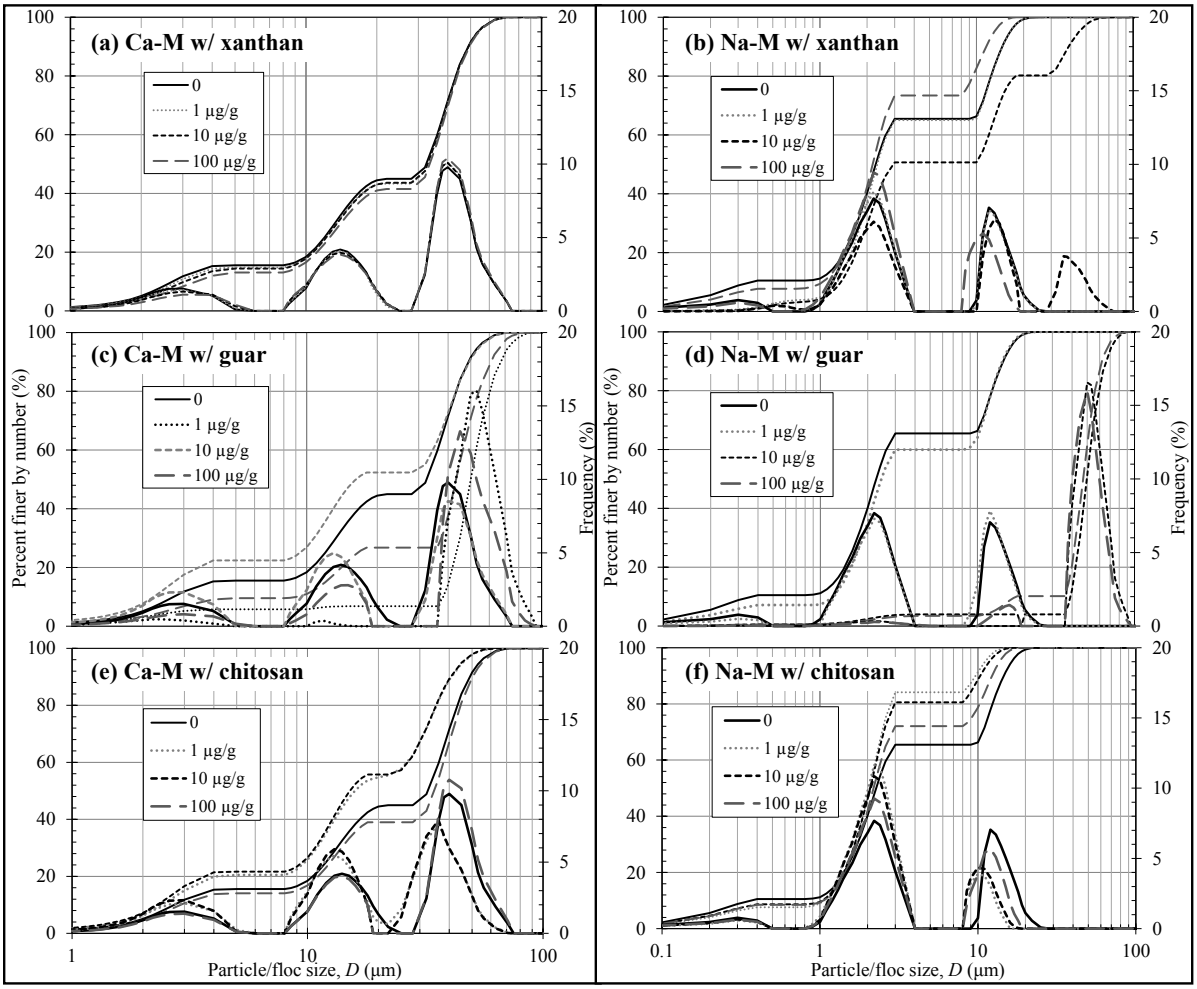

Figure 5.6 Effect of EPS on the PSD of Ca-M and Na-M at different concentrations (low pump speed).

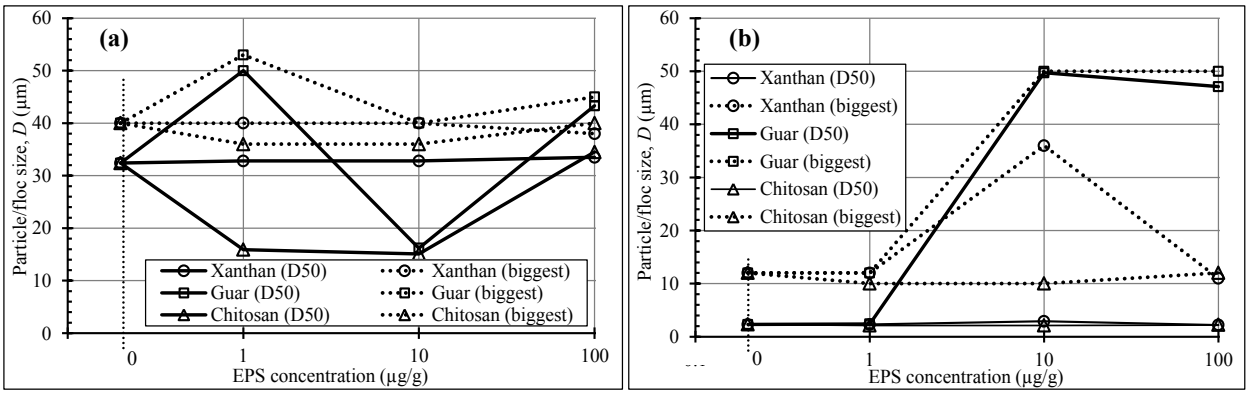

Figure 5.7 The D_{50} and largest floc size of (a) Ca-M and (b) Na-M with the EPS at different concentrations.

The difference in the interaction of Ca-M and Na-M with xanthan is caused by three mechanisms: (1) the negative layer charge of Ca-M is higher than that of Na-M (Table 5.1), which results in a higher electrostatic repulsion force between Ca-M and xanthan, preventing flocculation of Ca-M with xanthan; (2) the charge location is different: the isomorphous substitution in Ca-M exists only in octahedral sheets, while that in Na-M happens in both octahedral and tetrahedral sheets. The tetrahedral charges form stronger bonds with surface adsorbed cations than the charges in the sandwiched central octahedral sheets (Figure 5.1), which promotes the adsorption of xanthan to Ca-M through cation bridging via divalent Ca^{2+}, particularly in the presence of a background electrolyte (*Dontsova and Bigham*, 2005). For the highly swelling Na-M, since each 2:1 layer is an individual particle, more cations expose to water and hence attract the anionic parts of xanthan, which facilitates the flocculation at lower xanthan concentrations; (3) the unbalanced charge of the two clays are totally different, -0.04 for Ca-M and +0.025 for Na-M (Table 5.1). The negative unbalanced charge of Ca-M bestows the dominance of repulsion between xanthan. The small amount of positive unbalanced charge (i.e., caused by adsorbed cations) tends to attract and be balanced by the negative xanthan at low concentrations, which promotes the flocculation. However, in the high EPS concentrations (e.g., 100 μg/g), the negative charge density increases and the repulsion between particles also increases, preventing particles from flocculation as discussed in the previous two mechanisms. Such a reduction in the degree of flocculation may also be caused by the higher viscosity of the xanthan solution with a higher concentration, which can exert a higher flow-induced shear force on flocs, leading to more floc breakup.

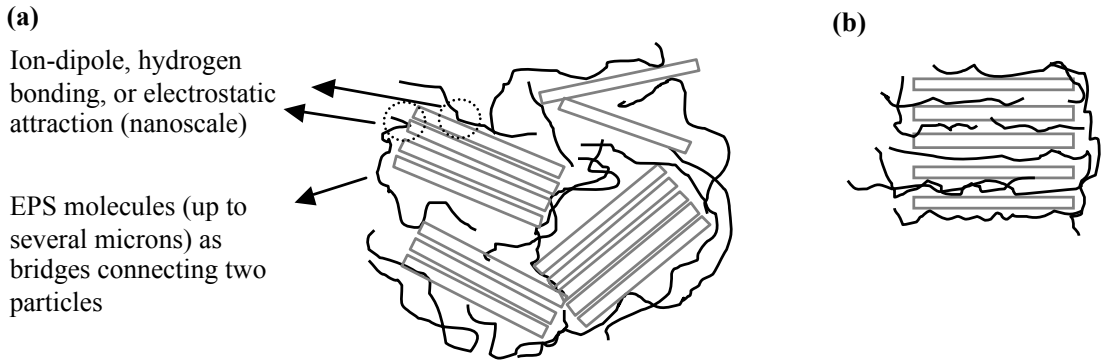

Figure 5.8 Schematic diagram showing clay and EPS interaction: (a) EPS facilitated flocculation; (b) intercalation of EPS into the swelling clay.

The neutral guar gum significantly changes the PSD of both clays by generating the largest flocs (e.g., up to 100 μm, Figure 5.6 c and d). For Ca-M, as the guar concentration increases, the PSD curve moves left, then right, and then left again. The highest degree of flocculation with a D_{50} of 50 μm occurs at a concentration of 1 μg/g, while the lowest one with a D_{50} of 16.2 μm at a concentration of 10 μg/g (Figure 5.7 a). The D_{50} of Ca-M at a guar concentration of 100 μg/g is 43.3 μm. For Na-M, the two intermediate concentrations (i.e., 10 and 100 μg/g) facilitate a higher degree of flocculation with D_{50} increasing from 2.3 to 49.7 and 47.1 μm, respectively. At a lower guar concentration of 1 μg/g, the Na-M slightly increases the particle size with D_{50} increasing from 2.3 to 2.4 μm. The higher degree of flocculation in Ca-M may be caused by the intercalation of guar molecules into the swelling clays (Figure 5.8 b) (*Theng*, 1982) together with the long-range polymer bridging and short-range ion-dipole interaction or hydrogen bonding between the hydroxyl groups of guar and the oxygen on clay

surface (Figure 5.8 a) (*Nugent et al.*, 2009), while the flocculation of Na-M and guar only results from the latter one. In addition, the molecule length of guar is the longest among the three EPS, which is the main reason for the generation of largest clay-EPS flocs.

Chitosan is insoluble in a neutral or alkaline aqueous solvent, but its amino functional groups are partly charged, resulting in the change of the two clays' PSD. Although the flocculation of clays caused by chitosan at a natural pH is not significant (*Chen and Chung*, 2011) (Figure 5.6 e and f), for both clays with the addition of chitosan, the particle size initially decreases at a concentration of 1 μg/g, and then increases at a concentration of 10 to 100 μg/g, The D_{50} of Ca-M decreases from 32.4 to 15.0 μm for 1 and 10 μg/g chitosan concentrations, but increases to 34.5 μm at 100 μg/g. The D_{50} of Na-M changes from 2.3 to 2.1 and 2.2 μm as the chitosan concentration increases. The largest-size peak of the two clays also shows the same trend of change. At a very low concentration, the positively charged chitosan molecules are adsorbed only onto the outer surface of particles or flocs, which results in partial separation of flocs (*He and Horikawa*, 2000) and hence a decrease in floc size. The positive charge of chitosan can neutralize the negative charge on clay surface (*Ghimici and Nichifor*, 2009), and its molecules can also enter the interlayer space of swelling clays (*Theng*, 1982). Therefore, as the chitosan concentration increases, the clay surface becomes saturated with adsorbed chitosan, and the excessive chitosan molecules re-flocculate the separated small particles or flocs through polycationic bridging as the long-range interactions as well as electrostatic attraction as the short-range interactions (Figure 5.8 a), resulting in an increase in floc size.

5.3.3 Effects of Salinity

As the salinity increases, the basal spacing of swelling montmorillonite may decrease by several angstroms (*Posner and Quirk*, 1964), which results in a slight decrease in particle size. On the other hand, according to Derjaguin-Landau-Verwey-Overbeek (DLVO) theory (*Derjaguin and Landau*, 1941; *Verwey and Overbeek*, 1948), the interaction between charged clay particles is a summation of van der Waals attraction and electrostatic repulsion due to double layer (DL) of counterions on clay surface, which can be compressed by increasing the cationic concentration of the environment. Thus, the addition of salt can decrease the electrostatic repulsion between montmorillonite particles and cause further flocculation or size increasing. These two competitive mechanisms co-exist in a saline clay suspension, resulting in particle size variations with salinity. For different types of montmorillonite and different salinities, the one that dominates flocculation may be different.

The characteristic length of the DL thickness, Debye length (t_D), on clay surface can be estimated by using the following equation (*Block*, 1978):

$$t_D = \sqrt{\frac{\varepsilon_0 \cdot \varepsilon \cdot k \cdot T}{\sum_{j=1}^{N} n_j \cdot q_j^2}} \qquad \text{Equation 5.9}$$

where ε_0 is the permittivity of vacuum, ε the dielectric constant, k Boltzmann constant, T the absolute temperature, and q_j and n_j the valance and mean concentration of the *j-th* ion species, respectively.

The dielectric constant of water decreases as the salinity increases, which is 80.4, 79.2, 77.9, and 71.8 for water at 0, 5, 10, and 35 ppt salinities, respectively (*Meissner and Wentz*, 2004; *Stogryn*, 1971). The major ions of the Instant Ocean® sea salt are Na^{+}, Mg^{2+}, K^{+}, Ca^{2+}, and Cl^{-}, SO_4^{2-}, TCO_2 (total carbon dioxide) with some other trace ions (*Atkinson and Bingman*, 1998). The DL thicknesses at a salinity of 5, 10, and 35 ppt are estimated as 0.92, 0.64, and 0.32 nm, respectively. Theoretically, the DL in pure water is infinity according to Eqn. (2), but the DL thickness of 960 nm in pure water at pH 7 was reported by (*Israelachvili*, 2007).

The effect of salinity on the PSD is shown in Figure 5.9. As the salinity increases from 0 to 35 ppt, the particle size of Ca-M decreases with D_{50} decreasing from 32.4 to 24.7 μm, while that of Na-M gradually increases with D_{50} increasing from 2.3 to 28 μm. As discussed previously, in the PSA's liquid circulation system, the limitedly swelling Ca-M maintains its tactoid structure. The presence of salt decreases the basal spacing and hence the thickness of the 2:1 layer particles will be significantly reduced. Additionally, the classical DLVO theory has limitation for predicting clay flocculation (*Furukawa and Watkins*, 2012) that it is not applicable to the limitedly swelling Ca-M (*Kjellander et al.*, 1988). Although the DL thickness deceases from 960 nm to ~1 nm, the attractive and repulsive forces between Ca-M interlayers may not change. Therefore, the slight decrease in the size of Ca-M in salt water is mainly caused by the decrease of basal spacing, but the change is not so significant. However, for the highly swelling Na-M, the addition of salt eliminates the small clay particles at ~0.3 μm (i.e., the leftmost peak disappears) and results in much larger flocs at ~35 μm (i.e., the rightmost peak appears). As the salinity increases, the particle size increases significantly. Thus, the dominant influence of salt on the Na-M's PSD is the repulsive DL thickness decreasing, which facilitates the flocculation of

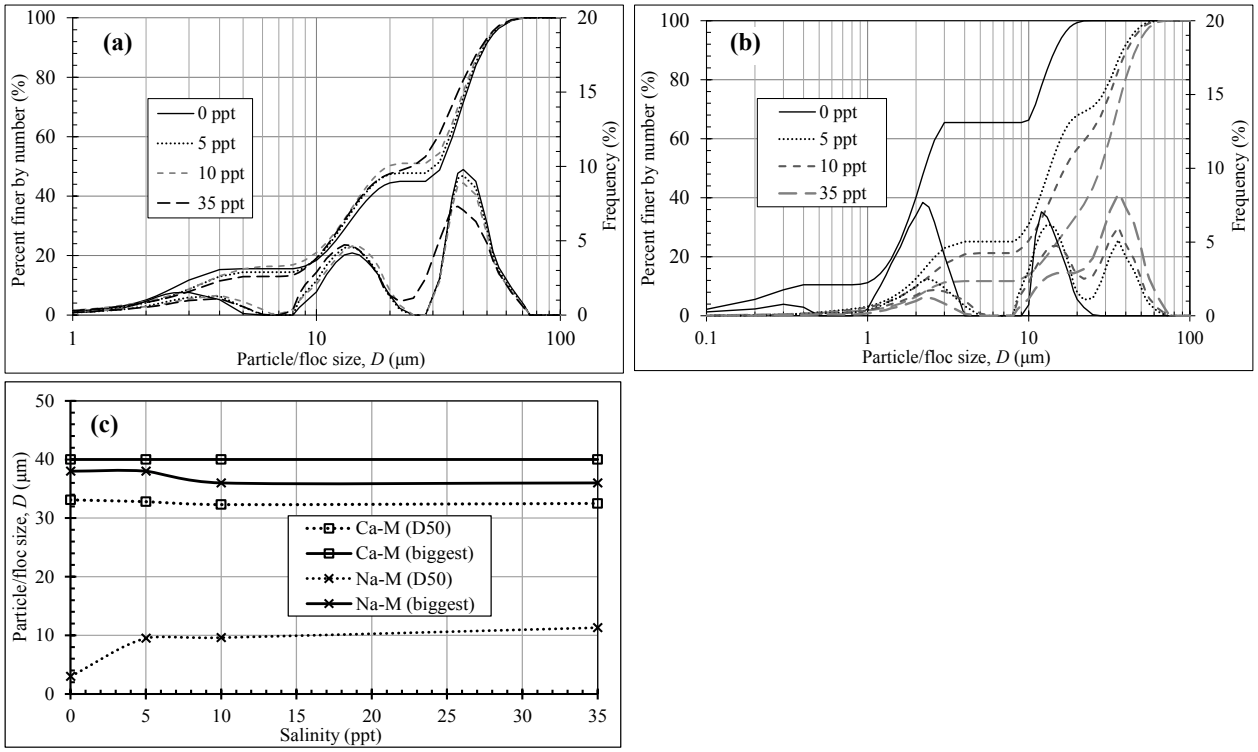

Figure 5.9 PSD of (a) Ca-M and (b) Na-M at 0, 5, 10, 35 ppt salinities (under low pump speed); (c) summary of D_{50} and the largest floc size of both clays at different salinities.

Na-M particles via face-face or face-edge association and other aforementioned mechanisms. As the salinity increases from 0 to 5 ppt, the DL thickness changes dramatically from 960 to 0.92 nm, and hence the D_{50} of the Na-M has the corresponding largest change from 2.3 to 13.0 μm (i.e., by one order of magnitude). As the salinity increases from 5 to 35 ppt, the DL thickness becomes smaller and smaller, and the D_{50} of Na-M keeps increasing from 13 to 28 μm.

5.3.4 Effects of Hydrodynamic Conditions

The size change and behavior of clay particles and flocs in aqueous flow are due to two competing effects, as shown in Figure 5.10: (1) flocculation by the increased collision possibility and hence more adsorption; and (2) breakup into smaller flocs or particles due to the flow-induced shear stress (*Jarvis et al.*, 2005; *Mietta et al.*, 2009; *Yeung et al.*, 1997). At a given hydrodynamic condition which is expected to exert a constant shear force, flocs of similar or higher strength tend to form, because the weaker ones can breakup and re-flocculate until they are strong enough to resist the shear stress exerted by the flow. To evaluate the influence of hydrodynamic factors on the PSD and flocculation behavior of the two expansive clays, the mean size (D_{50}) and the largest floc size (D_m) are selected from a series of PSD for comparison (Table 5.2). The hydrodynamic parameters of all clay suspensions in the PSA's liquid circulation system are summarized in Table 5.3. The concentration of the montmorillonite suspension is 0.4 g/L in this study, which is much smaller than 1.0 g/L, so the general flow behavior is Newtonian (*Guven and Pollastro*, 1992; *Vali and Bachmann*, 1988). The rheological properties of very dilute xanthan, guar, and chitosan solutions (0.0001-0.01 wt.% in this study) are different from their relatively higher concentration solutions (e.g., 0.5-10 wt.%). Therefore, the dilute EPS solution is also treated as a Newtonian fluid (*Fonseca et al.*, 2011). Their viscosity values (Table 5.3) were taken from literature, such as xanthan from (*He and Horikawa*, 1996) and chitosan from (*He and Horikawa*, 2000).

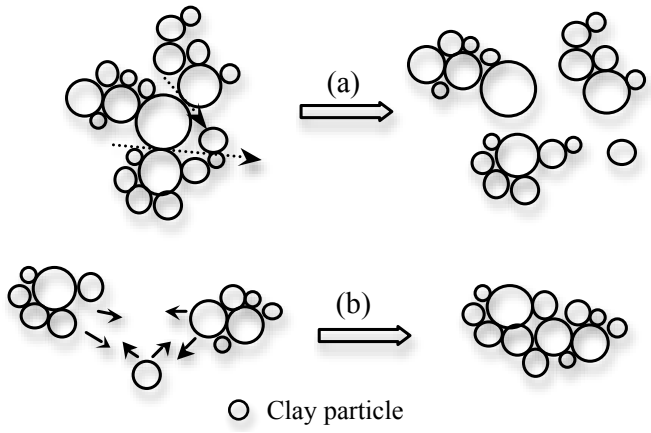

Figure 5.10 Schematic representation of the behaviors of clay particles and flocs in aqueous flow: (a) flocs break into smaller flocs or particles due to flow induced shear force; (b) flocculation by the increased collision possibility.

The low, medium, and high pump speeds result in different flow velocities and hence different types of flow in the pipe. For the DI water, salt water, and EPS suspension, the pipe flow is laminar (R_e <2000), transitional (2000< R_e <4000), and turbulent (Re >4000) flow for

low, medium, and high pump speed, respectively. The corresponding shear rates are also shown in Table 5.3.

Table 5.2 Particle or floc size (μm) under different hydrodynamic conditions.

Floc	Pump speed	Intrinsic (in EA)	DI water	Salinity (ppt)			EPS concentration (μg/g)								
							Xanthan			Guar			Chitosan		
				5	10	35	1	10	100	1	10	100	1	10	100
Ca-M D_{50}	Low	12.7	32.4	30.3	19.7	24.7	32.8	32.8	33.5	50.0	16.2	43.3	15.9	15.1	34.5
	Med	12.9	33.1	32.8	32.3	32.5	33.5	33.0	33.2	41.1	34.0	43.2	15.0	14.8	33.4
	High	13.1	32.6	32.4	31.7	32.2	32.9	32.7	33.0	35.6	34.2	42.5	15.0	14.7	33.1
Ca-M D_m	Low	16	40	40	40	38	40	40	38	53	40	45	36	36	40
	Med	16	40	40	40	40	40	40	40	45	40	45	36	36	40
	High	15	40	40	40	40	40	40	40	40	40	45	36	36	40
Na-M D_{50}	Low	12.3	2.3	13.5	16.8	28.0	2.3	2.9	2.2	2.4	49.7	47.1	2.1	2.1	2.2
	Med	12.3	3.0	9.5	9.6	11.3	3.0	3.0	2.2	2.4	35.2	43.9	2.1	2.1	2.3
	High	12.4	2.6	2.9	3.6	10.1	2.8	2.9	2.1	2.2	14.3	39.6	2.0	2.0	2.2
Na-M D_m	Low	16	12	36	36	36	12	36	11	12	50	50	10	10	12
	Med	16	38	38	36	36	38	38	11	12	40	45	10	10	12
	High	15	38	38	38	38	38	38	11	12	36	40	11	11	12

In alcohol, under the low and medium speeds, the flow is laminar, and it becomes transitional under the high speed. For both clays, D_{50} and D_m under low and medium pump speeds are almost the same, which may be caused by the fact that clay flocculation is the same in the same type flow. As the pump speed increases, their D_{50} slightly increases, but the largest floc size decreases. The increased fluid shear stress may be high enough to partially break the large-sized well-grown flocs (*Tambo and Hozumi*, 1979), and the separated particles re-flocculate with other micro-flocs, which causes more flocs with larger sizes.

Table 5.3 Reynolds number (R_e) and average shear rate (G) of different solutions or solvents in the stirring bath and flowing pipe (at room temperature).

Solution or solvent		Alcohol	Salinity (0-35 ppt)	EPS		
				Xanthan	Guar[a]	Chitosan
Concentration (μg/g)		NA	NA	1 - 100	1 - 100	1 - 100
Dynamic viscosity (mPa·s)		1.074	0.894 - 1.08	1.084 - 1.092	0.894 – 1.092	1.021 - 1.028
R_e in stirring bath		1377	2097 - 1783	1730 - 1717	2097 - 1717	1836 - 1824
G (s^{-1}) in stirring bath		149	184 – 170	167 – 167	184 – 167	172 – 172
R_e in pipe	Low speed	726	1091 - 921	899 - 893	1091 - 893	955 - 948
	Medium speed	1937	2908 - 2456	2399 - 2380	2908 - 2380	2547 - 2529
	High speed	3873	5817 - 4911	4797 - 4762	5817 - 4762	5093 - 5058
G (s^{-1}) in pipe	Low speed	92				
	Medium speed	293	344 - 324	320 – 319	344 – 319	327 – 326
	High speed	762	893 – 841	831 – 828	893 – 828	849 – 847

[a] The dynamic viscosity of very dilute guar was found between that of DI water and of xanthan solution at the same concentration.

In DI water, the D_{50} of both Ca-M and Na-M increases and then decreases as the flow velocity increases. The value of D_{50} under medium flow velocity is the largest. For swelling

clays, the flow turbulence may increase the collision-and-attachment possibility of clays and/or flocs and hence facilitate the flocculation to a certain degree. As the turbulence increases, the floc breakup is dominant, and hence the size of some weaker flocs decreases. The largest floc size of Ca-M remains the same, which means the hydrodynamic shear does not significantly influence the flocculation. The D_m of Na-M significantly increases from 12 to 38 μm as the flow velocity increases, which may be due to the presence of turbulent flow that can dramatically help the flocculation and the higher floc strength. These reasons can also explain the floc size change of the two expansive clays in salt water. The only difference is that the size of Na-M flocs in salt water keeps decreasing as the flow velocity increase. The salt-induced flocculation of Na-M may not increase the floc strength accordingly as the floc size increases (*Jarvis et al.*, 2005). Therefore, the appearance of turbulent flow largely decreases the floc mean size when the flow changes from low to medium speeds. As the flow turbulence increases, the floc size decreases. The addition of salt does not help the flocculation of Ca-M, so Ca-M in salt water shows the same behavior as in DI water.

For the EPS induced flocculation of the two expansive clays, in different type EPS and the different concentrations, the flocs size change caused by the flow velocity is different. Turbulent flow contains various eddies with different size intensities, which affect the flocculation in different ways. In the clay-EPS-water system, eddies may affect both EPS flocculation and floc breakup, and the turbulence may also significantly increase the rate of EPS adsorption on to clay surface (*Wågberg and Lindström*, 1987). Therefore, the size of clay-EPS flocs may also decrease or increase as the flow changes. The hydrodynamic factor does not significantly change the clay-xanthan and clay-chitosan flocs for both clays, and the small scale change (<1 μm) can be reasoned using the mechanisms discussed above for the same changes, or these flocs are relatively strong and resistant to breakup. For the clay-guar gum flocs, the size largely decreases (~14 μm) as the flow velocity increases, except for Ca-M in a 10 μg/g guar gum solution. The flocs induced by the flocculation with neutral guar gum are not as strong as with the other two charged EPS. Therefore, the increased shear stress will break the weak flocs and result in a decrease in size. This exception of Ca-M with guar gum is consistent with the above discussion that the strongest Ca-M-guar flocs occur at a concentration of 10 μg/g. The increased turbulence cannot break the flocs. On the contrary, it increases the adsorption of EPS onto clay surfaces, which facilitates flocculation.

5.3.5 Implications for Sediment Analysis

Cohesive sediment particles are transported in the form of flocs in most natural waters (*Mietta et al.*, 2009). Flocculation activity and PSD characteristics of suspended cohesive sediments in different aquatic environments, which change the properties of waterborne constituent particles and affect the transport of particle-bounded contaminants and nutrients, are of essential interest to marine, water, and environmental scientists (*Agrawal and Pottsmith*, 2000; *Droppo et al.*, 1997; *Guo and He*, 2011; *Walling and Moorehead*, 1989). Due to their unique properties, the flocculation and particle size variation of expansive clays are very sensitive to and highly dependent upon the environmental conditions. For sediments rich in expansive clays, in-situ sampling and subsequent laboratory characterization should consider the change of the chemistry and biological activities of its aquatic environment (e.g., salinity, EPS production or degradation), as well as the flow conditions. This laboratory-based experimental work sheds instructive light on the flocculation and PSD variation of expansive clays in fresh

water with and without EPS as well as in salt water of varying salinities. The results are expected to help understand the natural floc composition along with the dynamics and mechanisms of flocculation for field monitoring and numerical modeling of cohesive sediment flocculation and transport, particularly under varying aquatic chemical and hydrodynamic conditions.

Compared with non-swelling clays such as kaolinite and illite, the expansive ones are more sensitive to the environmental chemistry and hydrodynamic conditions, such as the polarity of solvent molecules and the presence of salt with different ions. For non-expansive clays, their PSD are also expected to vary with chemical, biological, and hydrodynamic factors that can promote or suppress flocculation. However, a dramatic difference is that these clays usually have a constant intrinsic PSD, or their primary particles have fixed sizes, while the expansive clays may exhibit different intrinsic or primary particle sizes due to swelling (i.e., particle thickness increases), partial or complete exfoliation (i.e., reduction in particle thickness), or interlayer intercalation of relatively large molecules (e.g., certain EPS). Moreover, the surface charges of expansive clays differ from their non-swelling counterparts, resulting in different surface reactivity and other chemical properties. This may lead to the formation of flocs with strength different from that of non-expansive clay flocs. Therefore, further work is warranted to characterize the strength of flocs formed by both expansive and non-expansive clays in different aquatic environments.

5.4 Conclusions

The PSD of two expansive clays, a Ca- and a Na-montmorillonite, under different dispersion methods and different chemical reagents were evaluated. The intrinsic PSD of these two expansive clays were obtained using highly purified ethyl alcohol, which is a less polar solvent inhibiting clay swelling. The two clays both show a bimodal lognormal distribution with particle sizes ranging from 0.2 to 50 μm with a D_{50} of ~13 μm.

The influence of different types of EPS at varying concentrations, different salinities, and hydrodynamic factors on the two clays' flocculation and hence PSD were also characterized. Anionic xanthan gum, neutral guar gum, and cationic chitosan can induce different degrees of flocculation for the two clays through long-range polymer bridging. Xanthan and guar can significantly increase the particle size of Na-M (e.g., from ~10 to ~50 μm for the largest flocs) and generate a higher degree of flocculation, while Chitosan decreases the particle size of both clays, owing to the formation of more compacted flocs resulted from polycationic polymer bridging. Increase in salinity facilitates the flocculation of Na-M by decreasing the repulsive electrical double layer thickness, while the particle size of limitedly swelling Ca-M is slightly reduced, which may be resulted from the basal spacing suppression. The flocculation of the two clays under laminar, transitional, and turbulent flows were also evaluated. Generally, the turbulence associated with higher shear rates facilitates the flocculation to different degrees of Ca-M in all of the studied conditions, while the Na-M floc size decreases to certain degrees when the shear rate increases. Therefore, the limitedly swelling Ca-M tends to form relatively stronger and larger flocs than the highly swelling Na-M.

5.5 Acknowledgments

This work was partially supported by the Office of Naval Research (Award No. N00173-10-1-G013) under program element number 0601153N. GZ was partially supported by the Overseas Collaboration Award of NSFC (Grant No. 51128901). XT received the LSU Graduate School Economic Development Assistantship and a Supplement Award. The facilities used in this study were purchased using the fund from the Louisiana Board of Regents Enhancement Program.

5.6 Notations

D_0 – internal diameter of pipe

D - mean diameter of all flocs and particles within a given size range

D_A - impeller diameter

ε_0 - permittivity of vacuum

ε - dielectric constant

$\bar{\varepsilon}$ - average turbulent energy dissipation per unit time and mass

f - friction factor

G - average shear rate

k - Boltzmann constant

l - diameter of a particle or floc

n - number of particles at a fixed size

n_j - mean concentration of the *j-th* ion species

N_p - power number of stirrer

Ω - angular velocity of impeller in the stirring bath of PSA

ρ - fluid density

q_j - valance of the *j-th* ion species

Q - flow rate in pipe

R_0 – internal radius of pipe

R_e - Reynolds number

t_D - Debye length

T - absolute temperature

μ - fluid dynamic viscosity

v_0 - mean flow velocity in pipe

v - kinematic viscosity of the liquid

V - volume of the stirring bath of PSA

5.7 References

[1] Agrawal, Y. C., and Pottsmith, H. C. 2000. Instruments for particle size and settling velocity observations in sediment transport, *Marine Geology*, 168, 89-114.

[2] Atkinson, M. J., and Bingman, C. 1998. Elemental composition of commercial seasalts, *Journal of Aquariculture and Aquatic Sciences*, 8, 39-43.

[3] Benchabane, A., and Bekkour, K. 2006. Effects of anionic additives on the rheological behavior of aqueous calcium montmorillonite suspensions, *Rheologica Acta*, 45, 425-434.

[4] Block, L. P. 1978. A double layer review, *Astrophysics and Space Science*, 55, 59-83.

[5] Brindley, G. W., Wiewiora, K., and Wiewiora, A. 1969. Intercrystalline swelling of montmorillonite in some water-organic mixtures *American Mineralogist*, 54, 1635-1644.

[6] Camp, T. R., and Stein, P. C. 1943. Velocity gradients and internal work in fluid motion, *Journal of the Boston Society of Civil Engineers*, 30, 219-237.

[7] Chang, I., and Cho, G. 2012. Strengthening of Korean residual soil with β-1,3/1,6-glucan biopolymer, *Construction and Building Materials*, 30, 30-35.

[8] Chang, T. S., Joerdel, O., Flemming, B. W., and Bartholoma, A. 2006. The role of particle aggregation/disaggregation in muddy sediment dynamics and seasonal sediment turnover in a back-barrier tidal basin, East Frisian Wadden Sea, southern North Sea, *Marine Geology*, 235, 49-61.

[9] Chen, C. Y., and Chung, Y. C. 2011. Comparison of Acid-Soluble and Water-Soluble Chitosan as Coagulants in Removing Bentonite Suspensions, *Water Air Soil Pollut.*, 217, 603-610.

[10] D422-63, A. S. 2007, Standard test method for particle-size analysis of soils, edited, ASTM International, West Conshohocken, PA, United States.

[11] Derjaguin, B., and Landau, L. 1941. Theory of the stability of strongly charged lyophobic sols and of the adhesion of strongly charged particles in solutions of electrolytes, *Acta Physico chemica URSS*, 14, 633.

[12] Devine, S. B., Ferrell, R. E., and Billings, G. K. 1972. A quantitative X-ray diffraction technique applied to fine-grained sediments of the deep gulf mexico, *Journal of Sedimentary Petrology*, 42, 468-475.

[13] Dontsova, K. M., and Bigham, J. M. 2005. Anionic polysaccharide sorption by clay minerals, *Soil Science Society of America Journal*, 69, 1026-1035.

[14] Droppo, I. G., Leppard, G. G., Flannigan, D. T., and Liss, S. N. 1997. The freshwater floc: A functional relationship of water and organic and inorganic floc constituents affecting suspended sediment properties, *Water Air Soil Pollut.*, 99, 43-53.

[15] Eirich, F. R. 1967, Rheology: Theory and Applications, Academic Press, New York.

[16] Fonseca, P., Dekker, R. F. H., Barbosa, A. M., Silveira, J. L. M., Vasconcelos, A. F. D., Monteiro, N. K., Aranda-Selverio, G., and da Silva, M. D. C. 2011. Thermal and rheological properties of a family of notryosphaerans produced by botryosphaeria rhodina MAMB-05, *Molecules*, 16, 7488-7501.

[17] Furukawa, Y., and Watkins, J. L. 2012. Effect of organic matter on the flocculation of colloidal montmorillonite: A modeling approach, *Journal of Coastal Research*.

[18] Gerbersdorf, S., Westrich, B., and Paterson, D. 2009. Microbial extracellular polymeric substances (EPS) in fresh water sediments, *Microbial Ecology*, 58, 334-349.

[19] Ghimici, L., and Nichifor, M. 2009. Flocculation properties of some cationic polysaccharides, *Journal of Macromolecular Science Part B-Physics*, 48, 106-113.

[20] Guo, L., and He, Q. 2011. Freshwater flocculation of suspended sediments in the Yangtze River, China, *Ocean Dynamics*, 61, 371-386.

[21] Gupta, B. S., and Ako, J. E. 2005. Application of guar gum as a flocculant aid in food processing and potable water treatment, *European Food Research and Technology*, 221, 746-751.

[22] Guven, N., and Pollastro, R. M. (Eds.) 1992, Clay-water interface and its rheological implications, The Clay Minerals Society, Aurora.

[23] He, M., and Horikawa, Y. 1996. Stability of allophane, allophanic clay, and allophane-halloysite floc in aqueous solutions of an anionic exocellular heteropolysaccharide (gum xanthan) from Xanthomonas campestris, *Soil Science and Plant Nutrition*, 42, 603-612.

[24] He, M., and Horikawa, Y. 2000. Partial deflocculation of mutual flocs of allophane and halloysite by xanthan and chitosan and relevance to particle arrangement in the flocs, *Soil Science and Plant Nutrition*, 46, 81-87.

[25] Hill, P. S. 1998. Controls on floc size in the sea, *Oceanography*, 11, 13-18.

[26] Hiltabrand, R. R., Ferrell, R. E., and Billings, G. K. 1973. Experimental diagnesis of Gulf Coast argillaceous sediment, *American Association of Petroleum Geologists Bulletin*, 57, 338-348.

[27] Hirst, C. N., Cyr, H., and Jordan, I. A. 2003. Distribution of exopolymeric substances in the littoral sediments of an oligotrophic lake, *Microbial Ecology*, 46, 22-32.

[28] Holland, F. A., and Chapman, F. S. 1966, Liquid mixing and processing in stirred tanks, Reinhold Publishing Corporation, New York.

[29] Ian W, S. 1994. Structure-function relationships in microbial exopolysaccharides, *Biotechnology Advances*, 12, 393-448.

[30] Israelachvili, J. N. 2007, Intermolecular and surface forces, 2nd ed., Elsevier Academic Press.

[31] Jarvis, P., Jefferson, B., Gregory, J., and Parsons, S. A. 2005. A review of floc strength and breakage, *Water Research*, 39, 3121-3137.

[32] Kjellander, R., Marcelja, S., Pashley, R. M., and Quirk, J. P. 1988. Double-layer ion correlation forces restrict calcium clay swelling, *J. Phys. Chem.*, 92, 6489-6492.

[33] Kleijn, W. B., and Oster, J. D. 1982. A model of clay swelling and tactoid formation, *Clay Clay Min.*, 30, 383-390.

[34] Labille, J., Thomas, F., Milas, M., and Vanhaverbeke, C. 2005. Flocculation of colloidal clay by bacterial polysaccharides: Effect of macromolecule charge and structure, *J. Colloid Interface Sci.*, 284, 149-156.

[35] Lagaly, G., and Ziesmer, S. 2003. Colloid chemistry of clay minerals: the coagulation of montmorillonite dispersions, *Advances in Colloid and Interface Science*, 100, 105-128.

[36] Lagaly, G., Ogawa, M., and Dékány, I. 2006, Chapter 7.3 Clay Mineral Organic Interactions, in Developments in Clay Science, edited by B. K. G. T. Faïza Bergaya and L. Gerhard, pp. 309-377, Elsevier.

[37] Laird, D. A. 2006. Influence of layer charge on swelling of smectites, *Applied Clay Science*, 34, 74-87.

[38] Lee, B. J., Fettweis, M., Toorman, E., and Molz, F. J. 2012. Multimodality of a particle size distribution of cohesive suspended particulate matters in a coastal zone, *Journal of Geophysical Research-Oceans*, 117.

[39] Luckham, P. F., and Rossi, S. 1999. The colloidal and rheological properties of bentonite suspensions, *Advances in Colloid and Interface Science*, 82, 43-92.

[40] Matsuo, T., and Unno, H. 1981. FORCES ACTING ON FLOC AND STRENGTH OF FLOC, *Journal of the Environmental Engineering Division-Asce*, 107, 527-545.

[41] Meissner, T., and Wentz, F. J. 2004. The complex dielectric constant of pure and sea water from microwave satellite observations, *Ieee Transactions on Geoscience and Remote Sensing*, 42, 1836-1849.

[42] Mermut, A. R., and Cano, A. F. 2001. Baseline studies of the Clay Minerals Society Source Clays: Chemical analyses of major elements, *Clays and Clay Minerals*, 49, 381-386.

[43] Mietta, F., Chassagne, C., Manning, A. J., and Winterwerp, J. C. 2009. Influence of shear rate, organic matter content, pH and salinity on mud flocculation, *Ocean Dynamics*, 59, 751-763.

[44] Moody, L. F. 1944. Friction factors for pipe flow, *Transactions of the A.S.M.E.*, 66, 671-684.

[45] Mosser-Ruck, R., and Cathelineau, M. 2004. Experimental transformation of Na,Ca-smectite under basic conditions at 150 °C, *Applied Clay Science*, 26, 259-273.

[46] Murray, H. H. 2000. Traditional and new applications for kaolin, smectite, and palygorskite: A general overview, *Applied Clay Science*, 17, 207-221.

[47] N.V, M., and Kumar, R. 2000. A review of chitin and chitosan applications, *Reactive and Functional Polymers*, 46, 1-27.

[48] Nair, R. R., Hashimi, N. H., Purnachandra, and Rao, V. 1982. Distribution and dispersal of clay minerals on the western continental shelf of India, *Marine Geology*, 50, M1-M9.

[49] Nugent, R. A., Zhang, G. P., and Gambrell, R. P. 2009. Effect of exopolymers an the liquid limit of clays and its engineering implications, *Transportation Research Record*34-43.

[50] Olejnik, S., Posner, A. M., and Quirk, J. P. 1974. Swelling of montmorillonite in polar organic liquids, *Clay Clay Min.*, 22, 361-365.

[51] Poli, A. L., Batista, T., Schmitt, C. C., Gessner, F., and Neumann, M. G. 2008. Effect of sonication on the particle size of montmorillonite clays, *Journal of Colloid and Interface Science*, 325, 386-390.

[52] Posner, A. M., and Quirk, J. P. 1964. Changes in basal spacing of montmorillonite in electrolyte solutions, *Journal of Colloid Science*, 19, 798-&.

[53] Pruett, R. J., and Webb, H. L. 1993. Sampling and analysis of KGa-1b well-crystallized kaolin source clay, *Clay Clay Min.*, 41, 514-519.

[54] Risica, D., Dentini, M., and Crescenzi, V. 2005. Guar gum methyl ethers - Part I. Synthesis and macromolecular characterization, *Polymer*, 46, 12247-12255.

[55] Sashiwa, H., and Aiba, S. I. 2004. Chemically modified chitin and chitosan as biomaterials, *Prog. Polym. Sci.*, 29, 887-908.

[56] Seo, Y. J., Seol, J., Yeon, S. H., Koh, D. Y., Cha, M. J., Kang, S. P., Seo, Y. T., Bahk, J. J., Lee, J., and Lee, H. 2009. Structural, mineralogical, and rheological properties of methane hydrates in smectite clays, *Journal of Chemical and Engineering Data*, 54, 1284-1291.

[57] Spicer, P. T., and Pratsinis, S. E. 1996. Shear-induced flocculation: The evolution of floc structure and the shape of the size distribution at steady state, *Water Research*, 30, 1049-1056.

[58] Stogryn, A. 1971. Equations for calculating the dielectric constant of saline water, *Microwave Theory and Techniques, IEEE Transactions on*, 19, 733-736.

[59] Tambo, N., and Hozumi, H. 1979. Physical aspect of flocculation process - II. Contact flocculation, *Water Research*, 13, 441-448.

[60] Theng, B. K. G. 1970. Interactions of Clay Minerals With Organic Polymers - Some Practical Applications, *Clay Clay Min.*, 18, 357-&.

[61] Theng, B. K. G. 1982. Clay-polymer Interactions - Summary and perspectives, *Clay Clay Min.*, 30, 1-10.

[62] Theng, B. K. G. 2012, Chapter 11 - Polysaccharides, in Developments in Clay Science, edited by B. K. G. Theng, pp. 351-390, Elsevier.

[63] Vali, H., and Bachmann, L. 1988. Ultrastructure and flow behavior of colloidal smectite dispersions, *J. Colloid Interface Sci.*, 126, 278-291.

[64] van Leussen, W. 2011. Macroflocs, fine-grained sediment transports, and their longitudinal variations in the Ems Estuary, *Ocean Dynamics*, 61, 387-401.

[65] van Olphen, H. 1964. Internal mutual flocculation in clay suspensions, *Journal of Colloid Science*, 19, 313-322.

[66] Verwey, E. J. W., and Overbeek, J. T. G. 1948, Theory of the stability of lyophobic colloids, Elsevier, Amsterdam.

[67] Wågberg, L., and Lindström, T. 1987. Kinetics of polymer-induced flocculation of cellulosic fibers in turbulent flow, *Colloids and Surfaces*, 27, 29-42.

[68] Walling, D. E., and Moorehead, P. W. 1989. The particle size characteristics of fluvial suspended sediment: An overview, *Hydrobiologia*, 176-177, 125-149.

[69] Winterwerp, J. C. 1998. A simple model for turbulence induced flocculation of cohesive sediment, *Journal of Hydraulic Research*, 36, 309-326.

[70] Wu, W. J. 2001. Baseline studies of the Clay Minerals Society Source Clays: Colloid and surface phenomena, *Clay Clay Min.*, 49, 446-452.

[71] Yeung, A., Gibbs, A., and Pelton, R. 1997. Effect of shear on the strength of polymer-induced flocs, *J. Colloid Interface Sci.*, 196, 113-115.

[72] Yokoi, H., Shiraki, M., Hirose, J., Hayashi, S., and Takasaki, Y. 1996. Flocculation properties of xanthan produced by Xanthomonas campestris, *Biotechnol. Tech.*, 10, 789-792.

[73] Yokoi, H., Yoshida, T., Hirose, J., Hayashi, S., and Takasaki, Y. 1998. Biopolymer flocculant produced by an Pseudomonas sp., *Biotechnol. Tech.*, 12, 511-514.

CHAPTER 6 MICROSTRUCTURE OF EXOPOLYMER-MODIFIED CLAY FLOCS

6.1 Introduction

Sedimentary cohesive soils usually originate from the particulate matter suspended in natural waters (e.g., riverine, estuarine, and coastal environments), including clay minerals, organic matter, phytoplankton, bacteria, and other live microorganisms (*Andrews et al.*, 2010; *Berlamont et al.*, 1993). Inorganic clay minerals (e.g., kaolinite, illite, and montmorillonite), typically as the dominant suspended matter, make up the major load-bearing solid skeleton after settling. However, microcrystalline colloidal clay minerals possess chemically active surfaces (e.g., permanent negative charges on face surface and pH-dependent charges on edge surface) resulting from isomorphous substitutions and other crystal defects (*Bergaya and Lagaly*, 2006; *Çelik*, 2004; *Schroth and Sposito*, 1997), and hence interact extensively with the organic matter in suspension to form clay-organic matter complexes (e.g., aggregates or flocs) (*Theng*, 1982), resulting in alterations to the particle size distribution (PSD), micromorphology, and microstructure of suspended particulate matter. Consequently, the settled bed deposit can inherit from the suspended clay-organic matter complexes these PSD and microstructure features that can affect its engineering behavior, such as resuspension and erosion shortly after settling, and the long-term post-depositional consolidation.

Of the various types of organic matter in natural waters, exopolymers or extracellular polymeric substances (EPS) of microbiological origin (*Azam and Malfatti,* 2007*; Fabricius et al.,* 2003*; Harris and Mitchell,* 1973*; Molobela and Ilunga,* 2012), are worth particular consideration due to their interactions with clay particles. They are the primary components of biofilms that are ubiquitous in natural aquatic environments, and consist of mostly polysaccharides and a small percentage of proteins and DNAs (*Decho*, 2000; *Decho and Kawaguchi*, 1999; *Decho et al.*, 2003). Polysaccharides are long chains of carbohydrate macromolecules consisting of repeating monosaccharide units joined by glycosidic bonds. In addition to the long backbone, they usually possess repeating side branches bearing functional groups, such as carboxyl (-COOH), hydroxyl (-OH), and amino ($-NH_2$) whose dissociation renders polysaccharide molecules anionic, neutral, and cationic polarity, respectively. As a result, the dissolved exopolymers can interact with the charged surfaces of suspended clay particles via intermolecular and surface forces (e.g., Coulomb forces, van der Waals attractions, ion-dipole interactions) (*Theng*, 1982). In fact, the important role of exopolymers in affecting suspended sediment flocculation (*Droppo,* 2004*; Hermawan et al.,* 2004*; Kranenburg, 1994; Lee et al.,* 2012) and stabilizing bed deposit has long been recognized, particularly for sediments in coastal and estuarine environments. Recently, *Tan et al.* (2012) and *Zhang et al.* (2013) studied the PSD kinetics of laboratory prepared clay-exopolymer suspensions, and found that exopolymers can remarkably induce clay flocculation. Similarly, exopolymers or other biopolymers can reportedly alter the index properties, strength, compressibility, and erosional resistance of bed deposit (*Chang and Cho*, 2012; *Droppo*, 2009; *Nugent et al.*, 2009), which is attributed partially to changes in soil microstructure induced by exopolymers.

Soil microstructure (i.e., referring to both soil fabric and interparticle forces) is as important in controlling a soil's physicochemical behavior and engineering properties as its

composition and stress history (*Lambe and Whitman*, 1969; *Mitchell and Soga*, 2005). With recent advancement in microcharacterization techniques such as electron microscopy, direct observation of fabric (i.e., particle arrangement and association) and interparticle cementation, is achievable (e.g., *Zhang et al.* (2004)). Most prior studies focused on relatively densely packed clay deposits. However, suspended clay flocs are usually tenuous, porous, and cluster-like aggregates with complex, fractal structures (*Furukawa et al.*, 2009; *Kranenburg*, 1994). Particularly, their extremely soft consistency and exceptionally high water content pose a significant challenge for probing their microstructure. Both direct observation techniques and indirect methods for floc structure characterization are evaluated in recent publications (*Chu and Lee*, 2004; *Droppo et al.*, 1997; *Jarvis et al.*, 2005a; *Jarvis et al.*, 2005b; *Lintern and Sills*, 2006). While direct observations yield images of different scales showing particle arrangement, they usually require sophisticated sample preparation (e.g., drying, staining, and fixation to increase image quality), which may disturb the microstructure of delicate flocs (*Danino and Talmon*, 2006). For indirect analysis, certain structural characteristics (e.g., density, fractal dimension) can be derived from some measured floc physical properties (e.g., settling velocity) (*de Boer et al.*, 2000). However, they alone can hardly provide microstructure details. Moreover, most previous studies focused on the microstructure of soils and flocs without organic matter or exopolymers. For example, *Du et al.* (2009) reported the microstructure of pure kaolinite aggregates via high resolution cryo-electron microscopy. In summary, although clay flocs microstructure was investigated in the past, an in-depth study of the microstructure of clay-exopolymer flocs involving different types of clay minerals has not been reported in the literature.

This chapter presents a systematical investigation of the microstructure of clay-exopolymer flocs prepared under controlled laboratory conditions. Four clay minerals abundant in both terrestrial and aquatic environments, namely kaolinite, illite, Ca^{2+}-montmorillonite (Ca^{2+}-Mt), and Na^{+}-montmorillonite (Na^{+}-Mt), were chosen as the representative inorganic components of flocs. Kaolinite and illite are non-swelling 1:1 and 2:1 clay minerals, respectively, while the two montmorillonites are swelling 2:1 clay minerals with different interlayer cations and interlayer swelling capacity. Both indirect PSD measurement and direct optical and electron microscopy were employed to characterize the microstructure of clay-exopolymer flocs.

6.2 Materials and Methods

6.2.1 Materials

Four highly pure source clay minerals (i.e., kaolinite, illite, Ca^{2+}-Mt, and Na^{+}-Mt), purchased from the US Clay Minerals Society (Purdue University, Indiana, USA), were chosen as the model inorganic clays. Table 6.1 shows their geographic origin and selected basic properties. Of the four clays, kaolinite, Ca^{2+}-Mt, and Na^{+}-Mt were supplied as dry powders containing the -44 μm fraction (i.e., via wet sieving through a #325 mesh) (*Pruett and Webb*, 1993), while illite was provided as small rock chips. To obtain a similar powder, illite rock chips were first slightly ground with a mortar and pestle and then wet ground with ethyl alcohol in a McCrone micronizing mill (McCrone Accessories and Components, USA) for 3 mins, which typically results in a fine powder with particle sizes ≤38 μm for most silicate minerals.

Table 6.1 Origin and basic properties of the four clay minerals[a].

Name	Origin	Layer charge[b] (unbalanced charge)		SSA[c] (m^2/g)	pH[d]	Chemical formula
		T	O			
Kaolinite (KGa-1b)	Washington County, Georgia	-0.06 (0)		10.05	5.97	$(Mg_{.02}Ca_{.01}Na_{.01}K_{.01})$ $[Al_{3.86}\ Fe^{3+}_{.02}Mn_{tr}Ti_{.11}]$ $[Si_{3.83}\ Al_{.17}]O_{10}(OH)_8$
		-0.17	0.11			
Illite (IMt-1)	Silver Hill, Montana	-1.68 (0)		30.00[e] or 24.9[f]	8.61	$(Mg_{.09}\ Ca_{.06}\ K_{1.37})$ $[Al_{2.69}Fe^{3+}_{.76}Fe^{2+}_{.06}Mn_{tr}Mg_{.43}Ti_{.06}]$ $[Si_{6.77}Al_{1.23}]O_{20}(OH)_4$
		-1.23	-0.44			
Ca^{2+}-Mt (STx-1b)	Gonzales County, Texas	-0.68 (-0.08)		83.79	7.32	$(Ca_{.27}Na_{.04}K_{.01})$ $[Al_{2.41}Fe^{3+}_{.09}Mn_{tr}Mg_{.71}Ti_{.03}]$ $[Si_{8.00}]O_{20}(OH)_4$
		0	-0.68			
Na^{+}-Mt (SWy-2)	Crook County, Wyoming	-0.55 (0.05)		31.82	6.44	$(Ca_{.12}Na_{.32}K_{.05})$ $[Al_{3.01}Fe^{3+}_{.41}Mn_{.01}Mg_{.54}Ti_{.02}]$ $[Si_{7.98}Al_{.02}]O_{20}(OH)_4$
		-0.53	-0.02			

[a] All data except those noted are taken from the US Clay Minerals Society Source Clay Physical/Chemical Data.

[b] The layer charge is based on per $O_{10}(OH)_8$ for kaolinite and $O_{20}(OH)_4$ for the other three minerals; O = charge from octahedral sheet; T = charge from tetrahedral sheets.

[c] SSA = specific surface area.

[d] pH of the suspension at a concentration of 0.4 g/L in deionized water at room temperature (23°C) obtained by a pH meter (Thermo Scientific Orion Star™ Series).

[e] Data from *Celis and Koskinen* (1999).

[f] Data from *Goldberg et al.* (1996).

Guar (Fisher ChemAlert Guide, Rochester, NY), a neutral plant polysaccharide from the seed of *Cyamopsis tetragonoloba*, was used as an exopolymer analog for the model organic constituent of flocs (Figure 6.1). Its aqueous solution is highly viscous and pseudoplastic (*Cheng et al.*, 2002). A low concentration guar solution can bring clay minerals to flocculation, while a high concentration solution may lead to steric re-dispersion (*Pawlik and Laskowski*, 2006). The lack of ionizable functional groups (e.g., -COOH) that are commonly found in anionic or cationic exopolymers renders guar neutrality in circum-neutral pH solutions. Its hydroxyl groups can dissociate only in very high pH solutions.

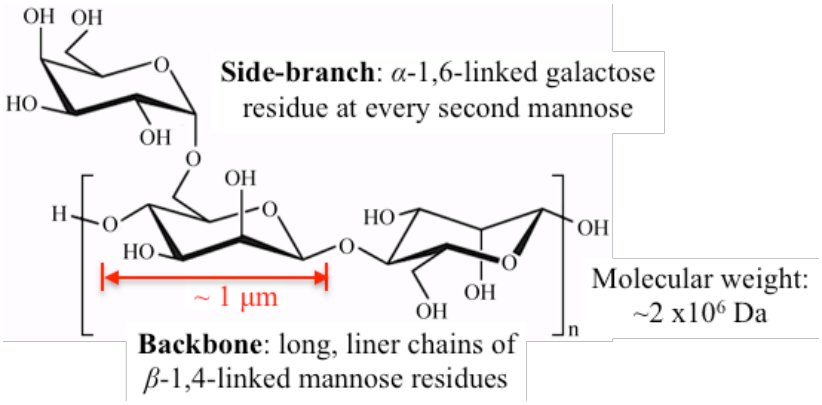

Figure 6.1 Chemical structure of guar.

6.2.2 Floc Preparation and PSD Measurement

Laboratory preparation of clay-guar flocs started with dispersing clay samples in deionized (DI) water to eliminate aggregates pre-existing in the dry powders. A Cilas® 1190 laser diffraction-based particle size analyzer (PSA) (Cilas Particle Size, Madison, WI, USA), which has a liquid dispersion and circulation system (Figure 6.2), was used to disperse clay samples, generate flocs, and perform PSD measurements. First, 0.2 g dry clay was soaked in 5 mL DI water for at least 16 hours, followed by dilution with additional 200 mL DI water in the PSA's sample bath. The clay suspension was dispersed by a built-in ultrasound disperser beneath the sample bath for a sufficient period of time. Then 50 mL guar solution with a concentration of 1000 µg/g was added to the sample bath, followed by adding more water to bring the total volume of the mixture suspension to 500 mL (i.e., the total volume of the PSA's bath and connection tubes), resulting in pre-designed final concentrations of 0.4 g/L and 100 µg/g for clay and guar, respectively. The 100 µg/g guar concentration was chosen to maximize clay-guar flocculation, because preliminary testing examining different concentrations (i.e., 0, 1, 10, 100, and 500 µg/g), selected from the range of 0-1000 µg/g in natural waters (*Gerbersdorf et al.*, 2009; *Hirst et al.*, 2003), showed that this concentration resulted in considerable flocculation of guar with all four clay minerals.

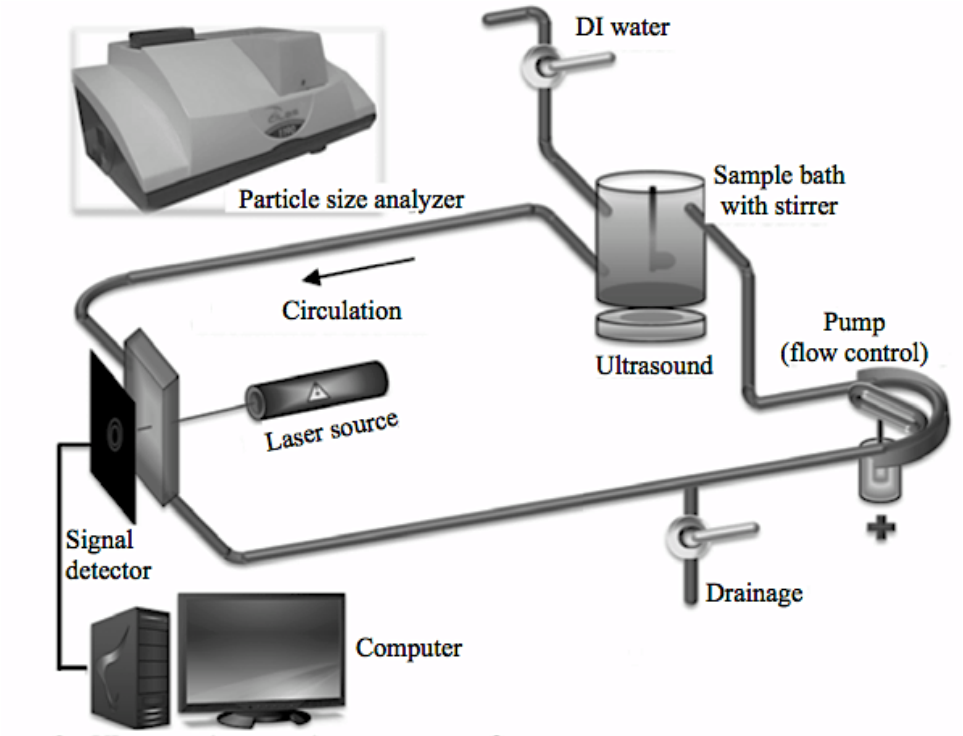

Figure 6.2 The liquid dispersion and circulation system of the Cilas® PSA used for preparing pure clay and clay-guar suspensions.

Liquid circulation, floc formation, and PSD measurement were then performed sequentially in the PSA. The mixture suspension was first circulated in the PSA's closed-loop liquid circulation system, driven by a pedal-like stirrer at a speed of 180 rpm inside the sample bath and a peristaltic pump at a speed of 30 rpm located in the tube section (Figure 6.2). This pump speed resulted in an average flow velocity of 150 mm/s, equivalent to laminar flow, in the

circulation tubes. Given that the dynamic viscosity of the 100 μg/g guar solution is 1.092 mPa·s (*Wientjes et al.*, 2000), a Reynolds number of 893 was calculated for the flow in the tubes. As such, the clay-guar flocs were formed in laminar flow condition. During circulation, the real-time flocculation process was monitored via measuring the PSD. Floc formation and breakage occurred simultaneously when the suspension was being stirred in the sample bath and circulated in the tubes. While flocculation of clay particles was caused by frequent particle collision facilitated by interparticle forces (e.g., van der Waals attractions, Coulomb forces), floc breakage was mainly controlled by flow-induced shear stress. At a given flow velocity, flocs with a strength greater than the shear stress can survive, while weaker ones breakup and then re-flocculate. Such floc breakup and reflocculation occur continuously until all flocs are strong enough to resist the flow-induced shear stress. Therefore, for all floc preparation, sufficient time (usually >15 mins) was allowed for the circulated suspension to reach a steady state (i.e., no further change in the measured PSD for prolonged circulation), followed by taking the final PSD measurement. The suspension with flocs was then transferred to a sealed beaker. Freshly prepared flocs were usually used immediately for microstructure characterization. Unused suspensions were stored in a refrigerator at 4 ± 0.1 ^{o}C to suppress biological activities for at most a week, after which the sample was discarded.

In addition to clay-guar mixture flocs, pure clay flocs from each of the four samples were also prepared at a clay concentration of 0.4 g/L by the same method. Results from the pure clay samples were obtained as the baseline data so that the changes caused by guar can be better compared. Moreover, some selected flocs were gently transferred to a fluid cell by a pipet, and a Leica DVM 2000 optical microscope was used to observe individual flocs submerged in the same exopolymer solution, with a particular attention to their size and surface morphology.

6.2.3 Electron Microscopy

Both scanning electron microscopy (SEM) and transmission electron microscopy (TEM) were employed to directly probe floc microstructure. Owing to floc's extremely soft consistency, exceptionally high water content, and large porosity, much effort was made in the preliminary phase to develop a suitable technique for preparing floc samples examined under electron microscopy. After many trials, freeze-drying and direct deposition methods were selected to prepare floc samples for SEM and TEM observations, respectively.

Preparation of floc samples for SEM observation is detailed as follows (Figure 6.3). A piece of flat aluminum foil was first glued onto the bottom of a petri dish at its edge by magic tape. Then several pieces of double-sided sticky carbon tape with a size of ~0.5 x ~0.5 cm were placed onto the foil. A pipet was used to withdraw the floc suspension that was being gently agitated, followed by dispensing a drop of suspension onto each carbon tape. The petri dish was covered by aluminum foil with tiny pierced holes (allowing water to sublimate), and then immediately placed into a freeze dryer (Model 35 XL Genesis, Virtis, Gardiner, NY). Upon freeze-drying completion, the aluminum foil attached to the petri dish was carefully removed, followed by cutting off each piece of carbon tape (but still glued onto the foil). A selected piece of aluminum foil together with freeze-dried flocs was glued onto an SEM stub, and sputter-coated with platinum in an EMS 550X sputter coater (Electron Microscopy Sciences, PA, USA). The coated samples were examined by an FEI Quanta 3D FEG Dual Beam FIB/SEM (FEI Company, Eindhoven, the Netherlands). Noteworthy is that folding and bending the aluminum

foil should always be avoided in these operations to minimize disturbance to the freeze-dried delicate flocs. Moreover, drops of pure clay suspension and pure guar solution were also freeze-dried for SEM characterization.

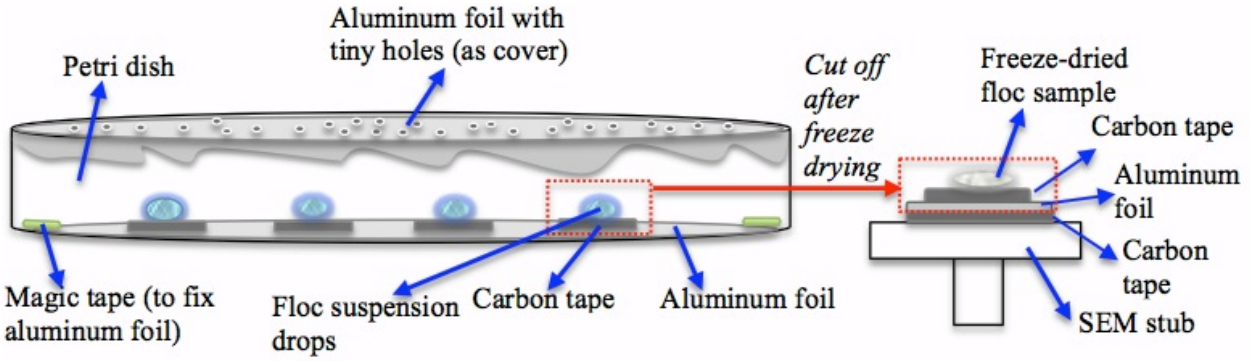

Figure 6.3 Schematic of the SEM sample preparation for freeze-drying and sputter-coating.

A relatively simple sample preparation method was chosen for TEM characterization. A small drop of clay-guar suspension was placed by a pipet onto a square copper mesh with conductive carbon film (CF-400-Cu, Electron Microscopy Sciences, PA, USA), which is usually used as the TEM sample stage. Excess water in the sample was gently removed by filter paper, followed by oven-drying the sample at 35^{o}C for 10 mins. Then the sample was immediately examined with a JEOL 100 CX TEM.

6.3 Results and Discussion

6.3.1 Particle Size Distribution

Figure 6.4 compares the PSDs of clay-guar suspensions with those of pure clay suspensions, which are plotted via both the probability density function (PDF, i.e., frequency) and cumulative distribution function (CDF, i.e., percent finer by particle number). The most striking feature is the remarkable shift of pure clay CDF curves to the right with the addition of guar, indicating that much coarser "particles" (which are actually flocs, as discussed later) are generated. In fact, the maximum size in pure clay suspensions is approximately 40, 30, 80, and 40 μm for kaolinite, illite, Ca^{2+}-Mt, and Na^{+}-Mt, respectively. With the presence of guar, however, this value is increased to approximately 500, 160, 500, and 500 μm for the four clays, respectively.

The second striking feature is the multimodality (i.e., multimodal distribution) for all eight PDF curves (Figure 6.4). This phenomenon was also reportedly observed for suspended particulate matter in natural waters (e.g., coastal zones) (*B J Lee et al.*, 2012; *Mikkelsen et al.*, 2006) and laboratory-prepared clay suspensions (*Tan et al.*, 2012; *Zhang et al.*, 2013). According to size, different particle groups, namely macroflocs, microflocs, flocculi, and primary particles, are assigned to each peak in the PDF curves (*Eisma*, 1986; *B J Lee et al.*, 2012; *van Leussen*, 1994) (Figure 6.5). Primary particles consist mostly of fine-grained individual clays and other fine particulates of 0.25-8 μm in size (*Andrews et al.*, 2010). Flocculus, a compound word for floc and nucleus (*van de Ven and Hunter*, 1977), is made of strongly bound primary clay particles and has a size of 10-40 μm. Flocculi are the smallest but densest clay-based flocs which barely

breakdown to the lower level primary particles even at the highest turbulent shear (*van de Ven and Hunter*, 1977), and hence are regarded as the basic and major building units of flocs (*van Leussen*, 1994). This concept is further verified in this study: all eight clay suspensions were pre-dispersed by ultrasound before adding guar for flocculation, yet flocculi were still present, indicating that flocculi are relatively strong and resistant to breakdown. Microflocs consist of flocculi and primary particles with a size range of 40-200 μm. Macroflocs are composed of microflocs, flocculi, and primary particles, and have a size range of 200-500 μm (Figure 6.5). This study further validates the concept of multimodality for laboratory prepared pure clay and clay-guar suspensions.

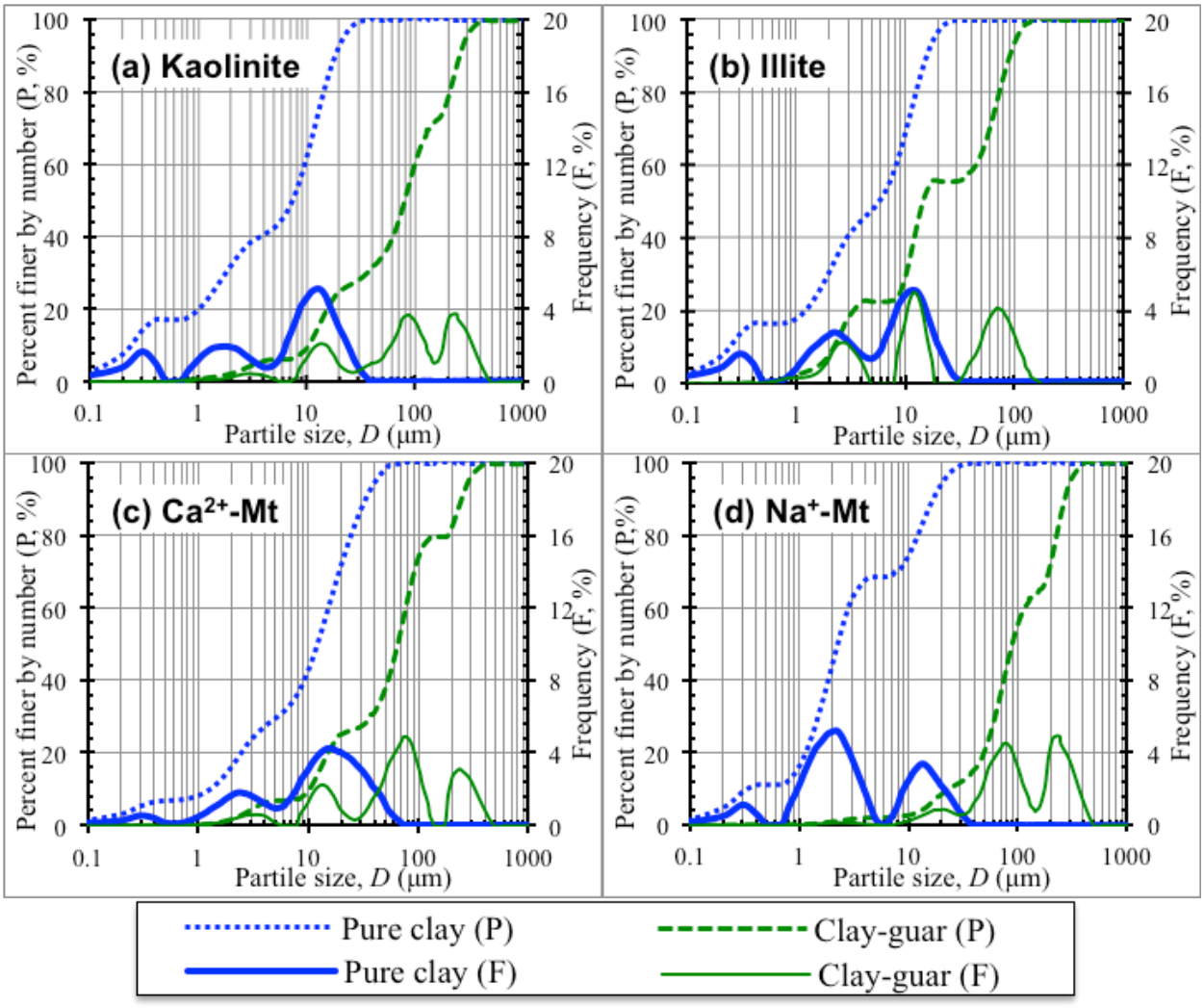

Figure 6.4 Particle size distributions (PSDs) of the pure clay and clay-EPS mixture suspensions.

Furthermore, in all four pure clay suspensions, only primary particles and flocculi are present, while all four discrete particle groups occur in clay-guar suspensions, except in the illite-guar suspension that lacks macroflocs. The addition of guar to clay suspensions causes the disappearance of, or decrease in the peak height of, finer particle groups (i.e., primary particles and flocculi), but the appearance of coarser ones (i.e., microflocs and macroflocs), suggesting that they are made of flocculi and primary particles, which may be interconnected by guar. In

fact, this hierarchical compositional relationship can be further demonstrated by the optical micrographs taken from submerged floc samples (Figure 6.6). Generally, the delicate, fluffy material is guar, while the isolated "grains" with noticeable boundaries are clay flocculi or microflocs. Particularly, flocculi can be easily identified inside the kaolinite-guar and Na^+-Mt-guar flocs (Figure 6.6 a and d). However, how these particle groups are arranged and associated with the organic guar inside the flocs cannot be deduced from the PSD curves or optical micrographs. Therefore, direct characterization via electron microscopy was performed to further probe the microstructure of clay-guar flocs.

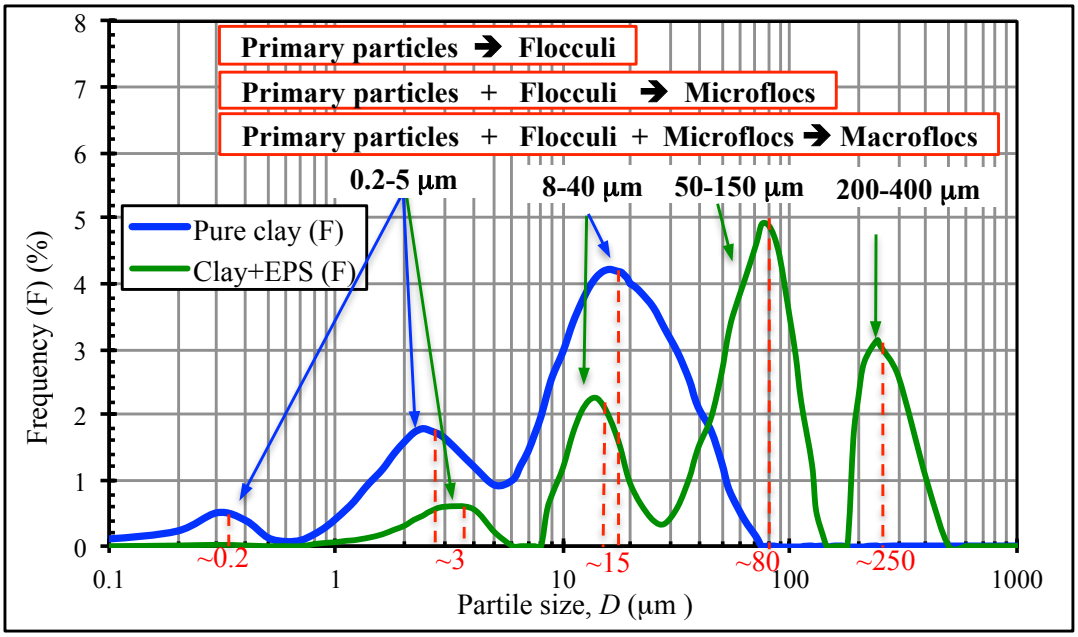

Figure 6.5 Hierachical four levels of particle groups in the PSDs of pure clay and clay-guar suspensions: primary particles, flocculi, microflocs, and macroflocs with the mean size of approximately 0.2-3, 15, 80, and 250 µm.

6.3.2 SEM Characterization of Pure Clay Flocs

For the purpose of subsequent comparison, this section presents the microstructure of pure clay samples observed by SEM. Previous PSD results indicate that microflocs and macroflocs are absent in pure clay suspensions, so the observed flocs are flocculi only. Figure 6.7 shows selected SEM images for the four clay samples. While individual, circularly or elliptically shaped flocculi of 10-30 µm in size look similar (Figure 6.7 a-b), the morphology and arrangement of individual particles within flocculi are different from each other for the four clays, as detailed by the high magnification SEM images (Figure 6.7 c-f). As expected, particles of all four clays have platy shapes with dimensions of ~2 µm, and the thickness and regularity of individual particles follow a decreasing order: kaolinite, illite, Ca^{2+}-Mt, and Na^+-Mt. Hexagonally shaped kaolinite has the lowest layer charge (i.e., -0.06 per $O_{10}(OH)_8$) and the least isomorphous substitutions (Table 6.1), resulting in thick, bulky morphology. Illite has the highest layer charge per $O_{20}(OH)_4$ and correspondingly the most structural defects. Ca^{2+}-Mt and Na^+-Mt can swell and further exfoliate their 2:1 aluminosilicate layers. The exfoliated and residual layers are much thinner than the non-swelling particles and hence they are flexible, soft, and easy to curl up (*Bihannic et al.*, 2001). Thus, particles of the two montmorillonites are thinner and more

irregular than those of illite. The highly swelling Na^{+}-Mt can swell until complete exfoliation so that each particle is only a 2:1 layer (*Lagaly*, 2006), while Ca^{2+}-Mt has limited swelling. Therefore, Na^{+}-Mt has even thinner, less regular, and more flexible particles than Ca^{2+}-Mt.

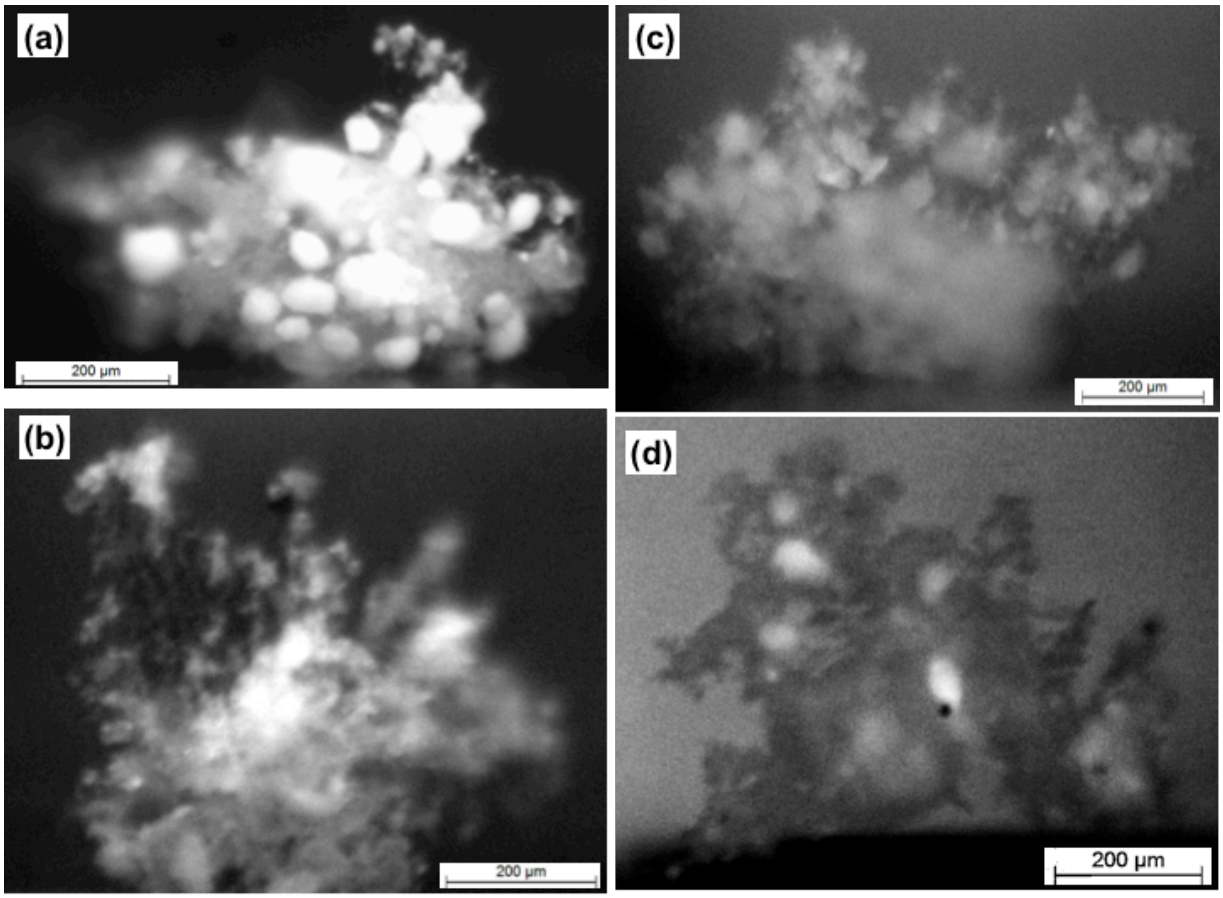

Figure 6.6 Optical images of clay-guar flocs submerged in suspension: (a) kaolinite, (b) Illite, (c) Ca^{2+}-Mt, and (d) Na^{+}-Mt.

The particle arrangement inside flocculi is also observable (Figure 6.7 c-f). Kaolinite particles are primarily face-to-face (FF) and secondarily edge-to-face (EF) associated. From Table 6.1, the tetrahedral and octahedral sheets of kaolinite 1:1 layers possess opposite electrical charges of -0.17 and +0.11, respectively. Under pH 5.97 (Table 6.1), the outmost octahedral sheet (as one face surface) exhibits positive charges, while the outmost tetrahedral sheet (as the other face surface) exhibits negative charges (*Gupta et al.*, 2011). The edge charge of kaolinite is also positive in this slightly acidic condition. As such, kaolinite flocculi are dominantly formed via electrostatic attractions in two different formats: primarily FF association between the tetrahedral sheet of one particle and the octahedral sheet of an adjacent particle and secondarily EF association between the external tetrahedral sheet of one particle and the edge surface of another. For the other three clays, the particle-scale microstructure within flocculi cannot be so definitively observed. However, the images suggest an EF association for most flocculi, which is consistent with previous work (*B J Lee et al.*, 2012; *van de Ven and Hunter*, 1977).

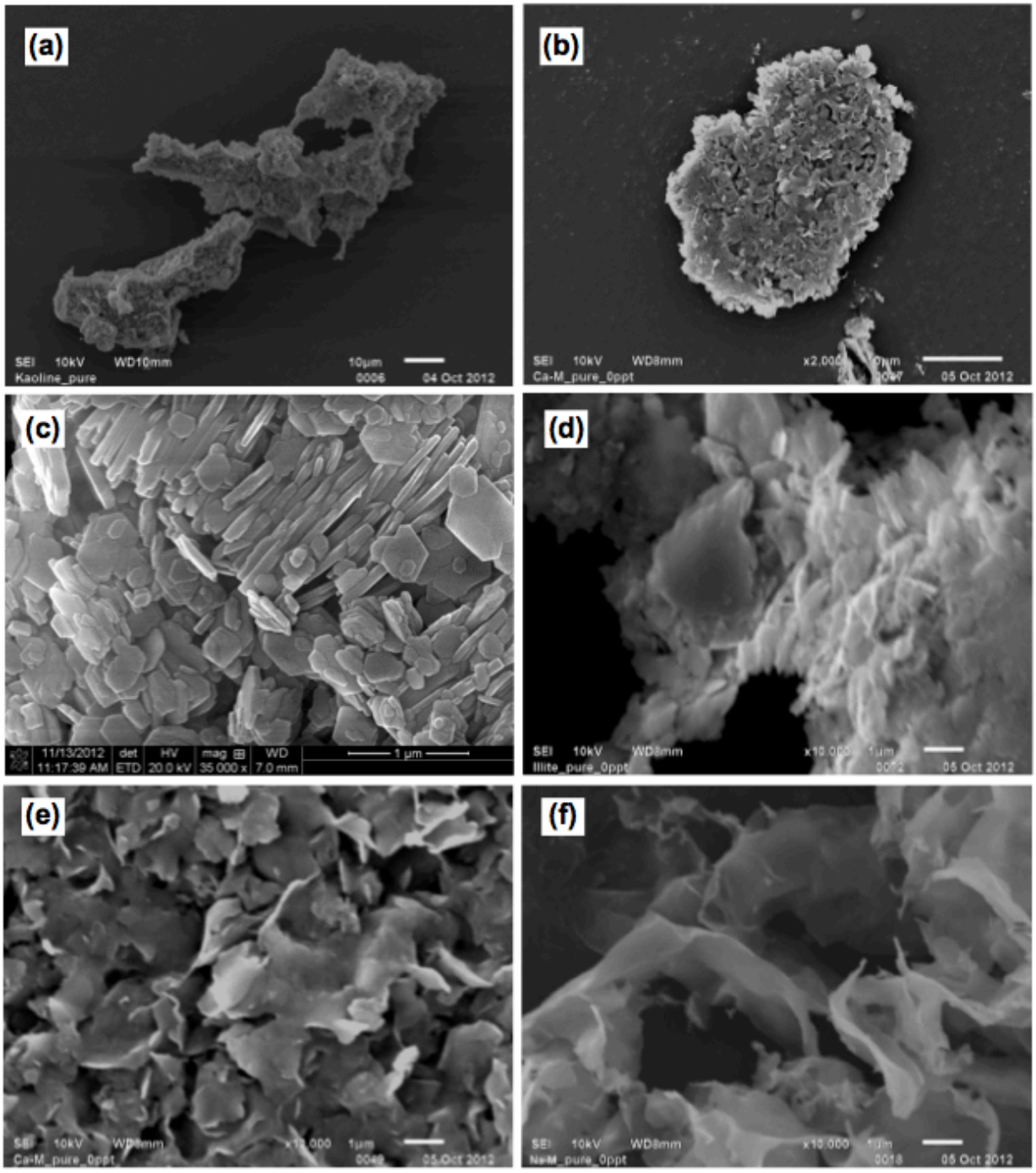

Figure 6.7 SEM images of the four pure clay samples: (a) kaolinite and (b) Ca^{2+}-Mt at a lower magnification, and (c) kaolinite, (d) Illite, (e) Ca^{2+}-Mt, and (f) Na^{+}-Mt at a higher magnification.

6.3.3 SEM Characterization of Clay-Guar Flocs

Figure 6.8 shows selected SEM images for the freeze-dried clay-guar samples. The lower magnification was chosen to present an overview of floc size and the distribution of guar. First, larger flocs (i.e., microflocs and macroflocs) are present, which is different from the pure clay samples where only smaller flocculi are observed. Second, compared with Figure 6.7, the space

between clay flocs is occupied by guar fibrils that are interconnected to form a network. These fibrils are believed to exist as "free" (i.e., not adsorbed onto clay surfaces) guar molecules in solution, and rapid freeze-drying prevents the condensation of the free guar onto clay surfaces. Third, the quantity of free guar fibrils varies with the clay type: kaolinite and Ca^{2+}-Mt have more free guar fibrils than the other two clays, and illite has the least free guar. Such a variation in free guar quantity is caused by clay surface properties, particularly layer charge and specific surface

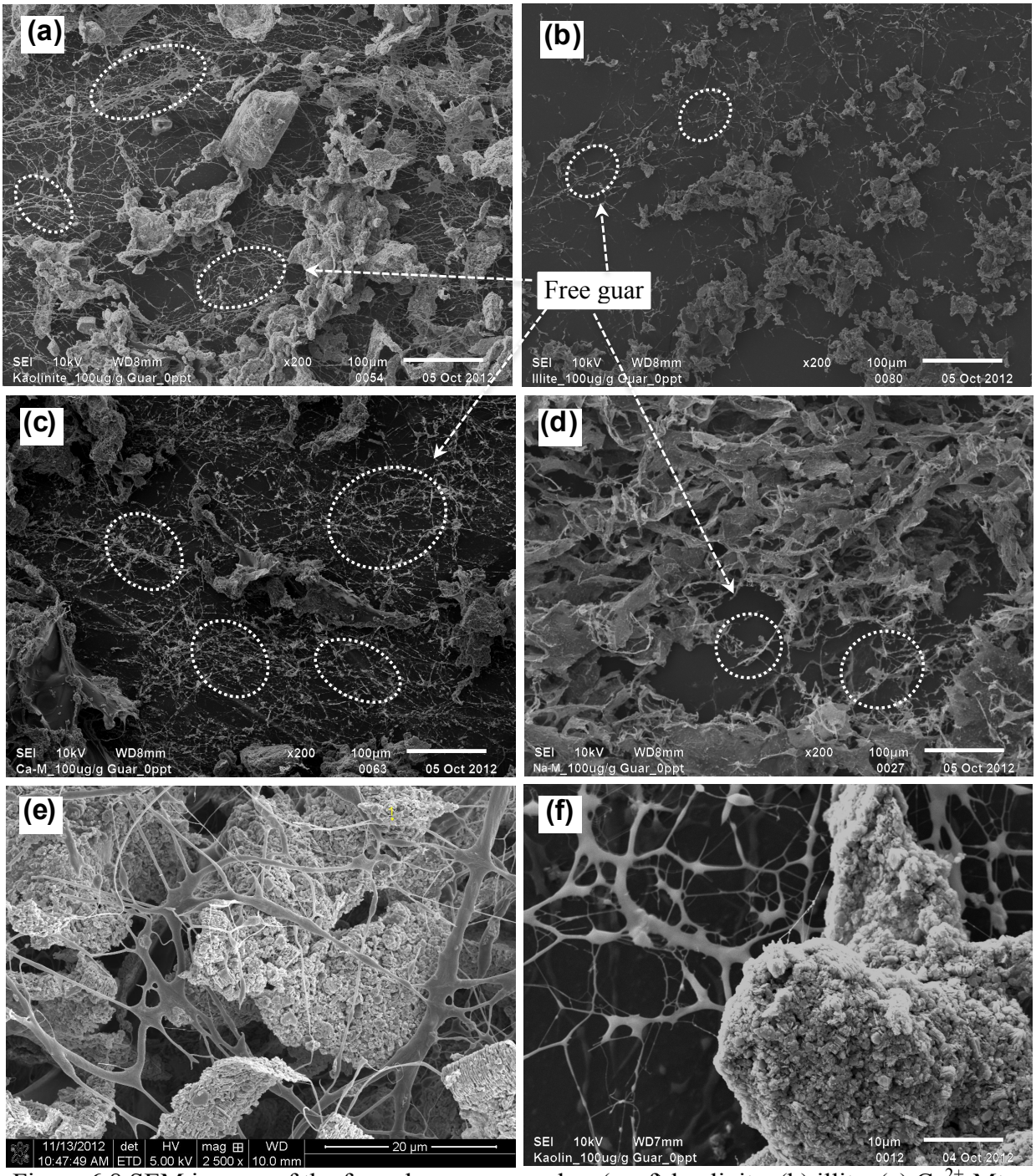

Figure 6.8 SEM images of the four clay-guar samples: (a,e,f) kaolinite, (b) illite, (c) Ca^{2+}-Mt, and (d) Na^{+}-Mt.

area (SSA). Generally, clay particles with a higher SSA and layer charge may adsorb more guar molecules onto their surfaces. From Table 6.1, of the four clays, illite has the highest layer charge (-1.68 per unit) and a relatively high SSA (30 m^2/g), and thus it can adsorb the most guar onto its surfaces, leaving the least free guar in solution. Highly swelling Na^+-Mt has a larger SSA than limitedly swelling Ca^{2+}-Mt, so there is much less free guar in the Na^+-Mt sample. Kaolinite has the smallest SSA and layer charge, and hence it contains the most free guar. Further work is warranted to quantify the free guar in each sample and correlate the SSA and layer charge with guar adsorption. Figure 6.8 e and f, at a slightly higher magnification, show the association of kaolinite flocculi (justified by size) and guar fibrils. The observed area may be part of a microfloc or macrofloc. Clearly, guar fibrils form an interconnected network that surrounds and interweaves around flocculi.

Figure 6.9 shows selected SEM images of clay-guar flocs at a much higher magnification, where characteristic microstructure features are observable. For comparison, Figure 6.10 shows a solution. Typically, the dissolved guar does not exist as individual molecules, but as fibrils (with a diameter of < 1 μm) and bundles (with a diameter of > 1 μm) that are connected to form a network structure (Figure 6.10). Such a feature is similar to the morphology of a collagen selected SEM image of the freeze-dried pure guar solution. These high-resolution images detailthe interactions between clay and guar in flocs as well as the morphology of guar in observed by a confocal microscope (*Lindström et al.*, 2010). In clay-guar suspensions, clay particles and flocculi are glued to or wrapped by guar fibrils and bundles. Careful examination points to three kinds of clay-guar associations at their interface: (1) film-like wide bundles that coat and wrap around individual clay particles and flocculi (Figure 6.9 a), (2) fibrils and bundles that bridge-connect clay particles, flocculi, and even microflocs (Figure 6.9 b), and (3) fibrils and bundles that are glued to clay particle surfaces (Figure 6.9 c-d). According to its molecular weight, the backbone length of a guar molecule ranges from 4.0 to 8.2 μm, which is estimated on the basis that the size of a glucose ring is ~1.0 nm (*Chang and Cho*, 2012). Such molecular lengths are greater than clay particles (i.e., ~2 μm). Additionally, the length of the connecting guar fibrils can be as long as >50 μm (Figure 6.10), greater than the size of flocculi. Therefore, bridging of clay particles and flocculi via guar fibrils and bundles to form larger flocs is feasible. Finally, another kind of association, which is difficult to be observed in SEM images, is the intercalation (i.e., insertion into the interlayer of swelling clays) of guar molecules or fibrils into swelling Ca^{2+}-Mt and Na^+-Mt, because neutral polymer molecules such as guar can penetrate into the expanding interlayer space (*Theng*, 1982).

It is worth discussing clay-guar interaction and flocculation mechanisms so that the observed microstructure features can be further interpreted and understood. Basically, in pure guar solution and clay-guar suspensions, the –OH functional groups in different guar molecules (Figure 6.1) can form short-range intermolecular hydrogen bonding through which multiple molecules are connected together, forming fibrils or even larger bundles. Moreover, since the –OH groups are in the repeating units of guar macromolecules, intramolecular hydrogen bonding may also develop. Therefore, neutral guar, although dissolved, does not exist as linear, individual molecules in suspension. Moreover, due to its chemical structure and functional groups, guar usually provides binding sites for colloidal particles such as clays (*Abu-Lail and Camesano*, 2003). For all four clay minerals, the interactions at the binding sites of guar molecules consist of both ion-dipole attraction between the –OH groups from guar and adsorbed cations on clay surface and hydrogen bonding between the –OH group from guar and -OH on hydroxylated clay

surfaces (e.g., as in kaolinite) or -O on siloxane clay surfaces (*S G Lee et al.*, 2013; *Theng*, 1982). These surface interactions provide the binding forces for clay-guar flocculation, as reflected by the aforementioned PSD changes.

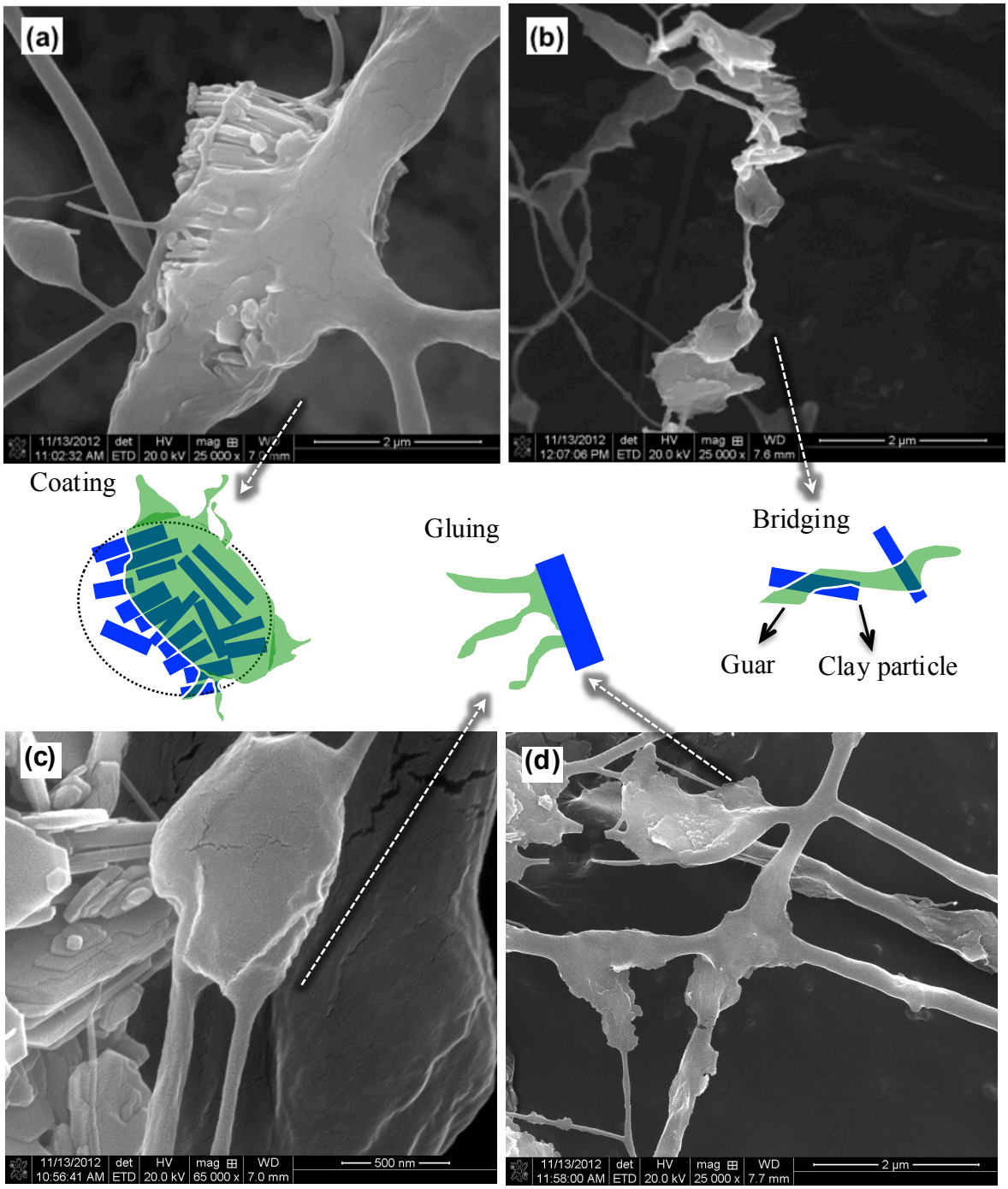

Figure 6.9 Selected SEM images as representatives for demonstrating the arrangement of clay and guar associations: (a) coating, (b) bridging, and (c,d) gluing.

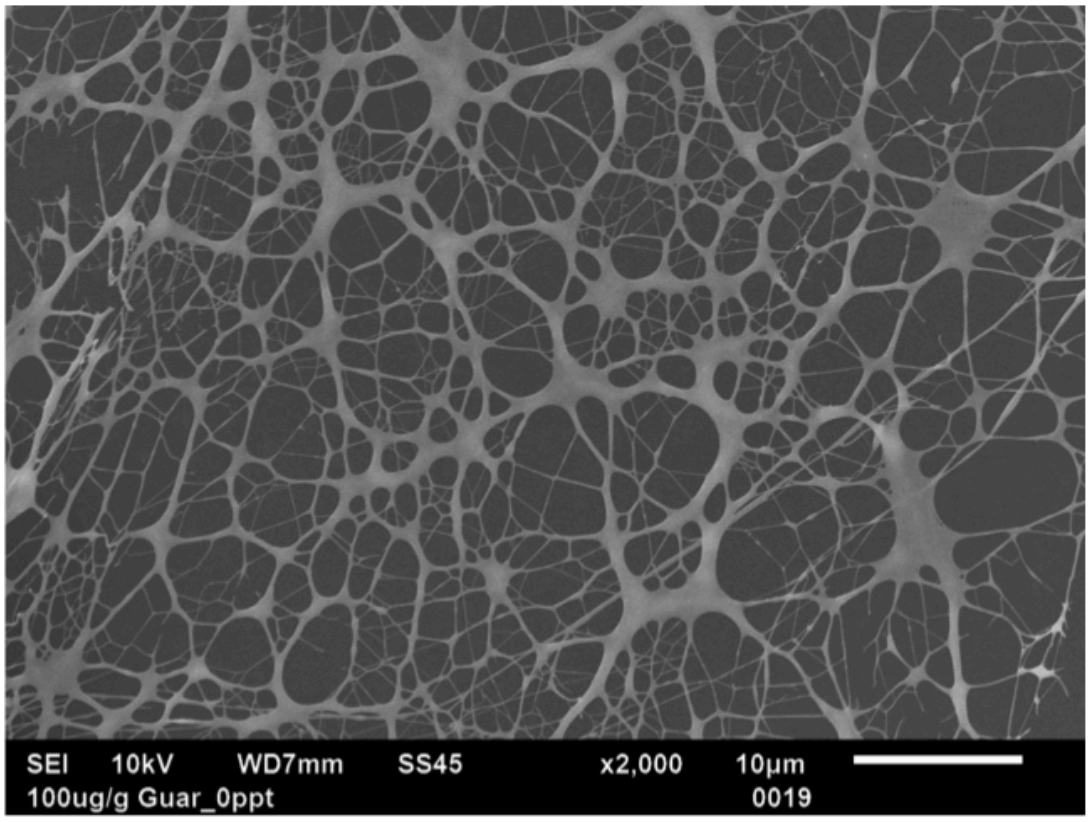

Figure 6.10 SEM image of the pure guar sample.

6.3.4 TEM Characterization

Under the extremely high resolution of TEM, large length scale features such as flocs and their sizes cannot be examined. Instead, TEM characterization was performed to observe the smaller scale microstructure details for clay-guar flocs. In addition, the comparison between TEM and SEM observations can verify whether floc microstructure was disturbed by the preparation of freeze-dried samples. Here only the results of kaolinite samples are discussed as examples. Figure 6.11 shows selected TEM images. The shape and size of kaolinite particles are clearly observed in the pure clay (Figure 6.11 a), while a network of interconnected guar fibrils or bundles is illustrated in the pure guar (Figure 6.11 b). With these two images as references, kaolinite particles and guar fibrils can be easily differentiated in the clay-guar mixture samples (Figure 6.11 c). The fibrous, porous, and less dense parts (absent in Figure 6.11 a) are guar, while the nonporous, bulky, and regularly shaped parts are individual kaolinite particles. Clearly, some fibrils are attached to the clay surface, forming bridge connections among particles. The other type of clay-guar association, surface coating, cannot be observed here, because of the principles of TEM imaging (i.e., the images are obtained by the electrons transmitted through the sample). These images also support the SEM observations discussed above, and indirectly verify that sample disturbance was not a major concern for the developed freeze-drying method.

6.3.5 A Conceptual Microstructure Model

A synthesis of the above PSD data and microscopy observations yields a clearer understanding of the clay-guar floc microstructure. On the basis of the developed understanding,

a conceptual microstructure model, consisting of four hierarchical levels with increasing length scales, is proposed to delineate the particle-level interactions and associations within a clay floc (Figure 6.12).

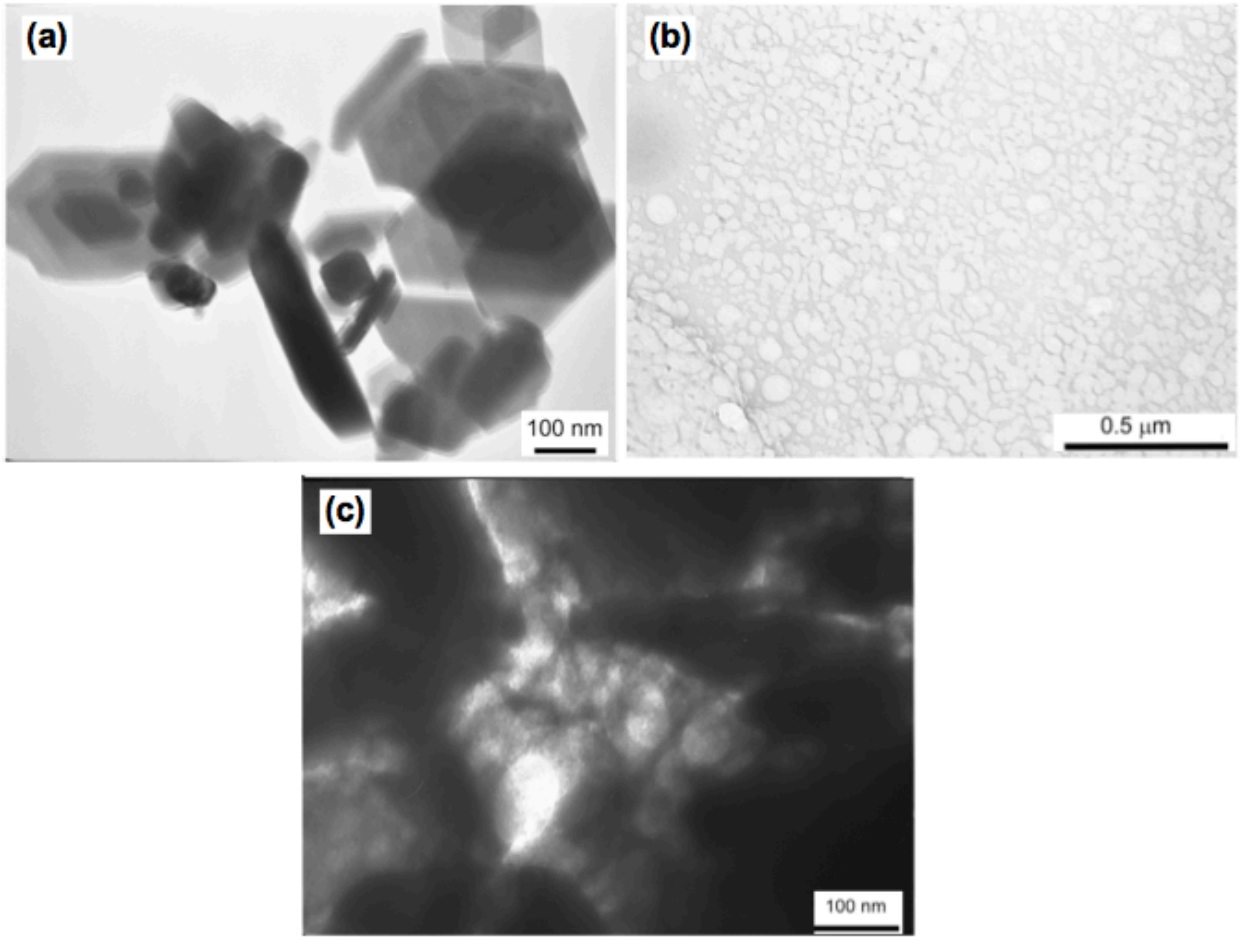

Figure 6.11 TEM images of (a) pure kaolinite, (b) pure guar, and (c) kaolinite-guar mixture.

The proposed microstructure model is constructed via a bottom-up (i.e., from smaller to larger scales) approach to facilitate interpretation and understanding. At the smallest length scale, Level I contains the primary clay particles and guar molecules. The latter in solution usually forms thin fibrils (<1 μm in diameter) and thick or wide bundles (>1 μm in diameter) via short-range intramolecular and intermolecular H-bonding. Relatively strong clay flocculi (8-40 μm in size) exist in Level II, which are formed mainly via short-range FF and EF associations, leading to a densely packed structure. In Level III, microflocs are formed via linking together flocculi and primary particles with guar fibrils and bundles. Such linkage can be further divided into three different types of associations according to the morphology: wide bundles coating around particles and flocculi, gluing onto particle surfaces, and bridging between particles and flocculi (Figure 6.9 and Figure 6.12). Finally, in Level IV, macroflocs are formed by linking together primary particles, flocculi, and microflocs. More specifically, a macrofloc is a nonhomogeneous, porous, hybrid inorganic-organic composite consisting of primary particles, flocculi, and microflocs, all of which are interconnected by guar fibrils and bundles to form a network structure.

As discussed above, clay flocculi are formed mainly via short-range surface-to-surface (i.e., EF and FF) associations, resulting in a densely packed microstructure. In contrast, clay-guar flocs are formed by long-range bridging where guar fibrils or bundles with a length greater than clay particles and flocculi interconnect particles and flocculi. Therefore, clay-guar flocs are much more porous and less dense than clay flocculi. Based on the four discrete particle groups, an ordered formation sequence can be postulated: primary particles are grouped to form flocculi, which can be further bridged by guar to form microflocs and even macroflocs (Figure 6.12). Therefore, higher-order flocs have a lower density and are more porous than lower-order ones, which is consistent with previous work (e.g., *Loch*, 2001).

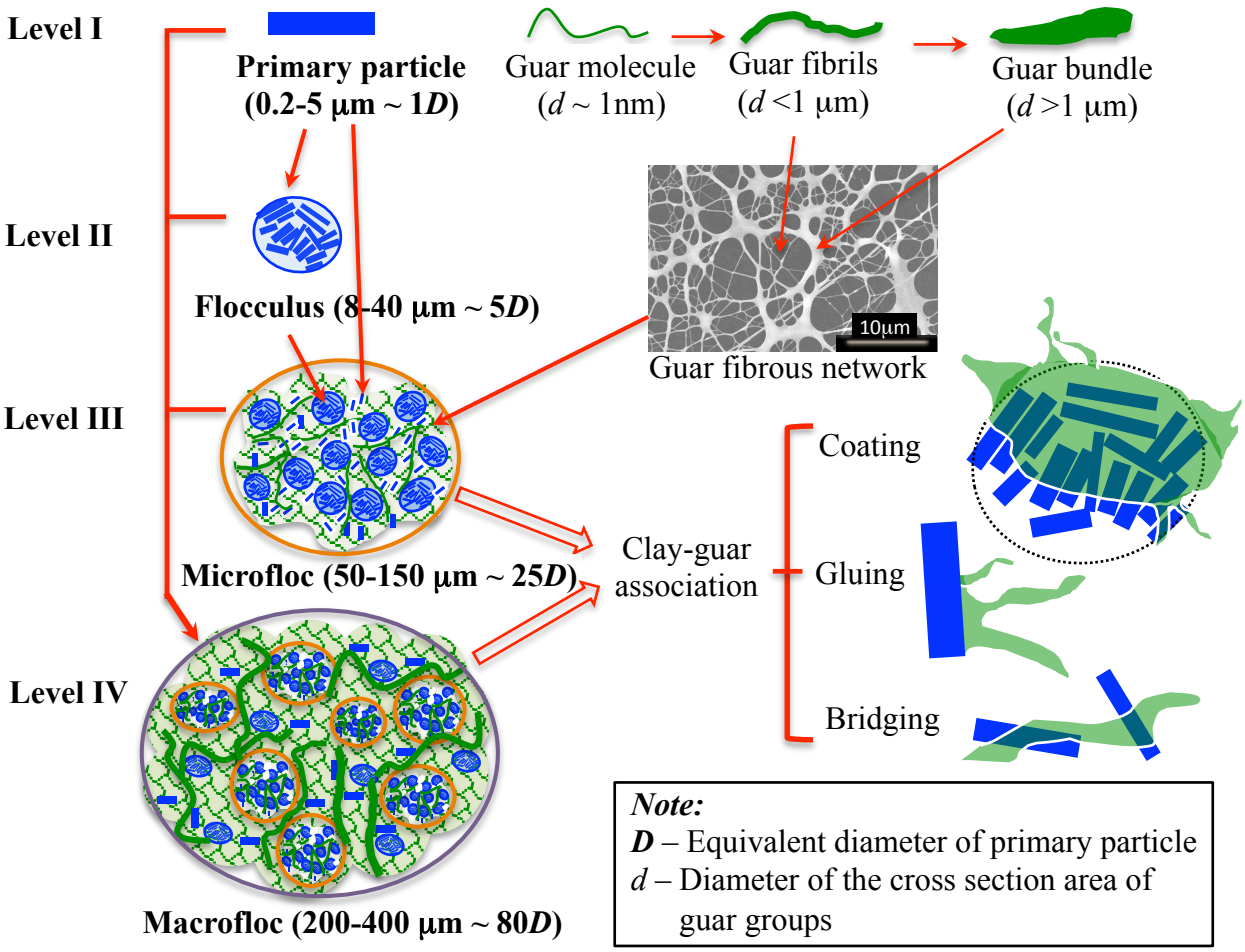

Figure 6.12 A conceptual model for the clay-guar floc microstructure.

6.3.6 Engineering Implications

As mentioned earlier, the microstructure of clay-exopolymer flocs can be preserved, at least during the initial stage shortly after settling, in the settled bed deposit. The flocs will then become the major load-bearing skeleton of the bed soil. The elucidation of floc microstructure can help understand some peculiar engineering behavior and properties of certain sedimentary soils, such as highly organic soils and fluid muds in coastal zones.

The four-level, hierarchical microstructure of clay-exopolymer flocs implies that flocs are highly porous and have exceptionally high water contents. This can result in a remarkably high compressibility for the sedimentary soils that are made up of clay-organic matter flocs. In fact, flocculation between inorganic clay particles and organic substances (e.g., exopolymers, humus) and the resulting high porosity may be the dominant reason for the high compressibility of most organic soils. Second, organic exopolymers have a much smaller specific gravity than clay minerals and other aluminosilicates. The high porosity and inclusion of exopolymers, together with the high water content, render the flocs an exceptionally low density, which could be comparable with that of salt water. As such, these flocs usually settle very slowly and, once settled, they may form a thick layer of fluffy fluid mud at the water-sediment interface. In fact, fluid muds that never settle or consolidate have been observed in some coastal zones. Third, such a network structure suggests that a floc may behave differently in response to tension and compression. The flexible, soft exopolymer molecules, fibrils, and bundles can better support tension than compression, and the exopolymer network can act as a net to entrap and anchor clay particles and aggregates. As such, such flocs and associated deposits may exhibit very low compressive strength, but their tensile strength may be enhanced when compared with that of pure clays. This could be one of the reasons why natural exopolymer-bearing cohesive soils show a better erosional resistance than soils without exopolymers. Fourth, such a hierarchical structure with four different levels also makes the characterization of particle sizes and their distribution difficult. In fact, their PSD tend to vary with the hydrodynamic forcing or the mechanical energy used for remolding samples. It is therefore suggested that the presence of EPS and other organic matter should be always considered in the index property measurements and soil classification. Finally, the conceptual microstructure model can be used to establish more realistic models for exopolymer or even organic matter rich soils. For example, nonhomogeneous, porous granular grains with smaller aggregates interconnected by exopolymer fibrils, instead of homogeneous solid particles, should be used as the fundamental soil units to model exopolymer-bearing, flocculated cohesive soils.

6.4 Conclusions

This chapter presents a systematical characterization of the microstructure of clay-exopolymer flocs using indirect PSD measurement and direct electron microscopy. Four abundant clay minerals (kaolinite, illite, Ca^{2+}-Mt, and Na^{+}-Mt) and a neutral plant polysaccharide, guar, were selected as the model systems studied in the laboratory. A series of conclusions are drawn as follows based on the experimental results and analyses.

First, clay-guar mixture suspensions exhibit multimodal PSDs that consist of discrete particle groups, namely primary particles, flocculi, microflocs, and macroflocs, the latter two of which are absent in pure clay suspensions. Second, the microstructure of clay-guar flocs directly probed by SEM and TEM observations is consistent with the indirect PSD results. Clay-guar flocs are a kind of highly porous, nonhomogeneous, extremely soft, hybrid inorganic-organic composites consisting of two different components: granular, densely packed clay flocculi and primary particles, and a network made of guar fibrils and bundles to which the clay particles and flocculi are connected. Third, clay-guar associations can be divided into three different types based on their morphology: coating, bridging, and surface gluing onto clay particles and flocculi. Finally, a conceptual microstructure model is proposed to delineate clay-guar flocs, which consists of four hierarchical levels with increasing length scales: primary particles and guar

fibers and bundles, clay flocculi, microflocs, and macroflocs, the latter two of which are composed of primary clay particles, flocculi, and guar fibrils network.

6.5 Acknowledgments

This study was partially supported by the Office of Naval Research (Award No. N00173-10-1-G013) under program element number 0601153N. Ms. X. Tan received the La BoR Economic Development Assistantship and LSU Graduate School Supplement Awards. Dr. Z. Lei was supported by the China Scholarship Council to visit LSU as a visiting scholar. The help from Dr. J. Losso and S. Earpina with freeze-drying is gratefully acknowledged.

6.6 References

[1] Abu-Lail, N. I., and Camesano, T. A. 2003. Polysaccharide properties probed with atomic force microscopy, *Journal of Microscopy*, 212, 217-238.

[2] Andrews, S., Nover, D., and Schladow, S. G. 2010. Using laser diffraction data to obtain accurate particle size distributions: the role of particle composition, *Limnology and Oceanography*, 8, 507-526.

[3] Azam, F., and Malfatti, F. 2007. Microbial structuring of marine ecosystems, *Nature Reviews Microbiology*, 5, 782-791.

[4] Bergaya, F., and Lagaly, G. 2006, Chapter 1 General Introduction: Clays, Clay Minerals, and Clay Science, in Developments in Clay Science, edited by F. Bergaya, B. K. G. Theng and G. Lagaly, pp. 1-18, Elsevier.

[5] Berlamont, J., Ockenden, M., Toorman, E., and Winterwerp, J. 1993. The characterization of cohesive sediment properties, *Coastal Engineering*, 21, 105-128.

[6] Bihannic, I., Tchoubar, D., Lyonnard, S., Besson, G., and Thomas, F. 2001. X-Ray Scattering investigation of swelling clay fabric: 1. The dry state, *Journal of Colloid and Interface Science*, 240, 211-218.

[7] Çelik, M. S. 2004, Electrokinetic behavior of clay surfaces, in Interface Science and Technology, edited by W. Fernando and S. Kestur Gundappa, pp. 57-89, Elsevier.

[8] Celis, R., and Koskinen, W. C. 1999. Sorption and desorption of triadimefon by soils and model soil colloids, *J. Agric. Food Chem.*, 47, 776-781.

[9] Chang, I., and Cho, G. 2012. Strengthening of Korean residual soil with β-1,3/1,6-glucan biopolymer, *Construction and Building Materials*, 30, 30-35.

[10] Cheng, Y., Brown, K. M., and Prud'homme, R. K. 2002. Characterization and intermolecular interactions of hydroxypropyl guar solutions, *Biomacromolecules*, 3, 456-461.

[11] Chu, C. P., and Lee, D. J. 2004. Structural analysis of sludge flocs, *Advanced Powder Technology*, 15, 515-532.

[12] Danino, D., and Talmon, Y. 2006, Direct-Imaging and Freeze-Fracture Cryo-Transmission Electron Microscopy of Molecular Gels, in Molecular Gels, edited by R. Weiss and P. Terech, pp. 253-274, Springer Netherlands.

[13] de Boer, D. H., Stone, M., and Levesque, L. M. J. 2000. Fractal dimensions of individual flocs and floc populations in streams, *Hydrological Processes*, 14, 653-667.

[14] Decho, A. W. 2000. Microbial biofilms in intertidal systems: an overview, *Continental Shelf Research*, 20, 1257-1273.

[15] Decho, A. W., and Kawaguchi, T. 1999. Confocal imaging of in situ natural microbial communities and their extracellular polymeric secretions using Nanoplast (R) resin, *Biotechniques*, 27, 1246-1252.

[16] Decho, A. W., Kawaguchi, T., Allison, M. A., Louchard, E. M., Reid, R. P., Stephens, F. C., Voss, K. J., Wheatcroft, R. A., and Taylor, B. B. 2003. Sediment properties influencing upwelling spectral reflectance signatures: The "biofilm gel effect", *Limnology and Oceanography*, 48, 431-443.

[17] Droppo, I. G. 2004. Structural controls on floc strength and transport, *Canadian Journal of Civil Engineering*, 31, 569-578.

[18] Droppo, I. G. 2009. Biofilm structure and bed stability of five contrasting freshwater sediments, *Marine and Freshwater Research*, 60, 690-699.

[19] Droppo, I. G., Leppard, G. G., Flannigan, D. T., and Liss, S. N. 1997. The freshwater floc: A functional relationship of water and organic and inorganic floc constituents affecting suspended sediment properties, *Water Air Soil Pollut.*, 99, 43-53.

[20] Du, J. H., Pushkarova, R. A., and Smart, R. S. C. 2009. A cryo-SEM study of aggregate and floc structure changes during clay settling and raking processes, *International Journal of Mineral Processing*, 93, 66-72.

[21] Eisma, D. 1986. Flocculation and de-flocculation of suspended matter in estuaries, *Netherlands Journal of Sea Research*, 20, 183-199.

[22] Fabricius, K. E., Wild, C., Wolanski, E., and Abele, D. 2003. Effects of transparent exopolymer particles and muddy terrigenous sediments on the survival of hard coral recruits, *Estuar. Coast. Shelf Sci.*, 57, 613-621.

[23] Furukawa, Y., Watkins, J. L., Kim, J., Curry, K. J., and Bennett, R. H. 2009. Aggregation of montmorillonite and organic matter in aqueous media containing artificial seawater, *Geochem. Trans.*, 10, 11.

[24] Gerbersdorf, S., Westrich, B., and Paterson, D. 2009. Microbial extracellular polymeric substances (EPS) in fresh water sediments, *Microbial Ecology*, 58, 334-349.

[25] Goldberg, S., Forster, H. S., and Godfrey, C. L. 1996. Molybdenum adsorption on oxides, clay minerals, and soils, *Soil Science Society of America Journal*, 60, 425-432.

[26] Gupta, V., Hampton, M. A., Stokes, J. R., Nguyen, A. V., and Miller, J. D. 2011. Particle interactions in kaolinite suspensions and corresponding aggregate structures, *J Colloid Interface Sci*, 359, 95-103.

[27] Harris, R. H., and Mitchell, R. 1973. Role of Polymers in Microbial Aggregation, *Annual Review of Microbiology*, 27, 27-50.

[28] Hermawan, M., Bushell, G., Bickert, G., and Amal, R. 2004. Characterisation of short-range structure of silica aggregates—implication to sediment compaction, *International Journal of Mineral Processing*, 73, 65-81.

[29] Hirst, C. N., Cyr, H., and Jordan, I. A. 2003. Distribution of exopolymeric substances in the littoral sediments of an oligotrophic lake, *Microbial Ecology*, 46, 22-32.

[30] Jarvis, P., Jefferson, B., and Parsons, S. A. 2005a. Breakage, regrowth, and fractal mature of natural organic matter flocs, *Environmental Science & Technology*, 39, 2307-2314.

[31] Jarvis, P., Jefferson, B., Gregory, J., and Parsons, S. A. 2005b. A review of floc strength and breakage, *Water Research*, 39, 3121-3137.

[32] Kranenburg, C. 1994. The fractal structure of cohesive sediment aggregates, *Estuar. Coast. Shelf Sci.*, 39, 451-460.

[33] Lagaly, G. 2006, Chapter 5. Colloid Clay Science, in Developments in Clay Science, edited by F. Bergaya, B. K. G. Theng and G. Lagaly, pp. 141-245, Elsevier.

[34] Lambe, T. W., and Whitman, R. V. 1969, Soil Mechanics, 553 pp., John Wiley & Sons, Inc.

[35] Lee, B. J., Fettweis, M., Toorman, E., and Molz, F. J. 2012. Multimodality of a particle size distribution of cohesive suspended particulate matters in a coastal zone, *Journal of Geophysical Research: Oceans*, 117, C03014, 03011-03017.

[36] Lee, S. G., Choi, J. I., Koh, W., and Jang, S. S. 2013. Adsorption of beta-D-glucose and cellobiose on kaolinite surfaces: Density functional theory (DFT) approach, *Applied Clay Science*, 71, 73-81.

[37] Lindström, S. B., Vader, D. A., Kulachenko, A., and Weitz, D. A. 2010. Biopolymer network geometries: Characterization, regeneration, and elastic properties, *Physical Review E*, 82, 051905.

[38] Lintern, G., and Sills, G. 2006. Techniques for automated measurement of floc properties, *Journal of Sedimentary Research*, 76, 1183-1195.

[39] Loch, R. J. 2001. Settling velocity – a new approach to assessing soil and sediment properties, *Computers and Electronics in Agriculture*, 31, 305-316.

[40] Mikkelsen, O. A., Hill, P. S., and Milligan, T. G. 2006. Single-grain, microfloc and macrofloc volume variations observed with a LISST-100 and a digital floc camera, *Journal of Sea Research*, 55, 87-102.

[41] Mitchell, J. K., and Soga, K. 2005, Fundamentals of Soil Behavior, 3rd Edition ed., 577 pp., John Wiley & Sons, Inc., New Jersey.

[42] Molobela, I. P., and Ilunga, F. M. 2012. Impact of bacterial biofilms: the importance of quantitative biofilm studies, *Annals of Microbiology*, 62, 461-467.

[43] Nugent, R. A., Zhang, G., and Gambrell, R. P. 2009. Effect of exopolymers an the liquid limit of clays and its engineering implications, *Transportation Research Record*34-43.

[44] Pawlik, M., and Laskowski, J. S. 2006. Stabilization of mineral suspensions by guar gum in potash ore flotation systems, *Canadian Journal of Chemical Engineering*, 84, 532-538.

[45] Pruett, R. J., and Webb, H. L. 1993. Sampling and analysis of KGa-1b well-crystallized kaolin source clay, *Clay Clay Min.*, 41, 514-519.

[46] Schroth, B. K., and Sposito, G. 1997. Surface charge properties of kaolinite, *Clay Clay Min.*, 45, 85-91.

[47] Tan, X., Zhang, G., Yin, H., Reed, A. H., and Furukawa, Y. 2012. Characterization of particle size and settling velocity of cohesive sediments affected by a neutral exopolymer, *International Journal of Sediment Research*, 27, 473-485.

[48] Theng, B. K. G. 1982. Clay-polymer Interactions - Summary and perspectives, *Clay Clay Min.*, 30, 1-10.

[49] van de Ven, T. G. M., and Hunter, R. J. 1977. Energy-dissipation in sheared coagulated sols, *Rheologica Acta*, 16, 534-543.

[50] van Leussen, W. v. 1994, Estuarine macroflocs and their role in fine-grained sediment transport, Universiteit Utrecht, Faculteit Aardwetenschappen, Utrecht.

[51] Wientjes, R. H. W., Duits, M. H. G., Jongschaap, R. J. J., and Mellema, J. 2000. Linear rheology of guar gum solutions, *Macromolecules*, 33, 9594-9605.

[52] Zhang, G., Germaine, J. T., Whittle, A. J., and Ladd, C. C. 2004. Soil structure of a highly weathered old alluvium, *Geotechnique*, 54, 453-466.

[53] Zhang, G., Yin, H., Lei, Z., Reed, A. H., and Furukawa, Y. 2013. Effects of exopolymers on particle size distributions of suspended cohesive sediments, *Journal of Geophysical Research: Oceans*, 118, 1-17.

CHAPTER 7 ROLE OF INTERMOLECULAR FORCES IN THE FLOCCULATION OF SUSPENDED KAOLINITE WITH EXOPOLYMERS IN FRESH AND SALT WATERS

7.1 Introduction

Clay minerals are characterized by chemically active surfaces with face surface possessing permanent negative charge (due to isomorphous substitution) and edge surface pH-dependent charges (i.e., negative if pH>7, positive if pH<7, due to imperfect crystal structure). The net negative charges are balanced by the counterions (i.e., cations) adsorbed onto the surfaces. Both of the clay mineral and exopolymer are macromolecules. Given that biopolymers usually possess charges of different quantity and polarity (i.e., polyanionic, nonionic and polycationic from -COOH, -OH and $-NH_2$, respectively), the interactions of clay particles with biopolymers are very complicated (*Theng*, 2012b), and different interactions between clays and biopolymer molecules usually coexist, which are dominated by their surface properties or functional groups, chemical structure, and conformation (e.g., the shape and association of polymer molecuels), and further influenced by the presence of different ions (e.g., ions in solution or adsorbed on clay surface).

Analyses of the interactions between different clay minerals and various exopolymers is of key importance but difficult, which mainly due to abusing of intermolecular forces (e.g., hydrogen bonding, van der Waals (VDW) force) or confusing of scales (i.e., atomic level or molecular level). *Theng* (2012b) summarized that the interaction between clay and exopolymers can be grouped into three categories according to the polarity of exopolymers. While a clearly discussion on the interaction details (i.e., type of the bonds and magnitude for different clays) still lacks. This study aims to present detailed and systematic clay and exopolymer flocculation mechanism, starting from the atomic level interactions with regard to the classification of intermolecular forces, by analyzing selected clay-exopolymer models.

There are four well-established, distinct forces in nature (*Israelachvili*, 2011), electromagnetic and gravitational forces (between atoms, molecules, elemental particles, etc.), strong and weak forces (between neutrons, protons, electrons, etc. in nuclear and high-energy physics). According to the chemical and physical property of clay and exopolymer, the interactions are electromagnetic forces. Since electromagnetic force is a wide and general definition, more detailed and further classification was performed. Electromagnetic forces, or intermolecular forces, can be roughly separated into four groups according to the properties of bonding or interaction (*Briscoe*, 2010; *Israelachvili*, 2007) (Figure 7.1): (1) Chemical bonding (i.e., covalent, ionic and metallic bonds with quantum mechanical nature) and steric repulsions (regarding to Pauli's exclusion principles), which are very short-ranged forces, e.g., covalent bond at 0.1-0.2 nm; (2) Coulomb force (or electrostatic force) between permanent charges and dipoles (i.e., charge-charge, ion-dipole) at a relatively long range (~0.3 nm); (3) Polarisation force between dipoles induced by nearby charges and permanent dipoles, including VDW force of three types (i.e., Keesom force, Debye force and London dispersion force) ranging 0.25-0.46 nm, which is considered as long ranged on molecular scale (~7 nm) but short-ranged on colloidal scale (1-10 μm); and (4) Hydrogen bonding (H-bonding), as special VDW force with some feature of covalent bond, of strong electromagnetic dipole-dipole attraction between hydrogen

donor and acceptor (i.e., N, O, F), which is typically considered as a short-ranged force ranging 0.26-0.25 nm.

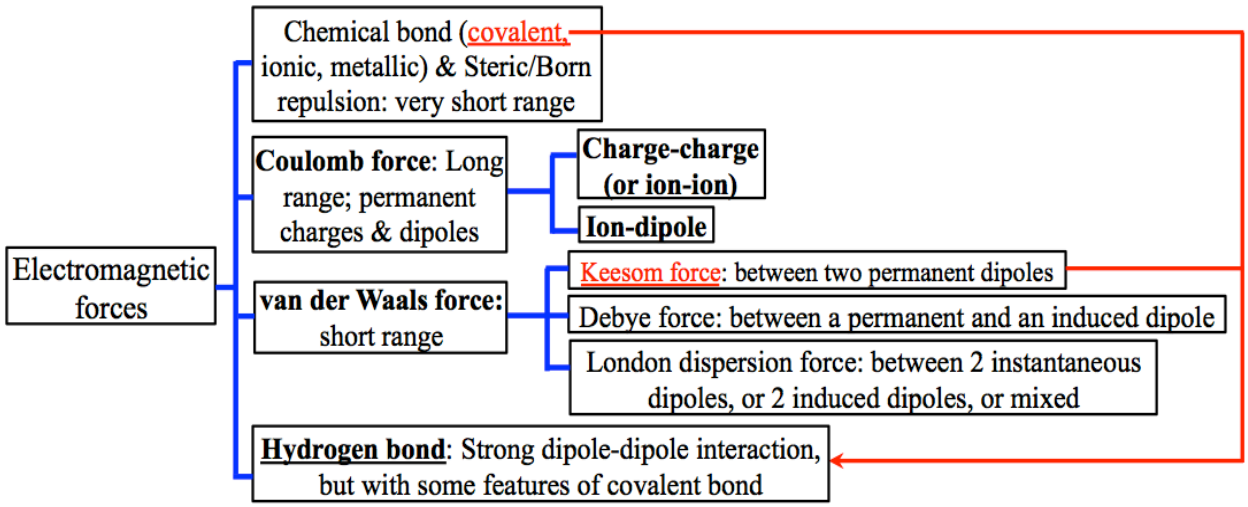

Figure 7.1 Classification of intermolecular forces.

This chapter aims to develop a systematic understanding about the details of clay-exopolymer flocculation in both fresh and salt waters with the appropriate nomenclature for all the involved intermolecular forces. Understanding of the fundamental mechanisms of clay-exopolymer flocculation is important for the studies in other areas, e.g., sediment transport, wastewater treatment, synthesis of inorganic-organic composite, etc.

7.2 Experimental Section

7.2.1 Materials

The high-purity clay mineral, kaolinite (KGa-1b), supplied by US Clay Minerals Society (Purdue University, Indiana, USA) as dry powders with the -44 μm fraction (i.e., via wet sieving through a #325 mesh) (*Pruett and Webb*, 1993), was chosen as the representative for inorganic components of the clay-exopolymer flocs or composites. As one of the most abundantly used source clay minerals, KGa-1b has been well analyzed and widely used by many studies as a reference clay mineral. Its geographic origin and basic properties are summarized in Table 7.1.

Interaction of clay and EPS typically depends on the polarity of exopolymers, thus EPS can be roughly grouped into three types: anionic, nonionic, and cationic (*Theng*, 2012b). Hence, to account for the varieties of naturally existing exopolymers, polyanionic xanthan gum (Spectrum®, Gardena, CA), nonionic guar gum (Fisher ChemAlert® Guide, Rochester, NY), and polycationic chitosan (Acros Organics, New Jersey, USA) were chosen as the EPS representatives that may induce flocculation of clay sediments. Chitosan was selected because it is the only commonly available natural polycationic exopolymer that has been found. While according to previous experiment and analysis, the unmodified chitosan is water-insolvable in circumneutral pH conditions (i.e., only dissolve when pH< 6.5 (*Sashiwa and Shigemasa*, 1999)), and the modified chitosan can be water-solvable but at the price of $-NH_2$ functional groups. Thus, the flocculation of kaolinite induced by only xanthan gum and guar gum was investigated.

Table 7.1 Origin and basic properties of the selected kaolinite[a].

Name	Origin	CEC[b] (meq/ 100g)	Layer charge[c] (unbalanced charge)		SSA[d] (m^2/g)	pH[e]	Chemical formula
			T	O			
KGa-1b	Washington County, Georgia	2.00	-0.06 (0)		10.05	5.97	$(Mg_{.02}Ca_{.01}Na_{.01}K_{.01})$ $\{Al_{3.86}\ Fe^{3+}_{.02}Mn_{tr}Ti_{.11}\}$ $\{Si_{3.83}\ Al_{.17}\}O_{10}(OH)_8$
			-0.17	+0.11			

[a] All data except those noted are taken from the Clay Minerals Society Source Clay Physical/Chemical Data.
[b] CEC = cation exchange capacity.
[c] The layer charge is based on per $O_{10}(OH)_8$; O: charge from octahedral sheet; T: charge from tetrahedral sheets.
[d] SSA = specific surface area.
[e] For pure kaolinite suspension with a concentration of 0.4 g/L in deionized water at room temperature (23°C).

Xanthan, as the polyanionic exopolymer analog, is a water-soluble bacterial extracellular polysaccharide produced via fermentation by *Xanthaomonas campestris* bacterium (Figure 7.2 a). Due to different bacterial strains and the growth environments, the molecular weight of xanthan varies but typically ranges 0.9-1.6 x 10^6 Da. Its negative charge is from the carboxyl (-COOH) in glucuronic acid and pyruvic acid groups on side chains (*Ian W*, 1994). Guar, as the nonionic exopolymer analog, is a plant polysaccharide from the seed of *Cyamopsis tetragonoloba* (Figure 7.2 b). Its aqueous solution is highly viscous and pseudoplastic (*Cheng et al.*, 2002). A low concentration guar solution can bring clay minerals to flocculation, while a high concentration solution may lead to steric re-dispersion (*Pawlik and Laskowski*, 2006). Length of the molecular backbone (L) for the two exopolymers (Figure 7.3) was estimated by using the method developed by *Chang and Cho* (2012), on the basis that the scale of a glucose is 1 nm. The morphology of macromolecules is very complicated that they may form intramolecular forces resulting in random coil or double-strained helix conformations, instead of existing as straight molecules. The mean end-to-end polymer distance (l) was also calculated using the method from *Stuart et al.* (1984) and *Swenson et al.* (1998) as Equation 7.1.

$$l \approx \sqrt{6} * \frac{M^{0.57}}{45} = \frac{M^{0.57}}{18.4} \qquad \text{Equation 7.1}$$

Additionally, to study the flocculation of clay and clay-exopolymer in salty conditions, an Instant Ocean® sea salt was chosen to prepare salt water. Compositions and major ions of this commercial salt has been reported by *Atkinson and Bingman* (1998). The characteristic length of the double layer, Debye length (t_D), on clay surface can be estimated by using the following equation (*Block*, 1978):

$$t_D = \sqrt{\frac{\varepsilon_0 * \varepsilon * k * T}{\sum_{j=1}^{N} n_j * q_j^2}} \qquad \text{Equation 7.2}$$

where ε_0 is the permittivity of vacuum, ε the dielectric constant, k the Boltzmann constant, T the absolute temperature, and n_j and q_j the mean concentration and valance of the j-th ion species,

respectively. After calculation, it was found that t_D decreases most significantly as salinity increases from 0 to 10 ppt (parts per thousand) (Figure 7.3). Thus, only the salinity of 10 ppt was chosen for preparing clay-exopolymer suspension samples.

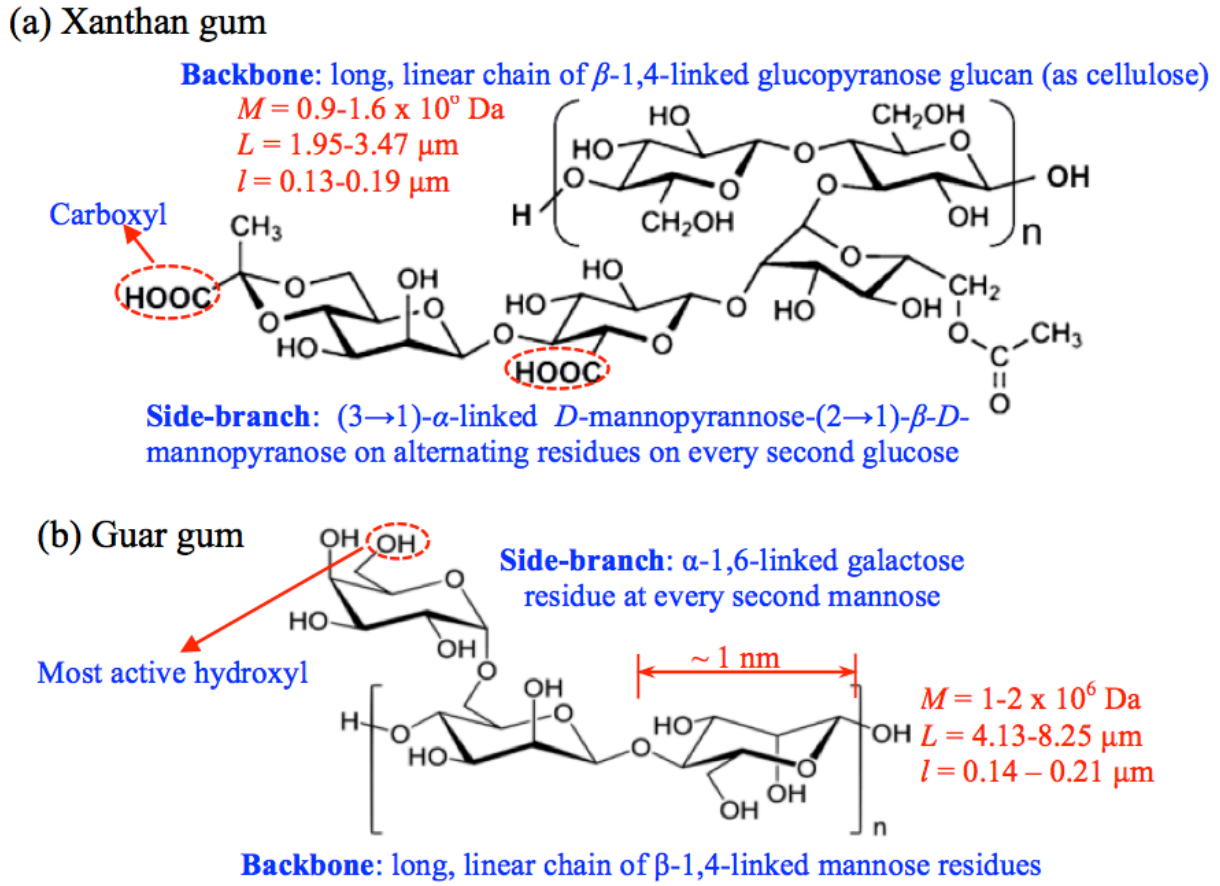

Figure 7.2 Chemical and molecular structure of (a) anionic xanthan and (b) nonionic guar (M - molecular weight, L - estimated length of molecular backbone, l – estimated mean end-to-end polymer distance).

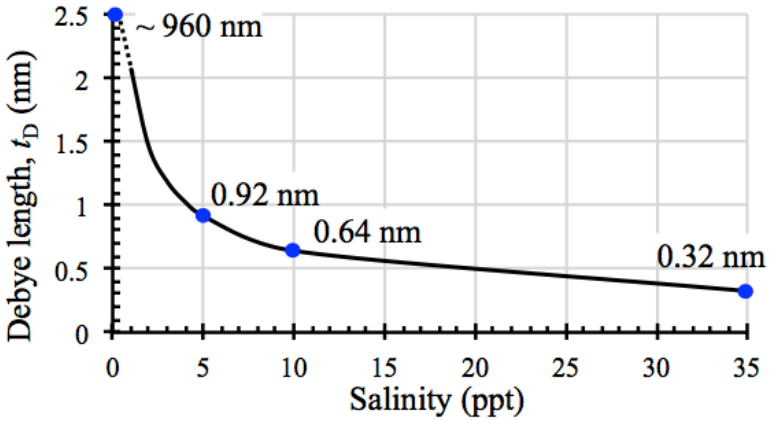

Figure 7.3 The decrease of Debye length (t_D) as salinity change from 0 to 35 ppt.

7.2.2 Floc Preparation and PSD Measurement

Laboratory preparation of clay-exopolymer flocs started with dispersing clay samples in deionized (DI) water or salt water to eliminate aggregates pre-existing in the dry powders. A Cilas® 1190 laser diffraction-based particle size analyzer (PSA) (Cilas Particle Size, Madison, WI, USA), which has a liquid dispersion and circulation system, was used to disperse clay samples, generate flocs, and perform PSD measurements. For floc samples in fresh water, firstly, 0.2 g dry kaolinite was soaked in 5 mL DI water for at least 16 h, followed by dilution with additional 200 mL DI water in the PSA's sample bath. The kaolinite suspension was dispersed by the built-in ultrasound disperser beneath the sample bath for a sufficient period of time. Then 50 mL exopolymer solution with concentrations of 10, 100, 1000 μg/g was added to the sample bath, followed by adding more DI water to bring the total volume of the mixture suspension to 500 mL (i.e., the total volume of the PSA's bath and connection tubes), resulting in pre-designed final concentrations of 0.4 g/L and 1, 10, 100 μg/g for kaolinite and exopolymer at different concentrations, respectively. For floc samples in salt water, all the DI water was substituted for with 10 ppt salt water and the procedures were the same. The 1, 10, 100 μg/g were chosen to examine different exopolymer concentrations or load levels varying from seasons and locations in natural water systems, selected from the range of 0-1000 μg/g (*Gerbersdorf et al.*, 2009; *Hirst et al.*, 2003). To better investigate the influence of exopolymers on kaolinite particle size, pure kaolinite samples in DI water and 10 ppt salt water were also prepared.

Liquid circulation, sample mixing, floc formation, and PSD measurement were then performed sequentially in the PSA. The mixture suspension was first circulated in the PSA's closed-loop liquid circulation system, driven by a pedal-like stirrer at a speed of 180 rpm inside the sample bath and a peristaltic pump at a speed of 30 rpm located at the tube section, which resulted in an average flow velocity of 150 mm/s in the circulation tubes. Given that the dynamic viscosity of the xanthan and guar solutions ranges from 0.894-1.092 mPa*s (*He and Horikawa*, 1996 et al.) and a corresponding Reynolds number of 893-1091 was calculated for the flow in the tubes. As such, all the clay-exopolymer flocs were formed in laminar flow condition. During circulation, the flocculation process was monitored via measuring the real-time PSD. Final PSD of the floc sample was measured when it arrives at a steady state.

In this chapter, the particle size obtained by the Cilas® PSA is defined as the diameter of equivalent spheres calculated based on the volume moment mean value of multiple particles at a given size range. That is:

$$D = \frac{\sum n*l^4}{\sum n*l^3} \qquad \text{Equation 7.3}$$

where D is the mean diameter of all flocs and particles within a given size range, n the number of particles at a fixed size, and l the diameter of a particle or floc.

The PSD of all samples were plotted via both the probability density function (PDF, or frequency) and cumulative distribution function (CDF, or percent finer by particle number). To better quantify the PSD compositions and change and understand flocculation behavior, the PSD data was further processed via decomposing their PDF or CDF, as the deconvolution routine developed by (*B J Lee et al.*, 2012; *Němeček et al.*, 2009; *Ulm et al.*, 2007; *Zhang et al.*, 2013).

7.3 Results

Particle sizes of all the laboratory-prepared systems, pure kaolinite, kaolinite-exopolymer, kaolinite-salt, and kaolinite-salt-exopolymer, were measured and the PSD curves (CDF – dashed line, PDF – solid line) are shown in Figure 7.4, 7.5 and 7.6. Generally, all the PSD curves have multimodal, subordinate lognormal distributions consisting of primary particles (0.2-5 μm), flocculi (8-40 μm), microflocs (30-150 μm), and macroflocs (200-500 μm). The most striking features are the remarkable shift of the pure clay CDF curve to the right with the addition of exopolymer and/or salt, accompanied with the appearance or disappearance, and location or fraction change of some distributions. Pure kaolinite suspension, considered as the 1st-level baseline for studying the exopolymer and/or salt induced flocculation, consists of only primary particles (41.4%) and flocculi (58.6%) distributions with the mean size at 0.3-2.44 and 12.97 μm, respectively (Figure 7.4 a).

7.3.1 Kaolinite-xanthan System

Addition of xanthan results in flocculation by generating microflocs or macroflocs (Figure 7.4 b-d). From the pure kaolinite sample to the kaolinite-xanthan with low level concentration (1 μg/g), the amount of primary particles and flocculi significantly decreases from 41.4% to 1.4% and 58.6% to 27.6%, respectively, with the generation of 27.6% microflocs and 65.6% macroflocs sizing 50-500 μm (Figure 7.4 a-b). As xanthan concentration increases to the medium level (10 μg/g), the CDF curve shifts to the left with the disappearance of macroflocs distribution on the right and a fraction increase for all the remaining distributions. The mean size of microflocs also remarkably decreases from 117.68 to 39.48 μm (Figure 7.4 b-c). When xanthan concentration keeps increasing to the high level (100 μg/g), the CDF continues shifting to the left, the fraction of microflocs decreases, simultaneously, and the fractions of both primary particle and flocculi increase (Figure 7.4 c-d). From the observation of the PSDs, it is found that xanthan with a relatively low level concentration (1 μg/g) can induce kaolinite flocculation significantly, while higher level concentrations impede the flocculation.

7.3.2 Kaolinite-guar System

Basically, similar to xanthan, the addition of guar results in the CDF curve shifting right with the generation of flocs (Figure 7.4 a, e-g), while the concentration for generating macroflocs is different from that of xanthan. When guar concentration increases from 0 to the low level (1 μg/g), only microflocs with a fraction of 62.8% were generated (Figure 7.4 a, e). As the concentration increases to the medium level (10 μg/g), the CDF curve remarkably shifts to the right by generating macroflocs with mean size of 254.82 μm and this is accompanied by the fraction decrease for primary particles and flocculi (Figure 7.4 e-f). As the guar concentration continues increasing to the high level (100 μg/g), the PSD curves don't have significant changes except that the mean size of microflocs increases from 56.74 to 87.86 μm and the fraction of macroflocs keeps increasing to 25.2% (Figure 7.4 f-g). According to these phenomena, guar is an efficient flocculant, and the efficiency keeps increasing as its concentration increases from 1 to 100 μg/g.

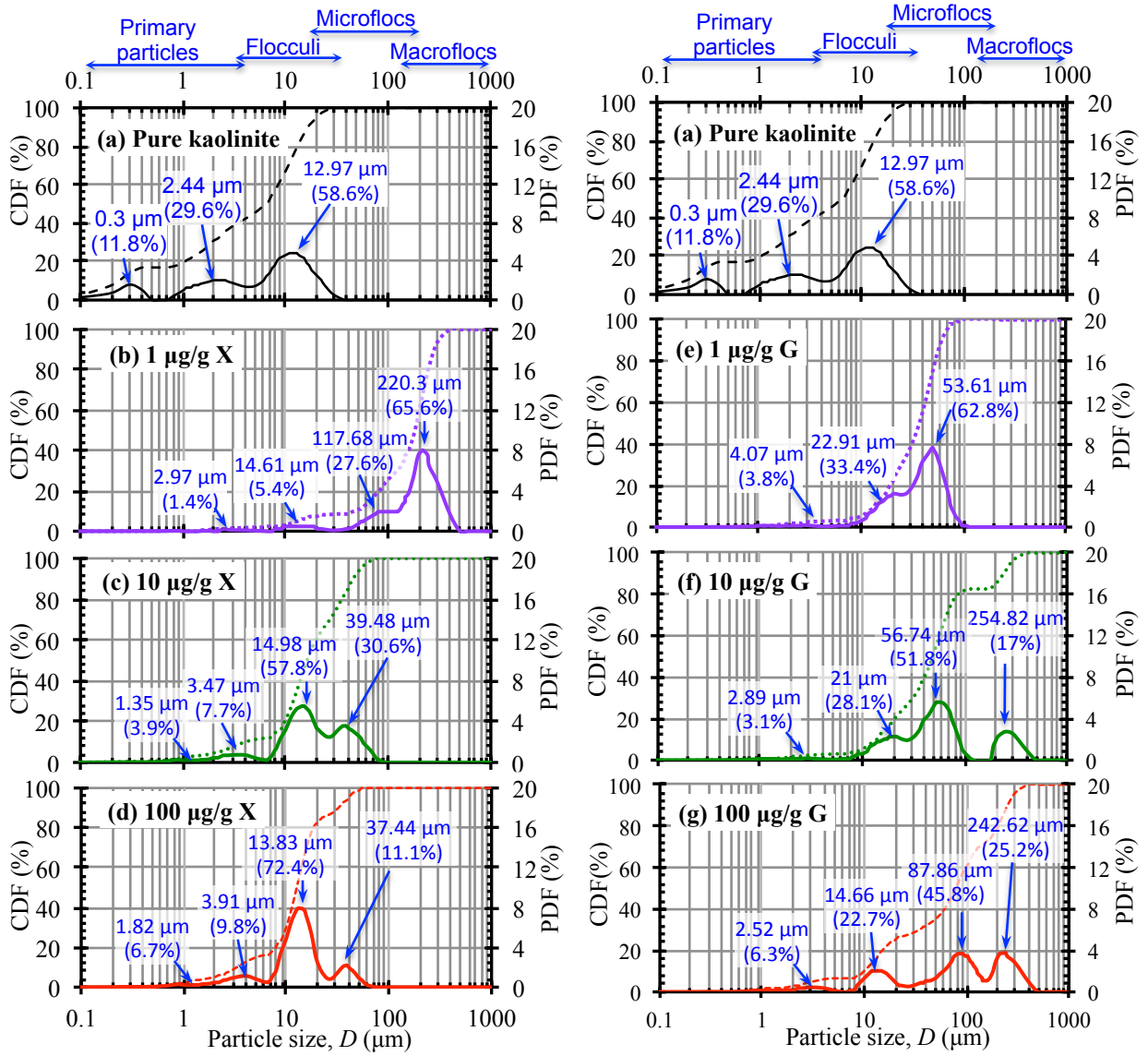

Figure 7.4 PSDs of kaolintie affected by xanthan (X) and guar (G) at different concentrations with the mean size and fraction changes of primary particles (0.2-5 μm), flocculi (8-40 μm), microflocs (30-150 μm), and macroflocs (200-150 μm).

7.3.3. Kaolinite-salt System

This kaolinite-salt system was selected to study the behavior of kaolinite in salt waters with different salinities, which is taken as the reference for choosing salinity for the kaolinite-salt-exopolymer system and as the 2nd-level baseline for understanding this complicated, three-element system. Particle size of kaolinite in salt waters changes as the salinity (Figure 7.5). Generally, the presence of salt with various ions does not create flocs for kaolinite, but the fraction of flocculi is increased and that of primary particles is decreased. When the salinity increases from 0 to 10 ppt (Figure 7.5 a-c), fraction of flocculi increases from 58.6% to 85.4% with the fraction of primary particles decreasing accordingly. Then the fraction of flocculi decreases slightly from 85.4% to 77.8% with the CDF curve shifting to the left, as the salinity

increases to 35 ppt (Figure 7.5 c-d). Thus, it is obvious that, salt water with 10 ppt most significantly changes kaolinite particle size and promotes the aggregation or coagulation of kaolinite.

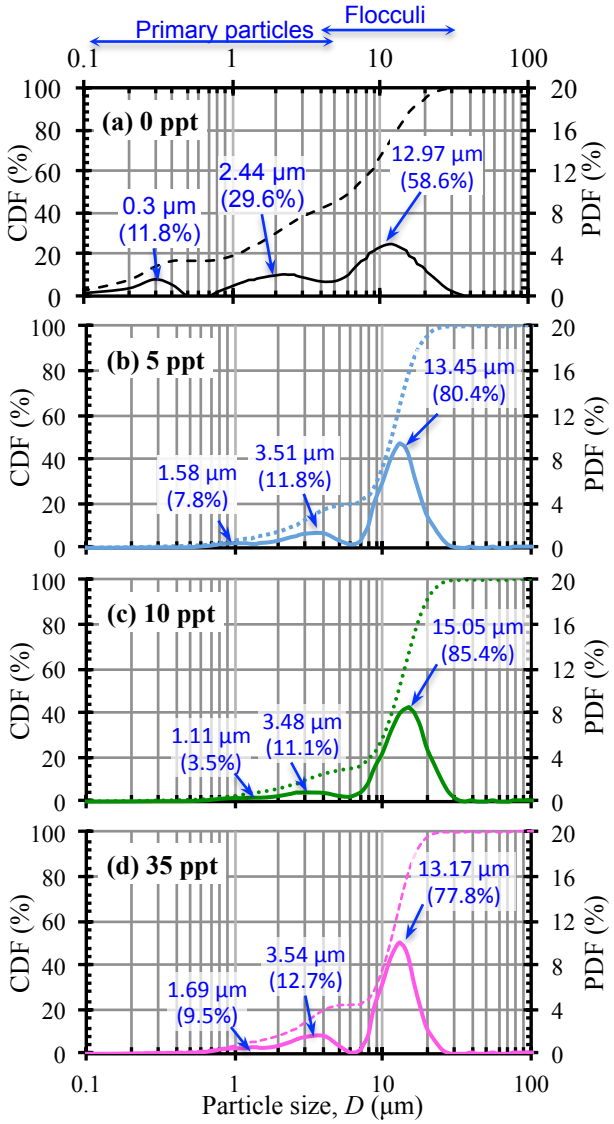

Figure 7.5 PSD of kaolinite in salt waters.

7.3.4 Kaolinite-salt-exopolymer System

According to the PSD result of kaolinite-salt system, salinity of 10 ppt was selected for preparing the kaolinite-salt-exopolymer system for both xanthan and guar with purpose of maximizing its difference from the kaolinite-exopolymer system. Figure 7.6 a-c shows the PSD of kaolinite-salt-xanthan system with comparison to both the kaolinite-salt and kaolinite-xanthan systems. With the addition of salt to kaolinite-xanthan system or of xanthan to kaolinite-salt system, the CDF curve remarkably shifts to the right with macroflocs appearing at ~200 µm, which indicates that kaolinite flocculation is mutually promoted by salt and xanthan. While for the kaolinite-salt-guar system, the addition of salt to the kaolinite-guar system does not increase

particle size via flocculation (Figure 7.6 a, d-e). On the contrary, the fraction of clay-guar macroflocs was slightly decreased from 25.2% to 15.7% after salt was added.

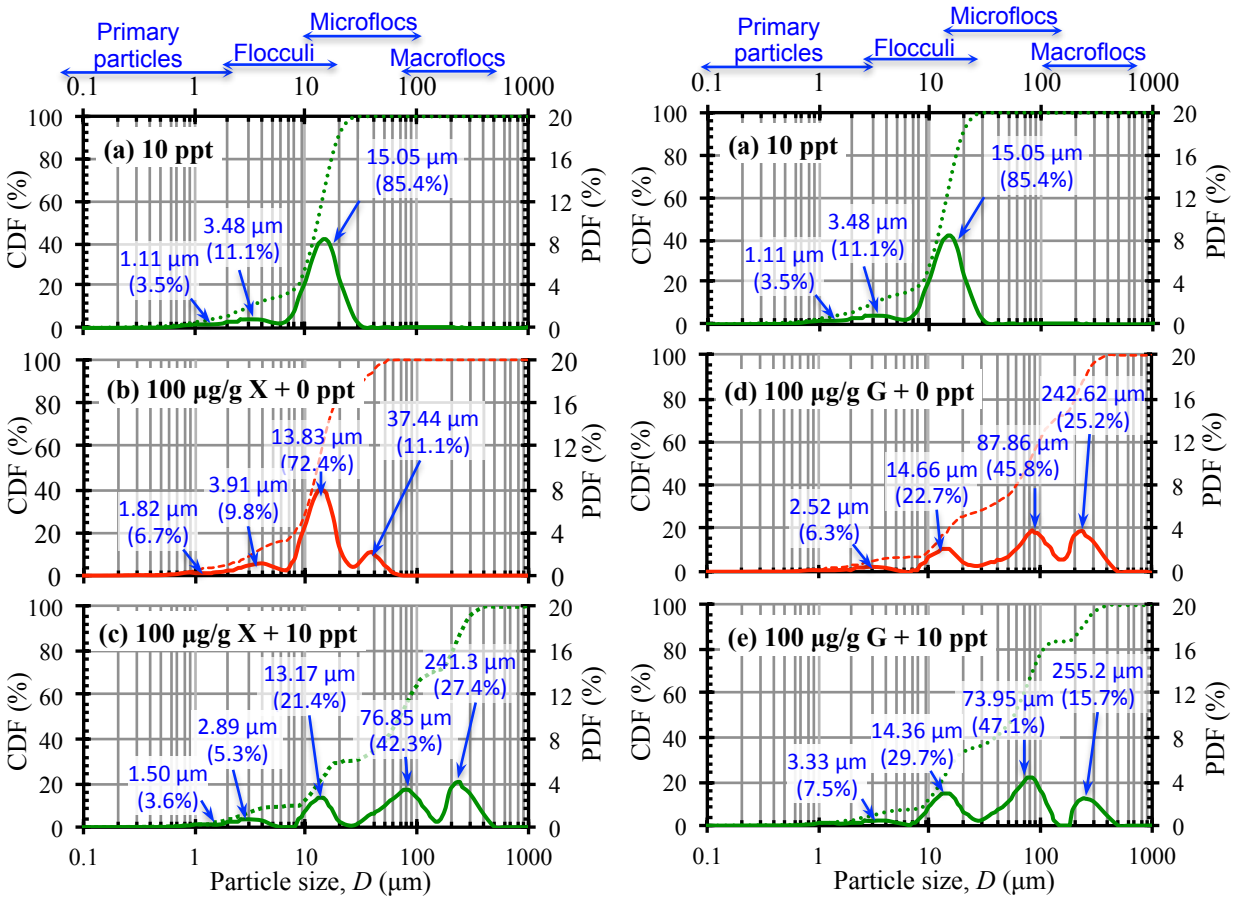

Figure 7.6 PSD of kaolinite with xanthan (X) and guar (G) in fresh and salt waters.

7.4 Discussion

Regarding the floc preparation process, floc formation (via interparticle interactions) and breakage (mainly controlled by flow-induced shear stress) occurred simultaneously when the suspension was being stirred in the sample bath and circulated in the tubes. At the given flow velocity, flocs with a strength greater than the shear stress can survive, while weaker ones break up (smaller flocs typically have greater strength than bigger ones) and then re-flocculate. Such floc breakage and reflocculation occur continuously until a steady state, at which the floc size can be an indication of both the floc strength (*Jarvis et al.*, 2005) and flocculation analysis.

The formation of clay-exopolymer flocs can be simplified as mainly a two-step process (*Gregory*, 1988; *Stuart*, 1990; *Tambo and Watanabe*, 1979): (1) adsorption of exopolymer molecules onto clay surfaces with the re-arrangement or re-conformation of exopolymer to an equilibrium configuration and (2) interactions among clay particles with adsorbed exopolymer to form flocs. Specifically, after adsorption, an exopolymer molecule usually forms a loop-train-tail conformation on the clay particle surface or substrate (*Stuart*, 1990; *Theng*, 1982) (Figure 7.7). The loop and tail parts of exopolymer are usually at the diffuse layer of the electrical double

layer, while the train segments can stay in the stern or inner layer of the electrical double layer of clay particle (*Theng*, 2012b), indicating that the 1st-step adsorption originates between the train segment of exopolymer and clay surface via short-range forces (Figure 7.7) and the 2nd-step of flocculation results from long-range interaction between the loop-tail parts and clay particle or flocculus (Figure 7.8).

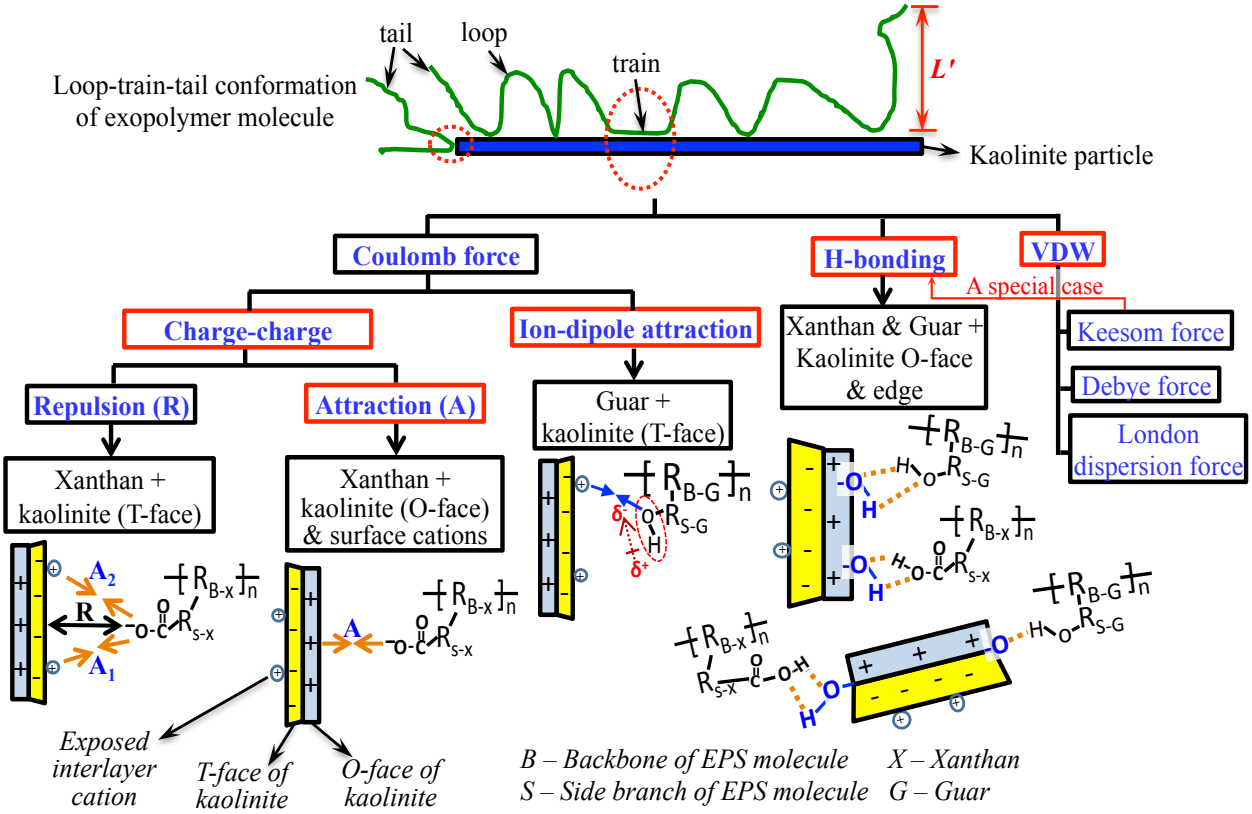

Figure 7.7 Adsorption of exopolymer molecules onto kaolinite surface as the 1st-step of flocculation.

7.4.1 Adsorption – 1st-step of Flocculation

To better describe and explain intermolecular interactions between kaolinite and exopolymers in the 1st-step of flocculation, intermolecular forces can be roughly grouped into three types according to the charge or polarity of participating molecules: Coulomb force (or electrostatic force) between charges or ions (including ion-dipole interaction), VDW force between two dipoles (i.e., permanent, induced, instantaneous), and hydrogen bonding. Moreover, based on the analysis of the molecular and chemical structure of kaolinite and the two exopolymers as well as the flocculation behavior indicated from PSD results, details of the short-range interactions are shown in Figure 7.7.

7.4.1.1 Kaolinite-xanthan (mainly Coulomb force)

Due to partial dissociation of –COOH on side-branches of xanthan at intermediate pH (*Young et al.*, 1994), dissolved xanthan contains both $–COO^-$ and –COOH, which renders xanthan the properties of a polyanionic and nonionic polymer, respectively. Thus, for kaolinite

and xanthan, the 1st-step short-range forces include mainly Coulomb force (charge-charge) and H-bonding. The charge-charge interaction occurs between dissociated carboxyl ($–COO^–$) and the charge sites on both T- and O-face surfaces of kaolinite. Specifically, the positive charge on kaolinite O-face surface, mainly located at Ti^{4+}, at which Al^{3+} has been isomorphously substituted. As a result, the charge-charge attraction is generated between $–COO^–$ and positive charge sites around Ti^{4+} on O-face surfaces. Likewise, the charge-charge repulsion regarding $–COO^–$ is seated at the negative charge sites around Al^{3+} on T-face surfaces. Particularly, the exposed interlayer cations (Mg^{2+}, Ca^{2+}, Na^+, K^+, Table 7.1) on T-face surfaces for balancing the negatively surface charge also interact with $–COO^–$ via charge-charge attraction. A schematical diagram of these details is shown at the bottom left of Figure 7.7. In addition to the H-bonding between kaolinite and xanthan, it is mainly generated between the –OH in undissociated carboxyl (–COOH) and –OH on O-face surfaces as well as exposed –O or –OH on edge faces of kaolinite (Figure 7.7). The other two forces, ion-dipole (i.e., between exposed interlayer cations and –COOH) and VDW (possibly among all atoms), also exist in kaolinite-xanthan system, but they make minor contribution to the exopolymer adsorption because these two forces are much weaker (Table 7.2). In summary, although they are both negatively charged in an overall view, adsorption of xanthan molecules onto kaolinite surfaces is still applicable, which results in kaolinite-xanthan flocs formation (Figure 7.4 a-d).

In addition, degree of dissociation for xanthan at the concentration of 1, 10, 100 μg/g is approximately estimated as 0.1, based on *Young et al.* (1994). Comparing the order of magnitude for the amount of total $-COO^–$ in the aqueous suspension and total cations on kaolinite O-face surfaces (Table 7.2), it is interesting to find that these two amounts have the same order of magnitude when xanthan concentration is 1 μg/g, which is possibly the reason for the generation of macroflocs. As a result, 1 μg/g xanthan is the optimum amount for the flocculation of kaolinite at 0.4 g/L. When xanthan concentration increases to 10 and 100 μg/g, the overdosed exopolymer produces steric stabilization (*Theng*, 2012a) and impedes the flocculation of kaolinite.

7.4.1.2 Kaolinite-guar (mainly H-bonding)

The most active hydroxyl (–OH, Figure 7.2 b) in guar only can dissociate in very high pH solutions. The lack of ionizable or dissociable functional groups (e.g., –COOH, $–NH_2$) that are commonly found in anionic or cationic exopolymers renders guar neutrality in circum-neutral pH condition (pH = 5.97, Table 7.1). Hence, unlike xanthan discussed above, guar is only considered as a nonionic exopolymer. Interactions between kaolinite and guar include mainly H-bonding and Coulomb force (ion-dipole attraction). H-bonding, similar to xanthan, is located on the O-face surfaces and exposed –O or –OH on edge faces of kaolinite. Ion-dipole attraction generates between the most active hydroxyl and the exposed interlayer cations on negatively charged T-face surfaces (Figure 7.7). The analysis matches other reported results. For example, as reported by (*S G Lee et al.*, 2013) with the results from density functional theory approach, it was found that H-bonding mainly forms between the hydroxylated surface (O-face surface) of kaolinite and nonionic exopolymers. Although –O in T-face surface can also be a hydrogen acceptor, it has less flexibility in the structure and hence is less efficient in the formation of H-bonding (*S G Lee et al.*, 2013).

With the parameter of basic properties for kaolinite (i.e., SSA and unit cell structure in Table 7.1, and the average aspect ratio of 5.3 (*Zbik and Frost*, 2009)), along with the assumptions that (1) kaolinite particles are all perfect hexagonal prism, (2) the average size of primary particles is D = 2 μm as the diameter of a equivalent sphere, and (3) kaolinite unit cell can be approximately treated as a cuboid with a = 1.026 nm, b = 0.889 nm, and c = 0.725 nm. The total number of hydroxyl on kaolinite particle surfaces was estimated, which is ~4.6×10^{18} for 0.4 g/L kaolinite with the volume of 500 mL (Table 7.2), and the total amount of the most active hydroxyl in guar solutions is 6.21×10^{17}, 6.21×10^{18}, and 6.21×10^{19} for 500 mL guar solution with concentration of 1, 10, and 100 μg/g, respectively. It is interesting to compare the total amount of the most active hydroxyl in guar and hydroxyl on kaolinite surface, with regard to kaolinite-guar flocculation. From Table 7.2, the amount of these two groups of hydroxyl is at the same order of magnitude only when guar concentration is 10 μg/g, at which H-bonding sites on kaolinite are saturated and kaolinite-guar macroflocs begin to generate (Figure 7.4 f). In guar solution with lower level concentration (1 μg/g), the amount of the most active hydroxyl is one order of magnitude lower than that on kaolinite, which results in only microflocs (Figure 7.4 e) without macroflocs due to insufficient H-bonding in the 1st-step adsorption. While with higher guar concentration (100 μg/g), the amount of the most active hydroxyl is one order of magnitude higher than that on kaolinite surface, since H-bonding sites on kaolinite are oversaturated and extra guar molecules mainly interact with themselves, which facilitate the 2nd-step flocculation via polymer bridging (as discussed below). Hence, compared with 10 μg/g guar, higher guar concentration only increases the fraction of macroflocs.

Table 7.2 Estimated chemical structure features of kaolinite, xanthan, and guar in their aqueous suspensions with volume of 500 mL.

Kaolinite (0.4 g/L)	Total charge on O-face surfaces	1.30×10^{17} (e, +)		
	Total charge on T-face surfaces	8.44×10^{16} (e, -)		
	Total cations on T-face surfaces	3.84×10^{16}		
	Total –OH on O-face surfaces	4.60×10^{18}		
Exopolymer Concentration (μg/g)		1	10	100
Xanthan	Amount of -COOH	6.52×10^{17}	6.52×10^{18}	6.52×10^{19}
	Estimated rate of dissociation	~0.1	~0.1	~0.1
	Amount of $–COO^-$	6.52×10^{16}	6.52×10^{17}	6.52×10^{18}
Guar	Amount of (the most active) -OH	6.21×10^{17}	6.21×10^{18}	6.21×10^{19}

7.4.2. Packaging – 2nd-step of Flocculation

The 2nd-step of the flocculation process, clay-exopolymer groups assembly or packaging, typically performs in two ways, polymer bridging and charge neutralization (*Adachi et al.*, 2012; *Gregory*, 1988; *Harris and Mitchell*, 1973; *Herrington et al.*, 1993; *Lagaly*, 2006; *Theng*, 2012b) (Figure 7.8). To achieve the former one, a single exopolymer molecule should be adsorbed (mainly via H-bonding and VDW force as in Figure 7.7) by no less than two particles or flocculi at the same time, which indicates that the maximum length of extending loops and tails (*L'*, Figure 7.7) should be at least larger than $2t_D$. The latter one, charge neutralization, happens between clay surfaces and exopolymer with opposite charges (adsorbed mainly via Coulomb force or charge-charge attraction as in Figure 7.7) with *L'* shorter than $2t_D$. After the charge of particles is neutralized (either partially or completely), charge-charge repulsion between particles will be decreased and other attraction forces (e.g., VDW force) become relatively greater. Moreover, neutralization of charge could also induce double layer compression or decreasing. If *L'* is greater than two times the compressed Debye length (t'_D), clay-exopolymer becomes being able to be packed via polymer bridging (Figure 7.7).

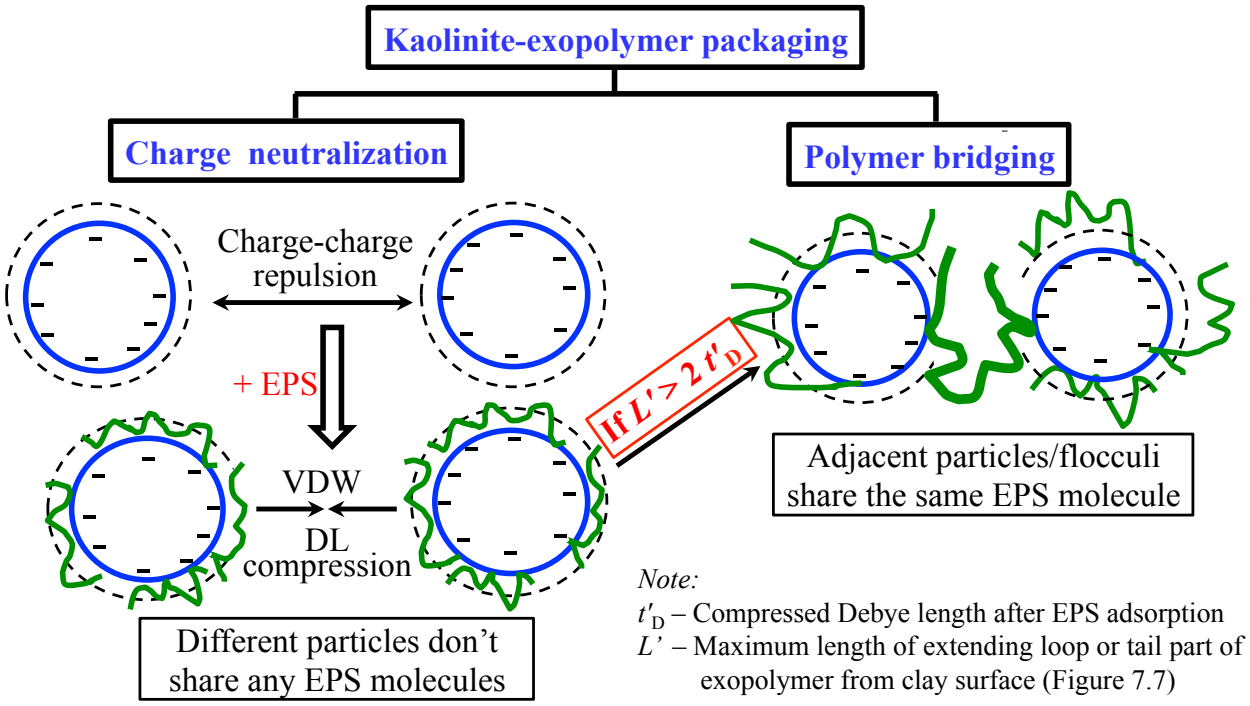

Figure 7.8 Packaging of kaolinite-exopolymer groups as the 2nd-step of flocculation.

Regarding the kaolinite-guar system, length of the molecule backbone (*L*) for nonionic guar is 4.13-8.25 μm (Figure 7.2), which is much greater than $2t_D$ for kaolinite in fresh water (Figure 7.3), 1.92 μm. Hence, kaolinite-guar packaging mainly results from polymer bridging. While *L* of xanthan, 1.95-3.47 μm, is only slightly greater than $2t_D$, the effect of polymer bridging for kaolinite-xanthan is much less than that for kaolinite-guar. Moreover, indicating that kaolinite has positive charge on one face surface (Table 7.1), kaolinite-xanthan packaging can be facilitated by charge neutralization (positive charges on O-faces neutralized by $-COO^-$) as well.

To better illustrate the 2nd-step of flocculation by polymer bridging, kaolinite-exopolymer suspension samples were characterized by using SEM and TEM. As in Figure 7.9, the exopolymers generally do not exist as single molecules; instead they connect together to form fibril- or bundle-like networks, which glue, hold, or link kaolinite particles or flocculi together to form the flocs.

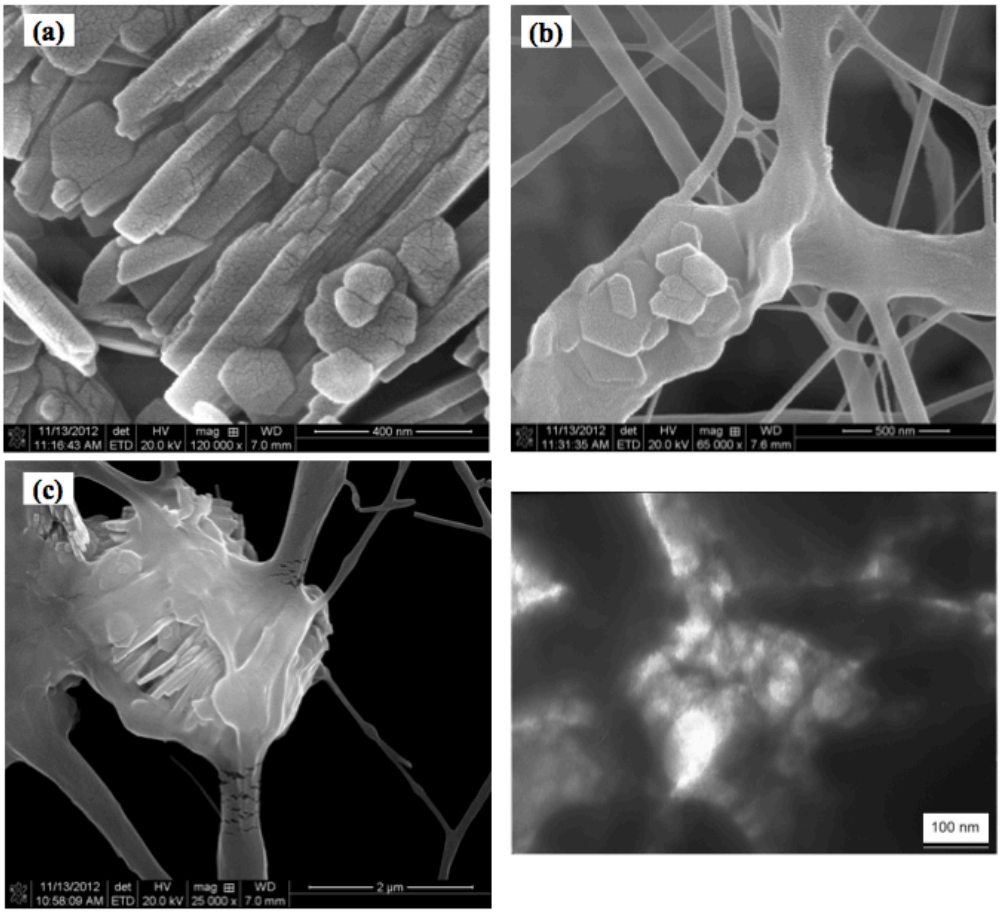

Figure 7.9 SEM images of (a) pure kaolinite, (b) kaolinite-xanthan (100 μg/g), and (c) kaolinite-guar (100 μg/g); and TEM image of (d) kaolinite-guar (100 μg/g).

7.4.3 Kaolinite-Exopolymer Affected by Salt

To better analyze the complicated, three-element kaolinite-salt-exopolymer system, it is necessary to understand the 2nd-level baseline, kaolinite-salt system. According to Equation (2), t_D monotonically decreases as salinity increases, hence the resulting repulsion force between particle face surfaces with the same polarity decreases, leading to more aggregation. Because T-face and O-face possess opposite polarities, as t_D decreases, attraction between T- and O-face surfaces is attenuated, which impedes kaolinite particle-particle aggregation. Thus, the effect of salinity on kaolinite aggregation is due to two competing effects: (1) the decrease of repulsion force between the face surfaces with the same polarity and hence more aggregation, and (2) the decrease of attraction between surfaces with different polarities and hence less aggregation. In fresh water, most kaolinite flocculi form via attraction between T- and O-face surfaces with different polarities (*Schofield and Samson*, 1954). It is observed from SEM image that kaolinite

particles mostly arrange as face-to-face (FF) (Figure 7.9 a). As salinity increases to 5 ppt, formation of kaolinite flocculi is promoted by mostly the slightly attenuated attraction between T- and O-face surfaces, and a small part of decreased repulsion among T-faces or O-faces. In 35 ppt salt water, the kaolinite flocculi formation is an opposite condition to that in 5 ppt. At 10 ppt salt water, the joint effect of attenuation and repulsion decreasing achieves the optimum level for kaolinite aggregation (Figure 7.5 c).

In light of the remarkable increase in kaolinite-xanthan PSD as well as the slight decrease in kaolinite-guar microflocs by adding salt to 10 ppt (Figure 7.6), there are two flocculation mechanisms for kaolinite-salt-exopolymer system: (1) divalent cation bridging (or cross-linking) and (2) double layer repulsion. As illustrated in Figure 7.10, divalent cations from salt (i.e., Mg^{2+}, Ca^{2+}) can form charge-charge attraction with both negatively charged xanthan and kaolinite T-face, which behaves as a bridge that connects these parts with the same polarity. In terms of the two-step flocculation, adsorption of xanthan onto kaolinite surface is increased, and intermolecular cross-linking can increase the effective length of xanthan molecules and enhance the possibility of polymer bridging for kaolinite-xanthan packaging, which both eventually facilitate the flocculation of kaolinite and xanthan. From Figure 7.3, t_D is significantly decreased from ~960 nm (*Israelachvili*, 2007) to 0.64 nm as salinity increases from 0 to 10 ppt. Then, relatively, L' is more possibly and much larger than t'_D, which also facilitates clay-xanthan packaging via polymer bridging. For the kaolinite-guar system, the addition of salt may induce collapse of polymer chains (*Gittings et al.*, 2001), which eventually impede the flocculation in certain levels and hence the kaolinite-guar macroflocs slightly decrease.

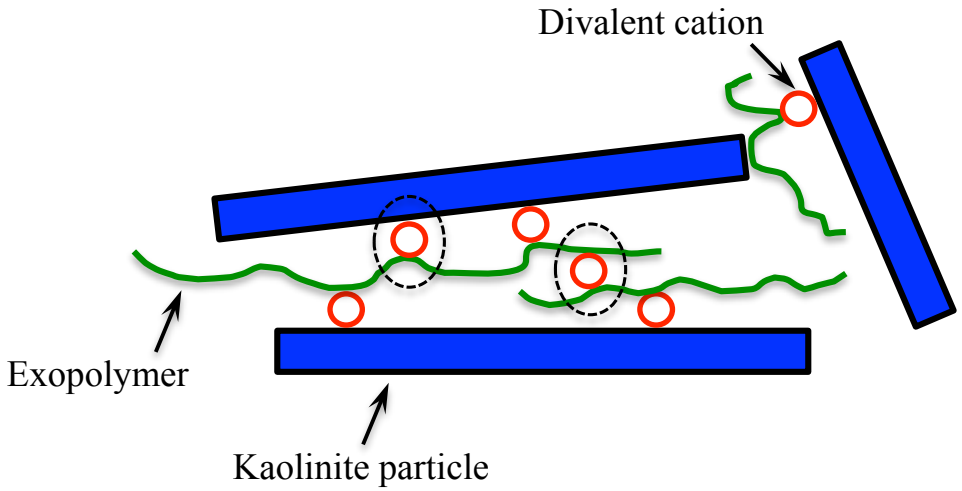

Figure 7.10 Schematic diagram of divalent bridging (in dashed circles) in kaolinite-salt-xanthan system.

7.5 Conclusions

This study aims to develop a systematic understanding about the details of clay-exopolymer flocculation in both fresh and salt waters with the appropriate nomenclature for all the involved intermolecular forces. The main findings can be grouped as three points as below.

Microscale and submicroscale interactions between the colloidal clay particle and exopolymer play a critical role in clay-exopolymer flocculation and hence in the understanding

the related research and industrial areas. While the interaction details and a systematic explanation of their flocculation still lack. One clay, kaolinite, and two exopolymers, xanthan and guar, were selected as the clay-exopolymer models. The other two types of model, pure clay and clay-salt, were also studied as the baseline for understanding the complicated clay-salt-exopolymer system.

Presence of xanthan and guar both induce the flocculation of kaolinite by generating microflocs (30-150 μm) or macroflocs (200-500 μm) in the particle size distribution (PSD) consisting of multimodal, subordinate lognormal distributions. The exopolymer-induced flocculation contains two main steps, adsorption of exopolymer onto kaolinite surface (1^{st}-step) and packaging of clay-exopolymer groups (2^{nd}-step). The 1^{st}-step results from submicroscale intermolecular forces including Coulomb force (i.e., charge-charge, ion-dipole), hydrogen bonding (H-bonding) and van der Waals force. According to the magnitude or energy of each forces, as well as the chemical structure of kaolinite and exopolymers, adsorption of xanthan onto kaolinite is mainly controlled by Coulomb force, while that of guar mainly H-bonding. Hence, the optimum concentration of exopolymers for the maximum flocculation is determined by the amount of participating functional groups on exopolymers and kaolinite face surfaces. The 2^{nd}-step of flocculation is microscale interaction that usually performs via charge neutralization or polymer bridging. Due to the lack of dissociable function groups, nonionic guar and kaolinite packaging is only through the way of polymer bridging, while polyanionic xanthan both ways.

Addition of salt to kaolinite-exopolymer system also shows different PSD change for xanthan and guar. Kaolinite-xanthan flocculation can be further promoted by divalent cation bridging and double layer compression induced more possibility in polymer bridging, which brings macroflocs in kaolinite-salt-xanthan system.

7.6 Nomenclature

EPS – extracellular polymeric substances

TEM – transmission electron microscopy

SEM – scanning electron microscopy

L – length of exopolymer backbone

L' – maximum length of extending loop or tail part of exopolymer on kaolinite surface

t_D – Debye length

t'_D – Compressed Debye length due to charge neutralization or salinity increase

T – tetrahedral sheet of a kaolinite layer

O – octahedral sheet of a kaolinite layer

7.7 Acknowledgments

This research was funded under the Accelerated Research Initiative "Strength of Flocs" that is funded under the NRL Base 6.1 program. GZ was partially supported by the Overseas Collaboration Award of NSFC (Grant No. 51128901). XT received the LSU Graduate School Economic Development Assistantship, Supplement Award and Dissertation Year Fellowship. The facilities used in this study were purchased using the fund from the Louisiana Board of Regents Enhancement Program.

7.8 References

[1] Adachi, Y., Kobayashi, A., and Kobayashi, M. 2012. Structure of colloidal flocs in relation to the dynamic properties of unstable suspension, *International Journal of Polymer Science*, 2012.

[2] Atkinson, M. J., and Bingman, C. 1998. Elemental composition of commercial seasalts, *Journal of Aquariculture and Aquatic Sciences*, 8, 39-43.

[3] Block, L. P. 1978. A double layer review, *Astrophysics and Space Science*, 55, 59-83.

[4] Briscoe, W. 2010, Chapter 16 Surface Forces, in Colloid Science: Principles, Methods and Applications (2nd Edition), edited by T. Cosqrove, pp. 329-361, Wiley-Blackwell.

[5] Chang, I., and Cho, G. 2012. Strengthening of Korean residual soil with β-1,3/1,6-glucan biopolymer, *Construction and Building Materials*, 30, 30-35.

[6] Cheng, Y., Brown, K. M., and Prud'homme, R. K. 2002. Characterization and intermolecular interactions of hydroxypropyl guar solutions, *Biomacromolecules*, 3, 456-461.

[7] Gerbersdorf, S., Westrich, B., and Paterson, D. 2009. Microbial extracellular polymeric substances (EPS) in fresh water sediments, *Microbial Ecology*, 58, 334-349.

[8] Gittings, M. R., Cipelletti, L., Trappe, V., Weitz, D. A., In, M., and Lal, J. 2001. The effect of solvent and ions on the structure and rheological properties of guar solutions, *Journal of Physical Chemistry A*, 105, 9310-9315.

[9] Gregory, J. 1988. Polymer adsorption and flocculation in sheared suspensions, *Colloids and Surfaces*, 31, 231-253.

[10] Harris, R. H., and Mitchell, R. 1973. Role of Polymers in Microbial Aggregation, *Annual Review of Microbiology*, 27, 27-50.

[11] He, M., and Horikawa, Y. 1996. Stability of allophane, allophanic clay, and allophane-halloysite floc in aqueous solutions of an anionic exocellular heteropolysaccharide (gum xanthan) from Xanthomonas campestris, *Soil Science and Plant Nutrition*, 42, 603-612.

[12] Herrington, T. M., Midmore, B. R., and Watts, J. C. 1993. Flocculation of kaolinite suspensions by polyelectrolytes, *Acs Symposium Series*, 532, 161-181.

[13] Hirst, C. N., Cyr, H., and Jordan, I. A. 2003. Distribution of exopolymeric substances in the littoral sediments of an oligotrophic lake, *Microbial Ecology*, 46, 22-32.

[14] Ian W, S. 1994. Structure-function relationships in microbial exopolysaccharides, *Biotechnology Advances*, 12, 393-448.

[15] Israelachvili, J. N. 2007, Intermolecular and surface forces, 2nd ed., Elsevier Academic Press.

[16] Israelachvili, J. N. 2011, Chapter 1 - Historical Perspective, in Intermolecular and Surface Forces edited by J. N. Israelachvili, pp. 3-22, Elsevier.

[17] Jarvis, P., Jefferson, B., Gregory, J., and Parsons, S. A. 2005. A review of floc strength and breakage, *Water Research*, 39, 3121-3137.

[18] Lagaly, G. 2006, Chapter 5 Colloid Clay Science, in Developments in Clay Science, edited by B. K. G. T. Faïza Bergaya and L. Gerhard, pp. 141-245, Elsevier.

[19] Lee, B. J., Fettweis, M., Toorman, E., and Molz, F. J. 2012. Multimodality of a particle size distribution of cohesive suspended particulate matters in a coastal zone, *Journal of Geophysical Research: Oceans*, 117, C03014, 03011-03017.

[20] Lee, S. G., Choi, J. I., Koh, W., and Jang, S. S. 2013. Adsorption of β-d-glucose and cellobiose on kaolinite surfaces: Density functional theory (DFT) approach, *Applied Clay Science*, 71, 73-81.

[21] Němeček, J., Šmilauer, V., and Kopecký, L. 2009, Characterization of Alkali-Activated Fly-Ash by Nanoindentation, in Nanotechnology in Construction 3, edited by Z. Bittnar, P. M. Bartos, J. Němeček, V. Šmilauer and J. Zeman, pp. 337-343, Springer Berlin Heidelberg.

[22] Pawlik, M., and Laskowski, J. S. 2006. Stabilization of Mineral Suspensions by Guar Gum in Potash Ore Flotation Systems, *The Canadian Journal of Chemical Engineering*, 84, 532-538.

[23] Pruett, R. J., and Webb, H. L. 1993. Sampling and analysis of KGa-1b well-crystallized kaolin source clay, *Clay Clay Min.*, 41, 514-519.

[24] Sashiwa, H., and Shigemasa, Y. 1999. Chemical modification of chitin and chitosan 2: preparation and water soluble property of N-acylated or N-alkylated partially deacetylated chitins, *Carbohydrate Polymers*, 39, 127-138.

[25] Schofield, R. K., and Samson, H. R. 1954. Flocculation of kaolinite due to the attraction of oppositely charged crystal faces *Discussions of the Faraday Society*135-145.

[26] Stuart, M. A. C. 1990, Polymers at Interfaces: Statics, Dynamics and Effects on Colloidal Stability, in The Structure, Dynamics and Equilibrium Properties of Colloidal Systems, edited by D. M. Bloor and E. Wyn-Jones, pp. 613-617, Springer Netherlands.

[27] Stuart, M. A. C., Waajen, F., Cosgrove, T., Vincent, B., and Crowley, T. L. 1984. Hydrodynamic thickness of adsorbed polymer layers, *Macromolecules*, 17, 1825-1830.

[28] Swenson, J., Smalley, M. V., and Hatharasinghe, H. L. M. 1998. Mechanism and strength of polymer bridging flocculation, *Physical Review Letters*, 81, 5840-5843.

[29] Tambo, N., and Watanabe, Y. 1979. Physical aspect of flocculation process .1. Fundamental Treatise *Water Research*, 13, 429-439.

[30] Theng, B. K. G. 1982. Clay-polymer Interactions - Summary and perspectives, *Clay Clay Min.*, 30, 1-10.

[31] Theng, B. K. G. 2012a, Chapter 2 - Polymer Behaviour at Clay and Solid Surfaces, in Developments in Clay Science, edited by B. K. G. Theng, pp. 47-75, Elsevier.

[32] Theng, B. K. G. 2012b, Chapter 11 - Polysaccharides, in Developments in Clay Science, edited by B. K. G. Theng, pp. 351-390, Elsevier.

[33] Ulm, F.-J., Vandamme, M., Bobko, C., Alberto Ortega, J., Tai, K., and Ortiz, C. 2007. Statistical Indentation Techniques for Hydrated Nanocomposites: Concrete, Bone, and Shale, *Journal of the American Ceramic Society*, 90, 2677-2692.

[34] Young, S. L., Martino, M., Kienzlesterzer, C., and Torres, J. A. 1994. Potentiometric titration studies on xanthan solutions *Journal of the Science of Food and Agriculture*, 64, 121-127.

[35] Zbik, M. S., and Frost, R. L. 2009. Micro-structure differences in kaolinite suspensions, *J. Colloid Interface Sci.*, 339, 110-116.

[36] Zhang, G., Yin, H., Lei, Z., Reed, A. H., and Furukawa, Y. 2013. Effects of exopolymers on particle size distributions of suspended cohesive sediments, *Journal of Geophysical Research: Oceans*, 118, 1-17.

CHAPTER 8 CONCLUSIONS

8.1 Summary and Conclusions

This dissertation focuses on uncovering and understanding the nanoscale interaction mechanisms between suspended clays and exopolymers, via designed or developed a multiscale characterization routine to probe the properties and microstructure of the flocs generated from clay-exopolymer flocculation process in coastal and estuarine environments. The main findings and their important engineering implications are summarized as below in four groups.

8.1.1 Evaluation and Recommendation of Intrinsic PSDs (Chapter 3 and 5)

As one of the most fundamental physical properties of soils, PSD is required by current soil classification standards and unified soil classification system. It is important to realize and understand the change of PSD under different conditions. A series of experimental study has been conducted to evaluate the PSD and their variability of four source clay minerals, kaolinite, illite, Ca^{2+}-Mt, and Na^{+}-Mt, under different dispersion or disaggregation methods, including dry dispersion in pressurized air and wet dispersion in water and EA with and without an interlayer expanding agent, glycerol, along with ultrasound disaggregation and NaHMP dispersion. According the results and detailed discussions, special cautions should be taken when selecting dry dispersion, chemical dispersion, or ultrasound disaggregation, which may result in PSD overestimation or unnecessary particle exfoliation or breakage. The intrinsic PSD of kaolinite and illite should be obtained by NaHMP dispersion, while those of the two smectites can be obtained by dispersing in EA or other less- or non-polar solvents. The PSD of most well dispersed clay minerals show a multimodal lognormal distribution consisting of primary particles (~2 μm) and flocculi (10-20 μm), the latter of which are resistant to disaggregation and can only be removed via sedimentation. As a result, the soil classification, depend on PSD analysis, tends to overestimate the silt-sized fraction, but underestimate the clay mineral-sized fraction.

8.1.2 Properties of Expansive Clays (mainly Chapter 5)

Flocculation and particle size variation of expansive clays are very sensitive to and highly dependent upon the environmental conditions. For sediments rich in expansive clays, in-situ sampling and subsequent laboratory characterization should consider the change of the chemistry and biological activities of its aquatic environment, as well as the flow conditions. The PSD and its variations of Ca^{2+}-Mt and Na^{+}-Mt affected by different types of exopolymers at varying concentrations, different salinities, and hydrodynamic factors were characterized by using laboratory-prepared sample. Generally, different exopolymers can induce different degrees of flocculation. Xanthan and guar can significantly increase the particle size of Na^{+}-Mt (e.g., from ~10 to ~50 μm for the largest flocs) and generate a higher degree of flocculation, while chitosan decreases the particle size of both clays, owing to the formation of more compacted flocs resulted from polycationic polymer bridging. Increase in salinity facilitates the flocculation of Na^{+}-Mt by decreasing the repulsive electrical double layer thickness, while the particle size of limitedly swelling Ca^{2+}-Mt is slightly reduced, which may be resulted from the basal spacing suppression. The flocculation of the two clays under laminar, transitional, and turbulent flows were also evaluated. Generally, the turbulence associated with higher shear rates facilitates the

flocculation to different degrees of Ca-M in all of the studied conditions, while the Na-M floc size decreases to certain degrees when the shear rate increases. Therefore, the limitedly swelling Ca-M tends to form relatively stronger and larger flocs than the highly swelling Na-M.

8.1.3 A Conceptual Model of Clay-Exopolymer Flocs (Chapter 6 and 4)

Since sedimentary cohesive soils usually originate from the particulate matter (dominantly clay-organic flocs or complexes) suspended in natural waters, investigation and elucidation of floc microstructure can help understand some peculiar engineering behavior and properties of certain sedimentary soils, such as highly organic soils and fluid muds in coastal zones. By synthesis the PSD and settling velocity results (as indirect observations) and electron microscopy images (as direct observation), a conceptual microstructure model consisting of four hierarchical levels (i.e., primary particles, flocculi, microflocs, and macroflocs) is proposed for the clay-exopolymer flocs.

According to the PSD results, clay-guar mixture suspensions consist of four discrete particle groups, including primary particles (0.2-5 mm), flocculi (8-40 mm), microflocs (50-150 mm), and macroflocs (200-500 μm). While the first two are present in both pure clay and clay-guar suspensions, the latter two only exist in the mixture suspensions, suggesting that microflocs and macroflocs are induced by guar and composed of primary particles and flocculi. With the same size, the settling velocity of clay-guar flocs is typically smaller than that of pure clay flocs, which is attributed to the reduced density of flocs caused by the exopolymer. The fractal dimension of these clay-EPS flocs estimated from settling velocity ranges from 1.39 to 1.47, which are smaller than that of pure clay flocs, indicating that these flocs are less compacted than the pure clay flocs. Direct electron microscopy characterization, which supports the PSD and settling velocity data, shows that densely packed flocculi are mainly formed via face-edge and face-face association of clay particles, and guar acts as fibrils and bundles coating, bridging, and surface gluing primary particles and flocculi, resulting in the formation of a loosely packed, porous microstructure for soft microflocs and macroflocs.

8.1.4 Flocculation Mechanisms of Clay-Exopolymer Flocs (mainly Chapter 7)

Microscale and submicroscale interactions between the colloidal clay particle and exopolymer play a critical role in clay-exopolymer flocculation and hence in the understanding the related research (e.g., removal of nutrients and contaminants from water, as well as the influence of involved organic matter on sediment yield). Kaolinite, xanthan and guar were chosen to construct the clay-exopolymer models. Considering the coastal or marine environment, clay-salt-exopolymer systems were also characterized. Based on the analysis of PSD result along with some theoretical calculation, the exopolymer-induced flocculation mechanism was explained as a two-step process:

(1) The 1st-step, adsorption of exopolymer onto clay surfaces, results from submicroscale intermolecular forces including Coulomb force (i.e., charge-charge, ion-dipole), H-bonding, and VDW forces. According to the magnitude or energy of each forces, as well as the chemical structure of kaolinite and exopolymers, adsorption of xanthan onto kaolinite is mainly controlled by Coulomb force, while that of guar mainly H-bonding. Hence, the optimum

concentration of exopolymers for the maximum flocculation is determined by the amount of participating functional groups on exopolymers and kaolinite face surfaces.

(2) The 2nd-step, packaging of clay-exopolymer groups, is microscale interaction that usually performs via charge neutralization or polymer bridging. Due to the lack of dissociable function groups, nonionic guar and kaolinite packaging is only through the way of polymer bridging, while polyanionic xanthan both ways. Addition of salt to kaolinite-exopolymer system also shows different PSD change for xanthan and guar. Kaolinite-xanthan flocculation can be further promoted by divalent cation bridging and double layer compression induced more possibility in polymer bridging, which brings macroflocs in kaolinite-salt-xanthan system.

Finally, the results of clay-exopolymer interaction can perform as a lower level structural model by scaling down from the proposed four hierarchical level microstructure model.

8.2 Possible Future Work

Based on current research in this dissertation and related literatures, some further work are recommended:

(1) In order to build a coherent, unified understanding of the nanoscale clay-exopolymer interactions, the experimentation-based study and theoretical analyzing may be still not sufficient. The interaction forces and energy need to be quantified to better understand the physical properties of clay-exopolymer flocs (e.g., floc strength). Hence, molecular dynamics (MD) simulation or density function theory (DFT) based calculation is strongly recommend to follow up, the addition of which can turn the study in this area an integrated experiment - theoretical analysis - computation work.

(2) Since this dissertation focuses on fundamental research of the properties of suspended cohesive sediments (i.e., flocculation mechanism and microstructure), some effort should be devoted to apply the results and findings into sediment transport modeling.

(3) The research object in this dissertation includes primary particles, flocculi, and flocs, which can be considered as the fundamental elements in settled floc bed. As a continuity from the conceptual floc model as presented in Chapter 6, a multiscale structural network model is deserved to built up by scaling up to floc bed. Further research is needed with focus on uncover the connections or relationship (e.g., scaling theory) between these different scales, which will play an important role in understanding and predicting the engineering property of floc or cohesive sediment bed.

APPENDIX: PERMISSIONS

The permission of reprinting or reusing Chapter 4 in this dissertation has been requested through Copyright Clearance Center's RightsLink service. The details are as below.

ELSEVIER LICENSE
TERMS AND CONDITIONS

Aug 09, 2013

This is a License Agreement between Xiaoling Tan ("You") and Elsevier ("Elsevier") provided by Copyright Clearance Center ("CCC"). The license consists of your order details, the terms and conditions provided by Elsevier, and the payment terms and conditions.

All payments must be made in full to CCC. For payment instructions, please see information listed at the bottom of this form.

Supplier	Elsevier Limited The Boulevard,Langford Lane Kidlington,Oxford,OX5 1GB,UK
Registered Company Number	1982084
Customer name	Xiaoling Tan
Customer address	Dept. of Civil & Environmental Eng. BATON ROUGE, LA 70803
License number	3177140826383
License date	Jun 27, 2013
Licensed content publisher	Elsevier
Licensed content publication	International Journal of Sediment Research
Licensed content title	Characterization of particle size and settling velocity of cohesive sediments affected by a neutral exopolymer
Licensed content author	Xiao-ling TAN,Guo-ping ZHANG,Hang YIN,Allen H. REED,Yoko FURUKAWA
Licensed content date	December 2012
Licensed content volume number	27
Licensed content issue number	4
Number of pages	13
Start Page	473
End Page	485
Type of Use	reuse in a thesis/dissertation
Title of your thesis/dissertation	Microstructure and Physics-Based Structural Models for Suspended Clay-Exopolymer Flocs
Expected completion date	Dec 2013

The permission of reprinting or reusing Chapter 5 in this dissertation has been requested through Copyright Clearance Center's RightsLink service. The details are as below.

SPRINGER LICENSE
TERMS AND CONDITIONS

Jan 22, 2014

This is a License Agreement between Xiaoling Tan ("You") and Springer ("Springer") provided by Copyright Clearance Center ("CCC"). The license consists of your order details, the terms and conditions provided by Springer, and the payment terms and conditions.

All payments must be made in full to CCC. For payment instructions, please see information listed at the bottom of this form.

License Number	3311520351548
License date	Jan 17, 2014
Licensed content publisher	Springer
Licensed content publication	Ocean Dynamics
Licensed content title	Flocculation and particle size analysis of expansive clay sediments affected by biological, chemical, and hydrodynamic factors
Licensed content author	Xiaoling Tan
Licensed content date	Jan 1, 2013
Volume number	64
Issue number	1
Type of Use	Thesis/Dissertation
Portion	Full text
Number of copies	1
Author of this Springer article	Yes and you are the sole author of the new work
Order reference number	
Title of your thesis / dissertation	Microstructure and Physics-Based Structural Model for Clay-Exopolymer Flocs
Expected completion date	May 2014
Estimated size(pages)	150
Total	0.00 USD
Terms and Conditions	

VITA

Ms. Xiaoling Tan was born in 1987 in Yicheng, Hubei Province, China. She earned her Bachelor of Engineering degree in Biomedical Engineering from Huazhong University of Science and Technology, China, in June 2009.

Ms. Tan joined the Department of Civil and Environmental Engineering (in the Ph.D. program of Engineering Science) in August 2009 as a Graduate Research Assistant. She has been involved in researches of a few areas including geotechnical and geophysical engineering, material science and engineering, clay mineralogy, sediment transportation, biogeochemistry, etc. Financially supported by the LSU Graduate School via three awards (Economic Development Assistantship Award 2009-2012, Supplement Award 2009-2012, and Dissertation Year Fellowship 2013-2014), Ms. Tan expects to finish all study and work, and receive the degree of Doctor of Philosophy in Engineering Science in May 2014.